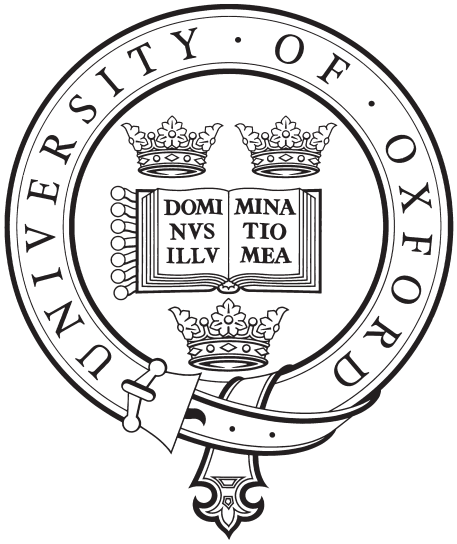
The properties of nitrogen in silicon

C.R. Alpass

Oriel College



Thesis submitted for the degree of Doctor of Philosophy

Trinity Term 2008

Supervisor: Dr P.R. Wilshaw

Abstract

The properties of nitrogen in silicon

Charles Alpass
Oriel College
Department of Materials, University of Oxford

Thesis submitted for the degree of Doctor of Philosophy
Trinity Term 2008

The behaviour of nitrogen in silicon is investigated using the dislocation unlocking technique. Specimens containing well-ordered arrays of dislocations are isothermally annealed for a controlled duration, during which nitrogen segregates to and pins the dislocations. The stress required to unlock the dislocations is then measured by three-point bending at elevated temperature. By analysing the dependence of this unlocking stress on anneal duration and temperature, information about nitrogen's transport and interaction with dislocations can be deduced.

Experiments are performed at anneal temperatures of 500 - 1050°C using float-zone silicon with $[\mathrm{N}] = 2 \times 10^{15}\,\mathrm{cm}^{-3}$. The results are analysed to give an expression for nitrogen's effective diffusivity of $D = 173,000 \exp(-3.24\mathrm{eV}/kT)\,\mathrm{cm}^2\mathrm{s}^{-1}$ in the 500 - 750°C range, showing for the first time that nitrogen transport at low temperatures behaves in the same way as measured at higher temperatures by other groups using secondary ion mass spectrometry. If analysed in terms of monomer-dimer dissociative transport, the results give a nitrogen monomer diffusivity of $D_1 = 28 \exp\left(-(1.1 \rightarrow 1.4\mathrm{eV})/kT\right)\,\mathrm{cm}^2\mathrm{s}^{-1}$, which is similar to that found by another analysis in the literature. The measurements also show that nitrogen's dislocation locking strength measured at 550°C is dependent on anneal temperature, peaking at 600 - 700°C and falling towards zero above 1000°C.

The dislocation unlocking technique itself is also investigated and characterized. It is found that the measured unlocking stress is dependent on the three-point bend duration, falling with increasing duration. Analysis of these results in terms of the theory of release of dislocations from pinning points indicates that nitrogen dislocation locking is likely to be by an atomic species. This effect also has implications for the results of previous nitrogen dislocation unlocking experiments, and the technique has been modified so that a standardised set of conditions is used for every test. Other measurements show that nitrogen's dislocation locking effect is lessened by the presence of transition metal contamination, and that dislocation velocity in silicon may be affected by the nitrogen present in the material.

A modified dislocation unlocking technique is developed to measure dislocation locking from near-surface ion-implanted impurities. Results from heavily N-implanted silicon show that nitrogen implantation can provide additional dislocation locking strength to that already given by the oxygen in the material. The scale of the dislocation locking effect in these experiments may provide evidence that nitrogen's effective diffusivity is reduced at high concentrations, indicating that nitrogen transport may be by a dissociative mechanism.

Preface

This thesis is an account of the work carried out by the author in the Department of Materials, University of Oxford, under the supervision of Dr P.R. Wilshaw, from Michaelmas Term 2004 to Trinity Term 2008. No part of this thesis has previously been submitted for a degree at the University of Oxford or elsewhere. The work of other authors has been freely drawn upon and is duly acknowledged in the text. A list of references is given at the end of the thesis.

Work presented in this thesis has been published as follows:

1. **C.R. Alpass**, J.D. Murphy, R.J. Falster, P.R. Wilshaw, *'Dislocation unlocking measurements of nitrogen in silicon'*, Journal of Applied Physics **105**, 013519 (2009).

2. **C.R. Alpass**, J.D. Murphy, R.J. Falster, P.R. Wilshaw, *'Nitrogen in silicon: diffusion at 500 to 750° C and interaction with dislocations'*, accepted by Materials Science and Engineering B (2008).

3. **C.R. Alpass**, J.D. Murphy, A. Jain, P.R. Wilshaw, *'Measurements of Dislocation Locking by Near-Surface Ion-Implanted Nitrogen in Czochralski Silicon'*, ECS Transactions **16**, 249 (2008).

4. **C.R. Alpass**, J.D. Murphy, A. Giannattasio, S. Senkader, R.J. Falster, P.R. Wilshaw, *'Out-diffusion of nitrogen from float-zone silicon measured by dislocation locking'*, Physica Status Solidi (a) **204**, 2256 (2007).

5. J.D. Murphy, **C.R. Alpass**, A. Giannattasio, S. Senkader, D. Emiroglu, J.H. Evans-Freeman, R.J. Falster, P.R. Wilshaw, *'Nitrogen-doped silicon: mechanical, transport and electrical properties'*, ECS Transactions **3**, 239 (2006).

6. J.D. Murphy, **C.R. Alpass**, A. Giannattasio, S. Senkader, R.J. Falster, P.R. Wilshaw, *'Nitrogen in silicon: transport and mechanical properties'*, Nuclear Instruments and Methods in Physics Research B **253**, 113 (2006).

7. J.D. Murphy, A. Giannattasio, **C.R. Alpass**, S. Senkader, R.J. Falster, P.R. Wilshaw, *'The influence of nitrogen on dislocation locking in float-zone silicon'*, Solid State Phenomena **108-109**, 139 (2005).

Charles Alpass, Oxford

18th July 2008

Acknowledgements

I would like to thank my supervisor Dr P.R. Wilshaw for his support, encouragement, and irrepressible enthusiasm. I'm sorry that I couldn't make any of the crazy ideas work! I am also grateful to the various members of the Semiconductor group for their support and friendship, including R.H. Haslam, W.A.T. Winborn, M. Bent, P.J. Lewis, B.C. Pygall, C. Wilson, N.J. Gregori, D.M. Jordan, K.J. Fraser, A.R. Walpole, D.J. Stowe, A. Giannattasio, S. Senkader, and particularly J.D. Murphy, who has been a true ally from the very start.

I would like to thank the Engineering and Physical Sciences Research Council for personal funding, and also the Institute of Physics and Oriel College, Oxford for travel funding which allowed me to present my work at international conferences. Those who have provided the silicon used in this work are also gratefully acknowledged, including Dr W. von Ammon of Siltronic AG, Dr O. Anderson of Topsil Semiconductor Materials A/S, Dr A. Jain of Texas Instruments Inc., Dr J. England of Varian Semiconductor Equipment Associates Inc. and Dr R.J. Falster of MEMC Electronic Materials Inc.

Finally, to my family who have always loved and looked after me, St Ebbe's who have been my family in Oxford, Oriel MCR for their fun and happiness, and my other friends in Oxford and elsewhere: thank you. I love you all.

I love you, O LORD, my strength.
The LORD is my rock and my fortress and my deliverer,
my God, my rock, in whom I take refuge,
my shield, and the horn of my salvation, my stronghold.
I call upon the LORD, who is worthy to be praised,
and I am saved from my enemies.

Psalm 18:1-3

Contents

1 Introduction **1**

1.1 Background 1

1.2 Growth of silicon crystals 2

1.2.1 Extraction of electronic grade silicon 2

1.2.2 The Czochralski method 3

1.2.3 The floating zone method 4

1.3 Oxygen in silicon 5

1.3.1 'Normal' diffusion of oxygen in silicon 6

1.3.2 Anomalous diffusion of oxygen in silicon 8

1.4 Nitrogen in silicon 9

1.4.1 The effects of nitrogen in silicon 9

1.4.2 The properties of nitrogen in silicon 10

1.4.3 Diffusion of nitrogen in silicon 16

1.4.4 Nitrogen-oxygen complexes 20

1.4.5 Measuring nitrogen in silicon 22

1.5 Impurity interactions with dislocations in silicon 23

1.5.1 Dislocations in silicon 23

1.5.2 Immobilization of dislocations by impurities 25

1.5.3 Dislocation locking by oxygen and nitrogen 27

1.6 Summary 28

1.7 This work 28

2 Previous dislocation unlocking experiments **30**

2.1 History of dislocation unlocking experiments 30

2.1.1 Introduction 30

2.1.2 Dislocation unlocking as a new way of measuring impurity transport 31

2.2 Dislocation unlocking used to measure oxygen transport in Cz-Si . . . 34

2.2.1 Transport analysis 35

2.2.2 Binding to dislocations 36

2.2.3 Oxygen transport in highly doped Cz-Si 37

2.2.4 Advantages of dislocation unlocking as an experimental technique 38

2.3 Dislocation unlocking used to measure nitrogen transport in FZ-Si . . 39

2.3.1 The need for measurements of nitrogen transport 39

2.3.2 Adapting dislocation unlocking to measure nitrogen 39

2.3.3 Results from nitrogen experiments 41

2.3.4 Analysis of dislocation locking by nitrogen: the identity of the locking species 48

2.4 Critical evaluation of previous nitrogen dislocation unlocking work . . 49

2.4.1 Was nitrogen locking really being measured? 49

2.4.2 Uncertainty with interpretation 50

2.4.3 Known problems with the experiments 53

2.5 Summary 55

3 The dislocation unlocking method as used in this work **57**

3.1 Specimen preparation 57

3.1.1 Cleaving and polishing 58

3.1.2 Clean and planar etch 59

3.2 Indenting 60

3.2.1 Micro-hardness tester 60

3.2.2 Nanoindenter 60

3.3 Bending set-up 61

3.3.1 Molybdenum bending jig 62

3.3.2 Full bending apparatus 63
3.3.3 Load application 66
3.3.4 Geometry 66
3.3.5 Four-point bend procedure 69
3.3.6 Three-point bend procedure 70
3.4 Annealing 71
3.4.1 Standard metallurgical furnaces 71
3.4.2 RTA furnace 73
3.4.3 Fast quench annealing 74
3.5 Evaluation of annealing techniques 75
3.5.1 Standard furnaces 76
3.5.2 RTA furnace 77
3.5.3 Fast-quench furnace 79
3.6 Etching 80
3.6.1 Planar etching 80
3.6.2 Preferential etching 81
3.7 Determination of unlocking stress 82
3.7.1 How specimens are measured 82
3.7.2 How unlocking stress is determined 83
3.7.3 The effect of standardising three-point bend conditions 85
3.8 Silicon used in this work 87
3.8.1 Float-zone silicon 89
3.8.2 Czochralski silicon 90

4 Characterization of the dislocation unlocking experimental method 93
4.1 Control experiments 93
4.1.1 Nitrogen-free control 93
4.1.2 Transition metal control 94
4.1.3 Instron performance 97
4.2 Results from High-[N] 2 silicon 99
4.2.1 Pre-anneal experiments to measure nitrogen out-diffusion . . . 100

4.2.2 Dependence of unlocking stress on three-point bend duration in High-[N] 2 NFZ-Si . . . 102
4.2.3 Nitrogen content of High-[N] 2 wafers . . . 103
4.3 Relationship between three-point bend duration and unlocking stress in uniform material . . . 103
4.3.1 Experimental results . . . 103
4.3.2 Analysis . . . 104
4.4 Summary of characterization experiments . . . 106
4.5 Errors in dislocation unlocking experiments . . . 108
4.5.1 Quantifiable error . . . 108
4.5.2 Other errors . . . 109
4.5.3 Measurements of the reproducibility of locking . . . 110
4.5.4 Summary . . . 111

5 Dislocation unlocking experiments using NFZ silicon 113
5.1 Nitrogen transport investigated by dislocation unlocking . . . 114
5.1.1 Nitrogen dislocation unlocking results . . . 114
5.1.2 Activation energy for the dislocation locking process . . . 114
5.1.3 Modelling Regime 1 to find nitrogen's effective diffusivity . . . 116
5.2 Analysis of the nitrogen effective diffusivity results . . . 120
5.2.1 Introduction . . . 120
5.2.2 Simple dimer diffusion . . . 120
5.2.3 Dissociative transport . . . 120
5.2.4 Discussion of dissociative diffusion and dislocation unlocking results . . . 123
5.3 The interaction between nitrogen and dislocations investigated by dislocation unlocking . . . 123
5.3.1 Regime 2 results . . . 123
5.3.2 [N]-dependence of Regime 2 locking stress . . . 124
5.4 Analysis of Regime 2 results . . . 125
5.4.1 Anneal temperature dependence of dislocation locking stress . 125

5.5 Discussion of nitrogen dislocation unlocking results 126
5.5.1 Diffusivity of nitrogen 126
5.5.2 Regime 2 126
5.5.3 Nature of the locking species 127
5.6 Dislocation velocity in dislocation unlocking experiments 130
5.6.1 Method of determining dislocation velocity 130
5.6.2 Dislocation velocity results 131
5.6.3 Dislocation velocity analysis 133
5.7 Unlocking discontinuity 134
5.8 Comparison with previous nitrogen dislocation unlocking work 134
5.8.1 Systematic error associated with changes in three-point bend duration 135
5.8.2 Effect of error on previous work 135
5.8.3 Reasons for having confidence in the new results 139
5.9 Summary 141

6 Nitrogen implant and nitrogen out-diffusion experiments 144
6.1 Nitrogen-implanted Cz silicon 144
6.1.1 Introduction 144
6.1.2 Motivation behind nitrogen-implant dislocation unlocking experiments 145
6.1.3 Stage 1: Modified experimental procedure 146
6.1.4 Experimental effectiveness of new technique 149
6.1.5 Experimental results 150
6.1.6 Analysis 153
6.2 Arsenic-implanted Cz silicon 156
6.2.1 Motivation 158
6.2.2 Experiments 158
6.3 Out-diffusion of nitrogen from NFZ-Si 159
6.3.1 Introduction 159
6.3.2 Experimental technique 160

6.3.3 Results and discussion 161
6.4 Summary 163

7 Summary and further work **165**
7.1 Nitrogen in silicon 165
7.1.1 Low-temperature transport 165
7.1.2 Interaction with dislocations 166
7.1.3 Nitrogen-implanted silicon 166
7.1.4 Interaction with transition metals 167
7.2 The dislocation unlocking experimental method 168
7.2.1 Improvement in technique 168
7.2.2 Usefulness of the dislocation unlocking technique 168
7.3 Suggestions for further work 169
7.3.1 Nitrogen dislocation unlocking experiments 169
7.3.2 Oxygen dislocation unlocking experiments 171
7.3.3 Nitrogen-implanted silicon 172

A Program used to model nitrogen's interaction with dislocations **173**
A.1 Fortran code 176

Chapter 1

Introduction

1.1 Background

Silicon continues to be the material of choice for modern microelectronics. The relentless miniaturization of transistor technology has meant that previously tolerable defects in silicon wafers can now have a catastrophic effect on device yields. The need for faster integrated devices is placing increasingly stringent demands on the basic silicon substrate, which must be defect-free at progressively smaller scales. Currently, the standard required for the most advanced devices can be achieved only by epitaxial growth or complex annealing schedules to remove defects from wafers.

It has been known since the 1990s that the addition of nitrogen to silicon crystals can improve their quality, and in the last few years this has started to become common practice amongst silicon manufacturers. Some of the most technologically important beneficial effects are thought to arise from the nitrogen's interaction with oxygen, which is also present in most silicon. This has created much interest in the nitrogen and nitrogen-oxygen systems in silicon, but despite this, they remain poorly understood.

In this chapter, a brief overview of the production of modern silicon is given, along with a summary of the effects of oxygen, an important impurity. The properties of nitrogen in silicon are then discussed. Finally, the interaction between impurities and dislocations is reviewed. Following this, a detailed examination of previous experi-

mental results found using the dislocation unlocking technique is given in Chapter 2.

1.2 Growth of silicon crystals

1.2.1 Extraction of electronic grade silicon

Silicon is the second most abundant element in the Earth's crust, and is familiar to most people as a constituent of common sand. However, since sand is contaminated with other oxides, crystalline quartz is used as the starting material for the production of silicon for electronic devices. Quartz is reduced to silicon by smelting, producing metallurgical grade silicon (MGS). The furnace is charged with a mixture of quartz, coal, coke and wood, which is heated by passing a current between the furnace walls and a submerged electrode. The quartz first undergoes thermal decomposition to form silicon monoxide:

$$2SiO_2 \rightarrow 2SiO + O_2$$

The silicon monoxide then reacts with carbon to form silicon carbide and carbon monoxide:

$$SiO + 2C \rightarrow SiC + CO$$

Finally, the silicon carbide reduces the quartz to form elemental silicon:

$$SiC + SiO_2 \rightarrow Si + SiO + CO$$

The dense molten silicon sinks to the bottom of the furnace and is removed. It is highly contaminated, particularly with iron and aluminium from the coal and coke, and must be further purified. MGS is usually refined using fractional distillation of $SiHCl_3$. MGS powder is reacted with hydrochloric acid to give the volatile $SiHCl_3$, which can be separated from the iron and aluminium chlorides which remain in solution. It is then reduced with hydrogen to give large bars of a polycrystalline material,

referred to as electronic grade silicon (EGS). This material is used to grow the silicon single crystals on which devices are fabricated. Two methods are used to grow crystalline silicon from EGS: the Czochralski method, and the floating zone method.

1.2.2 The Czochralski method

The vast majority of single crystal silicon sold today is grown by a method invented by Czochralski in 1916, which was originally conceived as a way of determining the crystallization velocity of metals [1]. Silicon crystals grown this way contained dislocations until the method was refined by Dash in 1958 [2], who introduced a crystal neck, allowing the growth of crystals that are entirely dislocation-free. A melt of EGS is held in a crucible, into which a seed crystal is dipped and then slowly withdrawn vertically, as seen in Figure 1.1. The liquid silicon crystallizes at the seed; growth velocities are of the order of 1mm per minute for 300mm diameter crystals. Once the silicon ingot is drawn from the melt it is sliced into wafers, which are then mirror polished on at least one side.

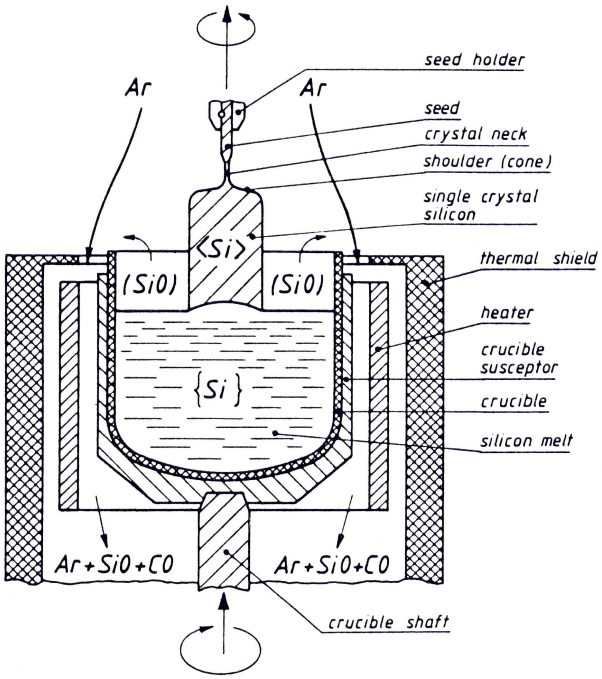


Figure 1.1: The Czochralski method for pulling silicon single crystals (*after Borghesi* [3]).

Silicon grown by the Czochralski method (Cz-Si) contains a significant amount of

oxygen, from the dissolution of the walls of the silica (SiO_2) crucible that holds the melt. Oxygen's segregation coefficient is greater than one, so it preferentially partitions into the solid during crystal growth. Cz-Si therefore typically contains oxygen in concentrations of 10^{17} to 10^{18}cm^{-3}. Oxygen is the most significant contaminant of Cz-Si, as most other impurities have much lower segregation coefficients (Table 1.1) and so are only present in low concentrations.

Cz-Si is the material of choice for the vast majority of very large scale integration (VLSI) device manufacture. This is because it is less expensive, and also generally has higher mechanical strength at the temperatures used in device processing than float zone silicon. It has long been known that Cz-Si wafers are less susceptible to slip than float zone wafers [3, 6], which is due to the presence of oxygen in Cz-Si. This is discussed further in §1.5. Cz-Si wafers are the largest in regular production today and 300mm diameter wafers are currently the standard for advanced device fabrication, with 450mm wafers being scheduled for 2012.

1.2.3 The floating zone method

To grow silicon crystals of the highest purity, it is necessary to remove all contact between the melt and the crucible and other contaminant sources. This can be achieved by zone-refining the crystals, taking advantage of the low segregation coefficients of most impurities at the liquid-solid transition. In the freely floating zone refining method, a floating zone created by radio-frequency induction heating is suspended between the melting and freezing interfaces (Figure 1.2). The whole apparatus is contained in an inert or nitrogen atmosphere, or held under vacuum.

Float zone (FZ) technology is the best method of growing high-purity crystals, and silicon ingots created this way can have unique properties that cannot be achieved using other techniques. For example, FZ-Si can be grown with resistivity exceeding

Impurity	Al	As	B	C	Cu	Fe	N	O	P	Sb
k_0	0.002	0.3	0.8	0.07	4×10^{-4}	8×10^{-6}	7×10^{-4}	1.25	0.35	0.023

Table 1.1: Segregation coefficients, k_0, for common impurities found in silicon (*after Pearce* [4], *except for N which is after Yatsurugi* [5]).

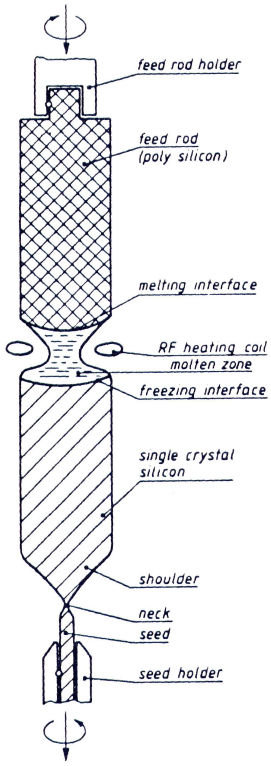


Figure 1.2: Float-zone growth (*after Zulehner* [7]). The entire apparatus is enclosed in a controlled atmosphere.

$10^5\Omega$cm because of the intrinsic process purity. It is, however, considerably more expensive than Cz-Si, and the largest wafers in regular production have a diameter of 200mm. Also, because of its negligible oxygen concentration it does not experience the benefits that oxygen provides, which are described below. FZ-Si is therefore only used when Cz-Si is unsuitable, for instance in high power applications, photodetectors, radio frequency devices and micro-electromechanical systems [8, 9].

1.3 Oxygen in silicon

The presence of oxygen in silicon is beneficial for two main reasons. Firstly, it is effective at pinning dislocations in silicon, which increases the mechanical strength of wafers by preventing slip [3, 6], allowing the use of more aggressive processing conditions. Secondly, oxygen precipitates deep inside the wafer can be used as internal gettering sites, capturing unwanted metal impurity atoms and preventing them from

harming the device structures at the wafer surface [10].

As significant amounts of oxygen are present in the majority of silicon sold, the way oxygen behaves in silicon is of great technological interest, and so the system has been studied extensively. Isolated oxygen atoms are most stable at interstitial sites in the lattice (Figure 1.3), as revealed by infra-red absorption measurements [11] and by small increases in the lattice parameter compared to FZ-Si [12]. At temperatures typical of device fabrication, oxygen is present in Cz-Si as a supersaturated solid solution, and below ∼1200°C, oxygen precipitates (SiO_2 particles) exist in the silicon crystal.

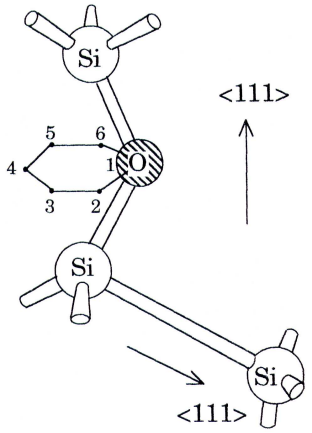


Figure 1.3: Interstitial position of an oxygen atom in the silicon lattice, covalently bonded with two neighbouring silicon atoms. The equivalent interstitial positions are indicated (*after Borghesi* [3]).

Oxygen in silicon at lower temperatures is less well understood, but there is evidence that some of the oxygen exists in the form of a fast diffusing dimer below 500°C [13]. Diffusion of oxygen can be the rate-limiting factor for the formation of oxide precipitates, so a full understanding of oxygen diffusion from room temperature to the melting point of silicon is desirable.

1.3.1 'Normal' diffusion of oxygen in silicon

Interstitial oxygen atoms, O_i, diffuse by jumping from one bond-centred site to one of the six adjacent sites [13]. Many studies have investigated oxygen's diffusivity, which is now thought to be understood for temperatures greater than approximately 850°C.

Early work used 100kHz and 300kHz acoustic waves to generate an oscillating

stress in a heated block of silicon [14]. The damping of the waves at high temperatures occurred with a broad superposed resonant peak, which, when analysed, gave a value for oxygen's diffusivity. More recently, secondary ion mass spectrometry (SIMS) has been used to deduce the diffusion coefficient of oxygen in silicon at high temperatures (Figure 1.4). The distributions of out-diffused $^{16}O_i$ [15,16] and in-diffused $^{18}O_i$ [17,18] were fitted to error function profiles, with results agreeing with the previous acoustic wave work.

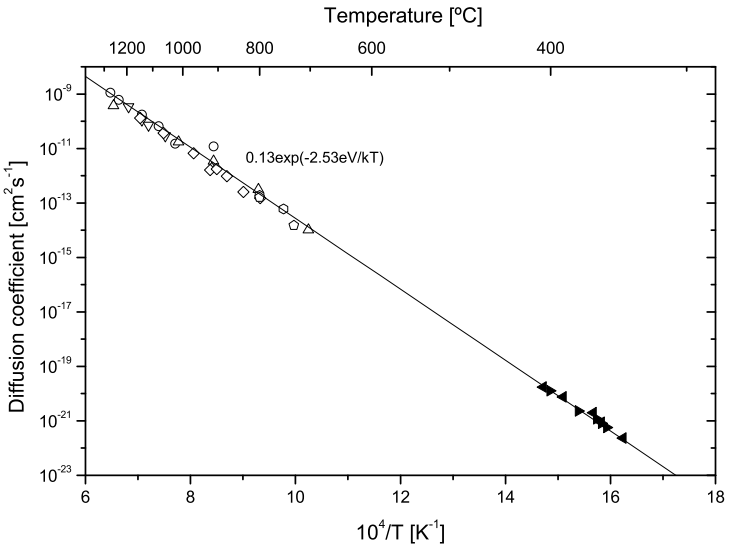


Figure 1.4: Measured values of 'normal' oxygen diffusion in silicon (*after Mikkelsen* [19]) The high and low temperature results are from SIMS and stress-induced dichroism, respectively (see [13, 20] for further details).

Diffusivities for the temperature range 330-400°C were determined by stress-induced dichroism. The results of Corbett *et al.* [21, 22], Stavola *et al.* [23] and Newman *et al.* [24] are also presented in Figure 1.4. These data, combined with those from SIMS, lead to the following expression for the diffusion coefficient in the 350 to 1325°C temperature range [13]:

$$D_{normal} = 0.13 \exp\left(-\frac{2.53\text{eV}}{kT}\right) \text{cm}^2\text{s}^{-1}$$

However, stress-induced dichroism, which measures oxygen diffusion by single jumps, is an IR technique and so cannot measure the diffusion above about 430°C,

and oxygen's diffusivity below about 650°C is too small to measure by SIMS. This left a gap in the measurements for this temperature range.

1.3.2 Anomalous diffusion of oxygen in silicon

The diffusivity measurements in Figure 5 might give the impression that oxygen's diffusion coefficient in silicon is well understood. However, investigations on a particular group of electrically active defects in silicon, known as thermal donors, revealed that this was not the case. These defects were known to be oxygen related, and because of this their formation kinetics presented a significant difficulty. At 450°C the diffusivity of oxygen implied by the TD formation rate is $2.5 \times 10^{-16}\mathrm{cm}^2\mathrm{s}^{-1}$ [25,26], whereas the expected diffusivity as determined by stress-induced dichroism is $6 \times 10^{-19}\mathrm{cm}^2\mathrm{s}^{-1}$ [23], more than two orders of magnitude lower. Several other experiments also indirectly indicated enhanced oxygen transport [27–30], shown in Figure 1.5. In 1983, Gösele and Tan [31] proposed the existence of a fast diffusing oxygen dimer to explain these measurements. Evidence for this was found recently by Senkader *et al.* [32], who also confirmed the enhanced oxygen transport effect by experiments which used the dislocation unlocking technique, as explained in Chapter 2.

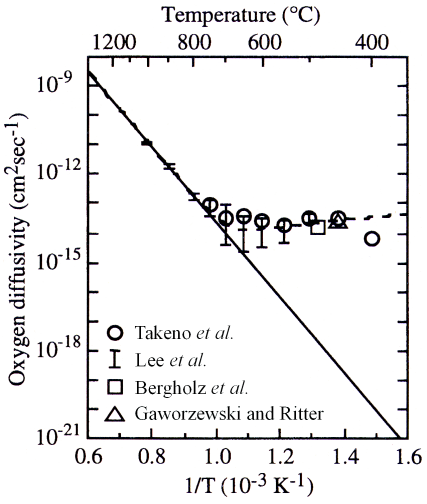


Figure 1.5: An Arrhenius plot of oxygen diffusivity indicating anomalous diffusion between 400 and 700°C (*after Takeno et al.* [27]). The data were taken by different authors using oxygen precipitation experiments. The solid line is the expression $D = 0.13 \exp(-\frac{2.53\mathrm{eV}}{kT})\mathrm{cm}^2\mathrm{s}^{-1}$, and the dashed curve indicates a calculated result using a speculative molecular oxygen model.

1.4 Nitrogen in silicon

1.4.1 The effects of nitrogen in silicon

Structural effects

It has been known for some time that the addition of nitrogen to FZ silicon is beneficial, as it reduces both interstitial (A-swirl) and vacancy-related defects (D-defects/crystal originated particles (COPs)/voids) respectively [33–41]. Surprisingly, the concentration of nitrogen required for this is so low, $\sim 10^{14} \mathrm{cm}^{-3}$, that until recently it could not be measured directly [39]. Nitrogen had been seen as an undesirable dopant in Cz-Si, as it was known to increase the formation of oxidation-induced stacking faults (OSFs) in Cz crystals [42–44]. Despite this, manufacturers have started adding small amounts of nitrogen to Cz-Si in the last few years, as this also has beneficial consequences.

Nitrogen affects the size and density distribution of voids in Cz-Si, creating a greater number of smaller voids [45–51]. This is preferable to having fewer larger voids, as the smaller defects are easier to anneal out [52], and are less likely to have damaging consequences for devices [34]. The mechanism for this is unclear, although vacancy aggregation is found to occur at a lower temperature after nitrogen-doping [53,54]. This indicates that nitrogen is unlikely to be the void nucleation centre, as the presence of a nucleating mechanism should make the void aggregation temperature higher [55]. The other major beneficial effect of nitrogen in Cz-Si is that it enhances oxygen precipitation, resulting in a greater density of precipitates [47,49,56–67], which improves the gettering of metallic impurities in devices [68, 69].

Nitrogen-doped float zone (NFZ-Si) wafers also have improved mechanical strength, since nitrogen pins dislocations [63,70–79], which are inevitably introduced during device processing. In Cz-Si this function is performed by oxygen [32, 80], but it is not yet known how the additional presence of nitrogen in Cz-Si affects dislocation locking. Additionally, it has been found that nitrogen increases the fracture strength of FZ-Si [77] and Cz-Si [78].

Electrical effects

Nitrogen has long been known to be largely electrically inactive in silicon [81–83], however, there are a few minor effects that arise when nitrogen is present, which have been used to gain information about the way it behaves in silicon. Shallow thermal donors (STDs), with an ionization energy of 35-37meV, have been found in as-grown nitrogen doped silicon after annealing over a wide range of temperatures, by investigations of far infra-red spectra and measurements of electron concentrations [84–93]. STDs generated in the middle temperature range (600 - 700°C) or observed in the as-grown state are believed to be due to a nitrogen-oxygen species [94–96], possibly an NO_n complex of one interstitial nitrogen atom with n oxygen atoms, most likely NO_2 - NO_4 [97]. STDs produced at a lower temperature, ∼470°C, have yet to be identified [85, 86, 91].

Nitrogen is also responsible for deep levels, which are produced by certain annealing conditions [98–100]. Investigations using deep level transient spectroscopy (DLTS) and electron paramagnetic resonance (EPR) have revealed levels at $E_c - 0.19$eV and 0.28eV [101], 0.42eV [102], 0.50eV [103] and 0.56eV [104]. The positions of levels in the bandgap created by impurities can be calculated by *ab initio* modelling, and reproducing these levels is an area of active interest for those engaged in the numerical simulation of nitrogen-related defects in silicon [55, 105, 106].

Other effects

Nitrogen is responsible for photoluminescence lines in silicon at around 1.1223eV [94, 107–110]. It has also been found to improve gate oxide integrity [111], although oxide film growth is retarded on substrates implanted by nitrogen [112–114].

1.4.2 The properties of nitrogen in silicon

Despite nearly fifty years of experimental investigation, the fundamental properties of nitrogen in silicon, such as its diffusivity and how it binds to defects, are poorly understood. This is largely because the low solid solubility of nitrogen in silicon (4.5×10^{15}cm^{-3}, *i.e.* one N atom for every ten million Si atoms, at the melting point) means

that in as-grown material it exists in concentrations beneath the normal detection limits of conventional techniques, including standard SIMS which is insensitive to nitrogen. This has not discouraged experimentalists, however, who have employed many different experimental techniques in an attempt to characterize the system, including:

- Infrared (IR) absorption spectroscopy [39, 115–118]
- Fourier transform IR spectroscopy (FTIR) [40, 60, 84, 99, 119–122]
- Low temperature FTIR (LTFTIR) [123]
- Optical measurements of refractive index [42]
- Hall effect [82, 97, 124]
- Study of dislocations [58, 63, 74, 79, 125]
- Spreading resistance profiling (SRP) [126, 127]
- Gold diffusion [47]
- Platinum diffusion [128, 129]
- Resistivity measurements [57, 82, 87, 121]
- MOS C-V measurements [82]
- Positron annihilation spectroscopy [38]
- Ion channeling [130–132]
- Rutherford backscattering spectrometry (RBS) [130]
- SIMS [56, 133–137]
- TEM [61, 64, 134, 136, 138–140]
- STEM [138, 141]
- Electron energy loss spectrometry (EELS) [133, 138]

- Photoluminescence [94, 107, 109, 110, 142–144]
- Electroluminescence [107]
- Laser-scattering tomography (LST) [121, 145]
- Infrared LST [49]
- Thermal warpage tests [75]
- Electron paramagnetic resonance (EPR) [98, 146–148]
- Mechanical testing [71, 76–78]
- Ion milling [137]
- Scanning bright field infrared interferometry [149]
- Charged particle activation analysis (CPAA) [150, 151]
- Electron-nuclear double resonance (ENDOR) [152]

A lot of this work used ion implantation to raise the nitrogen concentration to levels where it could be detected directly. Unfortunately it is not entirely clear whether results obtained this way are also representative of the as-grown situation, as ion implantation inevitably produces lattice damage which might not be fully annealed out. These difficulties do not affect theorists, however, who model nitrogen in silicon using *ab initio* calculations. Much of our present knowledge of the system has been obtained this way.

Identity of the nitrogen species

The simplest nitrogen defect, substitutional nitrogen (N_s), was identified by electron paramagnetic resonance using laser-annealed ion-implanted amorphous silicon [98, 146]. N_s was observed to be distorted to an off-centre structure at low temperatures, which was not expected at the time and prompted a number of theoretical investigations [153–161]. Ion channeling studies, however, have shown that the vast majority of nitrogen is not substitutional but resides at interstitial sites [130, 131].

FTIR studies [122,162,163] showed that most ion-implanted nitrogen in silicon forms pairs, with only about 1% or so becoming substitutional. Dimeric ^{14}N is characterised by two strong lines at 766 and 963cm^{-1} (749 and 937 for ^{15}N, with other lines at 759 and 948 for mixed isotopes, the two N atoms in the pair being equivalent [131]).

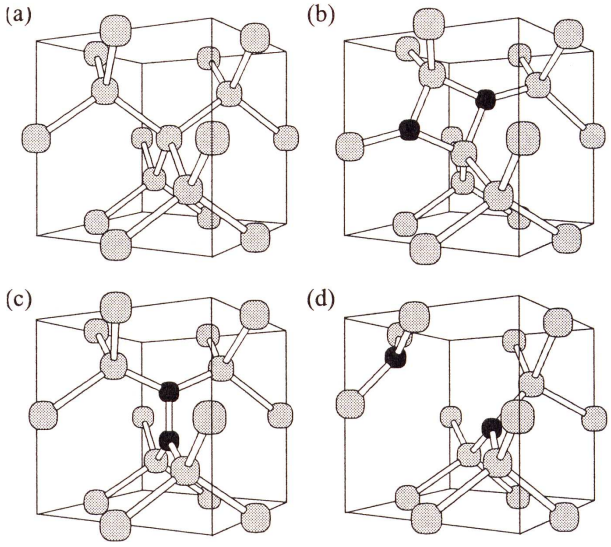


Figure 1.6: Representation of nitrogen dimer configurations (*after Jones et al.* [105]), with atom types as in Figure 1.7. (a) Si lattice, (b) the (N_i - N_i) complex, (c) (N_i - N_s), (d) (N_s - N_s).

The nitrogen pair (Figure 1.6) was identified by Jones *et al.* [131] as a split-interstitial dimer, (N_i - N_i), using *ab initio* local density functional theory calculations. There is general agreement amongst theoretical groups that this is the correct structure for the dominant defect [55,106,164–166], although earlier calculations had suggested that the N pair was unstable [160]. The binding energy of the dimer has been a matter of debate, with values ranging from ∼2eV [166] to ∼4eV [55], but latterly the higher value has been more widely accepted [106,167]. This would mean that the interstitial dimer is stable up to the melting point. Experimentalists have not yet been able to measure this binding energy. Calculations [106,164] of local vibrational mode (LVM) frequencies associated with the interstitial dimer have shown close correlation with the strong IR lines at 766 and 963cm^{-1} observed by Stein [122], but (N_i - N_i) is thought to be completely electrically inactive [105].

It is believed that the interstitial monomer (N_i) also occupies a split-interstitial position [106, 164], although there is a suggestion that the bond-centred position,

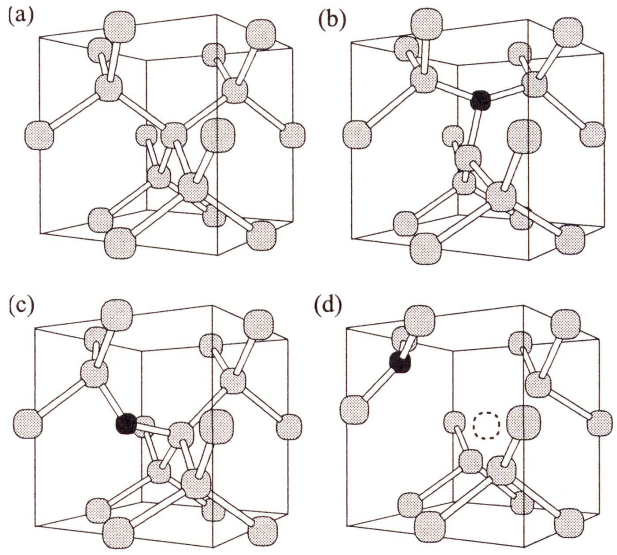


Figure 1.7: Representation of nitrogen monomer defect configurations (*after Jones et al.* [105]). Black and grey circles represent the N and Si atoms, respectively. (a) Fragment of Si lattice, (b) split-interstitial structure for N_i, (c) bond-centred structure for N_i, (d) the N_sV complex. The vacant site in (d) is marked by a dashed circle.

which has long been known to be the form taken by interstitial oxygen monomers [12,22], might be more stable at high temperatures [55] (see Figure 1.7). Calculations suggest that N_i has a small barrier to diffusion (0.4 - 0.5eV [55,106,164,168]), meaning that it is highly mobile even at low temperatures. A weak IR line at 653cm^{-1} that was originally assigned to substitutional nitrogen N_s [122] is now suspected of being due to N_i by modellers who have calculated LVMs of 664cm^{-1} [164] and 637cm^{-1} [106] for the defect.

Nitrogen and vacancies

The vacancy concentration in nitrogen-doped Cz-Si (NCz-Si) varies from approximately 10^{13} to 10^{15}cm^{-3} depending on temperature [39, 102, 129, 169]. Nitrogen-vacancy interactions in FZ- and Cz-Si have been the subject of much research, but little consensus has been reached. There is evidence for V-N complexes in annealed nitrogen-doped FZ wafers based on platinum diffusion [129], positron annihilation spectroscopy [38] and DLTS [102], and additionally there exists the well documented effect of nitrogen on vacancy aggregate density and size [45, 48].

Interstitial nitrogen monomers are calculated to bind to vacancies, forming the

substitutional monomer N_s, with binding energies of 3.6 - 3.8eV [55, 164], and some favour this as the most likely vacancy interaction [50], but this is contradicted by experiment which finds that 80% of nitrogen exists in pair forms [170] and that N_s accounts for less than 10% of the total nitrogen concentration in implanted material [98], which probably has a supersaturation of vacancies from implant damage [106]. The calculated binding energy is almost high enough for a nitrogen to 'kick out' a silicon atom and bind to the resulting vacancy [164] - vacancy formation energy estimates vary from 3.3eV [171] to 4eV [172]. Results from modelling also indicate that N_s should bind to a further vacancy, forming N_sV, with binding energy 1.6eV [105]. This defect is calculated to produce LVMs and electrical donor and acceptor levels, none of which have been observed experimentally.

Interstitial nitrogen dimers are expected to bind to vacancies via the reactions:

$$(N_i - N_i) + V \rightarrow (N_i - N_s) \tag{1.1}$$

$$(N_i - N_s) + V \rightarrow (N_s - N_s) \tag{1.2}$$

Most calculations show that (N_i - N_s) has a binding energy of 0.8 - 1.4eV [55, 106, 164, 167], although one group believes it to be unstable whilst remaining an intermediary species for the formation of (N_s - N_s) [173]. (N_s - N_s) is agreed by all groups to be highly stable, with a binding energy of approximately 4eV. Some calculations find that further complexing with vacancies to form (N_s - N_s)V [37] *etc.* is also energetically favourable (although the returns diminish with each extra vacancy added), while others find that these complexes are unstable [173, 174]. The substitutional dimer species all produce LVMs and electrical effects, which have not been observed in as grown material, leading most to conclude that the species are largely absent due to a lack of vacancies. Some extra LVMs have been detected in ion-implanted material [175] which have yet to be assigned [105].

1.4.3 Diffusion of nitrogen in silicon

Experimental work

The diffusion of nitrogen in silicon is another topic about which there is little consensus. The diffusion coefficient is not well known, despite nearly forty years of experimentation, and atomistic models of the diffusion mechanism are the subject of much debate. The first measurement of nitrogen diffusion was reported in 1968 by Clark *et al.* [124], who used Hall Effect measurements to determine the depth of a layer of implanted $^{14}N^{+}$ ions as a function of anneal time and temperature. The diffusion coefficient was found to be:

$$\mathrm{D}_N^{Clark} = 0.87 \exp\left(-\frac{3.29\mathrm{eV}}{\mathrm{kT}}\right) \mathrm{cm}^2\mathrm{s}^{-1} \tag{1.3}$$

This is not believed to be reliable, however, as it applies to substitutional nitrogen complexes created by the implant, which are thought to be of negligible concentration in as-grown silicon [122].

The next measurement was made in 1975 by Denisova *et al.* [176], who annealed clean FZ-Si in a nitrogen atmosphere between 700°C and 1200°C, then irradiated the specimens with 50keV neon ions, followed by a further 800°C anneal. This resulted in the formation of an inversion layer, whose depth was measured by a combination of oxidation etching and resistivity measurements. They found the diffusivity to be:

$$\mathrm{D}_N^{Denisova} = 0.03 \exp\left(-\frac{2.63\mathrm{eV}}{\mathrm{kT}}\right) \mathrm{cm}^2\mathrm{s}^{-1} \tag{1.4}$$

Unfortunately the results above 800°C were invalidated by the formation of a SiO_2 or Si_3N_4 film which inhibited diffusion. The technique is also very indirect, and this result is not generally held to be correct today.

In 1988 Itoh and Abe [177] made what is now widely considered as the most reliable measurement of nitrogen diffusion, using a specialised SIMS technique to measure out-diffusion profiles in as-grown NFZ-Si material. By comparing their out-diffusion concentration profiles with error function profiles, they found the diffusivity to be:

$$\mathrm{D}_N^{Itoh\ \&\ Abe} = 2700 \exp\left(-\frac{2.8\mathrm{eV}}{\mathrm{kT}}\right) \mathrm{cm}^2\mathrm{s}^{-1} \tag{1.5}$$

Itoh and Abe concluded that the diffusivity they measured was that of the nitrogen dimer. Other groups soon released similar results found using in-diffusion of nitrogen from the ambient [87, 102, 178, 179], and these measurements collectively became the most widely used reference for nitrogen diffusion in silicon.

Recent dislocation unlocking measurements made by Giannattasio [79, 180–184], made in the lower temperature range of 550 - 830°C, have indicated a much reduced barrier to diffusion of 1.45eV:

$$\mathrm{D}_N^{Giannattasio} = 6.8 \times 10^{-6} \exp\left(-\frac{1.45\mathrm{eV}}{\mathrm{kT}}\right) \mathrm{cm}^2\mathrm{s}^{-1} \tag{1.6}$$

This result is discussed further in Chapter 2.

Other experiments seem to indicate that the diffusion of nitrogen is more complicated. Hockett observed anomalous diffusion of nitrogen in ion-implanted specimens [185], which showed that a small fraction of the nitrogen diffused rapidly whilst the majority remained immobile. The same effect was observed by Mannino *et al.* [186] in nitrogen-implanted epitaxially grown films, and Voronkov and Falster [187] in out-diffusion profiles of as-grown material obtained with a nitrogen-optimised SIMS. Some of these results are shown in Figure 1.8.

Further instances of anomalous diffusion have been recorded. Mannino *et al.* [126] recently observed that nitrogen diffusion is enhanced in Cz-Si, something that had previously been found by Hockett [185]. This has been explained by Voronkov as being a consequence of the presence of oxygen, in conjunction with the dissociative mechanism [127], described below. Another recent measurement, by Stoddard *et al.*, reported massively enhanced nitrogen diffusion observed after ion milling of nitrogen-doped Cz silicon [137].

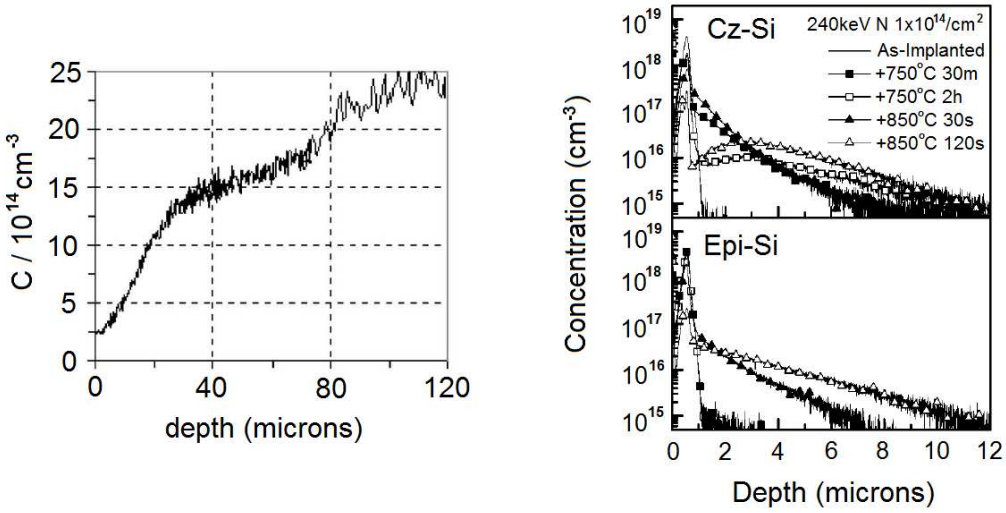


Figure 1.8: Two examples of anomalous nitrogen diffusion, found using SIMS. Left: An out-diffusion concentration profile of nitrogen in NFZ-Si exhibits three-regime behaviour (*after Voronkov and Falster* [187]). Right: annealing of N-implanted Cz- and epitaxially-grown silicon shows that a small fraction of the nitrogen is highly mobile, while the rest remains stationary (*after Mannino et al.* [126]).

Nitrogen's transport mechanism: dimer diffusion

Since nitrogen is known to exist in silicon mostly in the form of an interstitial dimer (§1.4.2), the mobility of this defect is of interest. Several theoretical studies have attempted to explain experimental measurements of nitrogen transport by calculating diffusion paths for the dimer. These give a range of different activation energies for dimer diffusion, depending on the particular path chosen: the most recent studies have produced values of 3-4eV [188], 2.69eV [189] and 2.38eV [190]. Some of these modelling predictions are presented in Figure 1.9.

These models fit some of the data well, but they do not explain the anomalous diffusion measured in other experiments. This has led others to consider more complex transport mechanisms. The model currently gaining acceptance is Voronkov and Falster's dissociative mechanism [187, 191].

Nitrogen's transport mechanism: dissociative diffusion

Dissociative diffusion has already been investigated in other systems, for instance hydrogen in silicon [192]. Voronkov and Falster's nitrogen mechanism is based on

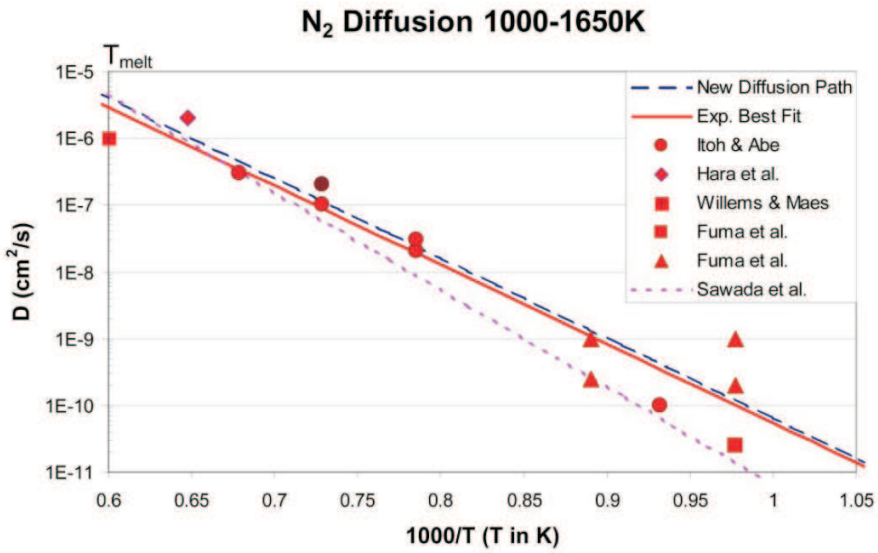


Figure 1.9: Experimental and theoretical data for nitrogen pair diffusion (*after Stoddard et al.* [190]).

the dimer as the prevalent defect, but concludes that it is practically immobile [127]. Instead, transport proceeds via dissociation of the dimer into monomers, which diffuse until they recombine. Nitrogen monomers are known to be highly mobile, with activation energies for diffusion calculated to be 0.4 - 0.5eV as discussed earlier. The behaviour produced by this dissociative diffusion can be approximated by a single effective diffusivity if the monomers and dimers are in equilibrium. However, if an experiment starts with the system out of equilibrium, and its duration is not long enough for equilibrium to be established, then anomalous results can be expected.

The dissociative mechanism includes an extra term, the 'dissociation time' of the dimer, to account for this effect. Voronkov and Falster modelled experimental results that showed anomalous diffusion, using this dissociation time as a fitting parameter. The results, some of which are shown in Figure 1.10, closely fitted the experimental data. However, the dimer dissociation times required for these fits did not scale intuitively: they increased with increasing temperature, leading some to believe that a different physical mechanism was responsible for the effect.

The monomer diffusivity expression obtained from the dissociative analysis is [191]:

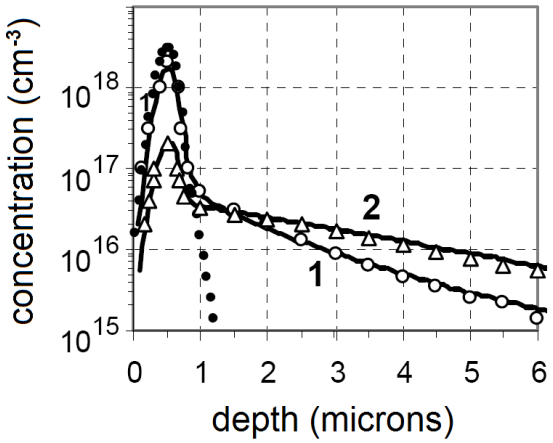


Figure 1.10: The theoretical fit for the SIMS data of Mannino *et al.* ([126], Figure 1.8) produced by dissociative mechanism modelling [127].

$$\mathrm{D}_N^{Voronkov} = 0.25 \exp\left(-\frac{1.25\mathrm{eV}}{\mathrm{kT}}\right) \mathrm{cm}^2\mathrm{s}^{-1} \tag{1.7}$$

This is a departure from the *ab initio* models of the defect, which give a lower energy of 0.4 - 0.5eV for the activation energy [168,193]. Another difference is that the binding energy of the dimer in Voronkov and Falster's analysis, 2.9eV, is considerably smaller than the majority of the estimates from theoretical work.

The dissociative mechanism was recently extended to include a secondary system of nitrogen hexamers (*i.e.* N_6) which split into fast-diffusing trimers (N_3), along with the dimer-monomer system and another component (thought to be N_4 or N_5) [187]. That such an exotic system can be credibly proposed shows how unusual the measurements of nitrogen diffusion are. Theoreticians are currently investigating this new model; for example, a recent paper by Fujita *et al.* found stable forms for N_3, but did not give any information about its diffusion [194].

1.4.4 Nitrogen-oxygen complexes

With the behaviour of nitrogen in silicon being so poorly understood, it should be of little surprise that no coherent model of nitrogen's interaction with oxygen in silicon exists either. The *effects* of the nitrogen-oxygen interaction are, by contrast, well-documented. Silicon manufacturers and others have made detailed investigations of

nitrogen's effect on oxygen precipitation in Czochralski-grown crystals [39,141,149]. A recent study by Rozgonyi *et al.*, for example, used a combination of HRTEM, STEM and EELS to probe individual precipitates, finding that the fraction of nitrogen they contained rose from 1% in the centre to 17% at the boundaries [138]. Similar efforts have been made by Karoui *et al.* [133] and Wang *et al.* [139]. Other effects attributed to nitrogen-oxygen complexes include:

- LVM lines at 801, 996 and 1026cm^{-1}, found in N- and O-implanted FZ-Si [195] and NCz-Si [116, 120] after annealing between 400°C and 700°C. These were initially believed to be due to NNO complexes [116], which was later confirmed by Jones *et al.* [196] using a combination of FTIR and *ab initio* calculation. The structure they determined was a weakly coupled combination of an interstitial nitrogen dimer and an interstitial oxygen atom O_i, which broke up above 700°C with the emission of the O_i.
- Enhanced diffusion of oxygen in the presence of nitrogen in NCz-Si [49,197,198].
- Reduced diffusivity of nitrogen by interaction with oxygen [40].
- An enhanced oxygen-dislocation interaction [142].
- Creation of STDs, attributed to an NO_x species [97].
- Interaction with vacancies to suppress voids [197].
- A reduction in the temperature at which oxygen precipitates dissolve [139].

Explanations for these effects are few and far between. Modelling groups have variously attributed the STDs to NO_2 [96], NO_3 [199], and (tentatively) to larger N-O clusters [115], whereas others think they are not N-O related at all but arise from Si interstitials [200]. Recent theoretical investigations have focused on the (N_s - N_s) complex, with calculations showing that it may act as a sink that can capture oxygen interstitials, forming stable (N_s - N_s)O_n complexes [173, 201]. However, as yet a complete treatment of N-O complexes has not been attempted, and more work, both theoretical and experimental, is needed.

1.4.5 Measuring nitrogen in silicon

Determining the concentration of nitrogen in silicon is not a new problem. A review of measurement methods published by Stein in 1986 [170] listed experiments using IR absorption [111, 202], EPR [98, 203, 204], luminescence [108, 205], resistivity [5, 206], Hall effect [130, 207], CPAA [150], DLTS [101], and SIMS, Rutherford backscattering spectrometry and Auger spectroscopy [208–210]. Some of these techniques had initially been used to measure nitrogen concentrations in silicon nitride dielectric layers, which was the relevant technological problem at the time (and is still researched today [211]). They were sufficient for the early nitrogen ion-implantation investigations, but most could not reach the sensitivities required to measure the concentrations below 10^{15}cm^{-3} found in as-grown material.

With nitrogen doping becoming a common practice amongst manufacturers in recent years, the problem has seen renewed interest. It has been shown that nitrogen starts to affect the properties of silicon at concentrations as low as $1 \times 10^{13}\text{cm}^{-3}$ [212], so being able to measure these concentrations is important. Lately, efforts have been centred around FTIR absorption and SIMS. SIMS measures the total nitrogen concentration, independent of its chemical state, but even specialised nitrogen machines have a detection limit of around $1 \times 10^{14}\text{cm}^{-3}$, limited by the background nitrogen concentration [213, 214].

FTIR absorption detects nitrogen in silicon via the presence of nitrogen-related vibrational modes. The traditional measurement, developed using FZ silicon, uses the nitrogen dimer lines at 963cm^{-1}, with a calibration coefficient of $1.83 \times 10^{17}\text{cm}^{-2}$ [150], and 766cm^{-1}, with a calibration coefficient of $4.45 \times 10^{17}\text{cm}^{-2}$ [120, 215]. However, in Cz silicon, in which a significant fraction of the nitrogen has formed complexes with oxygen, this method can underestimate the total nitrogen concentration [150]. It was proposed that the NNO IR lines at 996 and 1026cm^{-1} might be used to overcome this problem [216], and recently groups have claimed to be able to detect concentrations of approximately $9 \times 10^{13}\text{cm}^{-3}$ [118], $3 \times 10^{13}\text{cm}^{-3}$ [117] and $5 \times 10^{12}\text{cm}^{-3}$ [123], based on this method. As yet there is no agreed standard for calibrating the absorption to an absolute concentration. This can lead to practical difficulties, since manufac-

turers of nitrogen-doped silicon each measure [N] according to their own standard, so the quoted nitrogen contents of material from different sources cannot be directly compared.

1.5 Impurity interactions with dislocations in silicon

1.5.1 Dislocations in silicon

Modern silicon wafers are produced dislocation-free, but dislocations are inevitably introduced during device processing. High temperature stages during device fabrication can produce considerable thermal stresses [217], which, along with gravitational stress, can lead to dislocation generation, particularly around the edges of wafers [218]. This causes difficulties because the presence of dislocations will degrade the material's mechanical strength and eventually cause warpage of wafers, which is a significant problem for lithography and wafer bonding. A sufficient applied shear stress will cause dislocations to propagate to the surface of wafers, where they form microscopic steps known as *slip lines*. The presence of slip lines is known to cause failure of built-in MOS devices [219].

Dislocations can also act as gettering sites for metallic impurity atoms. This can be helpful if the dislocations lie away from the active areas of devices, as gettering impurities nullifies their harmful electrical effects. However, a dislocation decorated with metallic atoms which crosses a junction will become electrically active, degrading the junction's characteristics. Emitter-collector shorts, for example, constituted the dominant failure mechanism for shallow junction transistors (Figure 1.11) [220].

Dislocations move by crystallographic glide, whereby one part of the crystal slips, as a unit, across an adjacent part. The glide takes place on a surface known as the glide plane, whose orientation is determined by the structure of the lattice. Silicon has a diamond lattice structure and the dislocations glide in (111) planes [221]. Dislocations in silicon can be in the form of hexagonal loops [222], as in Figure 1.12, with Burgers vector $\mathbf{b} = \frac{a}{2}\langle\mathbf{110}\rangle$ (where a is the lattice constant), and dislocations can reduce the elastic strain energy by dissociating into two partial dislocations with Burgers vector

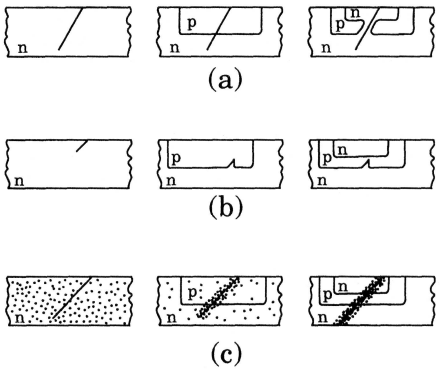


Figure 1.11: Models proposed to explain emitter-collector shorts (*after Lawrence* [220]): (a) enhanced diffusion of emitter dopant along crystal defect, (b) locally retarded base-dopant diffusion, (c) precipitation of fast-diffusing impurities.

$\frac{a}{6}\langle\mathbf{112}\rangle$, which bound a 4 - 8nm strip of stacking fault [223]. These are known as *Shockley partials*, as shown in Figure 1.13.

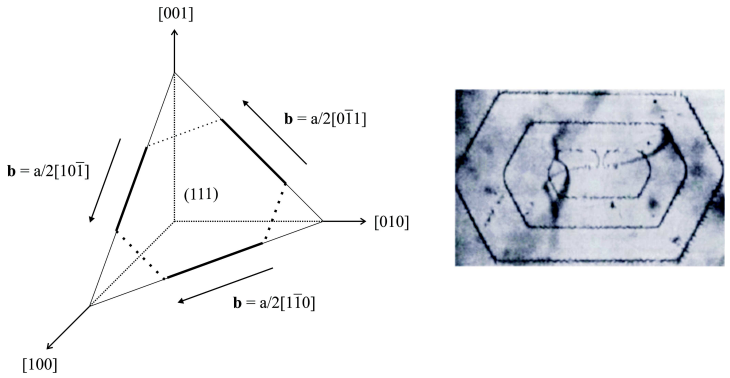


Figure 1.12: Three possible Burgers vectors for a hexagonal dislocation loop lying in the (111) plane, although only one is allowed in a real loop. Each defines a different glide system in silicon. The famous micrograph (*after Dash* [2]) shows copper-decorated dislocation loops in a silicon crystal.

Dislocations can be made to move by the application of a characteristic shear stress. Schmid introduced the concept of the *critical resolved shear stress* (CRSS) [225], which is the applied shear stress, τ, resolved onto the slip plane in the direction required for slip. If τ is greater than the CRSS then dislocations can move [226] with an average velocity:

$$v = v_0 \tau \exp\left(-\frac{U}{kT}\right) \tag{1.8}$$

where v_0 is a mobility coefficient, U is the activation energy for dislocation glide

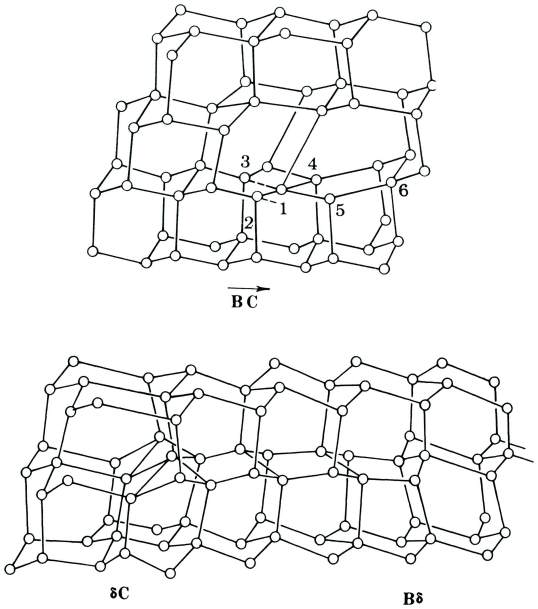


Figure 1.13: The 60° dislocation **BC** (top) dissociates into partial dislocations δ**C** (30° partial) and **B**δ (90° partial) (*after Hirth and Lothe* [224]).

and τ is the applied stress resolved on the glide plane along the glide direction. The values of m and U depend on the class of dislocations (edge, screw or mixed), but in silicon these values vary by only about 10%. In the case of 60° dislocations in silicon, the values are $v_0 = 1.0 \times 10^4 \text{ms}^{-1}\text{MPa}^{-1}$ and $U = 2.20\text{eV}$, and for screw dislocations $v_0 = 3.5 \times 10^4 \text{ms}^{-1}\text{MPa}^{-1}$ and $U = 2.35\text{eV}$ [227].

1.5.2 Immobilization of dislocations by impurities

Impurities in silicon are known to significantly affect dislocation motion. In the 1950s Cottrell [228] and Eshelby [229] developed a theory to describe the effect of a solute atmosphere on dislocations. An impurity in a crystal produces a strain field, which may interact with a dislocation, increasing or decreasing the elastic energy of the crystal. This, combined with electrical and chemical [230–232] interactions, makes up the interaction energy, E_i, of the impurity and the dislocation core. Because it is energetically favourable for impurities to be at the dislocation core rather than in the bulk, the concentration of impurities at the core will be greater.

The equilibrium concentration, $C(\mathbf{r})$, of an impurity at position $\mathbf{r}$ relative to a dislocation is given by Boltzmann statistics as:

$$C(\mathbf{r}) = C_0 \exp\left(-\frac{E_i(\mathbf{r})}{kT}\right) \tag{1.9}$$

This assumes there are a large number of vacant sites at the core, so that the impurities do not interact with each other. E_i can be expressed in terms of the variation in the binding energy (the Gibbs free energy ΔG), according to $-E_i = \Delta G = \Delta H - T\Delta S$, so in cylindrical polar coordinates the concentration profile is:

$$C(\mathbf{r}, \theta) = C_0 \exp\left(\frac{\Delta G(\mathbf{r}, \theta)}{kT}\right) \tag{1.10}$$

Thus, impurities tend to accumulate at the cores of dislocations, where ΔG is greater. Impurities become more mobile with increasing temperature so a greater number of impurity species are able to segregate to the dislocation core, although above certain temperatures they can have enough energy to evaporate off again, reducing the impurity concentration at the dislocation. An accumulation of impurity atoms at a dislocation core during an anneal may render the dislocation immobilised, an effect known as *dislocation locking*. Moving a locked dislocation requires the application of a stress, referred to as the *unlocking stress*, whose magnitude depends on the number of impurities at the core.

The unlocking stress is calculated to be [233, 234]:

$$\tau_u = \frac{N}{b^2}\left[\Delta G - kT \ln\left(\frac{LN\nu}{\Gamma}\right)\right] \tag{1.11}$$

where N is the line density of the locking particles, b is the magnitude of the Burgers vector of the dislocation, ΔG is the maximum interaction energy between the impurity and the dislocation, L is the dislocation length, and ν is the frequency of dislocation vibration, and Γ is the release rate of the dislocation from pinning particles. The equation predicts that if the pinning particles are of only one kind, the unlocking stress will depend linearly on temperature, and this has been verified experimentally (an example is given in §2.3.3).

1.5.3 Dislocation locking by oxygen and nitrogen

It was believed since the 1950s that oxygen would lock dislocations [235], and this was later shown by Hu [236] using a method based on indentation dislocation rosettes [237], despite earlier evidence to the contrary [238]. More recently, an *in situ* X-ray topographical technique was used by Sumino and Harada [239] to study the interaction between impurities and dislocations in silicon. In separate works published in 1983, Sumino and Imai confirmed that oxygen is effective at locking dislocations [226], and showed that mobile dislocations in an impurity doped crystal become locked when the applied stress falls below a certain value [240]. It is also possible for precipitates to form at dislocation cores under certain anneal conditions. Yonenaga and Sumino observed that the strength of Cz-Si increased during the early stages of oxygen precipitation (shown in a TEM micrograph in Figure 1.14), but then fell markedly as precipitation proceeded further [241]. This was explained as being due to the creation of additional dislocations from the precipitates.

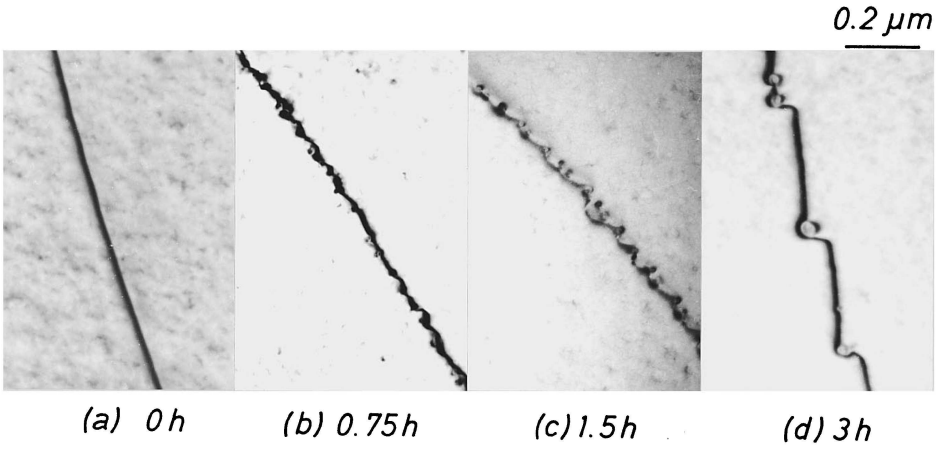


Figure 1.14: TEM micrograph showing oxygen precipitates developing with increasing anneal duration at 900°C (*after Yonenaga and Sumino* [241]).

Sumino and Imai also showed that nitrogen was extremely effective at locking dislocations; indeed, they found that locking by nitrogen can be equivalent to or even stronger than that from oxygen, even when the nitrogen is present in concentrations more than two orders of magnitude less [226]. This has recently been confirmed by Giannattasio and Murphy, in experiments which will be discussed in the next chapter. Despite these investigations, many aspects of the nitrogen-dislocation interaction still

remain unclear.

1.6 Summary

Nitrogen in silicon offers manufacturers flexibility in controlling oxygen precipitation, reduces the concentration of vacancy- and interstitial-related defects, and increases the mechanical strength of wafers by locking dislocations. It is largely electrically inactive, but does exhibit some minor effects, which have been investigated in an effort to understand the system. The dominant form of nitrogen in silicon is known to be an interstitial dimer, although substitutional forms are also thought to exist, particularly when a high concentration of vacancies is present. Most other aspects of nitrogen in silicon, for example its transport mechanism, interaction with defects, and interaction with oxygen, are poorly understood.

1.7 This work

The work presented in this thesis is mostly concerned with measurements of nitrogen transport in silicon, made using a novel experimental technique known as dislocation unlocking. This work is closely related to previous experiments performed using the same method, which are also described here in some detail. For clarity, the structure of this thesis and its main arguments are summarised here, to provide an outline of the work.

Chapter 2 gives a summary of the dislocation unlocking experiments carried out in Oxford prior to this present work. The measurements performed by Senkader with Cz-Si are briefly discussed and evaluated, and the transition from measuring oxygen locking in Cz-Si to nitrogen locking in NFZ-Si is explained. Giannattasio and Murphy's NFZ-Si work is then summarised.

Chapter 3 describes in detail the experimental methods used in this present work.

In **Chapter 4**, control experiments which have been used to characterize the dislocation unlocking technique are presented. Notably, it is shown that the measured

unlocking stress is dependent on the three-point bend duration, a variable that had not been standardised in Giannattasio and Murphy's NFZ-Si experiments.

Chapter 5 describes measurements which repeated Giannattasio and Murphy's NFZ-Si experiments, using a standardised experimental technique (as described in Chapter 3). These results are analysed in terms of nitrogen's effective diffusivity and interaction with dislocations in silicon. The difference between these new results and the previous NFZ-Si measurements is explained by a systematic error in the previous work, that arose from the lack of standardisation of experimental conditions.

Chapter 6 describes other experiments performed with nitrogen-implanted Cz-Si and NFZ-Si.

Chapter 2

Previous dislocation unlocking experiments

The work in this thesis is mostly concerned with measurements of nitrogen transport in silicon, using an experimental technique known as dislocation unlocking. This chapter gives a brief history of the dislocation unlocking technique, which was first developed in the late 1980s with the aim of measuring nitrogen's dislocation locking effect in silicon [242], and was then used extensively to measure and understand oxygen transport in silicon, and later still extended to return to the work on nitrogen in silicon.

2.1 History of dislocation unlocking experiments

2.1.1 Introduction

As described in the previous chapter, measurements of oxygen transport had been made using a combination of experimental methods. High temperature SIMS out- and in-diffusion and low temperature stress-induced dichroism measurements were consistent with each other, but left a gap in the middle temperature range of 400-700°C where these techniques could not be used. Some experiments indicated that oxygen transport was massively enhanced in this temperature range [29, 30], but this was difficult to measure directly. Another set of measurements performed by Senkader

et al. [32, 243–245], using the newly developed dislocation unlocking technique, have helped to resolve the uncertainties surrounding the issue. This technique will now be described.

2.1.2 Dislocation unlocking as a new way of measuring impurity transport

As previously discussed, one of the chief technological advantages of Cz-Si is that the high concentration of oxygen it contains helps to strengthen the material by locking dislocations. The desire to understand the transport processes underlying this effect partly motivated the oxygen diffusivity measurements outlined above, which used standard analysis techniques such as SIMS. The new dislocation unlocking method, however, elegantly exploited the dislocation locking effect, using a careful examination of its dependence on annealing conditions to infer information about oxygen diffusion. The technique used several stages, which are described here and illustrated in Figure 2.1. The work in this thesis also uses the dislocation unlocking technique, with some small modifications. This updated technique is described in more detail in Chapter 3.

Specimen preparation

Rectangular pieces of silicon with dimensions of approximately $30 \times 5 \times 0.7$mm were cleaved from (100) Cz-Si wafers. The long edges were then mirror-polished on both sides, after which the width was approximately 3mm. Throughout the whole of this process, great care was taken to keep the specimens as damage-free as possible. This is because the technique required that specimens be subjected to considerable mechanical stress, sometimes hundreds of MPa, so scratches or other surface damage had to be as small as possible to reduce the likelihood that the specimen would break. Also, the specimens were kept exceptionally clean, as the final step was to visually identify and measure microscopic surface features, which could be obscured by small amounts of dirt.

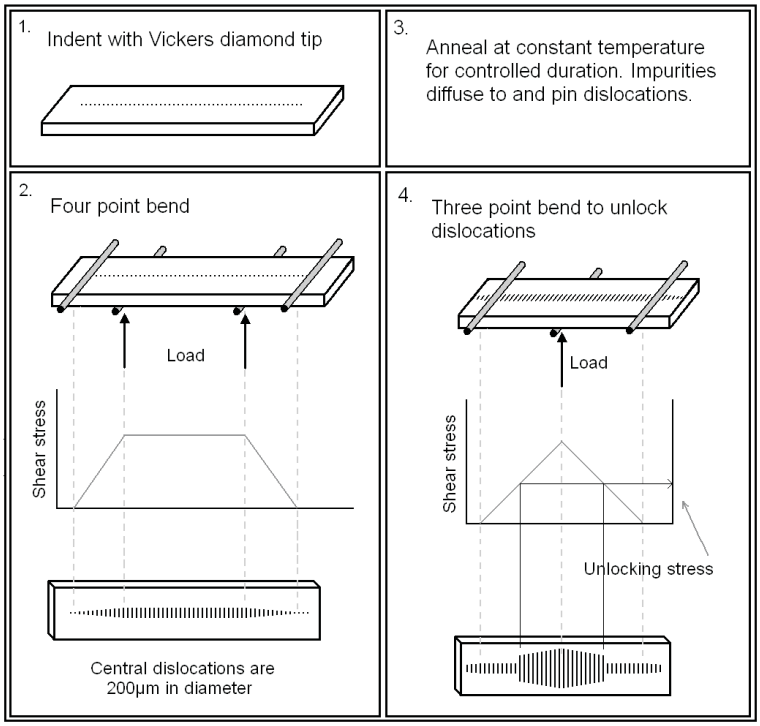


Figure 2.1: The different stages of the dislocation unlocking technique.

Indentation and dislocation growth

Modern single crystal silicon wafers are produced to be dislocation free, so dislocations had to be introduced into specimens intentionally. This allowed a level of control over the experiments that very few other materials could offer, since it was possible to produce a highly ordered and controlled array of dislocations in silicon specimens in a manner that was consistent and repeatable. A line of indents was made down the centre of each specimen, using a micro-hardness tester with a diamond Vickers tip, for a 5s dwell time at a 10g load. The indents were separated by 250μm. The specimen was then subjected to a four-point bend at 550 - 600°C, during which dislocation half-loops were generated at each indent, and expanded according to the stress they experienced. This created an array of dislocation loop sets with diameter $\sim$200μm along the centre of the specimen.

Anneal

Each specimen was then subjected to an isothermal anneal at elevated temperature. During this anneal, oxygen diffused and segregated to the dislocations, and the de-

gree to which this occurred was dependent on the anneal conditions. This created a dislocation locking stress, τ, which was believed to be proportional to the number of atoms at the dislocation core [32]. Each specimen was generally annealed once using a particular set of conditions; this was repeated so that, with many specimens, a range of temperatures and anneal times could be investigated. Anneals were carried out in an argon ambient, or occasionally in evacuated silica ampoules, to minimise surface oxidation, which could make dislocations hard to see and might have also introduced oxidation-induced stacking faults [246]. After annealing, specimens were etched so as to remove approximately 30μm of material, that might have been affected by oxygen out-diffusion during the anneal.

Determination of dislocation unlocking stress

The final stage was to subject the specimens to three-point bending at elevated temperature, typically 550°C, with the peak stress and bending duration chosen so that any resulting movement of dislocations would be as clear as possible, *i.e.* so that the first set of dislocations to have moved was easily distinguishable. The arrays of locked dislocations experienced a resolved shear stress which varied linearly along the length of the specimen, from zero at the outer knife-edges to the maximum stress τ_{max} at the central knife edge (see Figure 2.1). Those dislocations near the outer knife-edges which experienced a stress below the locking stress would not move during the three-point bend, and those towards the centre of the specimen which experienced a stress higher than their locking stress would move. Therefore, the lowest bending stress at which dislocations moved during this stage corresponded to the dislocation locking stress generated during the anneal. τ_{max} was typically chosen to be 1.5 - 2 times greater than the expected unlocking stress τ_u, so that the unlocking point would be away from the knife-edges, where the stress may have been non-linear. The duration of the three-point bend was chosen so that the first set of unlocked dislocations would have moved far enough away from the neighbouring locked set for the difference to be easily discernible. Typically this was set at 2 - 4 hours.

After the three-point bend, specimens were chemically etched with a defect-

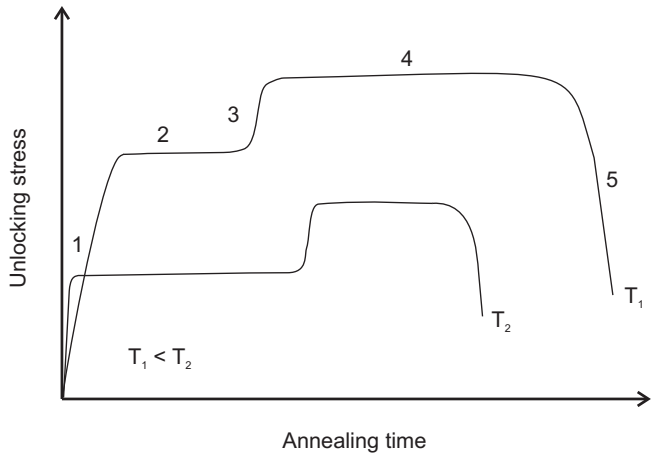


Figure 2.2: Schematic illustrating the variation in unlocking stress with annealing time and temperature, different regimes marked 1-5 (*after Senkader et al.* [80]).

revealing etch. This created etch pits where dislocations intersected the specimen surface, which could then be viewed with an optical microscope. The dislocation sets were measured, and the first set to have moved during the three-point bend was determined. By measuring the specimen, and the position of this set of dislocations relative to the knife-edges, the three-point bend stress at this point could be determined. This was the dislocation unlocking stress, τ_u. Analysis of the variation of unlocking stress with anneal temperature and duration provided information about oxygen transport, and how oxygen binds to dislocations.

2.2 Dislocation unlocking used to measure oxygen transport in Cz-Si

Senkader *et al.* found that the unlocking stress as a function of anneal duration had five distinct regimes, as illustrated by Figure 2.2. In the first regime, oxygen is building up at the dislocation core due to the diffusion process, giving an approximately linear rise in unlocking stress with annealing time. The gradient of this rise is strongly temperature-dependent. The steady-state second regime arises when a local equilibrium between the oxygen at the dislocation core and that in the bulk is established. The value of the unlocking stress in this regime is dependent on the anneal temperature and oxygen concentration. In the next regime the locking increases again,

due to oxygen precipitation at the dislocation core [32]. After further annealling the unlocking stress saturates again (Regime 4), before falling off rapidly (Regime 5).

Effective diffusivity

It is convenient at this stage to introduce the concept of *effective diffusivity*, which is useful when discussing the results of previous dislocation unlocking experiments, and also the new work presented in this thesis. In cases where impurity transport is not by a single species, diffusivity measurements can become complex. In the case of a two species system, with monomer and dimer components, the flux of atoms can be written as:

$$J = -D_1 \frac{dC_1}{dx} - 2D_2 \frac{dC_2}{dx} \tag{2.1}$$

where D_1, D_2 and C_1, C_2 are the diffusivities and concentrations of the monomer and dimer, respectively. In the general case this can be expanded to describe other species:

$$J = -D_1 \frac{dC_1}{dx} - 2D_2 \frac{dC_2}{dx} - \ldots - nD_n \frac{dC_n}{dx} = \sum_{i=1}^{n} -iD_i \frac{dC_i}{dx} \tag{2.2}$$

However, dislocation unlocking experiments are only sensitive to the total number of impurities at the dislocation core, and so cannot distinguish between the diffusion of different species. The experiments are therefore only sensitive to an effective diffusivity, defined by the expression:

$$J \approx -D_{\text{eff}} \frac{dC}{dx} \tag{2.3}$$

where $C = C_1 + C_2 + \ldots + C_n$. This analysis is shown in full for the new nitrogen dislocation unlocking work in Chapter 5.

2.2.1 Transport analysis

By analysing the gradients of the initial rises (Regime 1), Senkader *et al.* were able to deduce the activation energy of the dislocation locking process, which was believed

to be equal to the activation energy for the diffusion of oxygen to the dislocation core. At temperatures above 650°C, this value agreed well with previous work that had used a variety of techniques [19], as shown in Figure 2.3. At temperatures *below* 650°C, however, a lower activation energy for diffusion of approximately 1.5eV was deduced, indicating that enhanced transport of oxygen had been seen.

Describing oxygen diffusion to the dislocation core by:

$$\frac{\partial C_0}{\partial t} = D_0 \nabla \left(\nabla C_0 + \frac{C_0}{kT} \nabla (\Delta G) \right)$$

where D_0 is the oxygen diffusivity, they were able to deduce new values for the effective diffusivity of oxygen below 650°C. The three different oxygen concentrations they investigated, which they labeled low ($2.6 \times 10^{17}\text{cm}^{-3}$), medium ($6.3 \times 10^{17}\text{cm}^{-3}$) and high ($1.04 \times 10^{18}\text{cm}^{-3}$), gave effective diffusivities of:

$$\begin{aligned} D_{low} &= 2.04 \times 10^{-7} \exp\left(-\frac{1.51eV}{kT}\right) \text{cm}^2\text{s}^{-1} \\ D_{medium} &= 7.33 \times 10^{-7} \exp\left(-\frac{1.52eV}{kT}\right) \text{cm}^2\text{s}^{-1} \\ D_{high} &= 2.16 \times 10^{-6} \exp\left(-\frac{1.55eV}{kT}\right) \text{cm}^2\text{s}^{-1} \end{aligned}$$

These values are plotted in Figure 2.3, along with data obtained by SIMS and stress-induced dichroism (see §1.3.1).

The value of the activation energy for diffusion at low temperatures was recently confirmed by Yarykin and Vdovin [247], who measured oxygen loss from Cz-Si with a high dislocation density using infrared absorption techniques.

2.2.2 Binding to dislocations

The data also gave information about the way in which oxygen interacts with dislocations. Senkader *et al.* analysed the behaviour of Regime 2 - the steady-state where an equilibrium has been established between the oxygen at the dislocation cores and the surrounding oxygen in the bulk. By assuming a Maxwell-Boltzmann distribution between the two oxygen populations, they could deduce the binding enthalpy of the

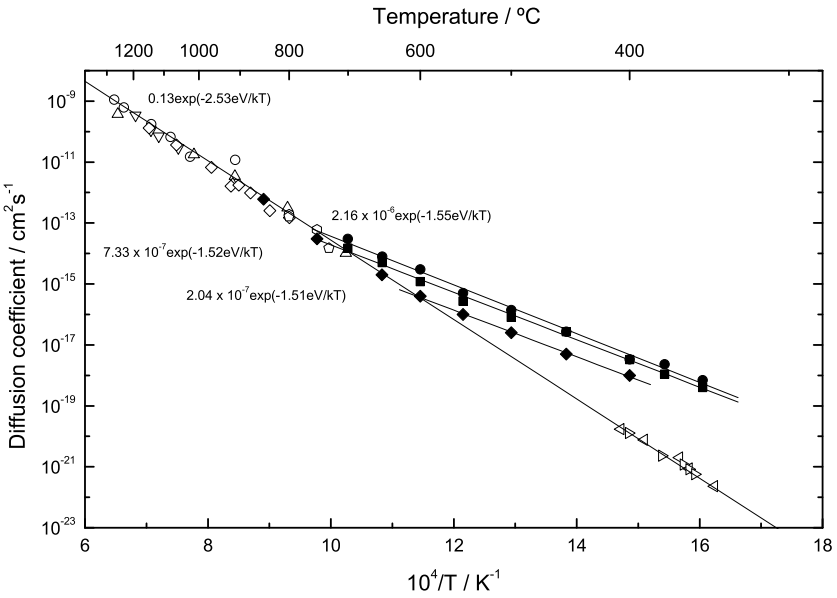


Figure 2.3: Oxygen diffusivity in Cz-Si (*after Senkader et al.* [80]), as obtained by dislocation unlocking (closed points) and SIMS and stress-induced dichroism (open points). Dislocation unlocking specimens with high (1.04×10^{18}cm^{-3}), medium (6.3×10^{17}cm^{-3}) and low (2.6×10^{17}cm^{-3}) oxygen concentrations are represented by circles, squares and diamonds respectively.

oxygen to the dislocation core. The Regime 2 unlocking stress values are shown in an Arrhenius plot in Figure 2.4. There are two binding enthalpies, 0.26eV and 0.74eV, with the change occurring at 650°C - the same temperature as the boundary between 'normal' and 'enhanced' diffusion that had been found from the Regime 1 gradients. This was a clear indication that different oxygen species were responsible for oxygen transport in the two temperature ranges. Furthermore, the scaling of effective diffusivity with oxygen concentration at the low temperatures was consistent with transport by an oxygen dimer[1], which had also been hinted at by other experiments [249, 250].

2.2.3 Oxygen transport in highly doped Cz-Si

Dislocation unlocking has also been used to investigate the effects of high levels of shallow dopants on oxygen transport in Czochralski silicon. A study by Murphy *et al.* found that while doping with antimony at 0.6 - 6×10^{18}cm^{-3} made no difference to

[1]The relevant analysis can be found in [248].

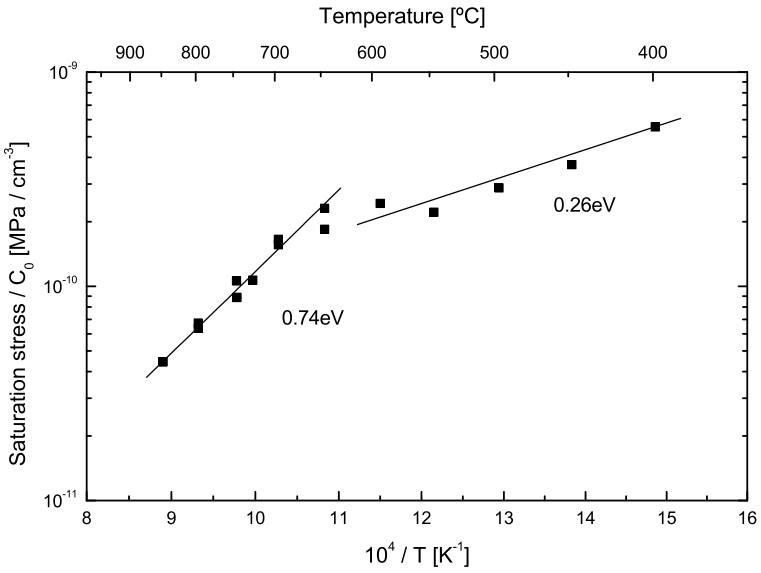


Figure 2.4: Saturation stress normalised by the oxygen concentration (*after Giannattasio et al.* [181]).

oxygen transport, doping with boron at 3 - 8×10^{18}cm^{-3} enhanced oxygen transport by up to a factor of 60 times in the temperature range investigated (350 - 550°C) [251, 252].

2.2.4 Advantages of dislocation unlocking as an experimental technique

The dislocation unlocking technique was highly successful as a means of investigating oxygen transport in regimes where standard techniques such as SIMS and stress-induced dichroism could not provide certainty. The advantages of the technique stem largely from the length scale of transport - to dislocations - that it measures. This means it is sensitive to diffusion at the sub-micron scale, and measures diffusion purely in the bulk where no surface effects are present. Dislocation unlocking can also be used to gain information about the interaction between the diffusing species and the dislocations, which for oxygen gave a confirmation of the change from monomer to dimer-dominated transport at 650°C.

Having been used so successfully to investigate oxygen transport in silicon, the

dislocation unlocking technique was then applied to nitrogen in silicon, another technologically relevant system. The work on the subject carried out by Giannattasio [253] and Murphy [254] is summarised here.

2.3 Dislocation unlocking used to measure nitrogen transport in FZ-Si

2.3.1 The need for measurements of nitrogen transport

As discussed in the previous chapter, nitrogen is deliberately added to some types of silicon by wafer manufacturers. Measurements of nitrogen's diffusivity are difficult to make. Nitrogen exists at very low levels (no more than $5 \times 10^{15}\text{cm}^{-3}$) in as-grown silicon, has no large electrical effects, and cannot be measured by standard SIMS due to problems with the background signal caused by out-gassing from equipment or residual air in the system. The most reliable technique, nitrogen-optimised SIMS, had only been used for temperatures greater than $\sim$750°C. Dislocation unlocking was ideally placed to make measurements below this temperature, given the apparent similarity of the oxygen and nitrogen systems. The technique was adapted to measure nitrogen-doped FZ-Si by Giannattasio [79, 180, 253].

2.3.2 Adapting dislocation unlocking to measure nitrogen

Whereas oxygen locks dislocations with a stress that can be greater than 250MPa, nitrogen in as-grown wafers gives a maximum of approximately 60MPa for high [N] material ($[\text{N}] > 10^{15}\text{cm}^{-3}$), and less than this if the nitrogen concentration is lower (data can be seen in Figure 2.6). This meant that the sensitivity of the experimental technique had to be increased by a considerable degree if the work was going to be successful, particularly since under some anneal conditions the unlocking stress would be below 10MPa.

Recall that in order to determine the unlocking point of a specimen, it is necessary to be able to distinguish the first set of dislocations that has moved during the three-point bend unlocking step. This means that in order to get a positive result,

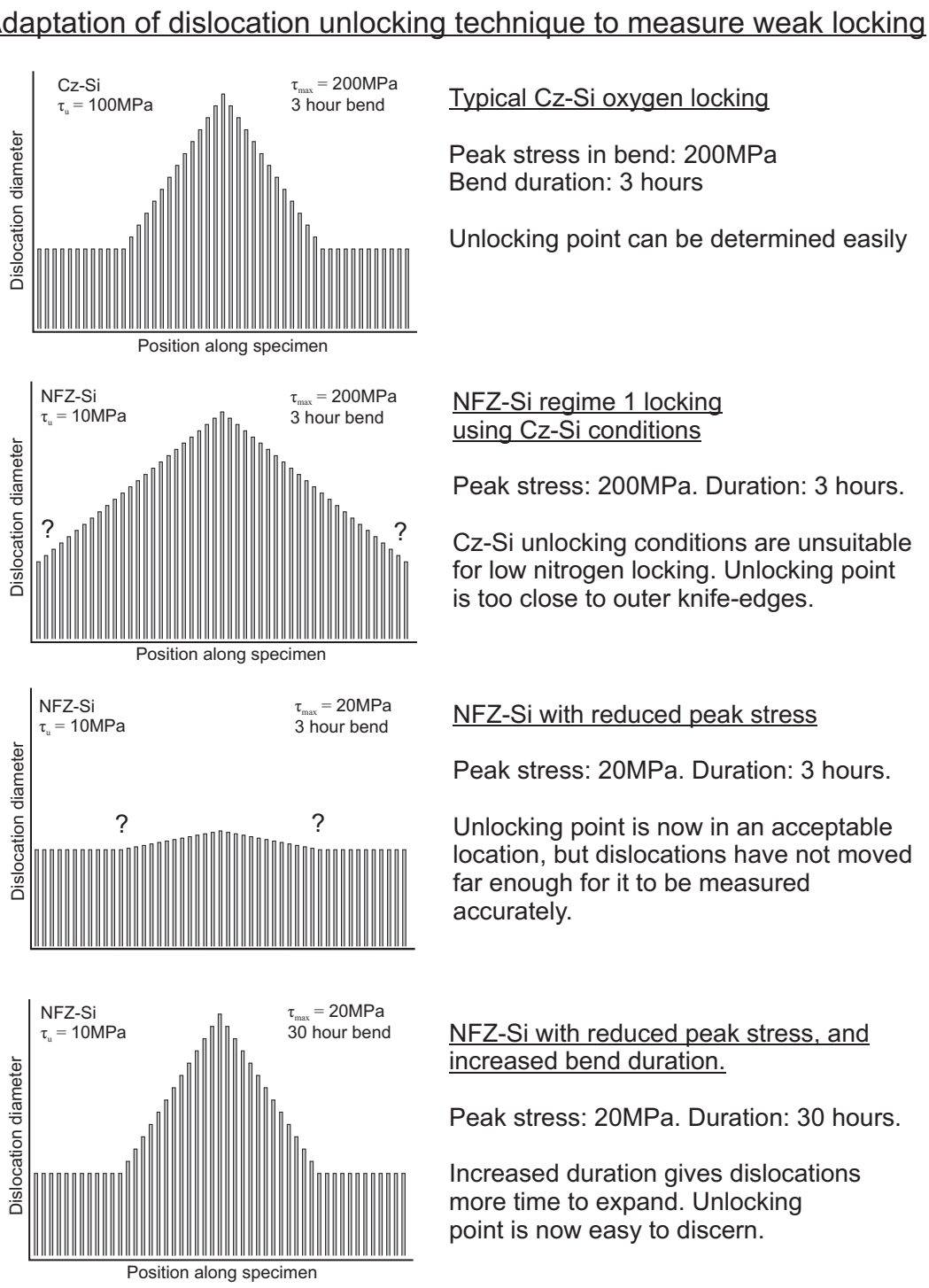


Figure 2.5: Schematic showing the effect of different three-point bend conditions. The total lengths of dislocation sets are plotted, using the method for identifying unlocking points that has been adopted in this work. This is explained in §3.7.2 and Figure 3.16.

the three-point bend stage must be set up so that this is possible. The three-point bend has two variables, load and duration (temperature having been standardised to 550°C). Giannattasio continued with the strategy used in the oxygen work, which was to set the load as approximately twice the expected unlocking stress, so that the unlocking point would be well away from the outer and central knife-edges. With the load decided, the bend duration could be set so that the first unlocked set of dislocations would move far enough to be easily distinguishable from those that remained stationary. This meant that specimens which were expected to have a high unlocking stress (i.e. long anneals) would be subjected to a high load for a short duration (4-8 hours) to unlock the dislocations during three-point bend, and specimens expected to have a low unlocking stress (short anneals) were given a low load, long duration three-point bend (8-20 hours). This is illustrated in Figure 2.5.

The first nitrogen dislocation unlocking experiments used NFZ-Si with a high nitrogen concentration, $[N] = 2.2 \times 10^{15} cm^{-3}$ [253]. This work was later complemented by a similar set of measurements using NFZ-Si with $[N] = 3 \times 10^{14} cm^{-3}$, approximately 7 times lower [254]. These later experiments pushed the sensitivity of the dislocation locking technique even further, with some three-point bends using such low loads that bend durations of over 60 hours were required.

2.3.3 Results from nitrogen experiments

Some of the results from the dislocation locking measurements performed on NFZ-Si are presented in Figure 2.6. At all temperatures, the variation of unlocking stress with anneal duration showed two regimes, similar to the first two regimes seen with oxygen in Cz-Si: an initial, linear rise (Regime 1), followed by a constant stress (Regime 2). The results were analysed in the same way that the earlier oxygen results had been. They were mostly self-consistent, but proved difficult to interpret.

Diffusivity from Regime 1

Regime 1 was seen at temperatures up to 900°C; above this, only Regime 2 results were seen, as the anneals required for Regime 1 were too short to be performed with

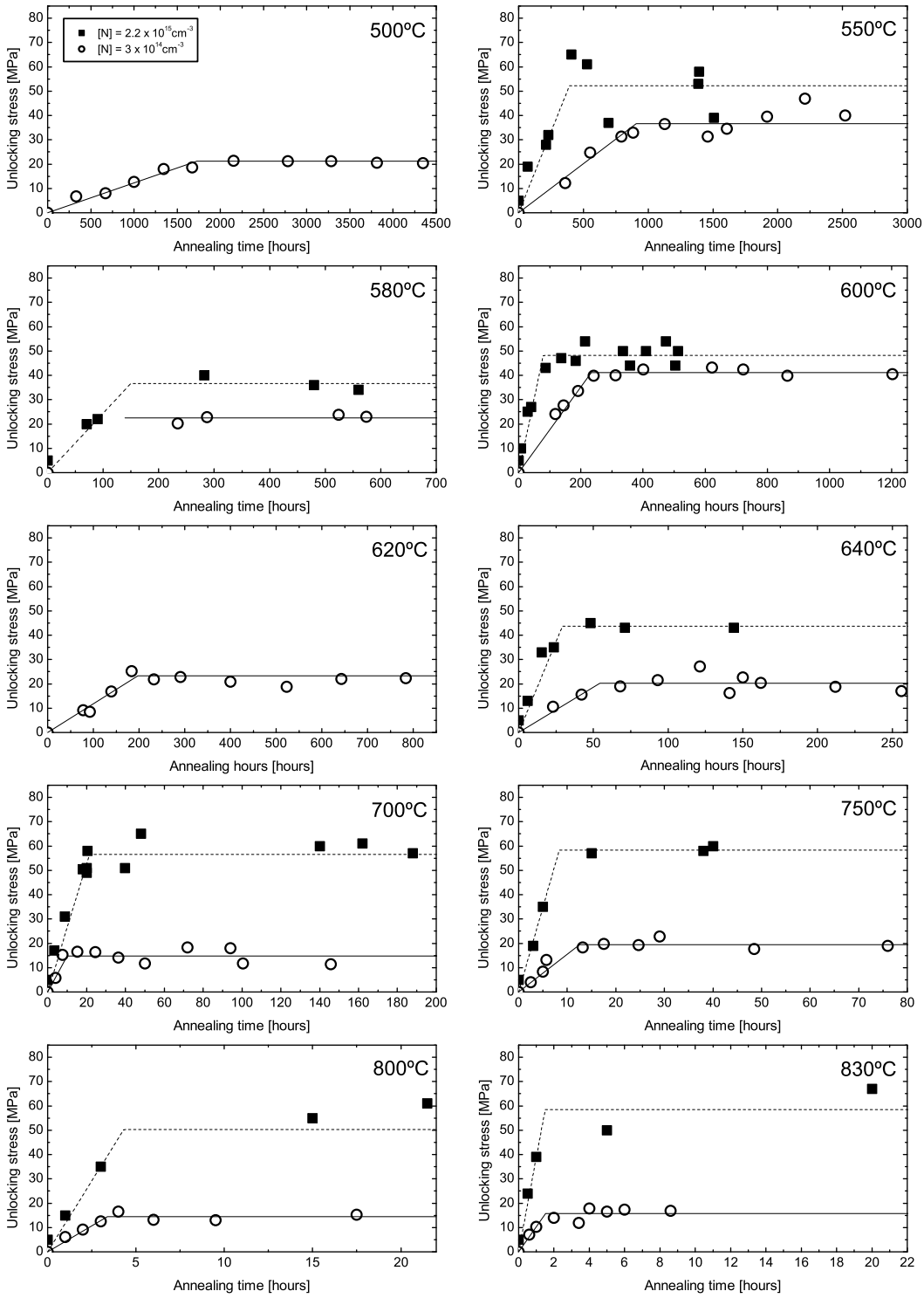


Figure 2.6: Dislocation unlocking stresses measured at 550°C for NFZ-Si. The closed squares were taken by Giannattasio using NFZ-Si with [N] = 2.2×10^{15}cm^{-3} [253], and the open circles by Murphy using NFZ-Si with [N] = 3×10^{14}cm^{-3}. The lines represent the average of the Regime 2 values, and a best fit for Regime 1 data (*after Murphy* [254]).

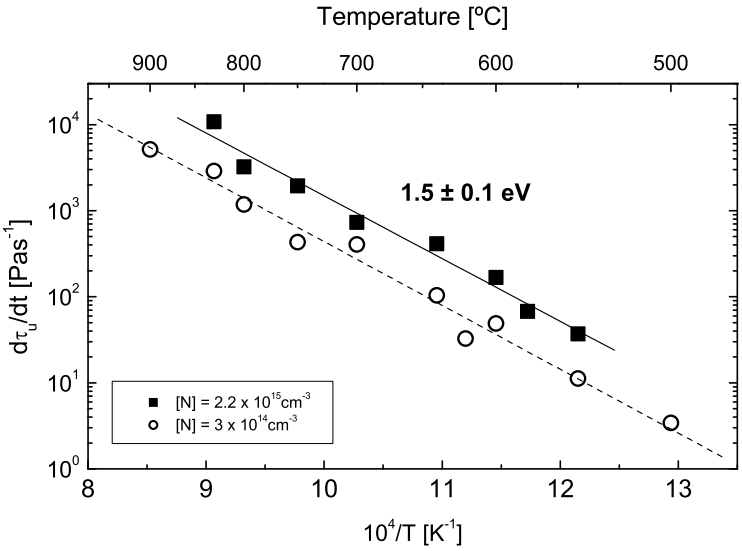


Figure 2.7: An Arrhenius plot of the gradient of the initial rise (Regime 1), $\frac{d\tau_u}{dt}$, found by Giannattasio (squares) and Murphy (circles) (*after Murphy* [254]).

the furnaces that were available. As with oxygen, the Regime 1 gradients were used in an Arrhenius plot to determine the activation energy for the dislocation locking process. The rate of increase of dislocation unlocking stress varies exponentially with temperature:

$$\frac{d\tau_u}{dt} \propto \exp\left(-\frac{E_{locking}}{kT}\right)$$

The rates of increase in dislocation unlocking stress were highly consistent, giving straight lines on the Arrhenius plot over three orders of magnitude (Figure 2.7). The high- and low-[N] results gave the same activation energy for the dislocation locking process, approximately 1.5eV. This low result was not understood, and was considerably different from the previous higher temperature SIMS studies, which had given an activation energy for effective nitrogen diffusion of 2.8eV [177]. By modelling nitrogen's locking of dislocations under the assumption that the system was similar to oxygen, absolute values for nitrogen's effective diffusivity could be estimated. These results are presented in Figure 2.8.

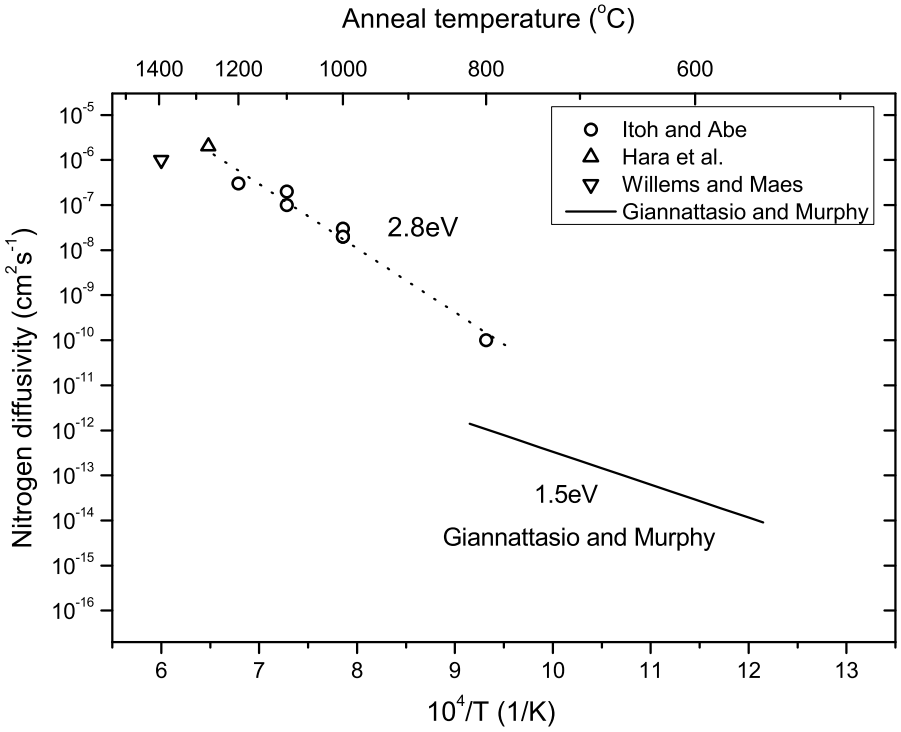


Figure 2.8: Nitrogen diffusivity values found by Giannattasio and Murphy [253, 254], and other authors [87, 177, 178].

Regime 2

The major difference between the dislocation unlocking behaviour of oxygen and nitrogen was the saturation regime. Recall that with oxygen, the magnitude of the locking stress in Regime 2 varied with anneal temperature, decreasing with increasing temperature (§2.2.2). Analysis of this effect provided information about the binding enthalpy of the locking species to the dislocations, and the change in behaviour at 650°C reinforced the evidence from Regime 1 for a change in locking species. The nitrogen data, in contrast, showed no coherent variation of Regime 2 saturation stress with anneal temperature (Figure 2.9).

The average value of Regime 2 stress for both sets of data is constant at all temperatures measured, although both sets contain some amount of scatter. The constant stress was surprising, particularly in the low-[N] data set where anneals had been performed at very high temperatures. This indicated that nitrogen was binding

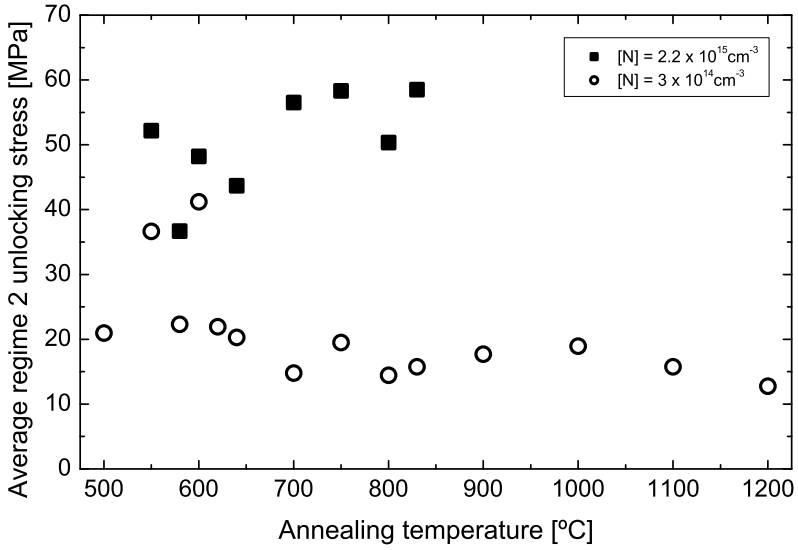


Figure 2.9: Average value of dislocation unlocking stress in Regime 2 measured at 550°C, found by Giannattasio (squares) and Murphy (circles) (*after Murphy* [254]).

very strongly to the dislocations; so strongly that it remained there even at 1200°C. A lower limit to the binding enthalpy to the dislocations was estimated as 2.4eV [254], a high value which was consistent with one theoretical study [63]. Nitrogen's high binding enthalpy received interest because it stood in contrast to oxygen, which 'boils off' dislocations above 800°C because it has a lower binding enthalpy of 0.74eV. Cz-Si wafers mostly lose the mechanical benefits of oxygen dislocation locking above this temperature. Could nitrogen therefore be useful as a substitute to give mechanical strength during high temperature device processing steps?

One other aspect of these data should be noted: the low-[N] saturation stress measurements at 550 and 600°C were twice as large as all the other temperatures investigated (which included 580°C, between the two). This could not be explained by random error, as the scatter in the underlying data sets was small, and the reason for these seemingly anomalous measurements was not understood.

Variation with nitrogen concentration

Giannattasio's high-[N] dislocation unlocking experiments were repeated with low-[N] silicon by Murphy because variation of unlocking behaviour with nitrogen concentration can yield important information about the identity of the locking species, if

locking is by atomic impurities (rather than precipitates). It was known that the majority species for nitrogen was the interstitial dimer (§1.4.2), but whether nitrogen transport is dominated by monomer or dimer diffusion was still an open question. Dislocation unlocking experiments had the potential to distinguish between the two cases.

By considering the flux of atoms to a dislocation in a population that contains a monomer and dimer species in equilibrium, expressions for the effective diffusivity can be derived for both the situation where the monomer is dominant (as with oxygen), and where the dimer is dominant (as with nitrogen) [255]. For nitrogen, it can be shown that if the dimer dominates transport then effective diffusivity will scale linearly with total nitrogen concentration; whereas if the minority monomer dominates transport, then the effective diffusivity will scale with the square root of total nitrogen concentration[2]. Since the gradients of Regime 1 are proportional to effective diffusivity, they should scale in the same way.

The silicon used by Murphy had [N] approximately 7 times lower than the material used by Giannattasio[3]. It was expected that nitrogen transport would be dimer-dominated, meaning that the Regime 1 gradients measured by Murphy should be $\frac{1}{7}$ as steep as those found by Giannattasio, and after a preliminary analysis of the results this indeed turned out to be the case. However, after the experiments had been completed a more thorough analysis of the data, including a re-calibration of the stresses applied to the dislocations, was performed. After this analysis it was found that the ratio of gradients found with high-[N] and low-[N] material was actually 3.5, not 7.

This ratio of 3.5 lay between that which would be expected for dimer-dominated transport (7) and monomer-related transport ($\sqrt{7} = 2.7$), but was closer to the latter. The tentative conclusion was therefore that the behaviour was inconsistent with dimer-dominated transport, but consistent with monomer-dominated transport, as a 25% error in the measurements was not improbably large [256].

[2]The analysis is given for the monomer-dominated case in §5.2.3.

[3]The precise ratio of concentrations quoted by the manufacturer was 7.3:1, but [N] is known to be hard to measure (§1.4.5).

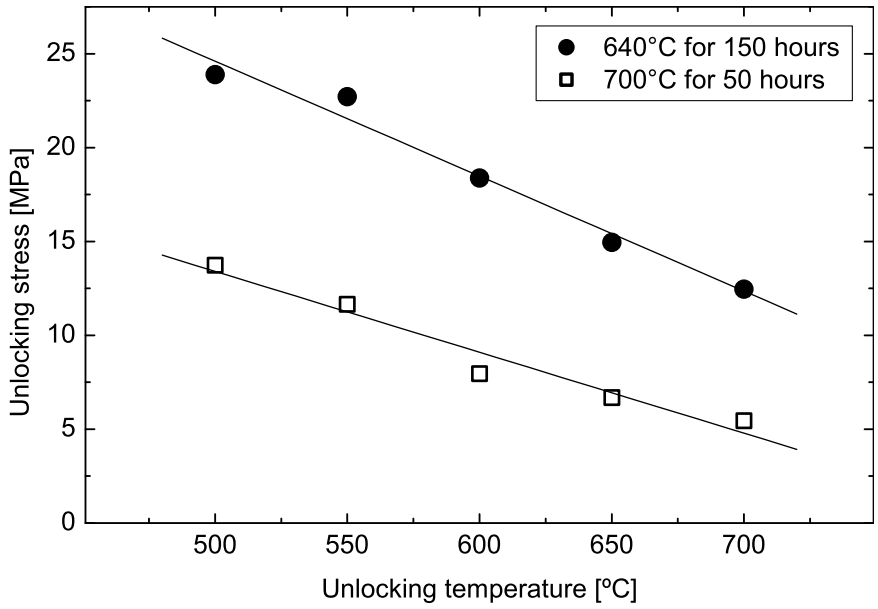


Figure 2.10: Variation of unlocking stress with unlocking temperature for NFZ-Si with [N] $= 3 \times 10^{14}\text{cm}^{-3}$ (*after Murphy* [254]).

Temperature dependence of unlocking stress

Another set of Murphy's experiments investigated how unlocking stress varied with unlocking temperature, *i.e.* the temperature at which the three-point bend stage is carried out. In the standard experiments this was standardised at 550°C whilst the main anneal was varied; in this experiment the main anneal conditions were kept constant, and the temperature of the three-point bend was varied, from 500°C to 700°C. This was carried out for two sets of specimens, which had been annealed at 640°C for 150 hours and 700°C for 50 hours (both in Regime 2 for their respective temperatures). The aim of these measurements was to provide evidence for the nature of the locking agent, as there was uncertainty as to whether locking was by nitrogen atoms or precipitates at the dislocation cores. The results are presented in Figure 2.10.

The results showed that for both annealing conditions, the unlocking stress was strongly dependent on unlocking temperature, falling linearly as the temperature increased. This was consistent with atomic locking of dislocations. The data were analyzed in terms of the theory of thermally activated release of impurities from dislocations, which had been used for dislocations in silicon by Sumino and Imai [226].

Using calculations of the relevant parameters taken from theoretical papers, Murphy was able to make a speculative estimate of the separation of individual nitrogen atoms along a locked dislocation (it came out as 150 Burgers vectors). However, another aspect of the data was noted: the unlocking stress for this set of samples showed a clear dependence on anneal temperature, with the specimens annealed at 640°C having greater unlocking stresses than those at 750°C, at all unlocking temperatures. This contradicted the main nitrogen dislocation unlocking experiments on other samples from the same wafers, which had shown that Regime 2 unlocking stress was constant at all anneal temperatures (apart from the anomalous results at 550 and 600°C). This inconsistency was not understood.

2.3.4 Analysis of dislocation locking by nitrogen: the identity of the locking species

Dislocation unlocking had been a highly effective experimental technique when used to measure oxygen locking in Cz-Si. The results agreed with other measurements of oxygen diffusivity where the temperature used was similar, and clearly showed that oxygen transport was dominated by monomers at high temperature and dimers at lower temperatures. Furthermore, the results indicated that the locking species was atomic, with a binding enthalpy to the dislocation core of 0.74eV. Unfortunately, the interpretation of the subsequent nitrogen results using the same technique was not nearly as straightforward. The experimental results, while mainly self-consistent, could not be explained by a single theory, since some aspects of the data indicated dislocation locking by atoms, but others by precipitates. Murphy offered separate analyses of the results for the two cases [257]:

Evidence for dislocation locking by atoms

- Measured 1.5eV activation energy could mean that dislocation unlocking experiments were sensitive to transport by a fast monomer.
- Regime 1 gradients seemed to scale linearly with anneal time, as expected for atomic transport, whereas for precipitates a $\sqrt{t}$ dependence might be seen. The

high level of random error in the data meant this was not completely certain, however.

- Regime 2 behaviour is consistent with locking by atoms with a high binding energy to the dislocation. With precipitates, a strong dependence of the unlocking stress on anneal temperature would be expected: the opposite of what was seen.

Evidence for dislocation locking by precipitates

- Regime 2 [N]-dependence results could not be explained by atomic locking.
- TEM studies had seen precipitates in nitrogen dislocation unlocking specimens, although the elemental composition was not determined.

Conclusions

The nature of the locking species in NFZ silicon could not be conclusively determined, given the difference between the two analyses and the problems with each. No firm conclusions were drawn in this area, and it was suggested that further TEM studies be undertaken.

2.4 Critical evaluation of previous nitrogen dislocation unlocking work

The results from the nitrogen dislocation unlocking experiments were unexpected, and considerable effort was put into explaining why this was the case. Some of the arguments are summarised here.

2.4.1 Was nitrogen locking really being measured?

The 1.5eV activation energy for transport found by the nitrogen dislocation locking experiments was very similar to that found for oxygen, raising questions about whether the experiments really were measuring nitrogen locking. Oxygen exists in FZ-Si at a level, depending on the manufacturing standards, of approximately 10^{15} -

10^{16}cm^{-3} (as opposed to $\sim 10^{18}$cm^{-3} in Cz-Si). Since this is comparable to the level of nitrogen in N-doped FZ-Si, it is not immediately obvious that a dislocation locking effect should be attributed solely to the nitrogen. However, dislocation locking by oxygen had already been studied in depth, using Cz-Si with different oxygen concentrations, and the locking strength was found to be concentration-dependent. An extrapolation of this effect down to the oxygen concentrations in FZ-Si showed that oxygen should not be expected to give significant dislocation locking in this material.

Direct evidence for nitrogen locking came from tests performed by Giannattasio, and later by Murphy. They performed identical experiments using both nitrogen-doped FZ-Si, and FZ-Si which was believed to be nitrogen-free. In all cases the nitrogen-free FZ-Si gave no dislocation locking. This showed that residual levels of oxygen, as well as any other impurities that might be present in the material or introduced during the experimental process, were not responsible for the dislocation locking effect. Murphy's low-[N] experiments provided further evidence, as they showed a correlation between locking strength and nitrogen concentration.

For these reasons, there was a high degree of confidence in the identification of nitrogen as the locking species.

2.4.2 Uncertainty with interpretation

The dislocation unlocking experiments with nitrogen-doped FZ silicon had produced results that could not be held together under one consistent interpretation. Potential explanations for this were:

- Problems with the interpretation of the results
- Experimental error
- Error in analysis
- A combination of the above

Problems with the interpretation of results

One possible reason for the failure of dislocation unlocking to give a consistent picture of nitrogen's interaction with dislocations in silicon was thought to be the interpretation of the experiments. Dislocation unlocking is an indirect method of measuring diffusivity, so it is unavoidably prone to ambiguity. The analysis used a model of the system which may have neglected important factors. For example:

- Transport to dislocations. Nitrogen transport in dislocation unlocking specimens could be complex, *e.g.* involving other impurities such as oxygen or other contaminants, or multiple nitrogen species as in the Voronkov model (§1.4.3).

- Are dislocations sufficiently isolated? The analysis assumes that the dislocations are sufficiently far apart that the effect of neighbouring dislocations on the local nitrogen concentration is negligible. This may not be valid.

- Unlocking of dislocations. Dislocations will unlock at the point where the applied stress first exceeds the local locking stress. If this occurs at certain 'special' points along the dislocation line it is not clear that the current analysis, which assumes unlocking of long uniform segments, would be sufficiently accurate.

- Locking strength of nitrogen. This is assumed to be proportional to the number of nitrogen atoms at the core. Locking by both atoms and precipitates was considered, but other options exist, *e.g.* those involving other impurities.

Unfortunately, most of these factors are such that they could not be easily discounted experimentally.

Experimental error

It is clear from data scatter that dislocation unlocking experiments contain a degree of random error, but this was not thought to affect the usefulness of the results (apart from minor aspects such as the inability to distinguish between a t and $\sqrt{t}$ Regime 1 dependence). However, there is also the possibility that the experiments were affected by systematic error, which is harder to identify. Dislocation unlocking is

a difficult and time-consuming technique, and comparable nitrogen experiments have only been reported by the Oxford group, so independent verification of the results was not possible (although members of the Oxford group regularly repeated each other's experiments to check for consistency). Under these circumstances the only way to minimise the risk of systematic experimental error was a detailed examination of the technique.

Some errors had been found and removed by changing aspects of the experimental method. For example, it was discovered that cooling down from the four-point bend stage could produce a small amount of additional dislocation locking, as this was effectively a short extra anneal. This led to the use of the 'cooling under load' procedure in some experiments, such as those of Murphy [254], which eliminated the error. As well as these known sources of error, the effects of potential undiscovered errors were estimated.

Dislocation unlocking experiments contain a number of procedures, but all are simple and well understood. Annealing and unlocking temperatures were thought to be the greatest possible error sources, since the relevant physical phenomena are strongly thermally activated, so small variations in temperature could change results appreciably [254]. After analysing the potential effect of an error in anneal or unlocking temperature, Murphy estimated that this could produce a maximum error of $\pm 25\%$ for a dislocation unlocking measurement in the worst case. The other potential source of error was the mechanical measurement involved in the determination of unlocking stress, but calculations showed that this was insignificant [258].

A $\pm 25\%$ potential undiscovered error might seem large, but in fact this is not the case. The unlocking measurements had been taken over many orders of magnitude, with anneal durations varying from minutes to thousands of hours, and a 25% error would be dwarfed at this scale. Transport measurements can be hard to make over many orders of magnitude, and diffusion coefficients for impurities in silicon are often only stated to a precision of one significant figure, so this potential error was not seen as being significant.

Another possible source of error is that certain experimental variables are not con-

trolled, as they are assumed to be unimportant. Adapting the dislocation unlocking method to measure nitrogen instead of oxygen had meant that three-point bend conditions had to be changed from specimen to specimen (§2.3.2), but tests performed at the time indicated that this had no effect on the final result.

Error in analysis

It is possible that the experiments and interpretation contained little error, but the analysis of the results had been performed wrongly (*e.g.* it contained algebraic mistakes or logical inconsistencies), but this is highly unlikely. The same analysis had been used successfully with the oxygen work, which was widely reported, and it was known to be sound.

2.4.3 Known problems with the experiments

As well as the difficulties of interpretation, and the potential risk of experimental error, other aspects of the experiments were known to be problematic.

Paucity of data

An observer not familiar with dislocation unlocking experiments might, understandably, question the confidence with which the 'lines of best fit' are drawn through some of the nitrogen dislocation unlocking graphs. As an example, consider the unlocking graphs for low-[N] silicon at 600 and 700°C, presented in Figure 2.6. In both cases the fit line for Regime 1 might not seem to be fully supported by the data: at 600°C there are no results on the lower half of the line, and at 700°C there is only one datum in Regime 1, through which the fit is plotted. The main reason for this is that dislocation unlocking experiments are extremely time consuming. This was especially true for the nitrogen experiments, for which only a limited quantity of silicon was available, and which used extremely long three-point bend durations, so that measurements could only be made at a rate of about one every two days.

This issue is discussed further in §5.8.2.

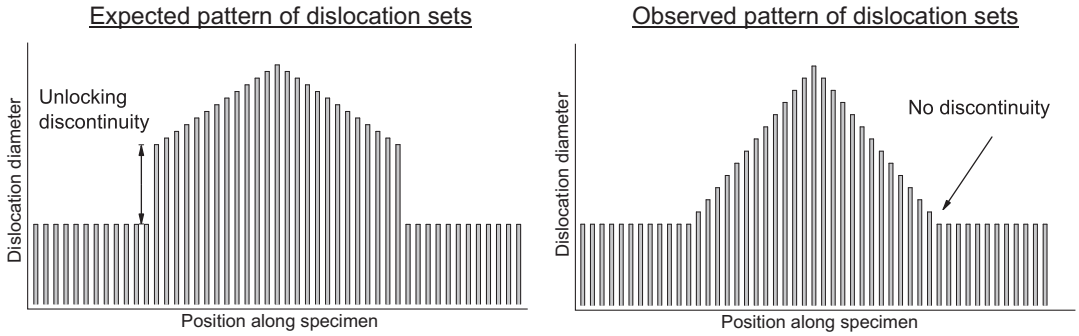


Figure 2.11: Schematic showing the pattern of dislocations usually observed, with no unlocking discontinuity.

The 'unlocking discontinuity'

Figure 2.11 shows a schematic representation of dislocation loop diameters after the three-point bend unlocking stage. In this schematic, the dislocations near the centre of the bar, which experience a resolved shear stress greater than τ_u, are shown as moving according to the stress they experience. This results in the characteristic pattern of unlocked dislocations, with a large gap between the first set of dislocations to move, and the set next to it which remained locked. This gap can be termed the 'unlocking discontinuity'.

The example of an unlocked dislocation set given by Senkader for the work on oxygen locking in Cz-Si showed a clear discontinuity (Figure 2.12). However, it was noted even at this time that this pattern was not representative of all of the specimens that had been examined [259]. In the case of the nitrogen work, most specimens contained dislocation sets which didn't show the unlocking discontinuity, as represented in Figure 2.11. The lack of a discontinuity was puzzling, since it seemed that the unlocked dislocations were not travelling with velocity proportional to the calculated stress during the three-point bend. This presented a challenge to the model of the experimental system that had been used to calculate unlocking stresses, and some effort was devoted to explaining it, without success (*e.g.* [260]).

The unlocking discontinuity issue has been investigated further for the specimens used in this work, and the results are presented in §5.7.

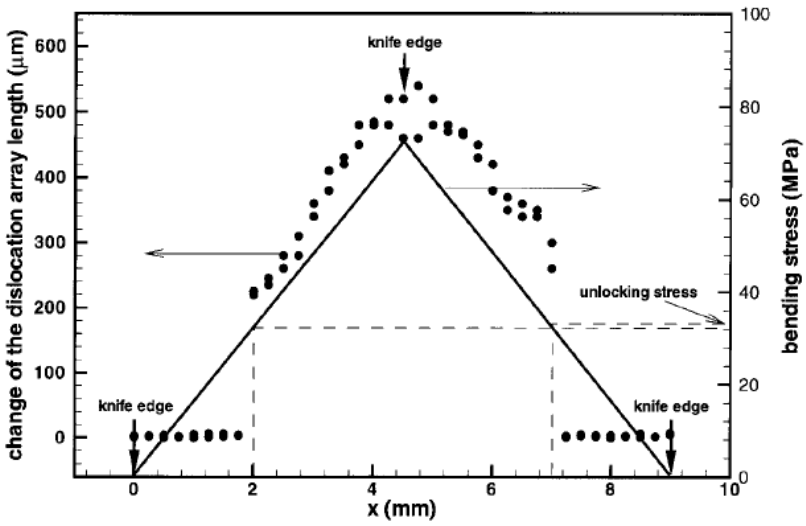


Figure 2.12: The example of unlocked dislocation lengths in a Cz-Si specimen given by Senkader *et al.*, showing a clear unlocking discontinuity (*after Senkader et al.* [32]). Note that the *change* in dislocation diameter is plotted, so dislocation sets that remained locked show as 0μm. This pattern is highly unusual in the nitrogen work (§5.7).

2.5 Summary

Dislocation unlocking had been extremely successful when used to measure oxygen transport in silicon, as it quantified enhanced transport at low temperatures due to a fast diffusing dimer. The technique was then developed to allow the sensitive measurements required to detect and quantify dislocation locking due to nitrogen. Three-point bend duration and load were varied on an experiment-by-experiment basis, to make the unlocking points clearer and give more precision at lower unlocking stresses. The results found using this changed technique were mostly self-consistent, but could not be explained by any single model for the system. This did not necessarily reflect negatively on the experiments themselves, however, as the wider context showed that nitrogen transport in silicon was poorly understood in general. The dislocation unlocking work formed just part of a field that contained a number of irreconcilable results, both experimental and theoretical.

The experimental technique had been examined closely, and there was a high degree of confidence that experimental error did not affect the final results significantly. This is not to say that there were no known problems, however. The missing unlock-

ing discontinuities in specimens showed that some aspects of the experimental system were not understood, but overall, this was not thought to affect the integrity of the results.

The dislocation unlocking experimental method, as used in the work in this thesis, is described in detail in the next chapter.

Chapter 3

The dislocation unlocking method as used in this work

The dislocation unlocking experimental procedure used in this work is broadly the same as that described in §2.1.2. The stages are:

- Specimen cleaving and polishing
- Indent to damage specimen surface
- Four-point bend to create dislocation array from indent damage
- Anneal to allow nitrogen to diffuse to dislocations
- Planar etch to remove $\sim 20\mu$m from surface of specimens
- Three-point bend to unlock dislocations
- Preferential etch to reveal dislocation positions
- Measure specimen to determine unlocking stress

Each aspect of the procedure will now be described in detail.

3.1 Specimen preparation

Dislocation unlocking specimens are time-consuming to prepare, because care must be taken at all stages to keep them clean and free of damage. Procedures were regularly

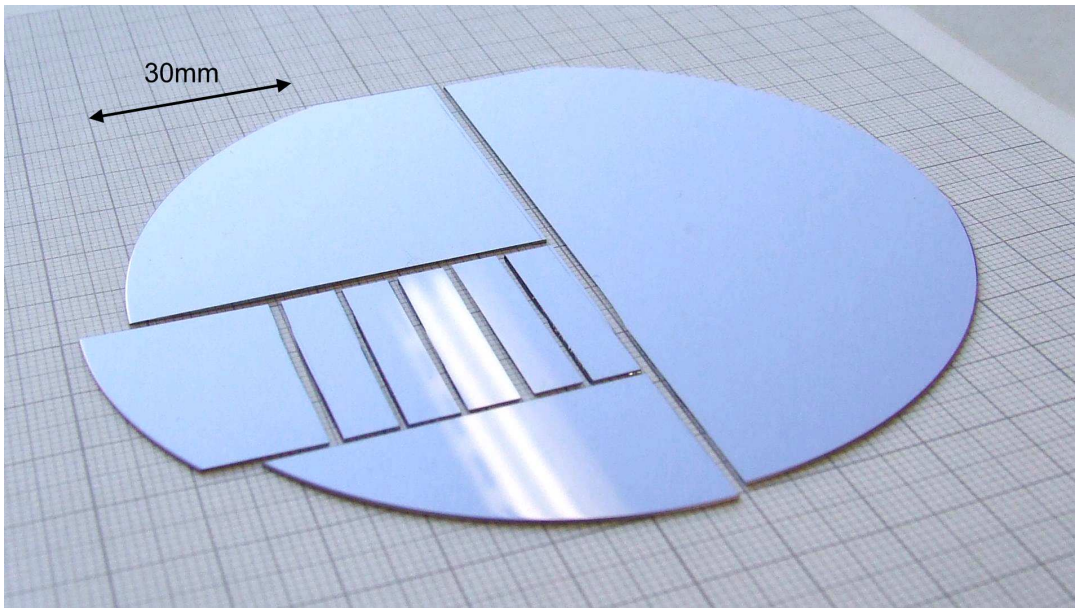


Figure 3.1: A 100mm diameter NFZ-Si wafer that has been cleaved to create some rectangular bars for dislocation unlocking experiments.

modified and refined, since improvements were always being sought. The specimen preparation procedure that was eventually settled on is described here.

3.1.1 Cleaving and polishing

All wafers used in this work were (100) orientation, with thicknesses varying from approximately 0.5 - 0.7mm. Most were mirror-polished on one side, some on both sides, and one on neither side. Rectangular bars along the [110] direction measuring approximately 28 × 5.5mm were cleaved from the wafers, using a diamond scribe (Figure 3.1). Bars were not taken from the very outer regions of wafers, as this part of the silicon crystal may have been affected by out-diffusion or any other surface effect. Sets of bars were then mounted in a polishing stub (made from an aluminium cylinder) with mounting wax (Figure 3.2).

The bars were then ground and polished using a sequence of progressively finer grades of silicon carbide paper and diamond polishing compound (usually 240 grit, 600 grit, 6μm, 1μm), with great care being taken to keep the polished surface orthogonal to the surfaces of the bars. When the bars were polished to a 1μm finish, the aluminium polishing stub was placed on a hot plate at ∼120°C until the wax had melted. The

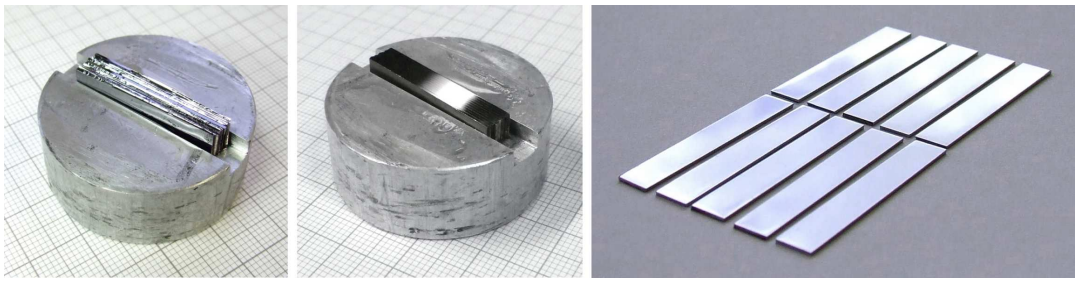


Figure 3.2: Polishing stub containing as-cleaved (left) and polished (centre) specimens. Right: specimens after cleaning and 5 minute planar etch. Polished specimens are approximately 28 × 4.5mm in size.

bars were turned over so that the polished side was face down, and the grinding and polishing procedure was repeated for the other side. After polishing, the width of the bars was 4 - 5mm.

It was important when polishing to make sure that the polished edges were parallel to the cleaved edges, as the calculation of the resolved shear stress experienced by the locked dislocations assumes that the specimens are oriented along the [110] direction (see §3.3.4). Also, bars had to be the same width at both ends, as the bend stress calculation is only valid for a rectangular specimen. In practice this could done satisfactorily using the naked eye; the widths of the two ends of the bars differed by only $\sim 50\mu$m on average.

One wafer was not polished on either face, so these specimens underwent the same polishing procedure for one of their faces. This used extra 0.3μm diamond paste and 'Syton' colloidal silica (70nm particle size) steps.

For some experiments, it was required that specimens be prepared only from certain areas of a wafer. In these cases the wafers were cleaved so as to maximise the number of specimens that could be made from the acceptable area of the wafer.

3.1.2 Clean and planar etch

After the second side was polished, the block of bars was put into a beaker of acetone and left until the mounting wax had softened sufficiently for the bars to separate. Bars were then individually wiped lightly with acetone-soaked tissue to remove the remaining wax, with particular care being taken to make the polished face of the

specimen stain-free. They were then dipped in methanol to remove the dry stain left by the acetone, and dried with compressed air.

After this, the bars were given a 5 minute planar etch using the mixture described in §3.6. This was to smooth off any scratches or other damage that might have remained after polishing.

3.2 Indenting

Micro-hardness and nano-hardness testers were used to indent specimens at room temperature, creating surface damage in an ordered, repeatable array. The damage creates residual stresses in the vicinity of the indent, and the crystal relaxes into a tangle of prismatic dislocation half-loops as the specimen is heated up before the four-point bend stage [261]. These half-loops then expand and multiply during the four-point bend.

3.2.1 Micro-hardness tester

Most of the experiments presented here used a micro-hardness tester made by Matsuzawa Seiki Co. Ltd to make indents, using a Vickers diamond tip. The indenter was set to apply a 10g load for a 5 second dwell time, the standard settings used for dislocation unlocking experiments in silicon. Specimens were aligned on the indenting stage using a rectangular glass slide to keep the specimen parallel to the movable stage's sides. The stage was then moved until the specimen's central axis was directly underneath the indenter tip. A line of indents approximately 18mm in length was made along the central region of the specimen, with the indents being 250μm apart.

3.2.2 Nanoindenter

The experiments described in §6.1 used an MTS NANO Indenter XP, which indented specimens with a three-sided Berkovich tip. This machine was computer controlled, and could be programmed to indent specimens in complicated arrays using different load and dwell time settings. Although the machine is much more advanced than the micro-hardness tester and can be used to generate detailed information about each

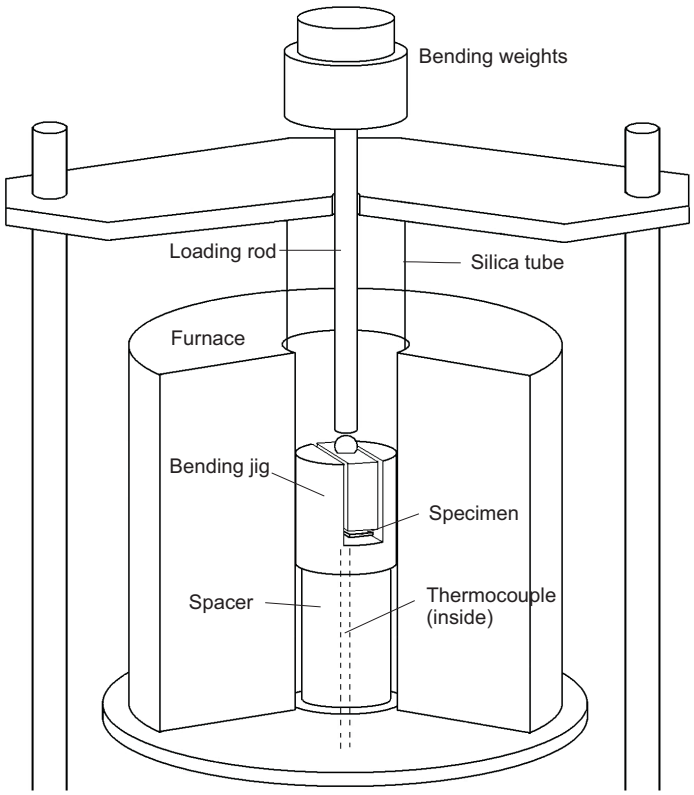


Figure 3.3: Bending rig schematic. The argon and water cooling loops have been omitted for clarity.

indent, the main benefit for this work was its ability to produce low-load indents, far below the minimum 10g load of the micro-hardness tester.

3.3 Bending set-up

In the standard technique, bending at elevated temperature was used first to expand dislocation half-loop sets created by indent damage so that they had a diameter of $\sim$200μm (four-point bend), and secondly after annealing, to expose specimens to a linearly varying stress which caused some dislocations to unlock and expand (three-point bend). The bending rig is shown in schematic form in Figure 3.3. The various parts of the apparatus will now be described.

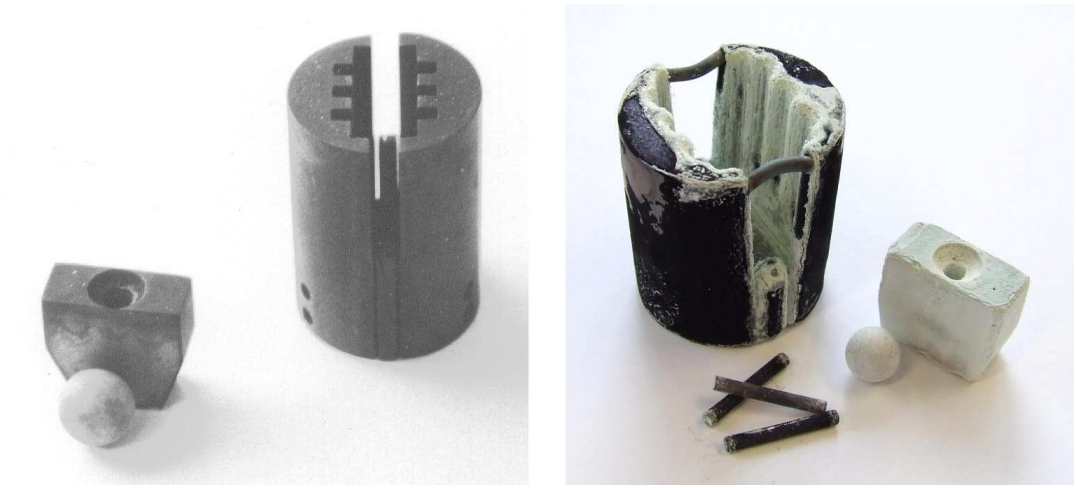


Figure 3.4: A molybdenum bending jig as new (left, *after Murphy* [254]) and the one used for this work (right).

3.3.1 Molybdenum bending jig

At the centre of the apparatus is the small molybdenum bending jig, shown in Figure 3.4. Molybdenum was chosen for its low solubility in silicon, and its mechanical strength at high temperatures. The jig is cylindrical, with a central slot above two outer knife-edges, crossed by three sets of vertical grooves which are used to align the knife-edges that come into contact with the specimen. The knife-edges are straight pieces of 1mm diameter molybdenum wire, approximately 15mm long, which were regularly replaced. With the specimen in place underneath the wire knife-edges, a small top-piece of molybdenum, with grooves cut to match the knife-edges, rests on top. The upper surface of this piece contains a depression, in which sits a steel ball-bearing of diameter 8mm, connecting it with the loading rod.

The jig is shown in Figure 3.4 in the condition it was in when the present work was complete, after it had been used daily for over 6 years. It is readily apparent that the condition has deteriorated, an effect of oxidation and subsequent cleaning. The sides have also bowed outwards, so two small pieces of molybdenum wire have been added across the top of the central groove, to help with alignment of the top-piece. The condition of the jig meant that more care had to be taken when aligning specimens inside, but otherwise is not thought to have affected the experiments.

The alignment of specimens inside the jig is shown in Figure 3.5. For a four-point

bend, specimens rest face-down on the jig's outer knife-edges, which are spaced approximately 24mm apart. Two wire knife-edges are then placed in the outer grooves, and sit on top of the specimen, with a gap of 12mm between them. The molybdenum top-piece rests on top of these two wire knife-edges. The useful part of the dislocation array is created between these two inner knife-edges, in the region of constant stress during the four-point bend.

Before three-point bending, ∼5mm is cleaved from each end of the specimen. It is then rested, face down, on the two outer wire knife-edges, and a third wire knife-edge is placed in the central slot on top of the specimen. The molybdenum top-piece balances on this central knife-edge. It is important that the specimen is aligned correctly at this stage, so that the central 12mm, which contains the array of full dislocation sets, is fully in between the outer wire knife-edges. This is shown in Figure 3.5.

A K-type thermocouple runs through a hole in the base of the jig, so that the temperature inside can be measured, a few millimetres away from the specimen.

3.3.2 Full bending apparatus

The full bending rig is shown in Figure 3.6. The molybdenum jig sits on two stacked cylindrical spacers, which are the right height to position the jig in the central zone of the furnace. The spacers have thin, axial holes through which the jig thermocouple passes. The spacers and jig sit inside a silica tube, which is part of the system that surrounds the jig with an argon ambient, reducing oxidation which is damaging to the jig and specimen (most notably, the oxidation of silicon can induce stacking faults [262]). Argon comes from a storage cylinder to the bottom of the bending rig, passes through the silica tube, then through the top of the rig and out to a bubbler. The argon system is kept at a slight over-pressure for the duration of each bend, to make sure that air is excluded.

The silica tube and bending jig are placed inside a cylindrical furnace manufactured by Severn Thermal Solutions Ltd. The furnace is controlled by its own thermocouple, but is set by hand to reach the desired temperature as measured by the jig thermocouple, which sits millimetres away from the specimen. Since the furnace

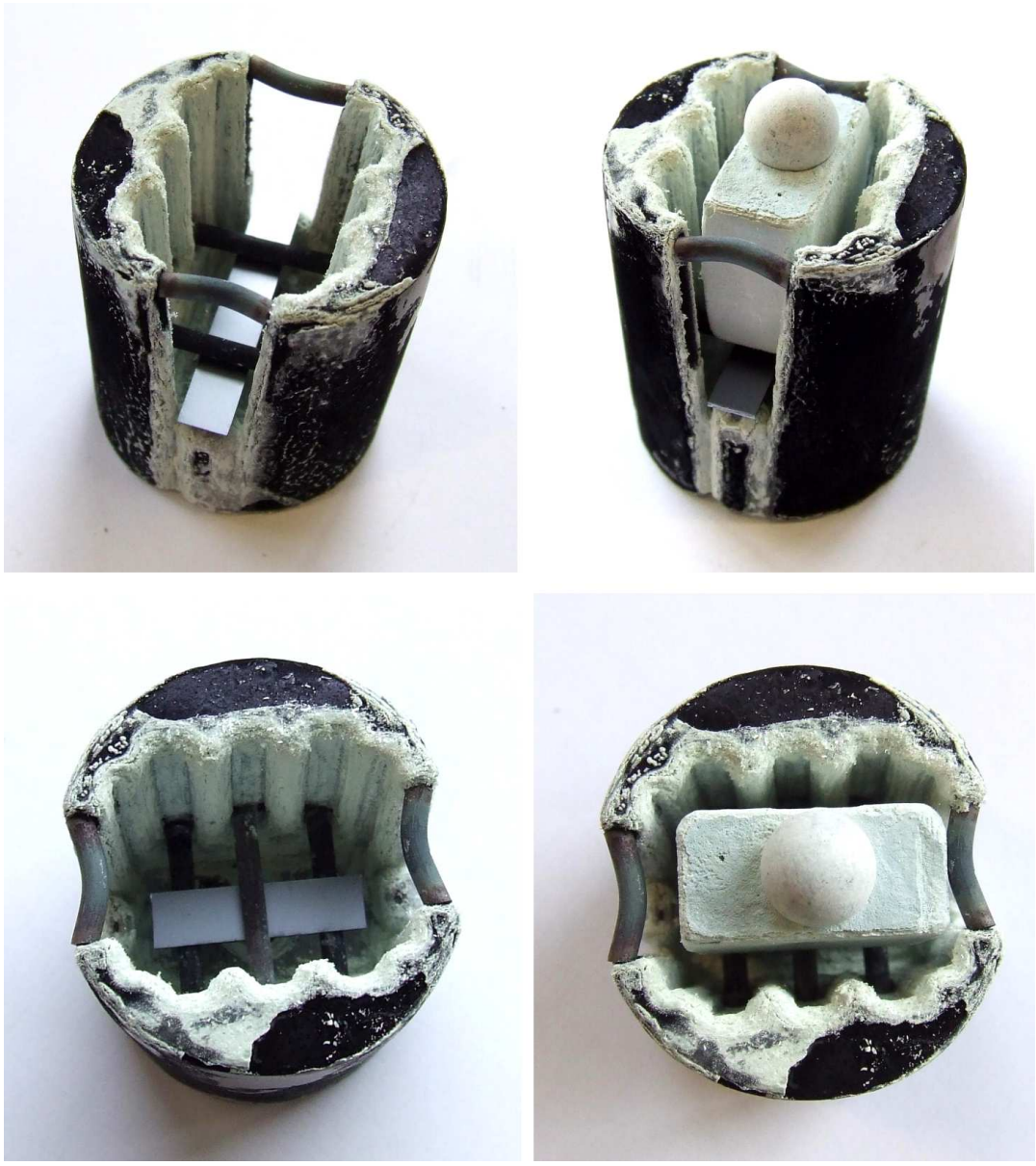


Figure 3.5: Specimen alignment in the bending jig, for four-point bending (top) and three-point bending (bottom).



Figure 3.6: Full bending rig in various stages of assembly, showing the molybdenum jig and the spacers (top left), the silica tube (top right), the Severn furnace (bottom left), and the full structure, with the loading rod being held just above the jig (bottom right).

is small, it has a small hot zone, which might seem non-ideal. However, the molybdenum bending jig, which surrounds the specimen, is an excellent thermal conductor and acts to keep the temperature homogenous.

Holding the top and the bottom of the rig is the supporting metal structure, which contains a water cooling loop to prevent the surrounding environment from heating up. The whole apparatus is mounted on the movable crossbar of an Instron 1195 mechanical testing machine, such that the machine can be used to apply load to the specimen. However, for most of this work the Instron was not used to apply loads for reasons discussed in §3.3.3 and 4.1.3.

3.3.3 Load application

The bending apparatus was mounted on the Instron machine so that it could be used to apply the bending loads, and historically this had been the common practice for dislocation unlocking experiments. However, since the move to measuring the lower unlocking stresses of nitrogen the Instron has been used less, as it was perceived to lack precision when applying low loads. Murphy, for example, only used it when using loads greater than 20N, as discussed in §4.1.3. The alternative was to use free weights, which rested on top of the loading rod. This was done for every experiment in this work apart from the high-load tests described in §6.1, as it guaranteed a stable, accurate load for the whole duration of a bend. It also allowed the loading rod to be set in place by hand, which reduced the risk of it being misaligned.

3.3.4 Geometry

Four-point bend

The four-point bend configuration is shown in Figure 3.7, along with the tensile stress distribution it produces. The stress σ rises linearly from the outer knife-edges to the inner knife-edges, taking a value in between the inner knife-edges ($\sigma_{constant}$) of [263, 264]:

$$\sigma_{constant} = \frac{3Pa}{wh^2} \tag{3.1}$$

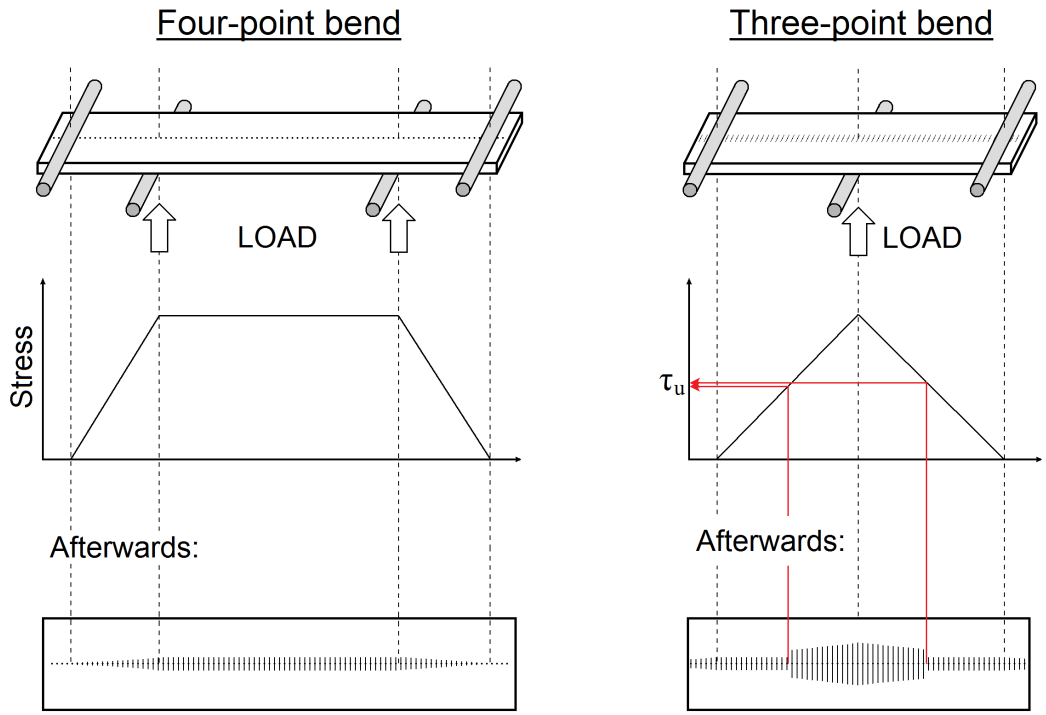


Figure 3.7: Schematic showing the stress distributions in four- and three-point bends.

where P is the applied load, a is the distance between outer and inner knife-edges, w is the specimen width and h the specimen thickness. Typical values of these parameters were a = 6mm (set by the dimensions of the jig), w = 4 - 5mm, h = 0.5 - 0.7mm, and P = 15 - 20N.

The purpose of the four-point bend is to expand the dislocations associated with the indent damage, until they have a diameter of approximately 200μm. Indenting silicon at room temperature produces a highly complex region directly underneath the indenter tip. This region includes various types of high-pressure phase, and amorphisation caused by plastic deformation [265]. The stresses associated with this damage are 'frozen in', and are relieved on heating up to four-point bend temperature by the throwing out of dislocation half-loops.

Dislocations may move when they experience a non-zero resolved shear stress, τ, in their glide plane. In these experiments the applied tensile stress is in the [110] direction, and $a/2[10\bar{1}](111)$ is the relevant slip system, as shown in Figure 3.8. To calculate the resolved shear stress experienced by the dislocations, the applied tensile

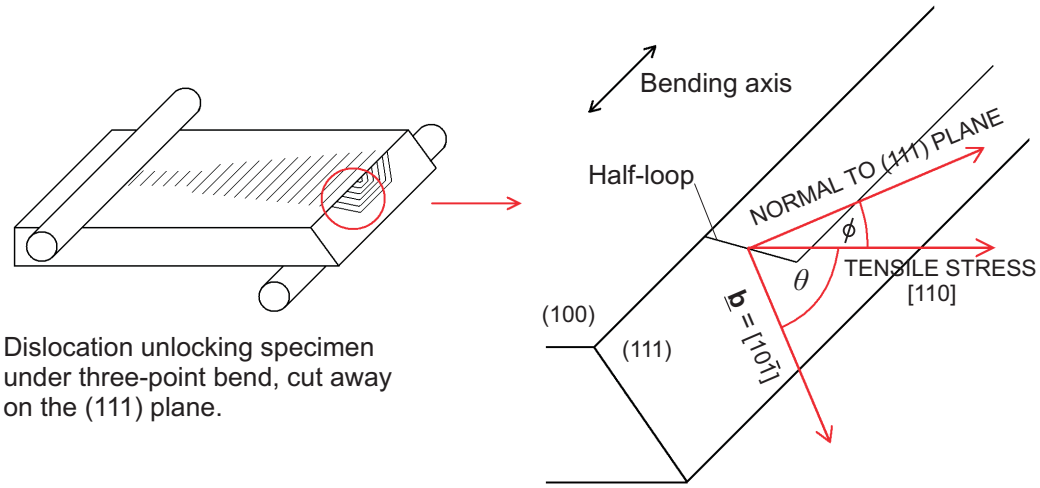


Figure 3.8: Schematic showing the geometry of the slip system in dislocation unlocking experiments.

stress must be multiplied by the Schmid factor. This is defined as $\cos\theta\cos\phi$, where θ is the angle between the applied tensile stress and the slip direction, and ϕ the angle between the applied tensile stress and the normal to the slip plane, as seen in Figure 3.8 [233]. For the slip system activated in this work, the Schmid factor is $\frac{1}{\sqrt{6}}$, and so the resolved shear stress is:

$$\tau = \frac{\sigma}{\sqrt{6}} \tag{3.2}$$

Three-point bend

The three-point bend configuration, and the stress distribution, is shown in Figure 3.7. The stress rises linearly from the outer knife-edges to the central knife-edge, where it takes a value of [263, 264]:

$$\sigma_{max} = \frac{3Pl}{2wh^2} \tag{3.3}$$

where l is the total span (the distance between the two outer knife-edges), and P, w and h are defined as before. The value of l is set by the dimensions of the bending jig as 12mm, although this was measured precisely for each individual specimen. Most experiments used a bending load P = 15 - 20N, but for some experiments it could be

as high as 150N.

Equation 3.3 applies for the case where the central knife-edge is equidistant from the outer knife-edges. With previous dislocation unlocking work, this condition was achieved practically with acceptable accuracy, as the knife-edge guide slots in the bending jig confined the central knife-edge with a high degree of precision. However, as can be seen in Figure 3.4, this was no longer the case in this work. Great care was taken to position the knife-edge as centrally as possible by hand, but measurements of specimens showed that occasionally the knife-edge had moved during the load application process.

For this reason, the maximum stress in the three-point bend had to be corrected to account for this factor. A more general expression for three-point bend maximum stress is [266, 267]:

$$\sigma_{max} = \frac{6Pxy}{lwh^2} \tag{3.4}$$

where x and y are the lengths between the central knife-edge and each outer knife-edge (so for a central knife-edge equidistant from the two outer knife-edges, $x = y = \frac{l}{2}$). This can be rewritten to show the correction to Eq. 3.3:

$$\sigma_{max} = \frac{3Pl}{2wh^2} \cdot 4\frac{x}{l}\frac{y}{l} \tag{3.5}$$

It should be noted that this correction was always small, with the corrected value rarely differing from the uncorrected value by more than 2%. As with the four-point bend, the Schmid factor is used to calculate the resolved shear stress.

3.3.5 Four-point bend procedure

All parts of the experimental procedure were standardised as much as was practicable. For this reason, the load used for the four-point bend was the same as that used for the three-point bend, and the duration was 35 minutes in every case, at 600°C.

First, the furnace was turned on and allowed to come up to temperature. While this was happening, an indented specimen was placed with care into the jig in four-

point bending configuration. When the furnace had reached full temperature, the apparatus was assembled, and argon and cooling water were turned on. The jig now heated up rapidly. The load was applied when the jig thermocouple had reached 500°C, and the 35 minute count was started when it reached 570°C, about 2 minutes later. Over the next few minutes, the jig temperature increased to the full 600°C. At 35 minutes, the load was removed and the specimen taken out of the rig and left to cool. Typically, another specimen would be put in immediately, and the process repeated.

This procedure was followed carefully in every case, and produced satisfactory dislocation arrays in a repeatable manner. The dislocation half-loops typically had a diameter of 150 - 200μm.

3.3.6 Three-point bend procedure

The three-point bend is more critical than the four-point bend, as it is where the dislocation unlocking takes place, so great care was taken to eliminate procedural inconsistency. As with the four-point bend, the first step was to turn on the furnace. The furnace was initially set to approximately 570°C, so that heating up to 550°C would be faster. While it was coming up to temperature, 5mm would be cleaved from each end of the specimen using a diamond scribe, so that it would fit in the centre of the jig for three-point bending. The specimen was then placed into the jig, and the knife-edges and molybdenum top-piece positioned around it. This positioning was very important, as the condition of the jig meant that the central knife-edge was not properly confined to a central position by the grooves, so it had to be placed there by hand.

Once this was done, the furnace was placed into the rig, and the whole apparatus assembled, with the loading rod held just above the jig with a clamp stand. The argon and cooling water were turned on at this point. When the specimen temperature reached 544°C, the furnace control was lowered to 565°C to slow the rate of temperature increase, and immediately the loading rod was placed with great care onto the ball-bearing on top of the jig's top piece, the bending weights were placed on

top of the loading rod, and the timing stopwatch was started. It was found that at the end of this procedure, the jig temperature would have reached 550°C. Over the next few minutes, the furnace control was steadily lowered, keeping the jig temperature at 550°C, until the controller itself was set to 550°C. With the temperature steady, the bend could be left alone.

Load was applied in the three-point bend for 4 hours (except where the effect of variation in the bend duration was being investigated), and at the end of the loading period, the specimen was removed from the bending rig and left to cool. The load was standardised to give ∼84MPa peak resolved shear stress, which is discussed further in §3.7.3.

3.4 Annealing

In the standard experimental technique, specimens are annealed at constant temperature for a controlled duration, to allow nitrogen transport to the dislocations that have been introduced via indentation and four-point bend. This is the stage where dislocation locking takes place, and as such, anneal conditions are very important. The annealing for this work was carried out in a number of ways, since no one type of furnace was suitable for the vast range of anneal temperatures and durations that were required. Particular attention was paid to warming and cooling rates - the transport analysis assumes a simple anneal where the effects of warming and cooling are negligible compared to the effects of the time spent at full temperature (see Chapter 5). For anneals lasting several hours, standard furnaces permit acceptably fast heating and cooling of specimens, but this is not the case for anneals lasting only seconds. The different annealing methods are described here.

3.4.1 Standard metallurgical furnaces

For anneals lasting more than about 7 minutes, Instron and Lenton furnaces were used (Figure 3.9). The furnaces contained silica tubes, through which argon was passed during annealing to exclude air and prevent oxidation of the specimens. The furnace was preheated to the required temperature, measured by a thermocouple located

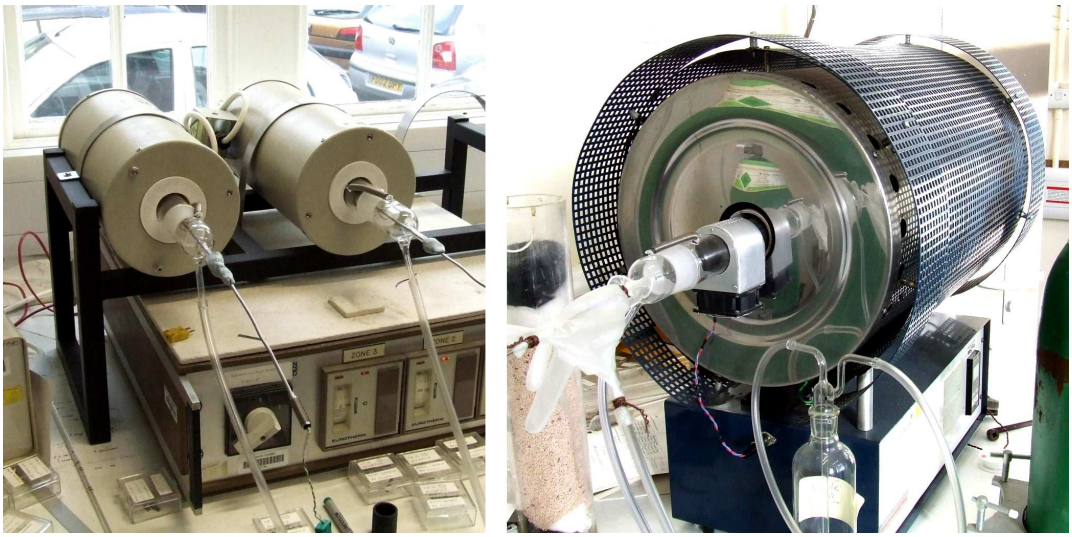


Figure 3.9: Furnaces in which specimens were annealed: Instron furnaces (left) and Lenton furnace (right).

directly over the position where the specimens would rest during the anneal, in the centre of furnace's hot-zone. The silica boat containing the specimen was then pushed into the centre of the furnace, with a precision of about ±2mm, and the silica tube quickly closed by hand. The specimen thermocouple was then monitored; the anneal period was determined to have started when the temperature reached 10°C below the required temperature, a convention that was used for every specimen annealed this way.

At the end of the anneal period, the silica boat was removed from the furnace and the specimen taken out of the boat as quickly as possible and left to cool. In general specimens were annealed one at a time, but this was not possible for the anneals at 500°C and some at 600°C because of the long durations involved (up to 7 months). In these cases, several specimens were stacked in the silica boat and annealed concurrently. The boat was quickly moved to the front of the furnace every time a specimen was removed, and quickly moved back to the hot zone. Specimens that remained in the boat until the end of a batch would have experienced a small amount of cumulative cooling because of this, but this has not been corrected for as it is negligible - the specimens affected had all been annealed for at least a hundred hours.



Figure 3.10: Jipelec Jetfirst Rapid Thermal Annealing Processor (RTA furnace) [268].

3.4.2 RTA furnace

Short anneals were performed using a Jipelec Jetfirst Rapid Thermal Annealing Processor (RTA furnace) (Figure 3.10), located in a clean room at the Begbroke Science Park. The RTA furnace heats specimens with radiant energy, and is able to produce far steeper temperature gradients than conventional furnaces. The furnace is computer controlled, and heating rate, anneal temperature and duration, and cooling rate, can be varied. Specimens are placed on a supporting 100mm silicon wafer, and the anneal temperature is measured by a thermocouple which touches the underside of this wafer, directly beneath the specimens. Anneals were performed in a nitrogen ambient as the RTA was not set up to use argon. There is not thought to be any risk of nitrogen in-diffusion into specimens, as the nitrogen concentration inside the specimens was already much higher than the solid solubility at all anneal temperatures used.

As the RTA furnace is located in a clean-room, all specimens had to be thoroughly cleaned before annealing. After standard cleaning (§3.1.2), specimens were further cleaned using the RCA procedure [269]:

Step 1: Immerse in a solution of distilled water, ammonium hydroxide (29%) and hydrogen peroxide (30%) in ratio 5:1:1 at 80°C for 20 minutes. Clean thoroughly afterwards with distilled water.

Step 2: Immerse in a solution of distilled water, hydrochloric acid (37%) and hydrogen peroxide (30%) in ratio 6:1:1 at 80°C for 20 minutes. Clean thoroughly

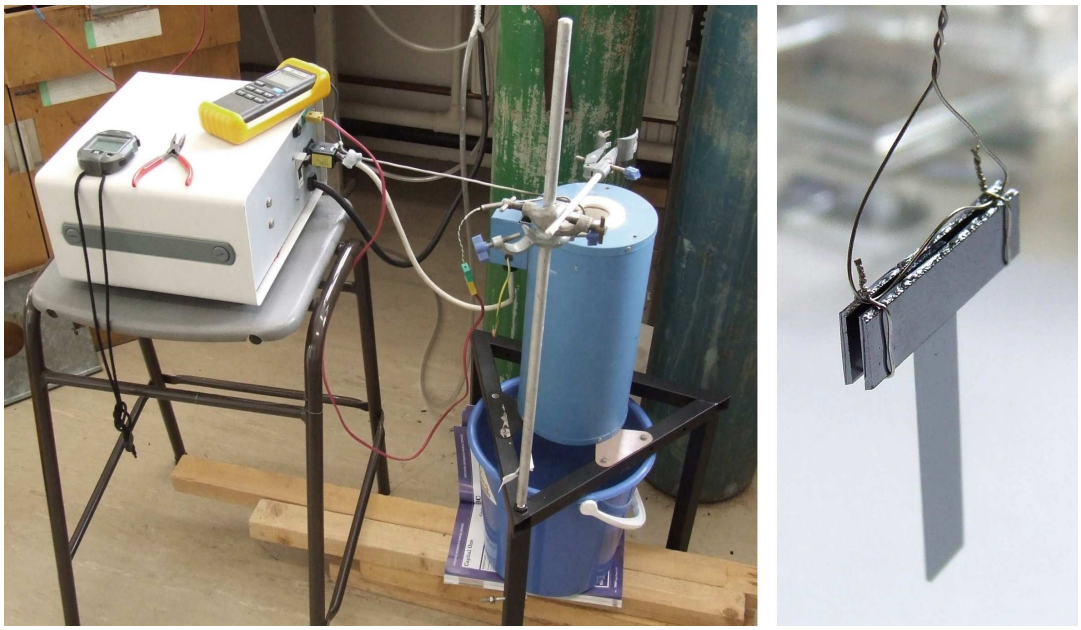


Figure 3.11: Left: the fast-quench Severn furnace, with Eurotherm controller and bucket of water. During anneals the top of the furnace was covered to prevent convection. Right: a fast-quench specimen.

afterwards with distilled water.

3.4.3 Fast quench annealing

For some high temperature experiments, the most important requirement is that the cooling rate after the anneal be as fast as possible (see §3.5). The RTA cooling rate is unacceptably slow in some situations, so annealing methods that give faster cooling have been sought. The standard method used in the past for dislocation unlocking was to seal specimens in evacuated silica ampules, anneal in standard furnaces, then water-quench immediately on removal from the furnace [270]. It is estimated that specimens handled this way could be cooled from high temperature in about 2 - 4 seconds. This method was used for a small set of experiments in this present work, described in §6.1.5.

However, some experiments in this work required faster cooling than this. The main factor that slowed cooling in the quench method described above was the insulation provided by the silica ampule, which had to be cooled itself before the specimen inside could reduce in temperature. Fast quenching in this work was performed us-

ing the annealing set-up shown in Figure 3.11. Specimens were clamped at one end between two pieces of silicon, which were bound with Constantan wire. This meant that only silicon was in contact with the specimen during the anneal. The specimen was then lowered with wire into a pre-heated Severn furnace, which was aligned vertically. A thermocouple was run inside the furnace, positioned in the hot-zone where the specimen would hang. The top end of the furnace was blocked to prevent convection through the hot zone, and the bottom end was left open. Directly underneath the furnace, with a gap of about 4cm, was a bucket of cold water. When the anneal was finished, the wire from which the specimen was suspended would be cut, and the specimen would fall through the furnace into the water.

This annealing method did not use an inert ambient. Specimens were directly exposed to air throughout, and so some oxidation of the surface will have taken place. However, subsequent chemical etching showed that no oxidation-induced stacking faults were produced.

3.5 Evaluation of annealing techniques

The analysis of dislocation unlocking results in the next chapter considers anneals as consisting of simple, rectangular time-temperature profiles, neglecting the warm-up and cool-down periods. This means that for the analysis to be valid, the temperature transient periods must have a negligible effect on the specimen, compared to the constant temperature part of the anneal. In terms of the thermal load on the specimens, this can be evaluated simply by comparing the durations of each part of the anneal; however, another consideration means that the cooling rate is particularly important for some experiments.

Chapter 2 described how the magnitude of the dislocation locking effect in Cz-Si reduced with increasing anneal temperature, falling to zero above 800°C. In order to measure this small high-temperature dislocation locking effect correctly, specimens had to be cooled quickly after the anneal: slow cooling would have allowed oxygen to start accumulating at the dislocations as the temperature dropped below 800°C, producing some dislocation locking. This is why silica ampoule quench cooling was

used by Senkader for high-temperature anneals using Cz-Si.

This quench cooling method was also used by Murphy for his high-temperature NFZ-Si anneals [270]. These experiments, in contrast to those with Cz-Si, detected dislocation locking at all anneal temperatures measured (up to 1200°C, §2.3.3). This was not thought to be affected by cooling rate, as calculations showed that nitrogen diffused too slowly to attach to dislocations in significant amounts in the short time it took specimens to cool after annealing. The work in this thesis, however, has shown that nitrogen transport in silicon is much faster at high temperatures than was measured by previous dislocation unlocking experiments (§5.1). This led to the development of a faster quench-cooling technique. The warm-up and cool-down rates for each type of furnace used in this work are evaluated in this present section.

As well as the warm-up and cool-down periods, specimen temperature measurement is another potential source of error, both when annealing and bending. With all annealing methods, temperatures were measured using K-type thermocouples. The thermocouples could not be placed in contact with specimens as this would cause damage and conductive heat loss, so they had to be placed as close as possible. This was done in different ways for the different furnaces, and the effect this had on the accuracy of temperature measurement in each case is estimated here.

3.5.1 Standard furnaces

The standard furnaces were used for most of the annealing in this work: all anneals at temperatures up to 750°C were performed this way, apart from those at 675 and 750°C which had durations of less than 7 minutes, where the RTA furnace was used. The warm-up and cool-down durations for these furnaces are of the order of a minute, which is negligible as the anneals were generally much longer than this. Temperature measurement was by a thermocouple positioned directly above the specimens and is thought to be accurate to ±5°C.

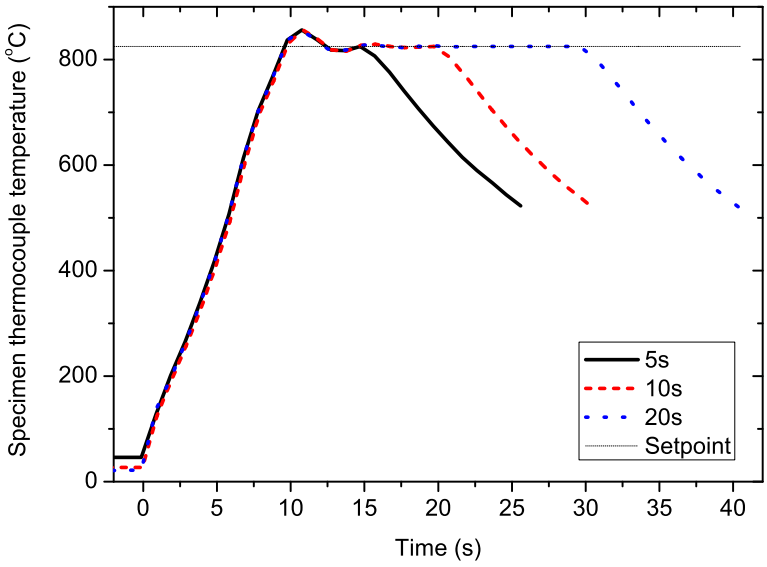


Figure 3.12: RTA furnace time-temperature profiles for three anneals at 825°C (durations indicated).

3.5.2 RTA furnace

The RTA furnace was used for most anneals above 750°C, apart from the fast-quench anneals described below, and also anneals at 675 and 750°C with durations below 7 minutes.

Warming and cooling

Since the RTA furnace is computer controlled, time-temperature profiles can be logged. Examples of these profiles, which give an indication of the capability of the furnace, are shown in Figure 3.12. The heating and cooling rates are faster than the standard furnaces, with specimens coming up to temperature in about 10 seconds and cooling almost as quickly. However, the anneal durations are also very short in some cases. The time-temperature profiles in Figure 3.12 show that for the shortest anneals, the warm-up and cool-down form a non-negligible part of the total thermal load. This has not been corrected for in the analysis presented in Chapter 5, as these measurements are not relevant to transport considerations, since no Regime 1 was

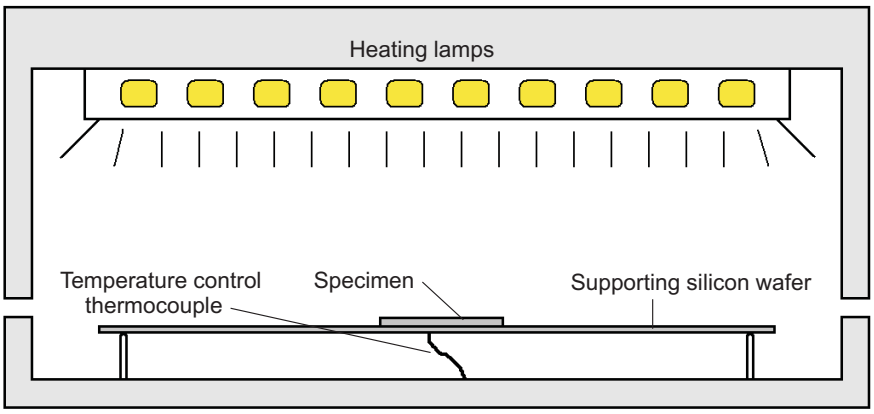


Figure 3.13: Schematic showing the positioning of the specimen and thermocouple in the RTA furnace.

seen at 825 and 900°C.

The cooling rate, while fast, is probably not superior to that achieved by the silica-ampule enclosed quench cooling in previous work. This means that the highest temperature anneals, at 825 and 900°C, could have been affected by dislocation locking on cool-down. However, comparison with the fast quench results (presented in the next chapter), shows that this is not a significant effect for these specimens. Another aspect of the profiles in Figure 3.12 is the small temperature overshoot at the start of the anneal. Temperature overshoots can be significant, since nitrogen transport is strongly thermally activated [177] so a small overshoot can have a disproportionate effect.

Temperature measurement

The RTA furnace contains two thermocouples and a pyrometer, with the thermocouple placed in contact with the underside of the supporting silicon wafer being used exclusively for temperature measurement (shown in Figure 3.13). Since silicon has a high thermal conductivity, and the thermocouple is very close to the specimens, it is thought that temperatures measured this way could also be as accurate as ±5°C.

Conclusion

The deviations from 'ideal' time-temperature profiles for specimens annealed in the RTA furnace are not thought to be a significant source of error.

3.5.3 Fast-quench furnace

Fast-quench cooling was used for one set of experiments, presented in the next chapter, that sought to measure nitrogen's dislocation locking ability at very high anneal temperatures (up to 1050°C). Specimens were kept at the desired anneal temperature for long enough to ensure that Regime 2 had been reached, then quenched into water.

Warming and cooling

The nature of the experiments meant that the warm-up was not important, as only the Regime 2 behaviour was being investigated. The important aspect of these experiments is the cooling rate, as specimens must drop in temperature quickly enough to prevent nitrogen accumulating at the dislocations during the cool-down. The quench cooling is shown in Figure 3.14. It is estimated that the specimen, having fallen through the furnace under gravity, would enter the water 0.2 seconds after the wire was cut. Cooling from high temperature in the water is estimated to have occurred in less than 0.1 seconds. This extreme cooling rate caused considerable thermal shock to the silicon, and more than half of all the specimens annealed this way shattered on quenching.

Temperature measurement

Temperature measurement in the fast-quench furnace was problematic. A thermocouple was positioned in the centre of the furnace, approximately 1 - 2cm away from the specimens. However, the furnace, being positioned vertically, acted as a chimney. Even with the top almost completely blocked, there would have been some convection through it, which is hard to quantify. Specimens also were surrounded by air, lacking the presence of the silica boat used in the standard furnaces or silicon wafer in the RTA furnace, which both acted to stabilise the temperature. For this reason

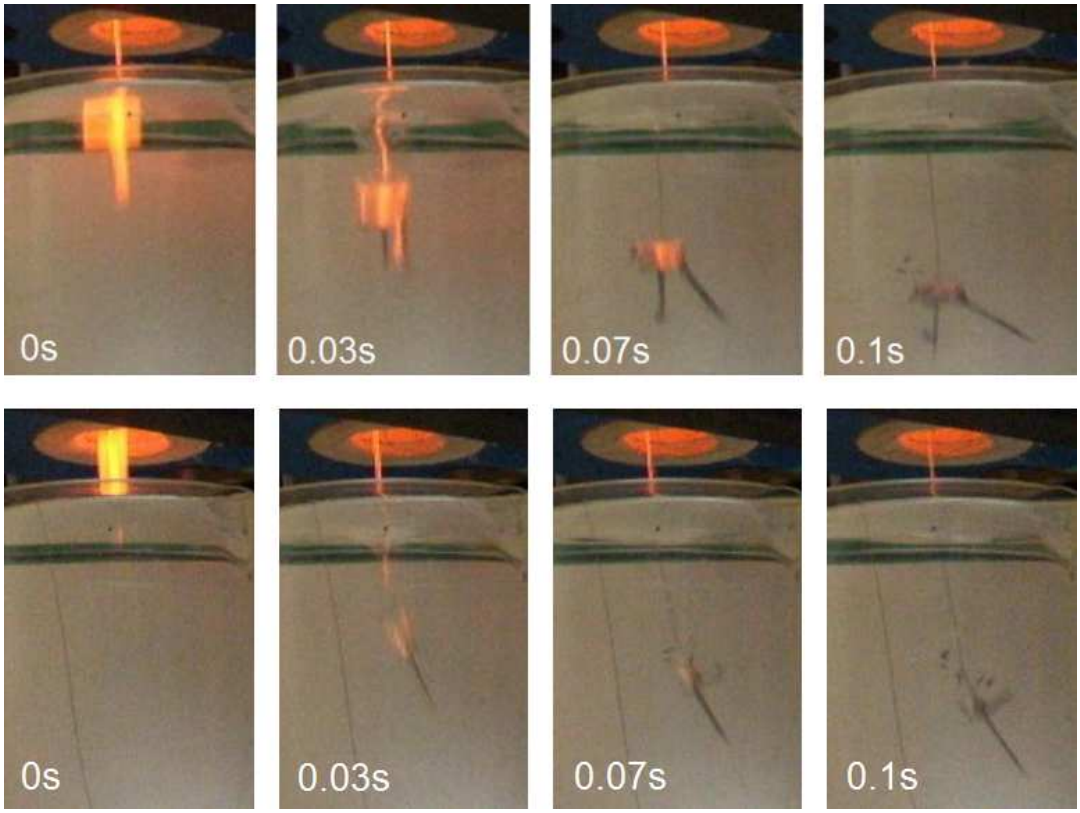


Figure 3.14: Two examples of specimens, annealed at ∼950°C, entering the water during fast-quench cooling. Top: holding pieces shatter, specimen breaks in two along its length. Bottom: holding pieces shatter, specimen does not break. The cooling rate is estimated from the colour of the specimens: silicon stops glowing in the visible range below about 600°C.

there is less confidence in the temperature measurements for these experiments, and a potential error of ±15°C in the anneal temperature is estimated.

3.6 Etching

3.6.1 Planar etching

Planar etching is used to strip away a layer of material from the surface of specimens after annealing, to remove any regions of specimens that might have been affected by out-diffusion of nitrogen, or other surface effects. It also removes the damage associated with the indents, which otherwise might nucleate new dislocations during the three-point bend stage. The etch attacks all surfaces at an equal rate, so it

has the effect of removing a uniformly thick layer from the top surface, and also smoothing out depressions or protrusions. For this reason it is also used briefly after specimen preparation, smoothing any scratches or surface damage that might remain after polishing.

The etch composition is nitric acid (79%), acetic acid (glacial), and hydrofluoric acid (40%) in the ratio 75:17:8. The standard procedure was to use ∼10ml of etch solution in a PFTE beaker, placing the specimen face-up at the bottom of the beaker, so that only the top face and sides would be exposed. Specimens were etched for 5 minutes after the initial cleaving and polishing, and 37.5 minutes after annealing. The chemical reaction produces hydrogen gas, which slowly forms bubbles on the specimen surface. This has the effect of initially lifting the specimen up from the bottom of the beaker, so for the long etches, specimens were gently pressed down again after about 10 minutes.

One set of experiments in this work used the depth of material removed by the planar etch as an experimental variable (§6.3), so this had to be measured accurately for these specimens. This allowed the planar etch rate to be calibrated. These results are presented in Figure 3.15, which shows that the standard 37.5 minute planar etch removed 15 - 20μm of material. It can also be seen that the etch rate reduces with time, as the active ingredients in the etch solution are used up.

3.6.2 Preferential etching

The position of dislocations after three-point bending is discerned by viewing etch pits created by a preferential etch. The etch preferentially attacks the silicon around dislocations, producing holes large enough to be identified using an optical microscope. The preferential etch is composed of 0.3M chromic oxide solution and hydrofluoric acid (40%) in the ratio 5:4. As with the planar etch, specimens were placed face up in a PTFE beaker which contained ∼10ml of etch solution, and left for 13 minutes, which was found to be long enough to give satisfactory etch pits.

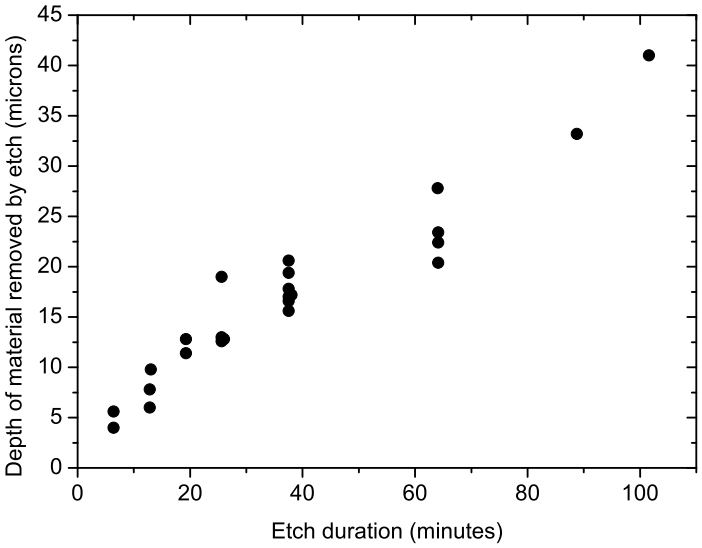


Figure 3.15: Depth of material removed by planar etch, for different etch durations. For the two longest duration specimens, the etch mixture was replaced after 65 minutes.

3.7 Determination of unlocking stress

Once specimens had been preferentially etched, the dislocation sets were measured to determine the unlocking point.

3.7.1 How specimens are measured

Specimens were viewed using an Olympus BH-2 optical microscope. Usually this was done at 200x magnification, using the microscope's calibrated graticule. The measurements made at the microscope were the total diameter of each set of dislocations, and the precise position of the outer knife-edges. In three-point bend the specimen sits in the bending jig with the top face against the outer knife-edges, and the damage they create is revealed by the preferential etch and can be easily identified under the microscope. Their position relative to the dislocation sets is measured to a precision of $\frac{1}{10}$ of the distance between dislocation sets, *i.e.* 25μm. The central knife-edge applies the load from the back of the specimen, and so does not damage the top face. Its position is inferred from the lengths of the unlocked dislocation sets later in the

process.

Due to the geometry of the specimens, two lines of dislocations intersect the surface for every dislocation set once some material is removed by planar etching. This could add uncertainty to the measuring process, since the two lines are rarely exactly the same length. The convention that had been used in previous dislocation unlocking work [253, 254] was that the diameter measured would be the distance between the outermost etch pits in either line, even if these outermost pits were isolated from the rest of the group. This convention has also been followed for this work. Starting at one end of the specimen, successive dislocation sets were measured, with the results being noted down to be analysed later.

Occasionally, dirt on a specimen obscured all or part of one or more sets of dislocations. Sometimes the dirt could be removed by briefly polishing the specimen with 'Syton' colloidal silica compound. If only one end of a dislocation set was obscured, an estimate of the total length could be made by measuring from the indent position to the visible end, and multiplying this value by two. On some occasions, however, a dislocation set diameter could not be measured. This was recorded, and its effect on the error in the final result was calculated. If this was unacceptably large, a new specimen was prepared and the experiment repeated.

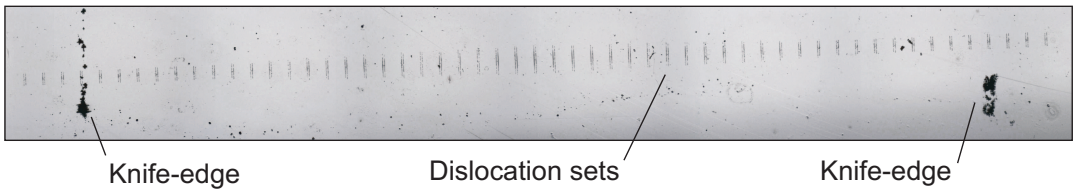
3.7.2 How unlocking stress is determined

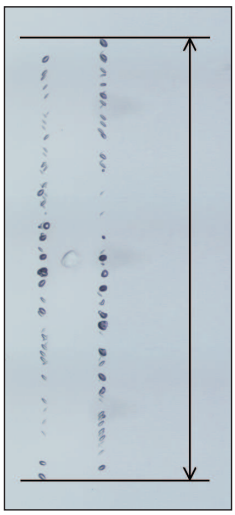
When the dislocation sets had all been measured, the data were plotted as a bar chart, as is shown in Figure 3.16. The overall shape of the chart was assessed, and the positions of the unlocking points and the central knife-edge were determined. Four lengths could then be found: the distance from the outer knife-edge to the unlocking point, and from the unlocking point to the central knife-edge, for each side of the specimen. Sometimes an unlocking point or knife-edge position could not be identified with confidence at a single set of dislocations; in these cases, a 'best guess' was made, with an appropriately large error being added to the final result.

This method differs from the way that unlocking points were determined in the past. In all previous dislocation unlocking experiments, unlocking points were iden-

Presentation of dislocation array data

Some of the work in this thesis is concerned with the detailed behaviour of dislocation unlocking specimens. These diagrams explain how dislocation data from specimens will be presented here.





Above: micrograph of the surface of a specimen after preferential etching, showing lines of etch pits from the dislocation arrays. The damage created by the outer knife-edges is also clearly visible.

Left: close-up of a dislocation set. Each dislocation set is measured individually using an optical microscope, with measurements taken from the outermost dislocations.

Below: the total lengths are plotted as a bar chart. The unlocking point can be discerned more reliably by examining this graph, rather than looking at the dislocations under the microscope.

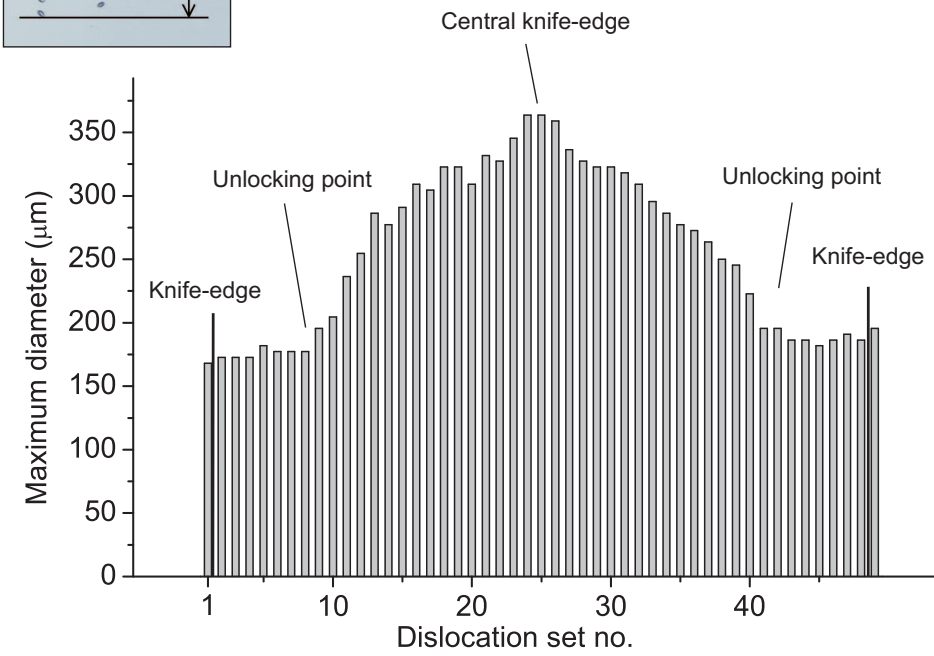


Figure 3.16: Presentation of dislocation unlocking specimen measurements.

tified under the microscope by comparing adjacent sets of dislocations. Since the microscope's field of view is limited, only 2-4 dislocation sets could be viewed at the same time, depending on the level of magnification used. The new method, illustrated in Figure 3.16, is thought to be an improvement on this, as the shape of the whole array of dislocation sets can be viewed and assessed at the same time using the bar chart of dislocation set diameters. This reduces the chance that random variation in diameters could lead to an unlocking point being misidentified.

The next stage was to measure the specimen with a screw micrometer. Measurements of thickness and width were made at both ends of specimens. These values were then used in the three-point bend stress formula described above to calculate the maximum resolved shear stress. Once this had been found, an unlocking stress could be evaluated for each side of the specimen, using the lengths measured from the specimen. The final value of τ_u was the average of these two unlocking stresses; for most specimens the difference between the two was not larger than the measurement error (see §4.5).

3.7.3 The effect of standardising three-point bend conditions

Recall that when the dislocation unlocking technique was adapted to measure nitrogen, the use of variable three-point bend conditions was introduced, as described in §2.3.2. This allowed low τ_u measurements to be made with greater precision. In this work, however, the three-point bend conditions have been standardised as described in §3.3.6, with a duration of 4 hours and a maximum stress τ_{max} of $\sim$84MPa being used (unless the effect of variation of these parameters was being explicitly investigated). The reason for this is that variation of the three-point bend duration affects the unlocking stress measured, as will be shown in §4.3.

The choice of the particular conditions used as the new standard, and the effect they have on measurement error, are described briefly here.

The choice of standardised experimental conditions

The data presented in §4.3 will show that measured unlocking stress drops as unlocking duration increases. For this reason, the short duration of 4 hours was chosen for the standard unlocking experiments, as it would give relatively large unlocking stresses, which are generally easier to measure. A secondary reason for this choice was that it would allow two experiments to be performed per day, which would speed up data collection considerably (recall that in previous work, durations of up to 60 hours were used (§2.3.2)).

The peak unlocking stress, τ_{max}, was also standardised for good experimental practice, although there was no evidence that varying it had an effect on the measured unlocking stress. The standard value was chosen in comparison with Giannattasio's nitrogen unlocking data, where the maximum unlocking stresses were ∼65MPa using similar unlocking conditions. ∼84MPa was therefore chosen to ensure that the locking stress would be exceeded in every case. Since specimens are polished to different thicknesses during specimen preparation, bending loads have to be altered accordingly to give a constant value for τ_{max}. Specimens are measured immediately after polishing, and the bending load is calculated to give 80MPa peak three-point bend stress; the actual value is slightly greater than this as the subsequent planar etch reduces the specimen dimensions slightly. This bending load is also used in the four-point bend.

The degree to which a standardised three-point bend peak stress was achieved is illustrated by Figure 3.17, a histogram of τ_{max} values for the FZ-Si specimens used in this work. This degree of uniformity is thought to be sufficient to remove any potential errors associated with variation in this parameter.

The effect of standardised conditions on measurement error

Since τ_{max} was set at ∼84MPa for every experiment, the unlocking points of specimens with $\tau_u = 10$MPa or less were close to the outer knife-edges. In addition to this, the low three-point bend duration of 4 hours meant that the first unlocked dislocations had not travelled very far in these cases, so the unlocking points were not as clear as with previous work where far longer durations were used. These two factors will

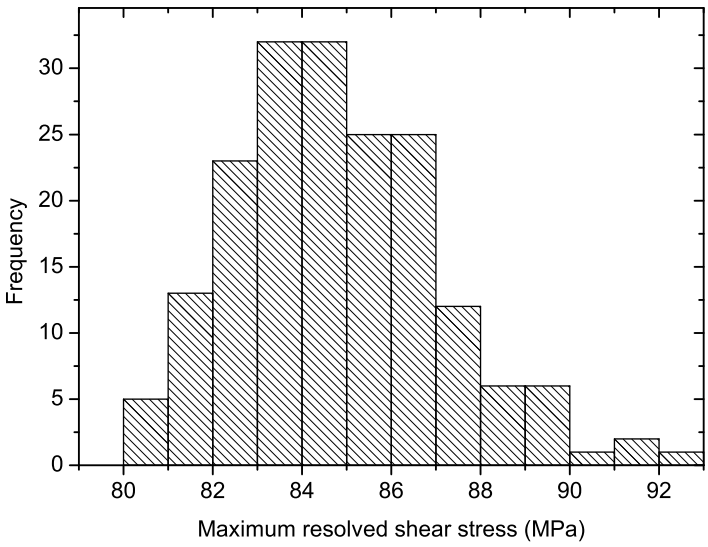


Figure 3.17: Histogram showing three-point bend τ_{max} values for the FZ-Si specimens used in this work.

unavoidably increase the measurement errors associated with low-τ_u specimens in this work. One consequence of this is that the minimum τ_u thought to be measurable under the standardised conditions is ∼6MPa, whereas with previous work this might have been 3MPa. Any specimens with less locking than this are presented as having zero locking (0MPa), and there is a potential error of up to 6MPa associated with these measurements.

3.8 Silicon used in this work

Several different types of silicon, both float-zone and Czochralski, were used in this work. All wafers were commercially grown, and of (100) orientation. Their properties are summarised in Table 3.1, and described in more detail below. For ease of reference, each type has been given a code, which is referred to throughout this thesis.

Type	Code	No. wafers	Doping (cm^{-3})	[O] ($10^{17}cm^{-3}$)	[N] ($10^{15}cm^{-3}$)	Use / Comment
FZ	Standard FZ	1	[B] = 9.6×10^{16}	< 0.1	Unknown	Thought to contain N (this work, §4.1.2)
	High-[N] 1	-	[P] = 2×10^{13}	< 0.1	2.2	Dislocation unlocking (Giannattasio [253])
	High-[N] 2	5	[P] = 1 - 2 $\times 10^{14}$	< 0.1	Variable (this work)	Nitrogen out-diffusion (§4.2)
	High-[N] 3	3	[P] = 6×10^{13}	< 0.1	2	Nitrogen dislocation unlocking
	High-[N] 4	1	Unknown	< 0.1	2.5	Nitrogen out-diffusion (§6.3)
	Low-[N] 1	1	[B] $< 1.3 \times 10^{12}$	< 0.1	0.3	Dislocation unlocking (Murphy [254])
	N-free	1	[P] $> 2 \times 10^{12}$	< 0.1	< 0.1	New N-free control (§4.1.1)
Cz	Cz 1	1	[B] = 1.5×10^{15}	6.32	< 0.1	Standard Cz
	$\overrightarrow{\text{N}}$Cz 1	1	[B] $\sim 7 \times 10^{14}$	Unknown	up to 30,000*	N-implanted (§6.1)
	$\overrightarrow{\text{N}}$Cz 2	1	[B] $\sim 7 \times 10^{14}$	Unknown	up to 200,000*	N-implanted (§6.1)
	Cz 2	1	[B] $\sim 7 \times 10^{14}$	Unknown	< 0.1	N-implant control wafer
	$\overrightarrow{\text{As}}$Cz 1	1	Unknown	Unknown	< 0.1	Arsenic-implanted (§6.2)
	$\overrightarrow{\text{As}}$Cz 2	1	Unknown	Unknown	< 0.1	Arsenic-implanted (§6.2)

Table 3.1: Properties of the different types of silicon relevant to this work. *Implanted concentrations - see Figure 3.18 for the nitrogen profiles.

3.8.1 Float-zone silicon

"Standard" FZ-Si

Standard Fz wafers were provided by Wacker Siltronic, had diameter 100mm and thickness 525μm, were mirror-polished on one side, and were p-type with [B] = 9.6×10^{16}cm^{-3} and $\rho = 0.2\Omega$cm.

Nitrogen-free FZ-Si

Nitrogen-free FZ-Si has been used as a control, being compared with NFZ-Si, in nitrogen dislocation unlocking experiments.

N-free are the control wafers described in §4.1.1, guaranteed to be nitrogen-free by the manufacturers Siltronic AG. They had diameter 100mm and thickness 525μm, were mirror-polished on one side, and were n-type with [P] $> 2 \times 10^{12}$cm^{-3} and $\rho < 2000\Omega$cm. The wafers contained defects that nitrogen normally suppresses: COPs (vacancy aggregates) from the centre to $\frac{2}{3}$ of the radius, and Lpits (interstitial aggregates) from $\frac{3}{4}$ of the radius to the edge [271].

NFZ-Si

NFZ-Si wafers have been used for nitrogen dislocation unlocking experiments. All measurements of nitrogen concentration were performed by the manufacturers, using IR absorption. Since there is no agreed calibration standard for nitrogen in silicon, measurements from different manufacturers cannot be accurately compared.

High-[N] 1 were the wafers used by Giannattasio for his nitrogen dislocation unlocking experiments, as discussed in Chapter 2. None of this material was available for the present work, but Giannattasio's results are compared to the results obtained in this thesis. The wafers, provided by Topsil Semiconductor Materials A/S, were (111) oriented, n-type with [P] = 2×10^{13}cm^{-3} and $\rho = 220\Omega$cm, and had [N] = 2.2×10^{15}cm^{-3}.

High-[N] 2 were 5 wafers used for the out-diffusion work described in §4.2, and also for the first measurements that showed the dependence of unlocking stress on three-point bend duration in dislocation unlocking experiments. They were provided

by Topsil Semiconductor Materials A/S, had diameter 100mm and thickness 500μm, were mirror-polished on one side, and were n-type with [P] = $1 - 2 \times 10^{14}$cm^{-3} and ρ = 20 - 40Ωcm. [N] was unknown but initially thought to be high, *i.e.* $> 10^{15}$cm^{-3}; however, subsequent investigation revealed that the wafers had probably been taken from different positions in the crystal ingot and so contained differing nitrogen concentrations. It was also suspected that [N] might vary radially across individual wafers. For this reason, these wafers are not considered suitable for further dislocation unlocking experiments.

High-[N] 3 were 3 wafers used for the repeat nitrogen dislocation unlocking measurements (Chapter 5). They were provided by Siltronic AG, had diameter 150mm and thickness 625μm, were mirror-polished on one side, and were n-type with [P] = 6×10^{13}cm^{-3} and ρ = 70Ωcm, and had [N] = 2×10^{15}cm^{-3}.

High-[N] 4 was a single wafer, used for variable-etch out-diffusion nitrogen dislocation unlocking measurements (§6.3). It was provided by Siltronic AG, had diameter 150mm, was not mirror-polished on either side, and had ρ = 100Ωcm and [N] = 2.5×10^{15}cm^{-3}.

Low-[N] 1 were the wafers used by Murphy for his nitrogen dislocation unlocking experiments, as discussed in Chapter 2. Repeats of some of these measurements, using this material, were also carried out in this work (§5.8.2). They were provided by Topsil Semiconductor Materials A/S, had diameter 150mm and thickness 490μm, were mirror-polished on both sides, and were p-type with [B] $< 1.3 \times 10^{12}$cm^{-3} and $\rho > 10,000\Omega$cm, and had [N] = 3×10^{14}cm^{-3}.

3.8.2 Czochralski silicon

Standard Cz-Si

Cz 1 was a wafer used in initial tests (Table 4.5), and also for the experiments measuring the dependence of unlocking stress on three-point bend duration in Cz-Si (§4.3). It was provided by MEMC Electronic Materials Inc., had diameter 200mm and thickness 740μm, was mirror-polished on one side, and was p-type with [B] = 1.5×10^{15}cm^{-3} and $\rho \sim 10\Omega$cm. [O] had been determined by FTIR as 6.32×10^{17}cm^{-3}

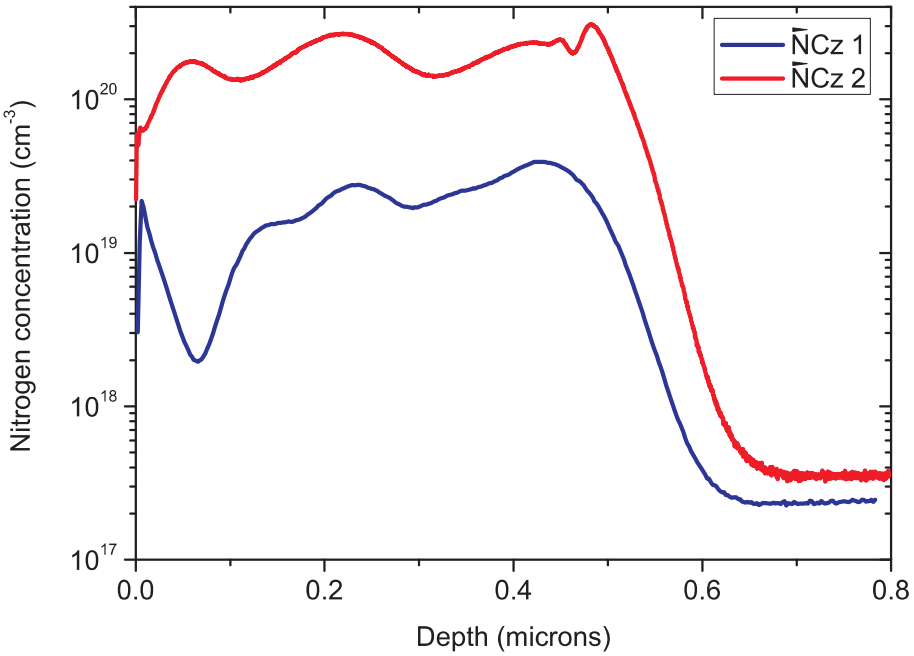


Figure 3.18: SIMS measurements of nitrogen concentration in N-implanted wafers (by Charles Evans & Associates).

(using the DIN 50438/I standard). The wafer had undergone an initial 1000°C, 15 minute anneal known as a *tabula rasa* treatment [272], which dissolved any grown-in precipitates and created a 3-4μm denuded zone at the surface.

Wafers used for nitrogen-implanted Cz-Si experiments

One set of experiments investigated dislocation unlocking in Cz-Si that had been implanted with nitrogen at very high local concentrations. These experiments are outlined in §6.1. Nitrogen-*implanted* wafers are designated as $\overrightarrow{\text{N}}$Cz, to be distinguished from NCz, nitrogen-*doped* Cz.

$\overrightarrow{\text{N}}$Cz 1, **$\overrightarrow{\text{N}}$Cz 2** and **Cz 2** were three of a matrix of nitrogen-implanted Cz-Si wafers provided by Texas Instruments Inc. They had diameter 200mm and thickness 720μm, were mirror-polished on one side, and were p-type with [B] $\sim 7 \times 10^{14}\text{cm}^{-3}$ and $\rho \sim 20\Omega$cm. [O] is not known, but was standard for Cz wafers ($\sim 10^{18}\text{cm}^{-3}$). They had been given an initial 50Å oxidation, and were then implanted with nitrogen at energies of 20, 80 and 180keV: **$\overrightarrow{\text{N}}$Cz 1** at doses of $1.20 \times 10^{14}\text{cm}^{-2}$, $3.20 \times 10^{14}\text{cm}^{-2}$ and $5.00 \times 10^{14}\text{cm}^{-2}$ respectively, and **$\overrightarrow{\text{N}}$Cz 2** at higher doses of $1.20 \times 10^{15}\text{cm}^{-2}$,

$3.20 \times 10^{15}\text{cm}^{-2}$ and $5.00 \times 10^{15}\text{cm}^{-2}$ respectively, using 5° tilt and 1.5° twist to reduce ion channeling. **Cz 2** was not nitrogen-implanted and served as the control. The effect of these staggered implants was to give an approximately square implanted nitrogen profile in the top 0.5μm of the wafers, as shown by the SIMS profiles in Figure 3.18. After implanting, the wafers were given a brief 1050°C spike anneal to spread the nitrogen and remove implant damage, and were then etched to remove the oxide layer.

Arsenic-implant experiments

Another set of experiments, described in §6.2, aimed to investigate locking by nitrogen of dislocation loops created by implant damage. They used Cz wafers (with standard [O]) that had been implanted with arsenic, designated $\overrightarrow{\text{As}}$Cz.

$\overrightarrow{\text{As}}$Cz 1 and **$\overrightarrow{\text{As}}$Cz 2** were two arsenic-implanted wafers provided by Varian Semiconductor Equipment Associates, Inc. They had diameter 200mm and thickness 720μm, and were mirror-polished on one side. They had been implanted with arsenic at 30keV at a dose of $5 \times 10^{15}\text{cm}^{-2}$, using 7° tilt and 22° twist. After implantation a 1050°C spike anneal had been performed on the wafers.

Chapter 4

Characterization of the dislocation unlocking experimental method

This chapter is concerned with a characterization of the dislocation unlocking technique, and an investigation of errors which may arise. New nitrogen results are presented here briefly and compared to previous work [253,254]; these new results are presented more fully and discussed in detail in Chapter 5.

4.1 Control experiments

4.1.1 Nitrogen-free control

To ensure that nitrogen is producing the dislocation locking effect in NFZ-Si, nitrogen-free specimens have been tested using the standard dislocation unlocking technique (with three-point bends of ∼84MPa for 4 hours). The wafers, designated **N-free** (N-type, (100) orientation, $\rho < 2000\Omega$cm), were confirmed to be nitrogen-free by the manufacturers Siltronic AG. They contained interstitial- and vacancy-related defects, which nitrogen normally suppresses. Specimens were taken from two regions of the wafers: a thin defect-free band, and a region that contained vacancy-related defects, which were 'crystal originated pits' - octahedral voids typically 150nm in diameter

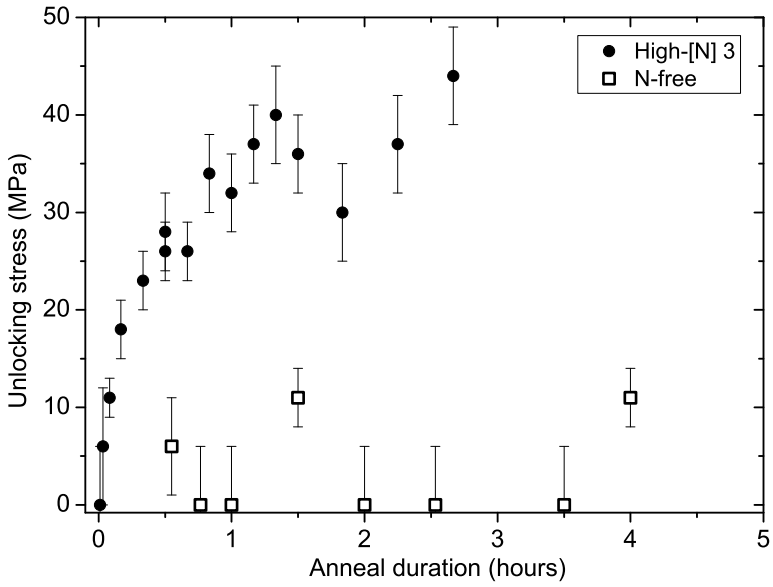


Figure 4.1: Dislocation unlocking stresses measured at 550°C, with anneals at 675°C. Shown are High-[N] 3 NFZ-Si, and the nitrogen-free control silicon, N-free.

[273]. Another region that contained interstitial-type defects was not used. The results of dislocation unlocking measurements using this material, with anneals at 675°C, are shown in Figure 4.1, along with measurements taken using NFZ-Si High-[N] 3 for comparison. It can be seen that there is no significant dislocation locking effect in the nitrogen-free control.

4.1.2 Transition metal control

Since dislocation unlocking experiments are not carried out under clean-room conditions, it is possible that specimens become contaminated with impurities other than nitrogen, which may be partially or entirely responsible for the dislocation locking effect. One possibility for alternative locking agents to nitrogen was transition metals, since such impurities could be introduced during specimen preparation or four-point bend.

The dislocation unlocking procedure could not be modified to remove all contact with metal. The most likely sources of contamination are the molybdenum bending jig and knife-edges, which are in contact with the specimen at elevated temperature during the four-point bend stage, prior to the anneal. Molybdenum has a low solubil-

	Copper	Iron	Nickel
15 minutes	3700	350	140
30 minutes	5200	490	200
45 minutes	6400	600	240
60 minutes	7400	700	280

Table 4.1: Approximate diffusion length $x = 2\sqrt{Dt}$, in microns, for copper, iron and nickel in silicon at 675°C for various anneal durations. The dislocations in specimens have a maximum depth of approximately 100μm during the anneal stage.

ity in silicon [274], but the pieces are not completely pure Mo and are likely to contain other metals. Since specimens could not be tested in metal-free conditions, the opposite approach was used: large amounts of metal contamination were deliberately introduced, to see if this would introduce significant extra locking.

The silicon used for this test was a **'Standard' FZ** wafer, which is believed to contain nitrogen, as described below. Specimens were prepared as per the standard technique, with indentation and four-point bending to create a dislocation array. After this, the whole of the top face of each specimen was rubbed with pieces of copper, iron and nickel (highly soluble, fast-diffusing elements which are usually the most significant metal contaminants in silicon devices [275]) before annealing at 675°C. Specimens were then planar etched, and unlocked at 550°C for 4 hours with τ_{max} ~85MPa. The metal rubbing procedure scratched the specimen surfaces considerably, but it was found that this damage was smoothed enough by the standard planar etch to avoid dislocation nucleation or specimen breakage during the three-point bend.

Table 4.1 shows the distances that the metal elements would be expected to diffuse in silicon for the 675°C anneals which were used. The distances are calculated using the approximation $x = 2\sqrt{Dt}$ [276], with values for D taken from a standard reference [277]. It can be seen that the three impurities move far enough to significantly affect the regions around the dislocations during the anneal; all move much deeper than the 20μm planar etch, even for the shortest duration anneal.

The results from the experiments are shown in Figure 4.2. Far from increasing the locking strength, the metal contamination seems to have resulted in a lower dislocation unlocking stress. The reason for this is unknown, but it could be that the metals interact with nitrogen in such a way as to reduce its dislocation locking capacity. A

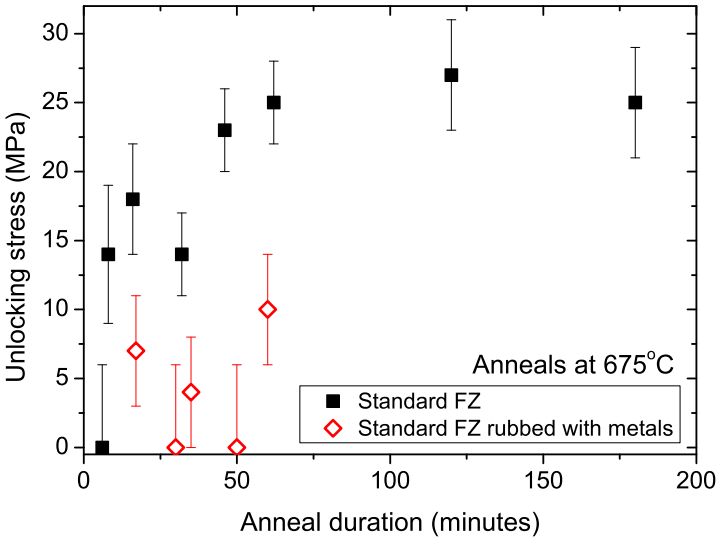


Figure 4.2: Dislocation unlocking stress measured at 550°C in 'Standard' FZ after anneals at 675°C, for uncontaminated specimens and specimens that had been rubbed with different metals prior to annealing.

search of the literature has not found any previous reporting of this effect.

Dislocation locking effect in 'Standard' FZ silicon

The results from the uncontaminated 'Standard' FZ silicon are presented again in Figure 4.3, along with results taken using High-[N] 3 NFZ-Si. It is noted that the 'Standard' FZ, while not being explicitly described by the manufacturers as containing nitrogen, nevertheless produces a dislocation locking effect that is comparable with that seen in NFZ-Si. Discussions with manufacturers have confirmed that this is likely to be the case: nitrogen doping of FZ-Si has been common practice since the 1990s [271]. Experimenters should therefore be aware that any FZ-Si manufactured recently may contain sufficient nitrogen to produce a significant dislocation locking effect, even if no nitrogen is mentioned in the product specification.

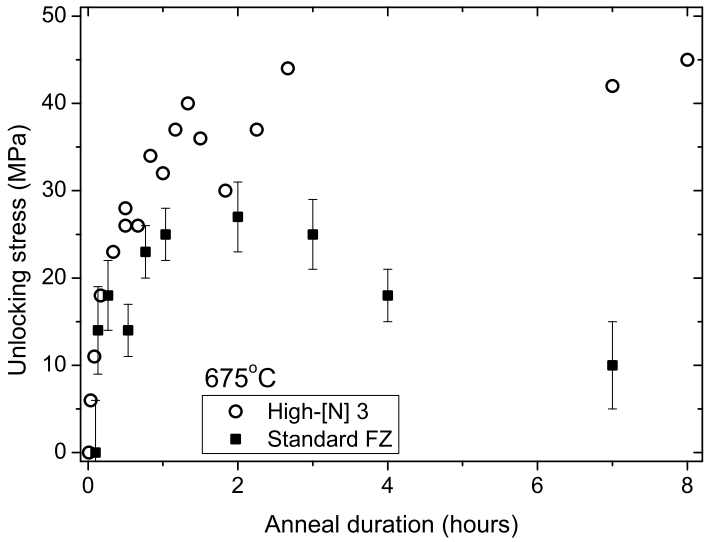


Figure 4.3: Dislocation unlocking stress measured at 550°C in 'Standard' FZ after anneals at 675°C, with results taken under the same conditions for 'High-[N] 3' NFZ-Si.

4.1.3 Instron performance

Figure 4.4 shows the bending apparatus used for dislocation unlocking experiments. The bending rig is mounted on the crossbeam of an Instron 1195 mechanical testing machine, which can be used to apply the loads in the four- and three-point bends. This was done by Senkader, whose Cz-Si tests regularly used loads of more than 100N, and also Giannattasio for the high-[N] NFZ-Si work. Murphy's low-[N] experiments required loads of less than 20N, and it was suspected that the Instron's load cell might not be sufficiently accurate in this low range. These experiments were therefore carried out using free weights to apply the load, a method more likely to be accurate.

Test experiments have been performed, using the Instron to apply the load for four- and three-point bends. The difference in the machine's load calibration between the start and the end of each bend was recorded, and these results are presented in Figure 4.5. The loads applied in these tests ranged from approximately 20 to 100N[1]. The results show that the Instron's calibration does change slightly while in use, to a degree that is significant for low-load dislocation unlocking experiments.

[1]It should be noted that the Instron's manual recommends that only loads greater than 1% of the load cell's capacity should be used [278]. The capacity is 5000N, so in some cases the machine was being operated outside its recommended conditions.

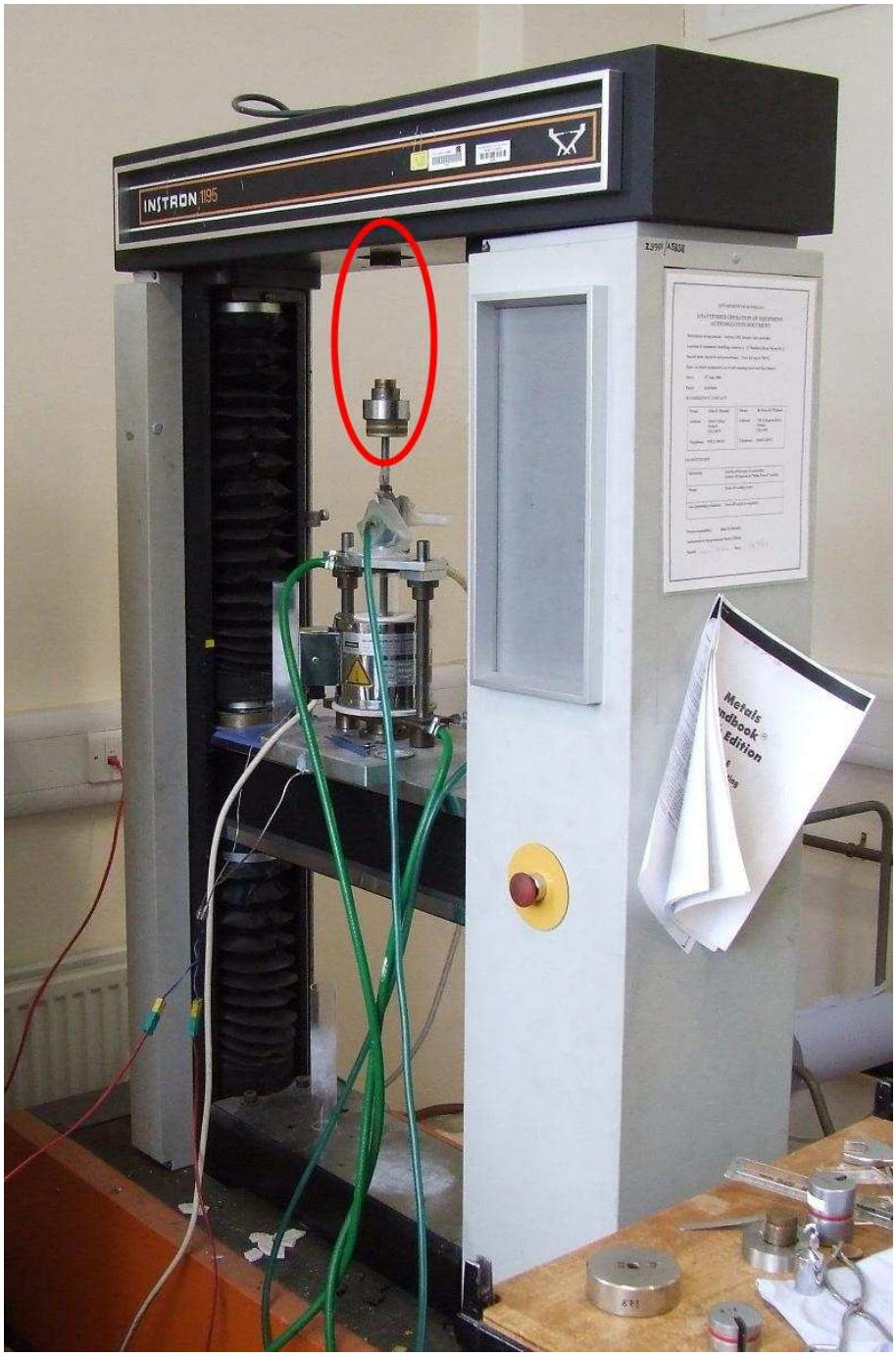


Figure 4.4: The bending rig, mounted on the Instron 1195 mechanical testing machine. Circled in red are the loading rod and the load cell attachment point (load is being applied using free weights). The rig is described in detail in Chapter 3.

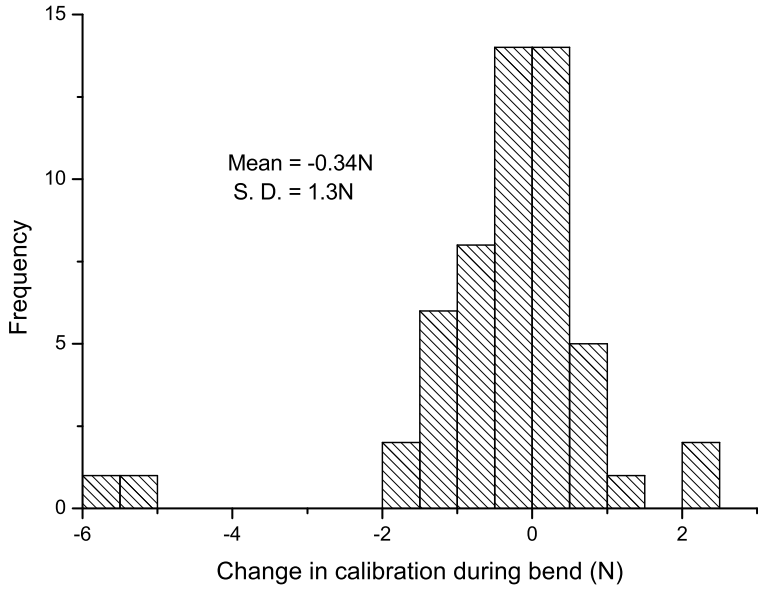


Figure 4.5: Change in Instron calibration for each bend performed during initial tests.

Another test of the Instron was also performed. The machine was switched on, with nothing attached to the load cell, and the load output was monitored. This was done twice, and the results are shown in Figure 4.6. In these tests the calibration wandered slowly with time, as had been recorded previously. However, one of the tests also revealed sharp 'spikes' in the output, of several Newtons. If translated into real load spikes in a bend test these could introduce significant error, as a short load spike could unlock dislocations which would then continue to move even when the load dropped again. The calibration drift and load spikes may have been responsible for some of the random error in Senkader and Giannattasio's dislocation unlocking measurements. For this reason, all the NFZ-Si experiments in this thesis were performed using free weights to apply the load.

4.2 Results from High-[N] 2 silicon

This section outlines the results taken using '**High-[N] 2**' NFZ-Si. The material was intended to be used to extend the work on nitrogen out-diffusion, which is described in §6.3. Other experiments which used High-[N] 2, also described in this section, investigated aspects of the dislocation unlocking technique itself.

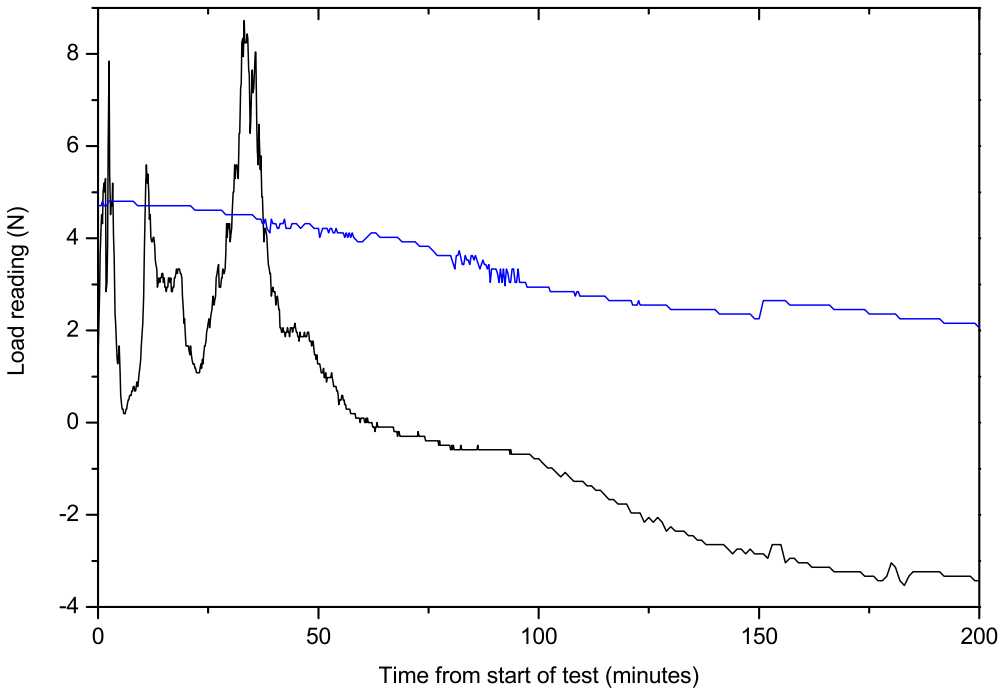


Figure 4.6: Two Instron load output tests. The machine was switched on, with nothing attached to the load cell, and the load output was monitored.

4.2.1 Pre-anneal experiments to measure nitrogen out-diffusion

Specimens from one set were given pre-anneals in order to investigate the effect of nitrogen out-diffusion on dislocation locking. This was intended to work as follows. The pre-anneal would be used to create an out-diffusion profile in the specimen, with regions near the surface being denuded of nitrogen. The subsequent dislocation unlocking procedure (with a Regime 2 anneal) would then reveal whether or not nitrogen had left the specimen in significant amounts: if standard Regime 2 unlocking stresses were measured then it could be concluded that nitrogen was still present, whereas if τ_u was lower than this, nitrogen must have either left the specimen during the pre-anneal, or been immobilized in some way. The pre-anneal duration should therefore affect the measured unlocking stress, with short pre-anneals giving standard Regime 2 stresses, and longer pre-anneals giving lower or zero τ_u.

Initial experiments were performed with High-[N] 4 silicon, of which only a small

Pre-anneal		Main anneal		Unlocking stress (MPa)
Temperature (°C)	Duration	Temperature (°C)	Duration	
1000	24 hours	640	48 hours	< 10
1000	24 hours	640	48 hours	< 10
1000	24 hours	640	48 hours	0
750	15 hours	750	15 hours	< 20
750	15 hours	750	15 hours	< 6
750	15 hours	750	15 hours	< 6

Table 4.2: Pre-anneal nitrogen out-diffusion results using High-[N] 4 NFZ-Si. The main anneals would be expected to give an unlocking stress of ∼50MPa in standard experiments.

Pre-anneal		Unlocking stress (MPa)
Temperature (°C)	Duration	
750	1 hour	0
750	1 hour	0
750	5 minutes	3
750	5 minutes	3
600	2.7 hours	9
600	1.2 hours	13
600	45 minutes	10
600	30 minutes	9
600	15 minutes	10
600	7 minutes	14
500	1 hour	0
500	20 minutes	7
500	7 minutes	0

Table 4.3: Pre-anneal nitrogen out-diffusion results using High-[N] 2 NFZ-Si. The second anneal was 48 hours at 750°C for each specimen.

amount was available, to test the feasibility of the new technique. The results, shown in Table 4.2, showed that large pre-anneals did indeed reduce the unlocking stress (measured at ∼50MPa in standard experiments with this material). With the technique having been shown to be successful, experiments were then performed using the High-[N] 2 silicon. In these experiments the second anneal was standardised at 750°C for 48 hours, with pre-anneals of varying durations at different temperatures being used. The results of these experiments are displayed in Table 4.3.

These High-[N] 2 results are inconsistent. Note, for example, that the 500°C pre-anneals represent a lower thermal budget than the four-point bend in the standard technique, yet they seem to have caused a complete loss of locking strength.

At the same time as these results were being collected, work was also being car-

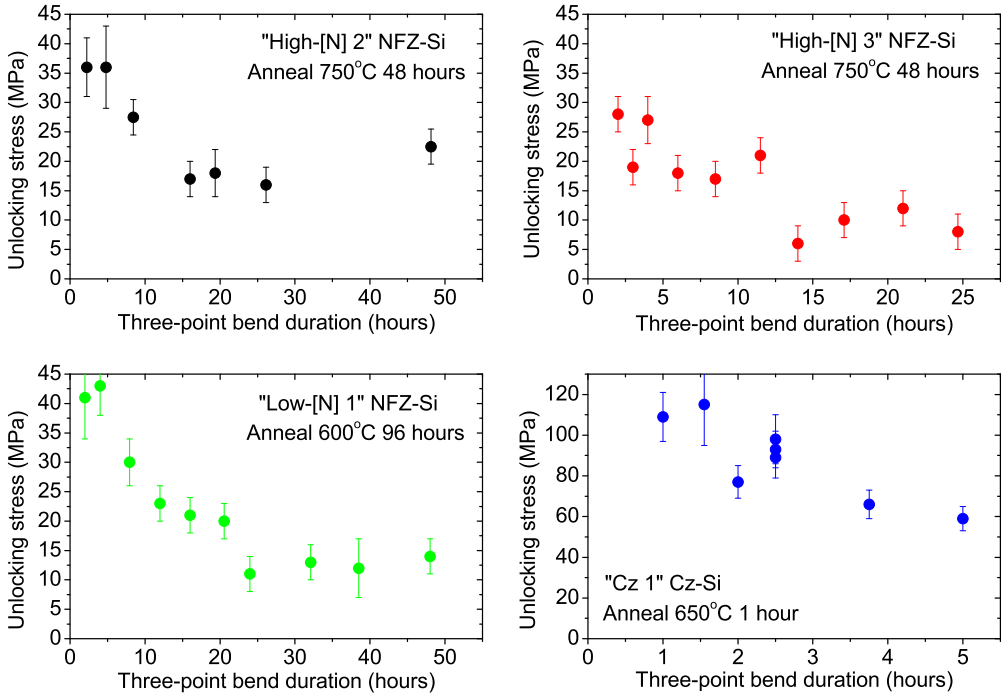


Figure 4.7: Variation of unlocking stress (at 550°C) with three-point bend duration for High-[N] 2 NFZ-Si and three other types of silicon.

ried out to investigate the dislocation unlocking technique itself, and some of this is described below.

4.2.2 Dependence of unlocking stress on three-point bend duration in High-[N] 2 NFZ-Si

Recall that when the dislocation unlocking method was adapted to measure nitrogen locking, the only change was that three-point bend conditions were altered on an experiment-by-experiment basis, to increase the sensitivity of the technique. The effect of variation in three-point bend duration on the unlocking stress has been measured using High-[N] 2 silicon. The results are displayed in Figure 4.7. They show that unlocking stress is dependent on three-point bend duration, falling as the duration increases.

4.2.3 Nitrogen content of High-[N] 2 wafers

While the dependence of the unlocking stress on the three-point bend duration was an interesting effect, it could not account for the results found in the pre-anneal nitrogen out-diffusion experiments. However, after eight months of experiments with High-[N] 2 silicon, increasing concerns about the lack of reproducibility of the results led to work with this material being halted. Discussions with the manufacturers of the silicon subsequently revealed that it could not be guaranteed that the High-[N] 2 wafers had been taken from adjacent positions in the crystal ingot. It is possible that some of the wafers had been taken from the end of the ingot, where [N] was varying quickly as a function of position. This effect would account for the lack of reproducibility in the results obtained using this material. For this reason, these wafers are thought to be unsuitable for further dislocation unlocking experiments, and no further attempt was made to analyse the measurements from this material.

4.3 Relationship between three-point bend duration and unlocking stress in uniform material

4.3.1 Experimental results

The experiments which showed the dependence of unlocking stress on three-point bend duration were repeated with different types of silicon, whose N or O content had been specified by the manufacturer (§3.8). Measurements were made using 'High-[N] 3' NFZ-Si ([N] = $2 \times 10^{15}\text{cm}^{-3}$), 'Low-[N] 1' NFZ-Si ([N] = $3 \times 10^{14}\text{cm}^{-3}$), and 'Cz 1' ([O] = $6.32 \times 10^{17}\text{cm}^{-3}$). The results are shown in Figures 4.7 and 4.8. The dependence of dislocation unlocking stress on three-point bend duration is present in all types of silicon tested, with τ_u decreasing as the duration increases. The effect exists both with NFZ-Si (nitrogen locking) and Cz-Si (oxygen locking), although in the latter case durations longer than 5 hours could not be measured, as specimens would break.

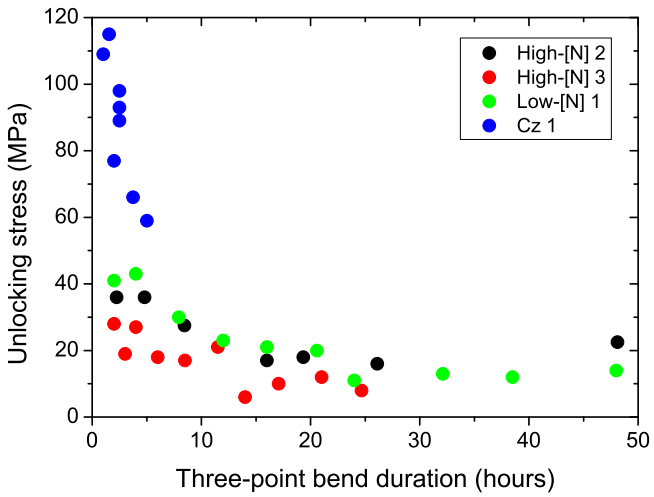


Figure 4.8: Variation of unlocking stress (at 550°C) with three-point bend duration for three types of NFZ-Si and one of Cz-Si. The data plotted are the same as Figure 4.7.

4.3.2 Analysis

Theory of dislocation release from pinning points

The drop in unlocking stress with increasing three-point bend duration can be understood in terms of the theory of release of dislocations from pinning points [233, 234]. If it is assumed that the interaction between the pinning points and the dislocation is of a short-range nature, and the pinning points are arranged discretely, then the releasing rate Γ of the dislocation is given by the theory of thermal activation as:

$$\Gamma = LN\nu \exp\left[-(E - \tau b^2/N)/k_b T\right] \tag{4.1}$$

where L is the length of the dislocation, N is the line density of the pinning points, ν is the frequency of dislocation vibration, E is the maximum interaction energy of the pinning point and the dislocation, τ is the applied stress, and b is the magnitude of the dislocation's Burgers vector.

Rearranging gives the unlocking stress, τ_u, as:

$$\tau_u = N\left[E - k_b T \ln(LN\nu/\Gamma)\right]/b^2 \tag{4.2}$$

	Low-[N] 1	High-[N] 2	High-[N] 3	Cz 1
N	$1.4 \times 10^8 \mathrm{m}^{-1}$	$8.8 \times 10^7 \mathrm{m}^{-1}$	$9.4 \times 10^7 \mathrm{m}^{-1}$	$4.3 \times 10^8 \mathrm{m}^{-1}$

Table 4.4: Values for the line density of pinning points along dislocations, inferred from the variation of unlocking stress at 550°C with three-point bend duration, for different types of silicon.

If the releasing rate Γ is thought of as a reciprocal 'unlocking time', $\frac{1}{t}$, then Equation 4.2 predicts that τ_u will fall off as this time increases, in broadly the same way as is seen in the data. Rearranging further gives the expression:

$$\tau_u = \frac{NkT}{b^2} \ln \Gamma + \frac{N}{b^2}[E - kT \ln(LN\nu)] \tag{4.3}$$

A plot of τ_u against $\ln \Gamma$ should therefore give a straight line, with gradient $\frac{NkT}{b^2}$. Such plots are shown in Figure 4.9, for the four sets of data taken with different types of silicon. The values of N, the line density of the pinning points, obtained from the gradients of these graphs are shown in Table 4.4. They show that nitrogen pinning points are separated by approximately 10nm in the three types of NFZ-Si, and 2.3nm for oxygen in Cz-Si. While the expression given in Equation 4.1 is only an approximation, these results do give an indication that locking in all these materials is by atoms rather than precipitates. It is also interesting that the pinning point line density and the absolute values of dislocation locking stress in Cz 1 are both about 4 times greater than the corresponding values for the three types of NFZ-Si. This indicates that the dislocation locking strength of nitrogen atoms is similar to that of oxygen atoms.

Conclusion

It is clear that changing the three-point bend duration in dislocation unlocking experiments can alter the measured unlocking stress considerably. This effect is significant: it will be shown in the next chapter that the variable three-point conditions used by Giannattasio and Murphy contributed to a systematic error in their measurements. The dislocation unlocking technique in this work has therefore been standardised to use the same three-point bend conditions for every test, as described in the previous

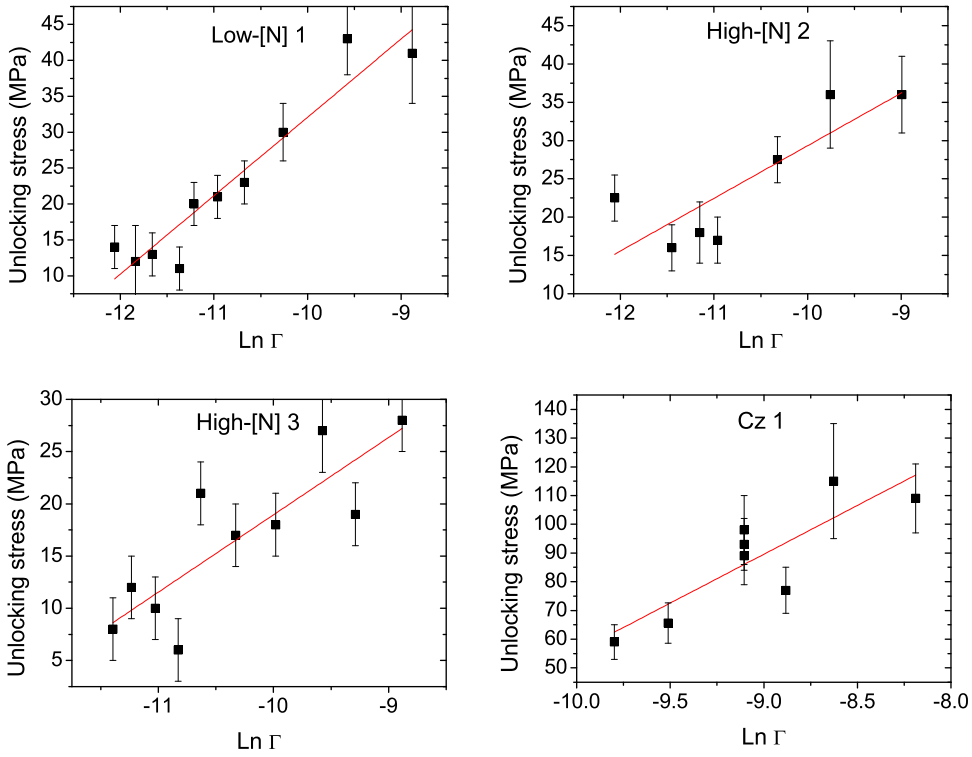


Figure 4.9: Unlocking stress measured at 550°C plotted against ln Γ, where $\Gamma = \frac{1}{t}$ and t is the three-point bend duration, in seconds. Results for four types of silicon are displayed: the data are the same as those shown in Figure 4.8.

chapter. All further results presented in this thesis have been taken in this way, unless it is explicitly mentioned otherwise.

4.4 Summary of characterization experiments

This chapter has described control experiments that have been carried out in an attempt to improve the understanding of and characterize the dislocation unlocking technique, in these ways:

- Measurements made using nitrogen-free FZ-Si found no locking stress, providing strong evidence that nitrogen is the dislocation locking agent in the NFZ-Si experiments.

- Transition metal contamination has been found to give no extra dislocation locking effect; indeed, the presence of transition metals has been shown to reduce

the locking strength of nitrogen in NFZ-Si.

- Experiments using 'standard' FZ-Si have found that it exhibits a dislocation locking effect comparable with that seen with nitrogen in NFZ-Si. Experimenters are warned that any float-zone silicon made since the 1990s may contain significant amounts of nitrogen.

- The Instron mechanical testing machine used in previous dislocation unlocking work has been tested and found to be unsuitable for low-load experiments, as its load output is not sufficiently stable.

- Initial tests have indicated that measurements using pre-annealed silicon could be used to investigate out-diffusion of nitrogen; however, further experiments using different wafers were unsuccessful, as this material did not contain a homogenous nitrogen distribution.

- The effect of variation of three-point bend duration on measured τ_u has been investigated; it is found that τ_u decreases with increasing unlocking duration. As will be discussed in the next chapter, this result has important implications for previous nitrogen experiments, where the unlocking duration was varied on a specimen-by-specimen basis. Analysis of these results in terms of the theory of release of dislocations from pinning points shows that NFZ-Si specimens have a pinning point line density of approximately $10^8 \mathrm{m}^{-1}$, giving an indication that dislocation locking is by atomic impurities.

These control experiments have resulted in the development of a slightly altered dislocation unlocking technique, which was outlined in the previous chapter. The next chapter describes repeats of previous nitrogen dislocation unlocking experiments that have been performed using this improved method. The errors associated with these measurements are outlined in the section below.

4.5 Errors in dislocation unlocking experiments

4.5.1 Quantifiable error

Detailed estimates of the error associated with dislocation unlocking experiments have already been made elsewhere. It was mentioned in §2.4.2 that Murphy's analysis gave a maximum percentage error of ±25% for any given dislocation unlocking specimen. For this work, quantifiable errors have been thought of in two groups: the combined error associated with the experimental process, and the uncertainty associated with the determination of the unlocking point for each individual specimen.

Combined procedural errors

The greatest potential error in dislocation unlocking experiments is thought to be that associated with anneal and unlocking temperatures, as identified by Murphy (§2.4.2). Other sources of error, thought to be smaller or negligible, are:

- Misalignment of the crystal [110] direction with the long axis of the specimen
- Error in anneal duration
- Error in three-point bend duration
- Error in three-point bend load
- Uneven application of load (*e.g.* if knife-edges are not sufficiently flat)
- Error in mechanical measurement of specimen dimensions
- Underestimation of specimen dimensions due to action of preferential etch, which is also planar to a small degree. Measurements are taken after the preferential etch, and so are slightly too small

The errors associated with these factors are insignificant compared to other error sources, and so have been neglected.

Determination of unlocking stress

The method used to determine unlocking stress was outlined in §3.7. Since the dislocation sets in specimens are discrete, separated by 250μm, an unlocking stress can only be known to a certain relative precision. In the best case the unlocking point can be clearly identified as being between two neighbouring sets of dislocations, one of which has unlocked, and the other not. The unlocking point is then chosen as the midpoint between these two sets[2], with an error large enough to cover the distance to the sets - about $\pm 2\%$ of τ_{max}, the maximum stress. If the unlocking position is not as clear as this, however, the uncertainty will be greater.

Since this error is a fraction of the maximum stress τ_{max}, it is of greater relative size for specimens with low values of τ_u if the same τ_{max} is used for all measurements. This value is used for the nominal error on each result. However, other aspects of the experimental system mean that this can sometimes underestimate the total error in dislocation unlocking measurements.

4.5.2 Other errors

It has already been noted that the experimental system is not completely understood (see, for example, the discussion about the unlocking discontinuity in §2.4.3). It has been assumed in the analysis of the experiments that locking and unlocking of dislocations are regular processes, but this may not be true. Dislocation unlocking experiments are sensitive to the least-strongly locked parts of dislocations, which move at lower stresses than other parts. If the degree of locking at a dislocation is non-uniform, this could add a degree of random error to the measurements.

Another possibility is that the locking impurity concentration, in this case nitrogen, is not distributed homogenously throughout silicon wafers. Specimens from different wafers, or different areas of the same wafer, would show different dislocation locking strengths according to the amount of nitrogen they each contained. This is al-

[2]It should also be noted that in all previous dislocation unlocking work, the unlocking point of a specimen was taken as the position of the first set of unlocked dislocations, rather than the mid-point between the first unlocked and last locked sets. This means that results in this work are about 2% smaller, overall, than they would have been using the old method. This is not problematic as the old and new results are not compared quantitatively.

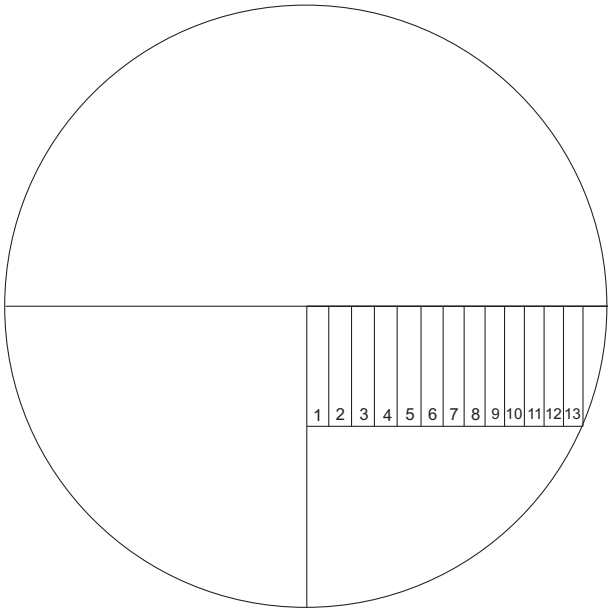


Figure 4.10: Pattern of specimens cleaved from High-[N] 3 wafer for a radial dislocation locking consistency test.

ready known to have affected some experiments, as described in §4.2. To test whether this would also affect the repeat NFZ-Si nitrogen dislocation unlocking experiments, which are described in the next chapter, one of the 'High-[N] 3' wafers was measured.

4.5.3 Measurements of the reproducibility of locking

Nitrogen distribution across a High-[N] 3 wafer was checked by taking specimens from the centre of the wafer to the edge, in the pattern shown in Figure 4.10, and performing identical dislocation unlocking tests. This served both to measure the reproducibility of dislocation unlocking measurements, and to check the wafer for potential nitrogen out-diffusion from the silicon ingot, which would leave the outer areas denuded of nitrogen. The specimens were annealed at 800°C for 17.5 hours in a standard furnace, and unlocked by three-point bend at 550°C for a 4 hour duration, with a maximum stress of ∼87MPa.

The results are presented in Figure 4.11. They show that unlocking stress does not fall off except possibly at the very edge of the wafer, meaning that out-diffusion of nitrogen has not occurred on a large scale. However, the scatter in the rest of the data is considerable, and is not accounted for by the errors calculated from measurement

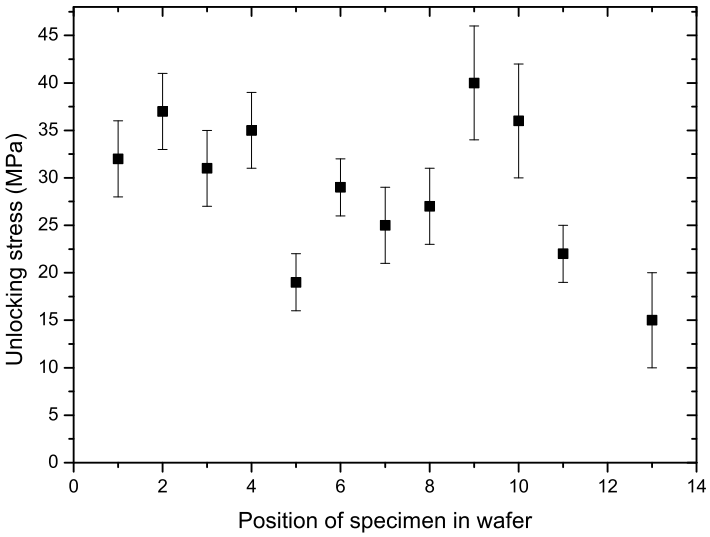


Figure 4.11: Unlocking stress measured at 550°C for a High-[N] 3 NFZ wafer tested at different positions (numbered as shown in Figure 4.10). The anneal was 17.5 hours at 800°C.

uncertainty (displayed for each data point). For these specimens, therefore, another source of random error was present.

This has not been the case with all dislocation unlocking work. Figure 4.12 shows typical results collected by Senkader for oxygen locking in Cz-Si [32], which contain minimal scatter, showing that dislocation unlocking experiments can have far less random error if the material used allows.

4.5.4 Summary

While it is possible to calculate the 'known' errors associated with dislocation unlocking measurements, results indicate that these are sometimes overshadowed by the lack of reproducibility, which cannot be quantified except by the scatter produced. Error bars will be displayed on some of the data; these largely reflect the uncertainty in the determination of the unlocking point for each specimen. They should be viewed only as an indication of the relative trustworthyness of results in this respect, rather than an expression of the accuracy of each measurement.

The scatter that exists in the results is important as it puts a limit on the usefulness

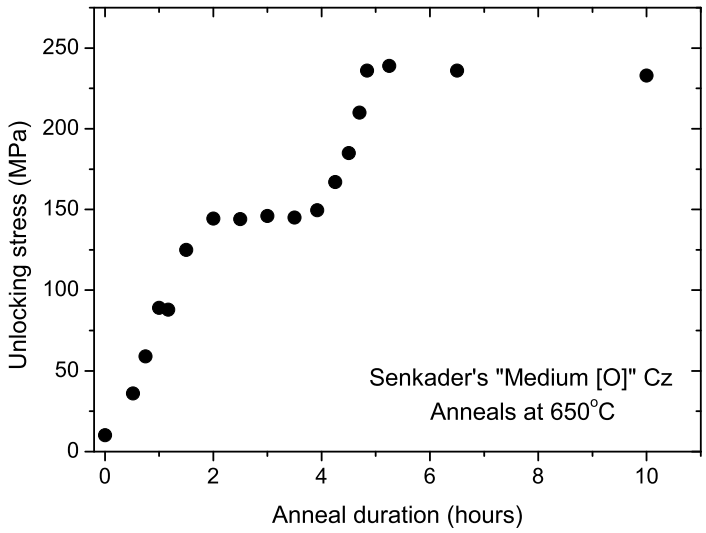


Figure 4.12: Oxygen dislocation unlocking stress measured at 550°C by Senkader, for Cz-Si with [O] = 6.3×10^{17}cm^{-3} which had been annealed at 650°C [32].

of the data. This can best be seen by looking at examples. It is noted in §5.1.1 that the new NFZ-Si 600°C anneal results seem to show a 'stepped' Regime 2 shape, not unlike that seen at the onset of precipitation in previous Cz-Si work. However, the data cannot justifiably be used to support this conclusion: the 'stepped' shape could just be a product of random error. On the other hand, the differences in Regime 2 saturation stresses at different anneal temperatures in the new data, discussed in §5.3.1, are large enough that they can be clearly identified, despite the scatter that is present.

Chapter 5

Dislocation unlocking experiments using NFZ silicon

New dislocation unlocking experiments using NFZ-Si, some of which were briefly presented in Chapter 4, are described and discussed in this chapter. Unless otherwise mentioned, all results are obtained using 'High-[N] 3' NFZ-Si, which has [N] = $2 \times 10^{15}\text{cm}^{-3}$. The nitrogen dislocation unlocking data will be presented and analysed first with respect to the Regime 1 behaviour (which gives information about nitrogen transport), and then the Regime 2 behaviour (which arises when transport to the dislocations is no longer the dominant factor controlling locking). Regime 1 gives information about the diffusivity of the locking impurity: for nitrogen in this work, this will be referred to throughout as the *effective diffusivity*, since it is believed that the dissociative mechanism may be responsible for nitrogen transport. Also presented and discussed are measurements of dislocation velocity inferred from dislocation movement during three-point bending.

5.1 Nitrogen transport investigated by dislocation unlocking

5.1.1 Nitrogen dislocation unlocking results

The dislocation unlocking technique described in Chapter 3 has been used to investigate nitrogen's behaviour at anneal temperatures of 500, 600, 675, 750, 825 and 900°C, for anneal durations of 0 - 5066 hours. These results are shown in Figure 5.1. Regime 1 was evident at 500, 600, 675 and 750°C; at the higher temperatures, it could not be seen as the available annealing methods were too slow.

Senkader's dislocation unlocking experiments in Cz-Si, measuring oxygen locking, found extra regimes which were a consequence of the onset of oxygen precipitation at dislocations (as shown in Figure 2.2) [32]. The previous NFZ-Si dislocation unlocking work by Giannattasio and Murphy, measuring nitrogen locking, only saw the first two regimes [253, 254]. This is also generally the case with the new data presented above, although the 600°C results do recall the double-step shape to some extent. Since this is only seen at one temperature, it is not possible to tell whether it is a real effect or an artefact created by random error.

5.1.2 Activation energy for the dislocation locking process

In Regime 1, the dislocation unlocking stress rises approximately linearly with anneal time, as impurity atoms diffuse to and pin dislocations. If dislocation locking is by an atomic species, the Regime 1 gradient $\frac{d\tau_u}{dt}$ is proportional to the background impurity concentration, C_0, and the diffusion to the dislocation core, D. This is a thermally activated process, so:

$$\frac{d\tau_u}{dt} \propto C_0 D \propto C_0 \exp\left(-\frac{E_A}{kT}\right) \tag{5.1}$$

where E_A is the activation energy for the dislocation locking process, and T is the anneal temperature. E_A can therefore be measured directly from the dislocation unlocking data shown in Figure 5.1.

The Regime 1 gradients for the data in Figure 5.1 are shown in an Arrhenius plot

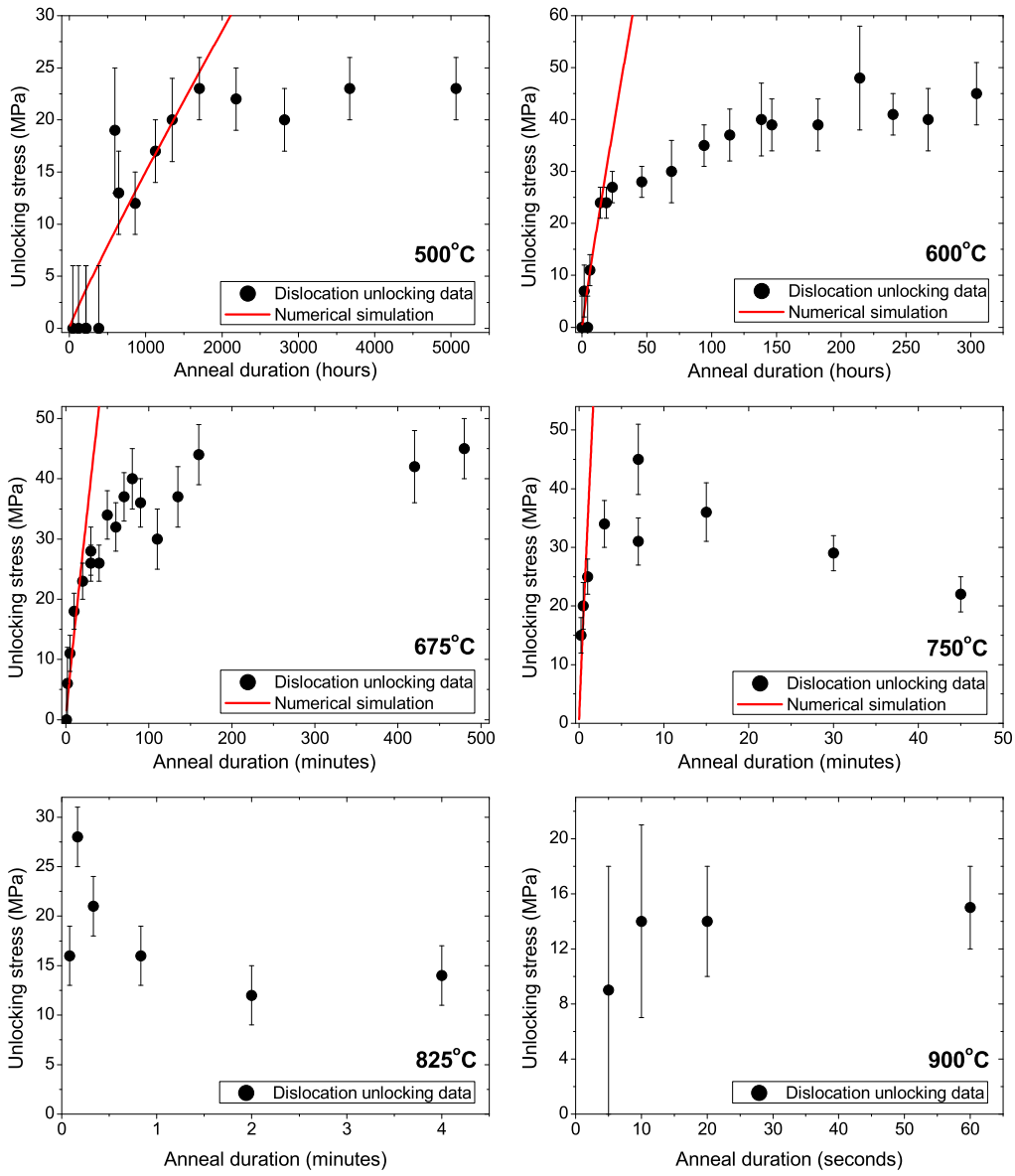


Figure 5.1: Dislocation unlocking stress measured at 550°C in 'High-[N] 3' NFZ-Si, at different anneal temperatures. The numerical simulations of Regime 1, also presented here, are discussed in §5.1.3.

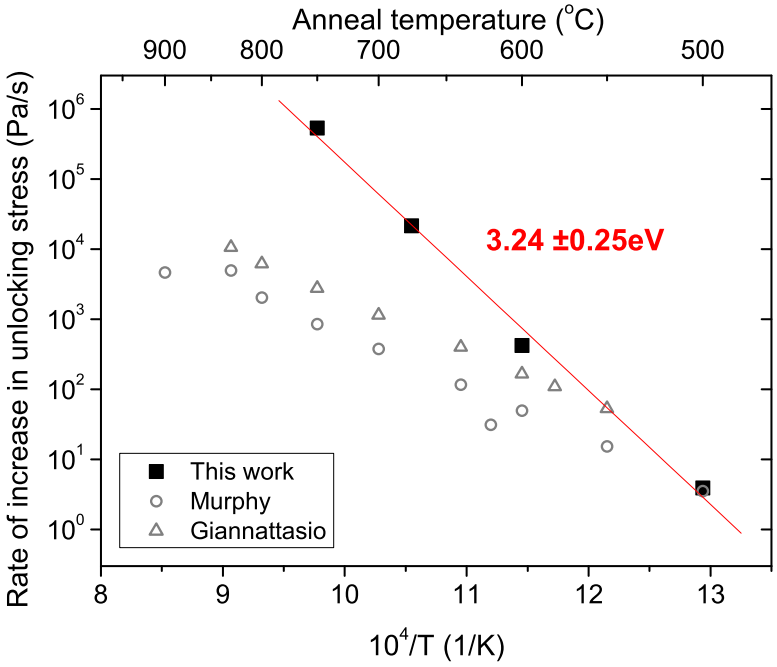


Figure 5.2: Regime 1 gradients found from dislocation unlocking experiments in this work, and also by Giannattasio [253] and Murphy [254].

in Figure 5.2, along with those found by Giannattasio and Murphy. The difference between the data sets can be seen clearly. The activation energy for the dislocation locking process, E_A, is found to be 3.24eV for the new data, with an error of $\pm$0.25eV.

E_A can be directly measured from Regime 1 in dislocation unlocking experiments. It is related to the more fundamental quantity, the activation energy of nitrogen's effective diffusivity. If transport to dislocations is by the majority species, which for nitrogen is the dimer, then E_A is the same as the activation energy for its diffusion. If dislocation locking is by another species, however, then more analysis is required (§5.2.3).

5.1.3 Modelling Regime 1 to find nitrogen's effective diffusivity

For the complete expression for nitrogen's effective diffusivity to be found, the diffusivity pre-factor must be calculated. This has been done using a modelling program, which was initially developed by Senkader to model oxygen's behaviour in Cz-Si dis-

location unlocking experiments [32]. The program, which is summarised here and explained in detail in Appendix A, models the system by simulating diffusion of impurities to a dislocation from a surrounding cylindrical region, and also capture by and re-emission from the dislocation core. The part of the model concerning transport, which applies for dislocation locking by atoms, finds a numerical solution to Fick's equation in this form:

$$\frac{\partial C}{\partial t} = D_{\text{eff}} \nabla \left[\nabla C + \frac{C}{kT} \nabla \left(\Delta G_{\text{binding}} \right) \right] \tag{5.2}$$

where C is the impurity concentration, D_{eff} the effective diffusivity, and $\Delta G_{\text{binding}}$ the binding energy of the impurity to the dislocation.

The equation describes transport to the dislocation. The first term models the diffusion of the impurity to the dislocation from the surrounding volume, and the second term models the interaction between the impurity and the dislocation (*i.e.* drift). The program was initially developed for the oxygen dislocation unlocking work [32], where both Regime 1 and Regime 2 were consistent with locking of dislocations by an atomic species. For Regime 2, this was shown by the dependence of saturation stress on anneal temperature - it gave a straight line on an Arrhenius plot, which allowed the binding enthalpy of oxygen to the dislocations to be measured, as shown in Figure 2.4.

Using this binding enthalpy and the bulk oxygen concentration, it was possible to calculate the number of atoms at the dislocation core in equilibrium with the bulk concentration at different temperatures. Thus, using the Regime 2 saturation locking stress, an absolute value for the dislocation locking stress per oxygen atom could be calculated. Senkader's experimentally-derived value of 7Pacm for this parameter [32] was close to a theoretical calculation from the literature.

In the new nitrogen results presented in this thesis, Regime 2 does not behave in the same way (as will be shown in §5.3.1). The saturation stress takes its highest value at anneal temperatures of 600 - 675°C and is lower at temperatures greater and lesser than this. This behaviour is not consistent with a saturation stress that is due to an equilibrium core concentration determined by a binding enthalpy, bulk

concentration and temperature. An Arrhenius plot of the new data, shown in Figure 5.5, *could* be interpreted as having a straight line portion above about 750°C, and this gives an activation energy of 0.5eV. However, if this value is assumed to be a binding enthalpy and is used to calculate an equilibrium nitrogen concentration at the dislocation core, it implies a locking strength per nitrogen atom of ∼1500Pacm, when taken with the measured values of locking stress. This is about 200 times greater than the value measured for oxygen atoms: a result that is assumed to be impossibly large. It is inferred from this that the temperature dependence of the Regime 2 stress is not due to an equilibrium between impurity atoms in the bulk and at the core, as is the case for oxygen.

The binding enthalpy of nitrogen to the dislocations, and the locking strength per nitrogen atom, cannot therefore be inferred from these experimental unlocking data. However, if it is assumed that the locking stress per nitrogen atom is of the same order as that for an oxygen atom (as was indicated by a comparison of the dependence of τ_u on three-point bend duration in Cz-Si and NFZ-Si (§4.3.2)), then an estimate of the effective diffusivity of nitrogen can be obtained. This has been done by using the numerical simulation program to fit the Regime 1 nitrogen dislocation unlocking results, using a locking strength per atom of 7Pacm (the same as with oxygen), whilst neglecting any thermal re-emission of impurities from the dislocation core, as is thought to be the case in Regime 1. The program was run at all anneal temperatures where a Regime 1 was seen in the new nitrogen data, using effective diffusivity as the sole fitting parameter. The values used for the model's other inputs are similar to those used previously [32], and are described fully in Appendix A.

The model's fits to the dislocation unlocking data are displayed in Figure 5.1, and the absolute values of effective diffusivity used to generate these fits are given in Table 5.1. These values are displayed in an Arrhenius plot, along with values from other work, in Figure 5.3. The expression for effective nitrogen diffusivity found from these results is:

$$D = 173,000 \exp\left(-\frac{3.24\text{eV}}{kT}\right) \text{cm}^2\text{s}^{-1} \tag{5.3}$$

Temperature (°C)	Nitrogen diffusivity (cm^2s^{-1})
500	1.75×10^{-16}
600	2×10^{-14}
675	1×10^{-12}
750	2.5×10^{-11}

Table 5.1: The diffusivities of nitrogen in silicon, found by fitting a simulation of diffusion to a dislocation to the experimental data in this work.

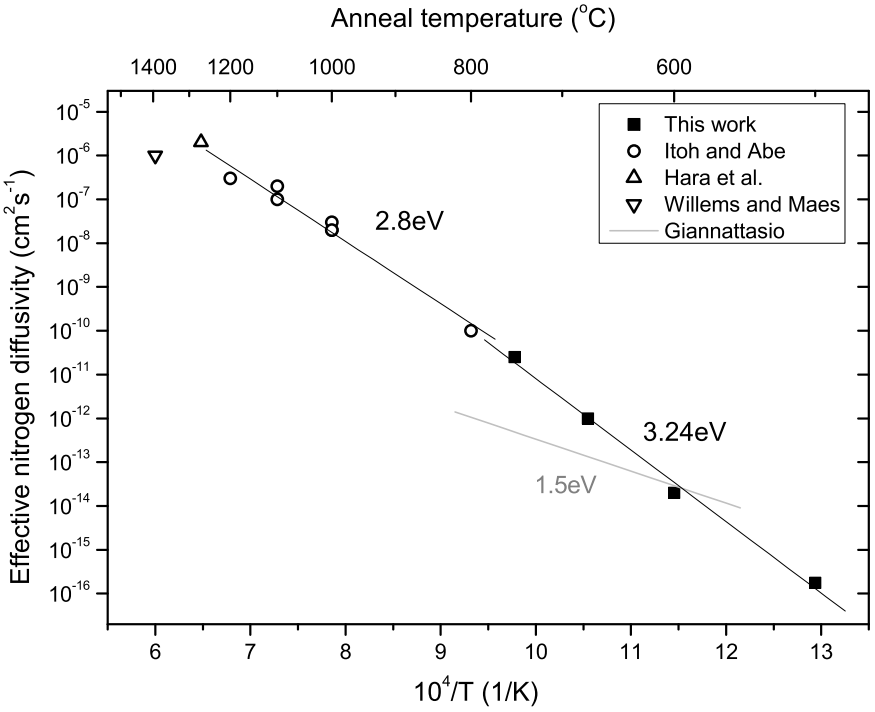


Figure 5.3: Nitrogen's effective diffusivity, from this and other work [87,177,178,253].

As above, the error on the activation energy is estimated to be 0.25eV. The diffusivity pre-factor depends on the locking strength per nitrogen atom, and it is also highly sensitive to changes in the activation energy, so this value is only thought to be accurate to within about two orders of magnitude.

It can be seen that the new results from this work are consistent with an extrapolation of those taken at higher temperatures using different methods. The 3.24eV activation energy is only slightly larger than that deduced from the SIMS data of Itoh and Abe [177]. For this reason it is believed that these dislocation unlocking measurements show that the same type of nitrogen transport is occurring over the complete range of temperatures that have been measured (500 - 1400°C).

5.2 Analysis of the nitrogen effective diffusivity results

5.2.1 Introduction

As discussed in Chapter 1, there is uncertainty in the literature as to nitrogen's transport mechanism in silicon. *Ab initio* models have calculated diffusion paths for the nitrogen dimer that are consistent with high-temperature SIMS diffusivity results; however, this simple model cannot account for measurements of anomalous diffusion, which has led others to consider dissociative transport.

Since dislocation unlocking experiments are only sensitive to an effective diffusivity, they cannot provide any specific information which could be used to differentiate between the two competing transport mechanisms, unless the variation of results with [N] is also investigated. The effective diffusivities measured in this work, shown in Figure 5.3, are consistent with the SIMS results at higher temperatures. Since both nitrogen transport models successfully explain these higher temperature results, both will therefore also account for the new dislocation unlocking measurements. Analysis in terms of the two models is presented below.

5.2.2 Simple dimer diffusion

For the case of simple dimer diffusion, nitrogen's diffusivity would simply be the expression given in Equation 5.3. The measured activation energy for effective nitrogen diffusion of 3.24eV is consistent with the broad range of dimer diffusion paths reported in the literature, so the new results do not contradict this transport mechanism. However, the diffusivity pre-factor of 173,000cm^2s^{-1} is extremely high. Species diffusing in silicon generally have pre-factors in the range 0.001 to 100cm^2s^{-1}, and it is not clear what physical mechanism could result in such a high value for the nitrogen dimer.

5.2.3 Dissociative transport

If diffusion is happening in a system which contains dimers and monomers in equilibrium, then the total flux of atoms is given by:

$$J = -D_1 \frac{dC_1}{dx} - 2D_2 \frac{dC_2}{dx} \tag{5.4}$$

where D_1, D_2 and C_1, C_2 are the diffusivities and concentrations of the monomeric and dimeric species, respectively. Equation 5.4 can be approximated by this expression:

$$J \approx -D_{\text{eff}} \frac{dC}{dx} \tag{5.5}$$

where $C = C_1 + 2C_2$ is the total nitrogen concentration, and

$$D_{\text{eff}} = \frac{C_1 D_1 + 2C_2 D_2}{C_1 + 2C_2} \tag{5.6}$$

The nitrogen dimer is known to be the dominant form, *i.e.* $C_2 \gg C_1$, so D_{eff} can be approximated as:

$$D_{\text{eff}} \approx \frac{C_1 D_1}{2C_2} + D_2 \tag{5.7}$$

Now, in equilibrium the monomer and dimer are related by $N_1 + N_1 \rightleftharpoons N_2$ and the concentration of dimers is:

$$C_2 = {C_1}^2 \frac{g_2 Z_2 \Omega_0}{{g_1}^2 {Z_1}^2} \exp\left(\frac{\Delta G_2}{kT}\right) \tag{5.8}$$

where g_1 and g_2 are the number of available sites per unit cell for the interstitial monomer and the dimer, Z_1 and Z_2 are the dynamic partition functions of the monomer and dimer, Ω_0 is the volume of a unit cell, and ΔG_2 is the binding energy of the dimer [192]. The full dynamic partition functions are not trivial to calculate, but are usually neglected as they are unlikely to alter the final result by more than a factor of two. Equation 5.8 can be re-arranged to give:

$$C_1 = \frac{\sqrt{C_2} g_1}{\sqrt{g_2 \Omega_0}} \exp\left(-\frac{\Delta G_2}{2kT}\right) \tag{5.9}$$

This expression for C_1 can then be substituted into the effective diffusivity expres-

sion, Equation 5.7. At this point, an assumption critical to the dissociative analysis is made: the dimer diffusivity, D_2, is neglected. Physically this reflects the assumption that the dimer is practically immobile. The following expression for effective nitrogen diffusivity is then found:

$$D_{\text{eff}} \approx \frac{C_1 D_1}{2C_2} = \frac{g_1}{2\sqrt{C_2 g_2 \Omega_0}} \exp\left(-\frac{\Delta G_2}{2kT}\right) D_1 \tag{5.10}$$

This can be compared with the experimental effective nitrogen diffusivity found from this work, given in Equation 5.3, to give a monomer diffusivity D_1 of:

$$D_1 = 346,000 \frac{\sqrt{C_2 g_2 \Omega_0}}{g_1} \exp\left(\frac{-(3.24 - \frac{|\Delta G_2|}{2})\text{eV}}{kT}\right) \text{cm}^2\text{s}^{-1} \tag{5.11}$$

The values of the parameters involved are: $g_1 = 12$ [106], $g_2 = 6$ [279], and $\Omega_0 = (5.43\text{Å})^3 = 1.601 \times 10^{-22}\text{cm}^3$ [280]. The nitrogen dimer binding energy ΔG_2 has never been measured, but, as mentioned in §1.4.2, recent theoretical calculations in the literature agree that it is high, giving values in the range 3.67 to 4.30eV [55,106,167]. Using these values in Equation 5.11 gives an expression for the nitrogen monomer diffusivity of:

$$D_1 = 28 \exp\left(\frac{-(1.1 \rightarrow 1.4\text{eV})}{kT}\right) \text{cm}^2\text{s}^{-1} \tag{5.12}$$

This is broadly consistent with the expression for monomer diffusivity given by Voronkov and Falster in their analysis of nitrogen diffusion data [191]:

$$\text{D}_N^{Voronkov} = 0.25 \exp\left(-\frac{1.25\text{eV}}{\text{kT}}\right) \text{cm}^2\text{s}^{-1} \tag{5.13}$$

As noted in Chapter 1, the activation energy for monomer transport of 1.25eV is different to the theoretical calculations of nitrogen monomer diffusion, which give a much lower barrier of 0.4 - 0.5eV [168,193].

5.2.4 Discussion of dissociative diffusion and dislocation unlocking results

The analysis presented above shows that a monomer diffusivity inferred from the new results is similar to that found by Voronkov and Falster's dissociative diffusion mechanism. This is not surprising, however, since the new dislocation unlocking results are broadly consistent with the higher temperature SIMS results which were included in their analysis. It should be emphasised that dislocation unlocking does not provide any evidence for this particular transport mechanism. Multi-species transport is need to explain the 'anomalous' SIMS diffusion profiles, some of which were shown in §1.4.3, but dislocation unlocking is sensitive only to an effective diffusivity, which may be simple or complex. The only indication of non-Fickian diffusion from the results presented in this chapter is the effective diffusivity pre-factor of 173,000$\mathrm{cm^2s^{-1}}$, which is orders of magnitude larger than those found for simple systems.

The physical implications of dissociative transport can be surprising, particularly at low temperatures. For example, if the dimer binding energy is 4eV, the concentration of monomers at 500°C in the silicon used in this work is only $10^6\mathrm{cm^{-3}}$. In the monomer-dimer dissociative mechanism, these $10^6\mathrm{cm^{-3}}$ monomers are completely responsible for nitrogen transport, producing the dislocation locking effect that is measured in these experiments.

5.3 The interaction between nitrogen and dislocations investigated by dislocation unlocking

5.3.1 Regime 2 results

The Regime 2 data obtained using standard annealing, together with the drop-quench anneal results, are presented in Figure 5.4, plotted against anneal temperature. Anneal duration for the drop-quench experiments was standardised at 5 minutes for all temperatures, on the assumption that at such high temperatures the Regime 2 unlocking stress is reached very quickly, and is independent of anneal duration. It should be noted, however, that the thermal budget experienced by the higher temperature

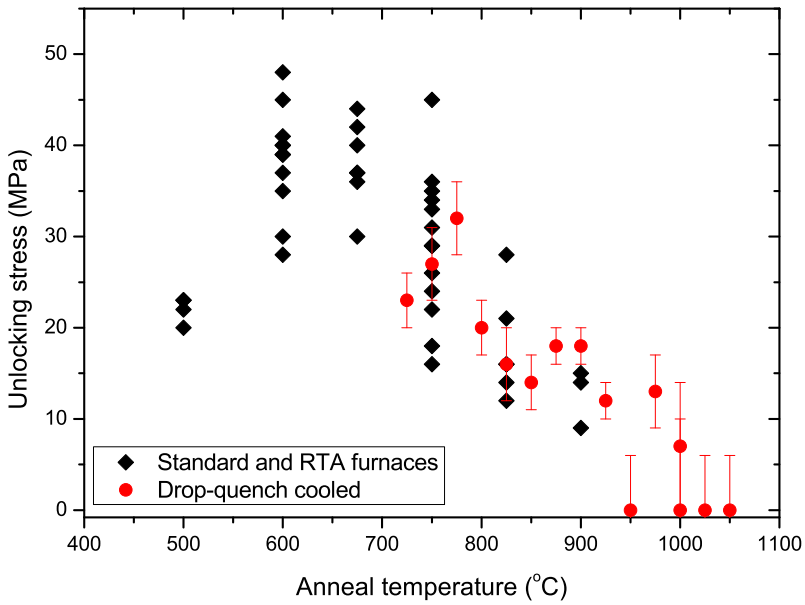


Figure 5.4: Regime 2 values of dislocation unlocking stress measured at 550°C in 'High-[N] 3' NFZ-Si, at different anneal temperatures.

drop-quench anneals (up to 1050°C) is far greater than for the lower temperature ones (around 750°C).

The results show that the dislocation unlocking saturation stress (Regime 2) is temperature-dependent, peaking at 600 - 675°C and falling to zero (within experimental error) at around 1000°C. This is in contrast to the behaviour found by Senkader with oxygen locking, where saturation stress decreased monotonically with increasing temperature [32]. It is also different to the behaviour seen in previous nitrogen dislocation unlocking experiments, where saturation stress was independent of temperature, as discussed in §2.3.3. The Regime 2 results are shown in an Arrhenius plot in Figure 5.5.

5.3.2 [N]-dependence of Regime 2 locking stress

For reasons outlined in §5.8.2, a small number of experiments were carried out to test the Low-[N] 1 NFZ-Si that had been used by Murphy, using standardised three-point bend conditions. The results of these experiments are displayed fully in Figure 5.11

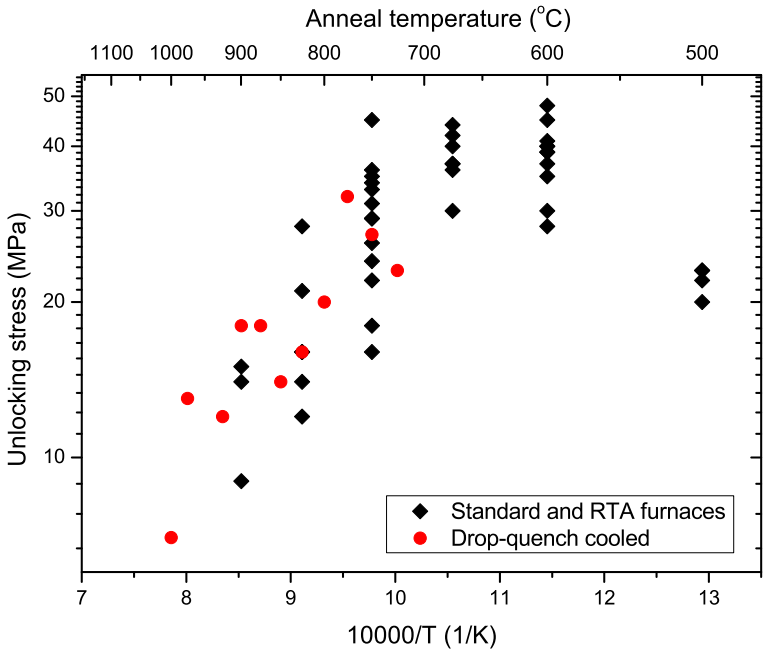


Figure 5.5: Regime 2 values of dislocation unlocking stress measured at 550°C in 'High-[N] 3' NFZ-Si, at different anneal temperatures, in an Arrhenius plot.

below. Most of the results fell into Regime 2, and these data are displayed in Figure 5.6, alongside the results from the nitrogen work presented above. They show that the low-[N] silicon behaves in the same way as the High-[N] 3 material, with locking stress falling off with increasing anneal temperature. This is in contrast to most of the previous experiments that used this silicon, which found that the Regime 2 locking stress took a constant value up to anneal temperatures of 1200°C (§2.3.3).

5.4 Analysis of Regime 2 results

5.4.1 Anneal temperature dependence of dislocation locking stress

The broad temperature-dependent peak in Regime 2 dislocation locking stress, shown in Figure 5.4, is not understood. The shape is similar to those seen for precipitation processes, but the large temperature range over which it occurs means that this is unlikely. The results are discussed briefly in terms of the nature of the locking species in §5.5.

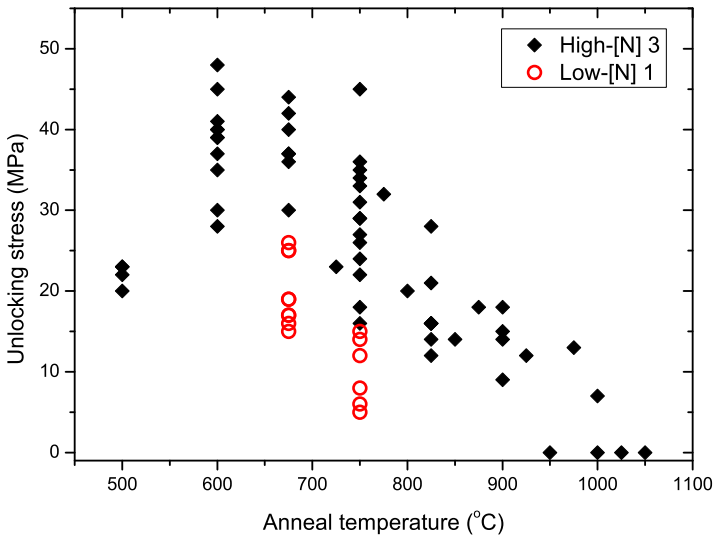


Figure 5.6: Regime 2 values of dislocation unlocking stress measured at 550°C in High-[N] 3 and Low-[N] 1 NFZ-Si. The specified nitrogen concentrations (2×10^{15}cm^{-3} and 3×10^{14}cm^{-3}, respectively) should not be compared directly, as the [N] measurements were made by the respective manufacturers using their own standards.

5.5 Discussion of nitrogen dislocation unlocking results

5.5.1 Diffusivity of nitrogen

The main conclusion of the new nitrogen dislocation unlocking experiments is that nitrogen's effective diffusivity has been shown to exhibit similar behaviour in the 500 - 750°C temperature range to that measured at higher temperatures using other methods, as shown in Figure 5.3. It is therefore believed that a single mechanism is likely to be responsible for nitrogen transport from 500°C up to the melting point. These corrected dislocation unlocking experiments are the first in the literature to show low-temperature behaviour that is consistent with the higher temperature SIMS results.

5.5.2 Regime 2

Regime 2 data show the locking strength, measured at 550°C, after anneals at other (usually higher) temperatures. They are sensitive to the effect at 550°C of the nitrogen that is left on the dislocations after the main anneal. This locking strength has been

found to vary with the temperature of the main anneal, peaking at 600 - 700°C and falling towards zero at 1000°C.

In terms of the practical applications of nitrogen in silicon, the new results are disappointing. The previous work by Giannattasio [253], and in particular Murphy [254], had indicated that nitrogen could provide mechanical strength to silicon wafers at up to 1200°C, which could have been extremely useful in high-temperature industrial processes. The new results presented in this thesis show that nitrogen's locking strength falls off with temperature in a similar manner to oxygen's. If there is any strength benefit associated with the presence of as-grown nitrogen when oxygen is already present, it is not large.

The difference in the high-temperature Regime 2 results from this and previous work is accounted for by the faster post-anneal cooling methods used in this work. For an accurate high-temperature result to be seen, cooling from high temperature must be fast enough to prevent significant amounts of nitrogen segregating to the dislocations during the cool-down after the anneal. The methods used previously were relatively slow, although this was thought to be adequate at the time, since nitrogen transport at high temperatures was thought to be much slower than has been shown in this thesis. It is believed that the results from these previous experiments were affected by this slow cooling, and that the faster cooling used in this present work has allowed a more accurate picture of nitrogen's high temperature interaction with dislocations to be discerned.

5.5.3 Nature of the locking species

As discussed in §2.3.4, previous nitrogen dislocation unlocking experiments could not be consistently interpreted by atomic locking, so precipitates were also considered. The new results, outlined in this chapter, are consistent with the SIMS data when interpreted in terms of atomic transport to dislocations. Locking of dislocations by an atomic (or diatomic, *etc.*) species is the simplest explanation, but the results do not show conclusively that this is the case. Different aspects of the data, and their relevance regarding the nature of the locking species, are discussed briefly here.

Variation of three-point bend duration with unlocking stress

If the results showing that unlocking stress decreases with increasing unlocking duration are analysed in terms of the theory of release of dislocations from pinning points (§4.3.2), consistent values for the line density of pinning points are found: they are separated by about 10nm in NFZ-Si and 2nm in Cz-Si. Since the NFZ-Si and Cz-Si results are comparable and dislocation locking by oxygen is thought to be by an atomic species, this gives an indication that nitrogen locking is also atomic.

Regime 1 shape

Murphy's analysis found that while the Regime 1 unlocking stress should rise linearly with anneal time for locking by atomic impurities, this might not be the case for precipitates, where locking strength might increase linearly with their radius. Since precipitate radius varies with time according to $r \propto \sqrt{Dt}$ [281], the Regime 1 unlocking stress might rise with $\sqrt{t}$ if precipitates are responsible for locking. In Murphy's case this was an argument against precipitates since his Regime 1 data were linear, but the new results presented in Figure 5.1 are more ambiguous in this sense. Unfortunately, the high level of random error in these experiments means that the data are not clear enough to support either conclusion.

Activation energy for nitrogen transport

Since locking stress might increase according to $\sqrt{D}$ for precipitate locking, the activation energy for nitrogen transport would be double that for the dislocation locking process. This is the main reason precipitates were considered by Giannattasio and Murphy as an explanation for their results, as doubling their measured 1.5eV gave an energy close to the 2.8eV measured by SIMS. With the new data presented in this work this is not the case: the measured 3.24eV is broadly consistent with the SIMS measurements. This, therefore, is an argument in favour of atomic locking of dislocations by nitrogen.

Regime 2 unlocking stress temperature dependence

Heterogenous precipitation is a highly temperature-dependent process. If this were occurring at dislocations in NFZ-Si, it would be expected that the locking strength would also be highly temperature-dependent, forming a peak over a narrow temperature range. A peak *is* seen in the new data, as shown in Figure 5.4, but it is over a large temperature range, 500 to 1000°C. With simple atomic locking the Regime 2 stress would be expected to fall with increasing anneal temperature, giving a straight line on an Arrhenius plot, and this is only seen above 750°C in the new data. The measured behaviour is therefore not easily explained by either atomic or precipitate locking.

Conclusions

The data do not conclusively support either atomic or precipitate locking of dislocations, but there is more evidence in favour of atoms than precipitates as the locking agent. No experiments specifically designed to confirm the identity of the locking species have been carried out in this work, but they would not be hard to design. For example, the dependence of unlocking stress on unlocking temperature (*i.e.* three-point bend temperature - standardised at 550°C in this work) could be measured. For atomic locking τ_u is expected to fall with increasing unlocking temperature, as individual atoms are bound to dislocations weakly (0.74eV with oxygen, for example [32]). This is not the case with precipitates.

Another experiment could use NFZ-Si specimens which had been annealed into Regime 2 at 600 - 700°C to give a large amount of locking strength. A high temperature second anneal would then be performed; if locking were by atoms this would quickly establish a new equilibrium at the dislocations and the locking stress would fall. This would not happen immediately with precipitates, which would take much longer to dissolve.

5.6 Dislocation velocity in dislocation unlocking experiments

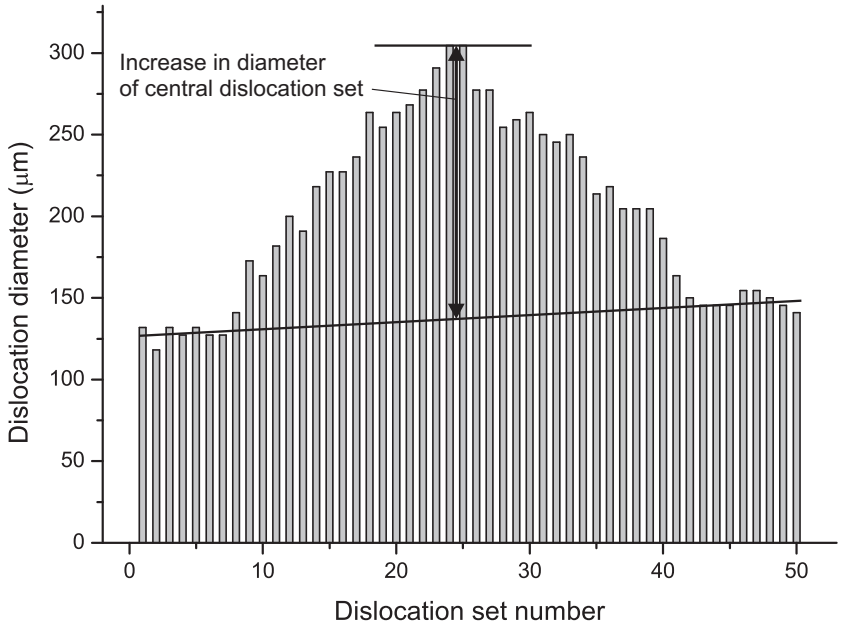
It is known that impurities can affect the mobility of dislocations in silicon. For instance, boron [282] and phosphorous [283] have been found to enhance dislocation velocity, whereas dislocations are significantly retarded in material co-doped with boron and germanium [284].

Most experimental work investigating the effect of nitrogen on dislocation velocity has used NCz-Si. Some studies found that dislocations moved more slowly if nitrogen was present, with potential explanations being that the greater oxide precipitate density in NCz-Si hindered dislocation motion [125], that an N-O complex is responsible for the effect, or that nitrogen enhances diffusion of oxygen to dislocations [285]. A more recent study, however, found that nitrogen doping did not affect dislocation motion in either Cz- or FZ-silicon [63].

Unlocked dislocations in dislocation unlocking specimens have travelled a measurable distance under a known stress for a known duration, so these experiments can be used for a dislocation velocity investigation. A brief analysis of the specimens used for this work is presented here.

5.6.1 Method of determining dislocation velocity

The dislocation velocity of the unlocked dislocations during three-point bend is determined for each specimen from its dislocation loop diameter diagram, using the process outlined in Figure 5.7. First, the average diameter of the locked dislocations next to each outer knife-edge is determined. The mean of these two values is taken, and this is assumed to be approximately equal to the diameter of the dislocations in the centre of the specimen after the four-point bend stage. The unlocked dislocation diameter at the central knife-edge is then measured, correcting for any irregularities by considering the whole set of unlocked dislocations. The four-point bend dislocation diameter is then subtracted from this value, to give the diameter increase of the central dislocations, which can be used to determine the dislocation loops' rate of



centering

Figure 5.7: Diagram illustrating how dislocation set diameter increases have been measured.

diameter increase per MPa using the bend duration and central resolved shear stress τ_{max}. This is then halved, to give the rate of radius increase, *i.e.* the velocity at which the dislocation moves across the specimen surface[1].

5.6.2 Dislocation velocity results

Collected results

In total, 176 specimens have been measured, using different types of FZ-Si. The rates of dislocation loop radius increase for all these specimens are shown in Figure 5.8. The mean dislocation velocity at 550°C found from a Gaussian fit of these results is $7.5 \pm 1.2 \times 10^{-11} \mathrm{ms}^{-1}\mathrm{MPa}^{-1}$. The empirical expressions for the velocity of screw and 60° dislocations in silicon, given in Chapter 1, give velocities of $1.4 \times 10^{-10} \mathrm{ms}^{-1}\mathrm{MPa}^{-1}$ for screw dislocations, and $3.4 \times 10^{-10} \mathrm{ms}^{-1}\mathrm{MPa}^{-1}$ for 60° dislocations, at 550°C. The value found using the dislocation unlocking specimens is smaller than these, although by less than one order of magnitude. The difference is not surprising: it is well-known that dislocation velocity measurements in silicon can give slightly different answers to

[1]For a perfect hexagonal half-loop, this value could be multiplied by $\frac{\sqrt{3}}{2}$ to give the velocity perpendicular to the line direction.

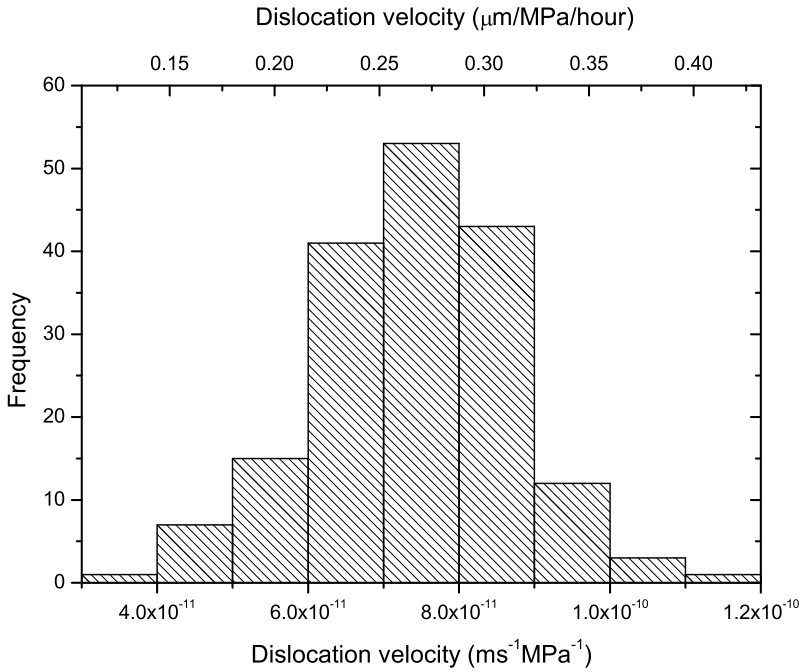


Figure 5.8: Histogram of dislocation velocities measured at 550°C from NFZ-Si and FZ-Si specimens used in this work.

the standard values if pinning impurities are present [286]; and in any case, dislocation motion in dislocation unlocking specimens is not fully understood, as evidenced by the unlocking discontinuity problem (§5.7).

Dislocation velocity in different anneal regimes

The results presented above can be broken down in several ways, to test different hypotheses about the motion of unlocked dislocations in NFZ-Si. One such hypothesis suggested that unlocked dislocations might not move completely away from the impurities that had been pinning them. Nitrogen atoms might be able to diffuse fast enough to keep up with a dislocation, if they remained close enough to be influenced by its stress field. These impurities might then exert a 'dragging' force on the dislocation, which could reduce its velocity.

Mean dislocation velocities for NFZ specimens which had zero measured locking stress, a Regime 1 stress and a Regime 2 stress are shown in Table 5.2. It can be seen

	Mean velocity ($ms^{-1}MPa^{-1}$)	No. specimens
No locking	7.6×10^{-11}	15
Regime 1	7.4×10^{-11}	25
Regime 2	7.5×10^{-11}	96

Table 5.2: Dislocation velocities at 550°C for unlocked NFZ-Si specimens. Specimens where no locking was measured had been given either short duration or very high temperature anneals.

Silicon	[N] (cm^{-3})	Mean velocity ($ms^{-1}MPa^{-1}$)	No. specimens
High-[N] 3	2×10^{15}	7.4×10^{-11}	106
Standard FZ	Unknown	7.4×10^{-11}	14
Low-[N] 1	3×10^{14}	8.0×10^{-11}	19
N-free	$< 10^{14}$	9.2×10^{-11}	8

Table 5.3: Dislocation velocities at 550°C for unlocked FZ-Si specimens, for different types of silicon. Note that as there is no agreed standard for the measurement of [N], values given by different manufacturers cannot be directly compared.

that the dislocation velocity is not dependent on the specimens' anneal regime.

Dislocation velocity for different silicon types

Dislocation velocities sorted by silicon type are shown in Table 5.3. The data seem to indicate a slight trend, with dislocation velocity decreasing as nitrogen concentration increases - something never reported before for nitrogen in FZ-Si at the stresses used here. Unfortunately, there are not enough results from the nitrogen-free silicon, N-free, to show this with more certainty. The effect, if it exists, is small.

5.6.3 Dislocation velocity analysis

The analysis of dislocation velocities from the different anneal regimes shows that there is no difference in velocity between specimens with no locking, Regime 1 locking and Regime 2 locking. This indicates that dislocations, once unlocked, are no longer influenced by the locking species in such a way as to alter their mobility.

The effect of bulk nitrogen concentration on dislocation velocity, shown in Table 5.3, is of more interest. It seems that the presence of nitrogen slows down dislocations by a small amount. This is a tentative conclusion, however, as the number of data for the Low-[N] and N-free material is small: more experiments would have to be performed before the effect could be demonstrated conclusively. However, the results

Discontinuity	No. Specimens
None	191
Partial / Unclear	58
Full	5

Table 5.4: Frequency of different dislocation set shapes for specimens used in this work.

as they stand do indicate that a dislocation-slowing effect probably exists.

The data do not allow any conclusions to be drawn regarding the mechanism responsible for this effect.

5.7 Unlocking discontinuity

The lack of an unlocking discontinuity in most dislocation unlocking specimens was mentioned in §2.4.3. The unlocked dislocation sets in each specimen used in this work have been assessed, in order to investigate this effect. Specimens were sorted into three categories by the shape of their unlocked dislocations: no discontinuity, partial or unclear discontinuity, and full discontinuity (i.e. what would be seen if dislocations behaved as expected). The results of this process are shown in Table 5.4.

Clearly, a full unlocking discontinuity is a rare event, and partial discontinuities are significantly outnumbered by those specimens that showed no discontinuity at all. As mentioned in §2.4.3, some effort was previously devoted to this problem [260], but no consistent explanation for the lack of the unlocking discontinuity was found. This situation has not improved with the present work, as there are no apparent common factors in the specimens that contain full discontinuities or partial discontinuities.

5.8 Comparison with previous nitrogen dislocation unlocking work

The measurements of nitrogen's effective diffusivity presented in this thesis are considerably different to those made previously. The reasons for this will be discussed in this section.

5.8.1 Systematic error associated with changes in three-point bend duration

The results presented in §4.3 showed that the unlocking stress measured in dislocation unlocking experiments is dependent on the three-point bend duration used. This has implications for the nitrogen dislocation unlocking experiments performed by Giannattasio and Murphy. Recall that in the previous nitrogen dislocation unlocking technique, discussed in Chapter 2, three-point bend durations were altered on an experiment-by-experiment basis, to increase the precision of the low-τ_u results. Specimens expected to be annealed to Regime 2 (large unlocking stress) would be given short three-point bends, and for Regime 1 the duration would be made progressively longer with shorter and shorter anneal times, as the expected unlocking stress dropped towards zero. The results in §4.3 show that the progressively longer three-point bend durations would act to *create* progressively falling unlocking stress measurements. This means that the tailored unlocking conditions used in the previous work had the potential to create a false Regime 1, where none existed.

This 'three-point bend duration error' is only possible if a clear expectation of the outcome of measurements exists; however, this is not unusual with dislocation unlocking experiments, since Regime 1 gradients have a simple exponential temperature dependence and so can be easily predicted. As the experimental technique is very time-consuming, setting up each test individually to give a clear result was thought to be a good way of maximising the number of results taken.

The magnitude of the discrepancy that can be created by the error depends on whether the expectation is for a faster or slower Regime 1 than reality, as illustrated in Figure 5.9. This shows that if the real Regime 1 behaviour is slower than expected then the error has little effect, but if the real Regime 1 is faster than expected, then the measured gradient could be far lower than it should be.

5.8.2 Effect of error on previous work

The nitrogen dislocation unlocking results from this thesis are presented in Figure 5.10 alongside those taken in previous work. They are similar at 500°C, but the old

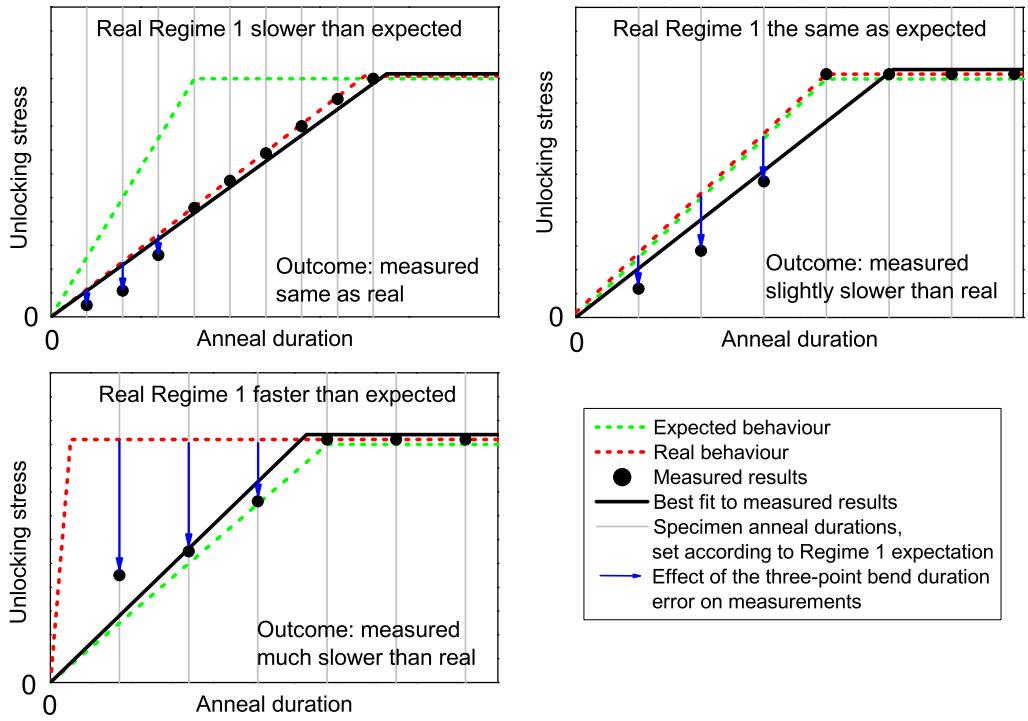


Figure 5.9: Schematic showing the effect of the three-point bend duration error, for three different types of expectation. The magnitudes of the discrepancies caused by the error are approximations.

Regime 1 results indicate progressively slower locking than the new results as the anneal temperature is increased.

The three sets of experiments were performed using three different types of silicon. None of the material used by Giannattasio was available, but the material used by Murphy has been re-tested using the same standardised three-point bend conditions as were used with the new NFZ-Si experiments presented in this chapter. The results are shown in Figure 5.11. It can be seen that under the standardised conditions, the Low-[N] 1 material used by Murphy gives results consistent with the new results presented in this thesis.

Since Murphy recorded the three-point bend durations used in his experiments, it is possible to examine his results to see whether the discrepancy between his data and the present work can be accounted for by the three-point bend variation alone. At some temperatures there is a such a correlation, but at others there is not. Two examples of sets of three-point bend durations, for data taken at 620°C and 800°C,

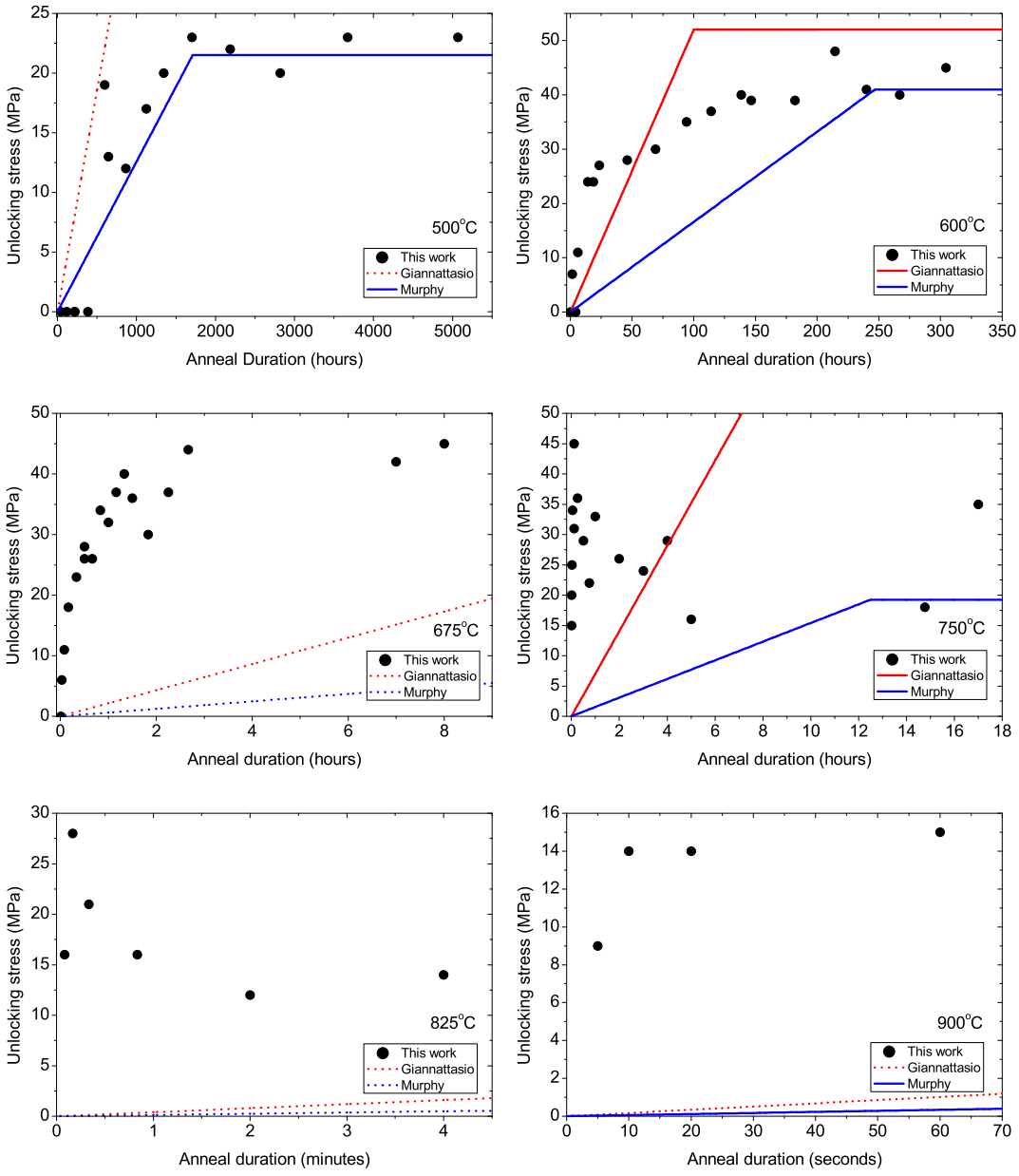


Figure 5.10: Dislocation unlocking stress measured at 550°C in NFZ-Si for this work, and the best-fit lines of Giannattasio [253] and Murphy [254] (the dashed Regime 1 gradients are interpolated and extrapolated from their $\frac{d\tau_u}{dt}$ data at other temperatures, as no experiments were performed at these temperatures by these authors).

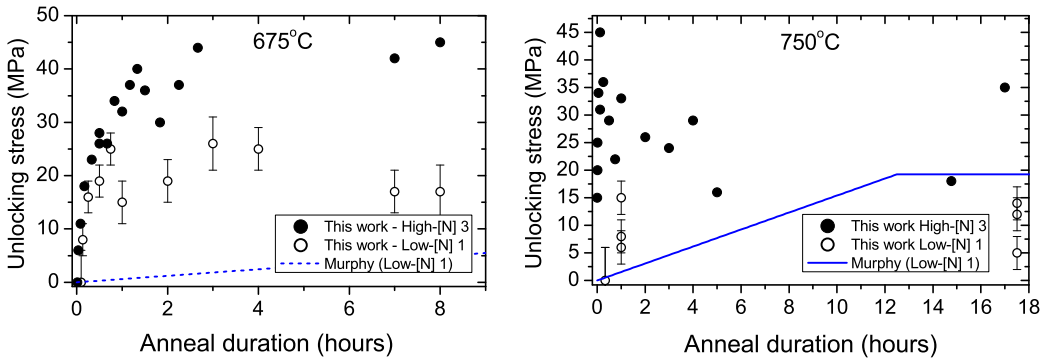


Figure 5.11: Dislocation unlocking stresses measured at 550°C, with anneals at 675°C and 750°C. The unfilled circles are results taken using the low-[N] NFZ-Si that was used by Murphy [254]. As in Figure 5.10, Murphy's 675°C Regime 1 gradient is interpolated from other data, as he didn't perform experiments at this temperature.

are shown in Figure 5.12 with the corresponding graphs of results.

It can be seen that at 620°C the two low Regime 1 measurements had longer three-point bend durations of 68 and 43 hours, while the rest of the measurements used the shorter duration of ∼20 hours, as was standard for Regime 2. The results at this temperature are consistent with the hypothesis that Regime 1 could have been an artefact, created by the three-point bend duration effect. At 800°C, however, this is not the case, as the ∼20 hour unlocking standard was used for all except one of the measurements. At this temperature, another explanation for the low Regime 1 measured values must be sought.

A broader view of Murphy's results can be obtained by plotting τ_u vs three-point bend duration for the whole set of data. This is shown in Figure 5.13. Since the anneals used by Murphy were far longer than those used in this present work, nearly all his specimens were annealed into Regime 2 (as found in the present work). The few that were not - 7 data at low temperatures - have been omitted from this plot, so that all the data presented are from Regime 2 anneals.

The results are ambiguous, as was shown with the two individual temperatures given in Figure 5.12. The data taken at long anneal durations (40 - 70h) are all low unlocking stresses, which is consistent with the systematic error hypothesis. However, at the ∼20h duration, where most of the data lie, there is a full range of stresses, from 6 to 47MPa. This means that the change in three-point bend duration was not the

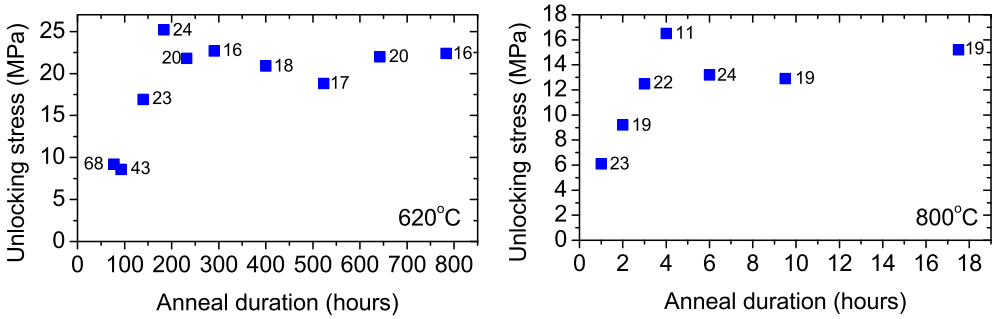


Figure 5.12: Murphy's low-[N] dislocation unlocking results at 620°C (left) and 800°C (right) [254], with the three-point bend duration (rounded to the nearest hour) for each point.

only reason for changes in unlocking stress. It seems, therefore, that even if the three-point bend duration error had been large enough to explain the discrepancy, it was not relevant in some cases.

5.8.3 Reasons for having confidence in the new results

It is believed that the new nitrogen dislocation unlocking results presented in this work are correct, and the previous results were affected by experimental error. The reasons for this are summarised here.

Standardised technique

As described in Chapter 3, the new experimental technique used a standard three-point bend load and duration for every measurement. This eliminated the potential systematic error associated with intentional variation of three-point bend duration, explained above.

Repeat using Low-[N] 1 silicon

The results presented in Figure 5.11 show that when the low-[N] silicon used by Murphy is tested under standardised conditions, it gives results consistent with the new results presented in this work. None of the silicon used by Giannattasio was

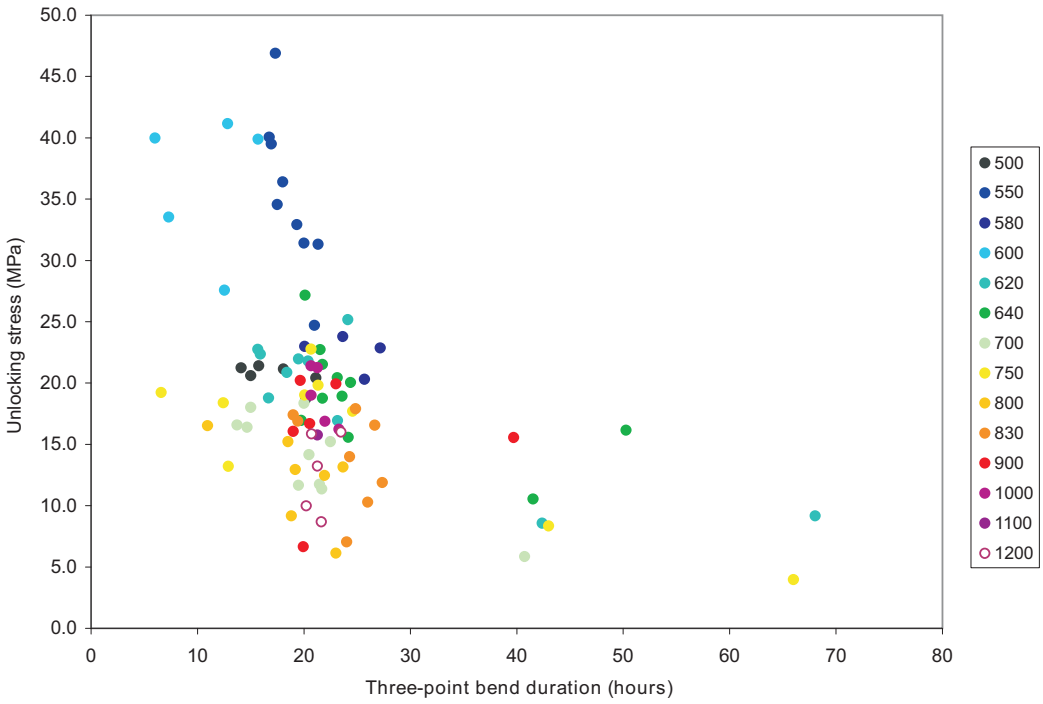


Figure 5.13: Murphy's low-[N] NFZ-Si three-point bend durations at all anneal temperatures, plotted against unlocking stress measured at 550°C [287]. Anneal temperatures are colour-coded as shown.

available and so could not be re-tested in this way, however, it seems unlikely that the difference between the results could be explained solely by differences in the material.

Number of measurements

It was noted in §2.4.3 that the previous NFZ-Si dislocation unlocking graphs, some of which were presented in Figure 2.6, do not have a large number of data in Regime 1. Practical constraints limited the number of experiments that could be performed, and there was a large amount of confidence in the general shape that the results would take. This meant that the minimum number of measurements were taken in Regime 1 at each temperature, as if simply to confirm the behaviour had been expected.

Table 5.5 shows the average number of Regime 1 measurements made per temperature investigated, for Senkader (oxygen locking), Giannattasio (high-[N] nitrogen locking), Murphy (low-[N] nitrogen locking), and this work (high-[N] nitrogen lock-

ing)[2]. It suggests that the conclusions drawn from the new results presented in this work have a better grounding in the experimental data than those drawn from the previous nitrogen dislocation unlocking work.

Senkader	Giannattasio	Murphy	This work
7.1	2.4	2.1	4.8

Table 5.5: The average number of data in Regime 1 for each temperature in different sets of dislocation unlocking work.

Identification of unlocking points

The method by which unlocking stress is determined in this work, outlined in §3.7.2, uses a bar chart representing the entire specimen to identify the unlocking points. This is thought to be an improvement on the previous method, where unlocking points were identified under the microscope, which has a limited field of view.

Comparison with other measurements of nitrogen diffusivity

As shown in §5.1, the new results presented in this thesis give an effective diffusivity of nitrogen that is consistent with previous SIMS experiments at higher temperature. This is not the case for the previous nitrogen dislocation unlocking results. The new results are also consistent with experiments which measured out-diffusion of nitrogen using a modified dislocation unlocking technique, which are presented in the next chapter.

5.9 Summary

The NFZ-Si dislocation unlocking experiments have been performed at anneal temperatures of 500 to 1050°C. The results have been used to infer an effective diffusivity of nitrogen in silicon in the 500 - 750°C range of:

[2]The categorisation of data into Regimes has been done subjectively, using the criterion that Regime 1 points should be lower than the lowest Regime 2 point at each temperature. The single 'no anneal' result, plotted at each temperature in Giannattasio and Murphy's graphs, has not been included.

$$D = 173,000 \exp\left(-\frac{3.24\text{eV}}{kT}\right) \text{cm}^2\text{s}^{-1} \tag{5.14}$$

These measurements have shown for the first time that nitrogen transport at these low temperatures is consistent with the behaviour measured at higher temperatures using SIMS. This effective diffusivity is consistent with both of the competing models for nitrogen transport - dimer diffusion, and the monomer-dimer dissociative mechanism. If the results are analysed in terms of the latter case, an expression for the nitrogen monomer diffusivity is found:

$$D_1 = 28 \exp\left(\frac{-(1.1 \rightarrow 1.4\text{eV})}{kT}\right) \text{cm}^2\text{s}^{-1} \tag{5.15}$$

However, since dislocation unlocking experiments are only sensitive to overall nitrogen transport, the measurements do not provide any evidence for one model rather than the other.

The effective nitrogen diffusivity measured in this work is different to that found by previous nitrogen dislocation unlocking experiments. This is believed to be largely a consequence of the standardisation of experimental conditions in this present work, which has eliminated a systematic error due to intentional variation in three-point bend duration that affected the previous work. Confidence in the new results is based on the improved methodology in these experiments, repeat measurements of the silicon used in previous work, the greater number of data taken at each temperature in this present work, and a comparison with higher temperature SIMS results.

The Regime 2 results show that nitrogen's dislocation locking strength is dependent on anneal temperature, peaking at 600 - 700°C and falling towards zero above 1000°C. This result is empirically useful, as nitrogen is already being used to strengthen silicon wafers, with further applications being actively researched in industry. It indicates that nitrogen does not have a constant locking strength up to 1200°C as previously reported [254], however, nitrogen may still provide some benefit over oxygen in terms of high-temperature dislocation locking strength.

The dislocation velocity during three-point bend has been calculated for the FZ-

Si specimens used in this work. The average velocity of all the measurements is broadly consistent with expressions for dislocation velocities in silicon reported in the literature. It is found that while the anneal regime of NFZ-Si specimens has no effect on the velocity during three-point bend, the nitrogen content does: dislocation velocity decreases slightly as the nitrogen content of the material increases.

The next chapter outlines experiments performed with ion-implanted silicon, and another measurement of nitrogen's effective diffusivity using an out-diffusion technique.

Chapter 6

Nitrogen implant and nitrogen out-diffusion experiments

This chapter gives details of novel experiments performed with non-standard dislocation unlocking techniques, that have been carried out as part of a wider investigation into the properties of nitrogen in single-crystal silicon. The work falls into two categories: experiments using ion-implanted Cz-Si, and measurements of out-diffusion of nitrogen from NFZ-Si.

6.1 Nitrogen-implanted Cz silicon

6.1.1 Introduction

This section outlines experimental work that was carried out as part of a collaboration with Texas Instruments Inc., which explored effects associated with nitrogen implanted into Cz-Si to give near-surface concentrations of up to $2 \times 10^{20}\text{cm}^{-3}$. The experiments used the dislocation unlocking technique, which was modified to accommodate the shallow concentration profile of the implanted nitrogen (shown in the SIMS profiles in Figure 3.18). The aims of this work were both to increase the fundamental understanding of the system, and also to make measurements that might be relevant to technological applications.

6.1.2 Motivation behind nitrogen-implant dislocation unlocking experiments

One of the surprising aspects of nitrogen's behaviour is that it is able to give significant improvements to FZ-Si's mechanical strength, despite being present at concentrations of 10^{15}cm^{-3} or below - concentrations at which oxygen gives no such benefits (§1.4). Oxygen does not provide a large amount of dislocation locking strength in Cz-Si above about 800°C [32], so dislocation generation and propagation can be problematic during high-temperature stages of device manufacture. This has become particularly apparent with the recent introduction of strain-engineered transistor channels, which enhance device speed by increasing carrier mobility, but are especially prone to dislocation nucleation [288].

One possible solution would be to implant nitrogen into the surfaces of wafers, to lock dislocations in the device regions. Since local nitrogen concentrations in implanted material could potentially be 10^5 times as high as in as-grown material, even a very small high-temperature dislocation locking effect could be significant, if it increased with increasing nitrogen concentration. The experiments described in this chapter investigated nitrogen's interaction with dislocations in heavily nitrogen-implanted Cz-Si, with the hope of advancing the physical understanding of the system, and providing physical inputs for a modelling effort carried out by Texas Instruments. The experiments used the dislocation unlocking technique, which was modified, as described below.

Planned experiments

A large group of nitrogen-implanted Cz-Si ($\overrightarrow{\text{N}}$Cz-Si) wafers was received, several of which were suitable for dislocation unlocking experiments. The properties of the wafers are described in detail in §3.8. The wafers were grouped into four sets, which had been implanted with different amounts of nitrogen at different energies. SIMS data showing the nitrogen concentration for the two wafers used in the dislocation unlocking experiments are shown in Figure 3.18. The procedure that was planned for the experimental effort was as follows:

Stage 1: Modify the dislocation unlocking technique so that it is sensitive to the extremely high concentration of near-surface nitrogen in the implanted wafers, instead of a uniform nitrogen distribution as with NFZ-Si.

Stage 2: Perform initial experiments under the most favourable conditions for nitrogen dislocation locking: using the highest [N]-implanted material, with the anneal conditions most likely to give a large locking effect. This would allow the magnitude of the effect to be gauged quickly, after only a few experiments. Once dislocation locking had been seen with the high-[N] silicon, the experimental work could be broadened to investigate how locking was affected by changes in nitrogen concentration and anneal conditions. Unfortunately this work was not completed, for reasons described below.

6.1.3 Stage 1: Modified experimental procedure

The standard dislocation unlocking procedure, outlined in Chapter 3, is as follows:

- Specimen cleaving and polishing
- Indent to damage specimen surface
- Four-point bend to create dislocation array from indent damage
- Anneal to allow nitrogen to diffuse to dislocations
- Planar etch to remove $\sim$20μm from surface of specimens
- Three-point bend to unlock dislocations
- Preferential etch to reveal dislocation positions
- Measure specimen to determine unlocking stress

The nitrogen-implanted silicon required a modified technique:

- Specimen cleaving and polishing
- Nano-indentation to damage specimen surface
- Anneal to allow nitrogen to diffuse to dislocations

- Planar etch using lacomit masking
- Three-point bend to unlock dislocations
- Preferential etch to reveal dislocation positions
- Measure specimen to determine unlocking stress

The main changes to the technique are the use of nano-indentation, and the omission of the four-point bend dislocation expansion step. This was so that the dislocation loops would be small, close to the shallow near-surface nitrogen implanted region. The alterations to the technique are now described briefly.

Cleaving and polishing

The cleaving and polishing procedures were the same as with the standard technique, except that specimens were only ∼16mm long, since the modified technique omitted the four-point bend stage.

Nanoindentation

An MTS Nano Indenter XP nano-hardness tester, described in Chapter 3, was used to make indent damage on the surface of specimens. Testing initially used a spread of indent loads on $\overrightarrow{\mathrm{N}}$Cz-Si specimens, so that the optimum setting could be found. Staggered arrays of 0.3, 1, 3 and 10g load indents were made on specimens, which were then immediately subjected to three-point bend at 550°C with a maximum stress of about 100MPa, so that dislocation generation and expansion from the different indents could be examined. These specimens were not annealed before the three-point bend. Some examples of the indents and dislocations are shown in Figure 6.1. It was found that dislocations associated with the 0.3g and 1g indents appeared only sporadically, and not reliably enough for useful dislocation unlocking measurements. Dislocation generation from the 3g and 10g indents was more consistent, but not as reliable as with the standard technique.

The three-point bend stress required to generate dislocations was ∼30MPa for the

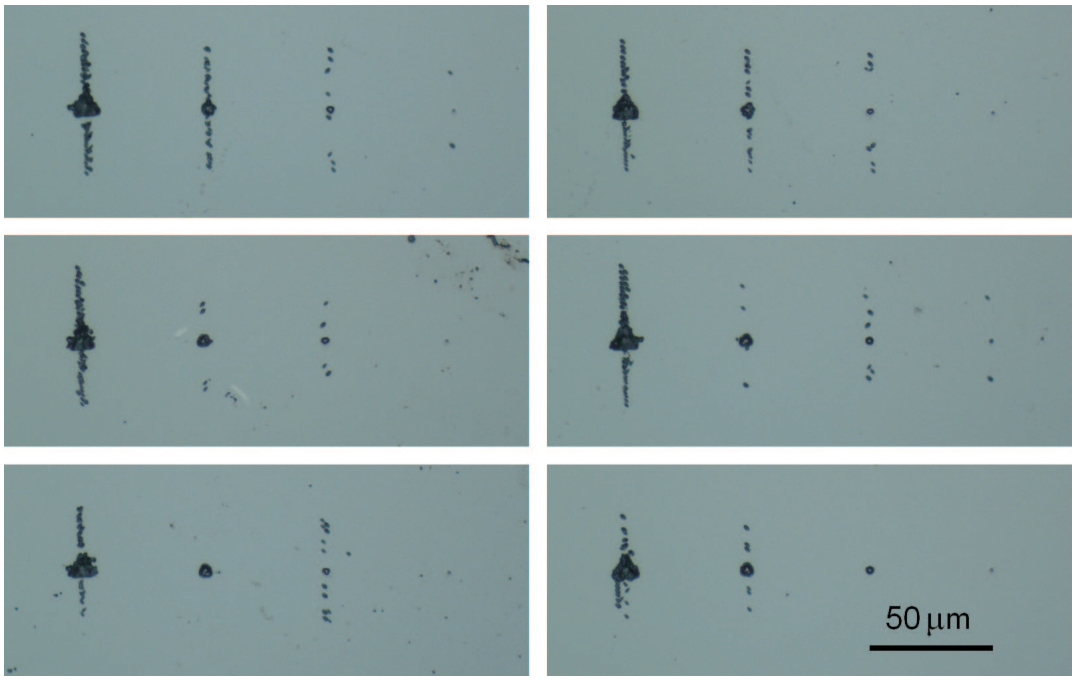


Figure 6.1: Six sets of 10g, 3g, 1g and 0.3g indents from the near the centre of an $\overrightarrow{\text{N}}$Cz 1 specimen that had been indented, then subjected to three-point bend at 550°C with a maximum stress of about 100MPa. The indents in each set are separated by 50 microns. The inconsistency of dislocation growth from the lower-load indents is readily apparent.

10g indents, and ∼50MPa from the 3g indents[1]. Below these stresses, no dislocations were visible after three-point bending. These stresses therefore represent the 'baseline' for subsequent annealed specimens: any extra oxygen- or nitrogen-induced dislocation locking would be added to these values. This represents a significant difference to the standard technique, where dislocations are grown to a large diameter by four-point bend before annealing.

It was decided that annealed specimens would contain arrays of 1, 3 and 10g indents (although ultimately, consistent unlocking stress measurements could only be made with the 3g and 10g indents). As with the standard technique, indents for each load were made down the centre of the specimen, separated by 250μm. The different arrays were offset by 50μm, as shown in Figure 6.1, so that the indents of each did not overlap.

[1]The difference is thought to arise from the dislocation loop geometries associated with the different load indents: the smaller 3g indent loops take more stress to grow, as the stress required to expand a loop is proportional to the inverse of its diameter [233].



Figure 6.2: Two nitrogen-implanted specimens in the final state (after preferential etching to reveal dislocations). The effect of the lacomit-masked etching can be seen.

Lacomit-masked etching

For reasons described in §6.1.4, the modified technique could not use a standard planar etch after the anneal, as the specimen's top surface had to be preserved. Initial tests omitted the planar etch entirely, but specimens fractured from edge damage during the three-point bend stage. Lacomit varnish was therefore used to cover the top surface, leaving the edges exposed, and specimens were immersed in planar etch solution (§3.6) for about 5 minutes. After etching the lacomit was peeled off. This procedure was found to smooth specimens enough to prevent fracture during three-point bend. Two specimens etched in this way are shown in Figure 6.2.

6.1.4 Experimental effectiveness of new technique

Sensitivity to shallow implanted nitrogen

As mentioned above, the experimental technique was modified to improve its sensitivity to the nitrogen contained in the 0.5μm thick implanted layer. Dislocations are approximately 100μm deep after four-point bending in the standard technique; this is acceptable when nitrogen is present throughout the bulk, but not if it is all contained in a shallow layer, since it would then have to diffuse down to the dislocations before being able to lock them. Dislocation depth is therefore the most important aspect of the modified technique, and unfortunately this was not measured directly. The implications of this are discussed further in §6.1.6.

Random error

The unusual conditions used for these experiments affected the level of random error in the results. The large diameter half-loops of the standard experiment are far closer to the 'ideal' conditions of independent, unstressed dislocations than the small loops associated with indent damage used in the modified experiment. This caused a greater level of random error in the $\overrightarrow{\mathrm{N}}$Cz-Si experiments, with values of $\pm$10 - 15% for τ_u being typical.

Oxygen locking test

One of the reasons for using the planar etch in the standard technique is to remove the indent damage before the three-point bend. This is to ensure that no new dislocations are nucleated there during the bend: if indents were acting as dislocation sources, then the technique might be sensitive to the dislocation nucleation stress, rather than the dislocation unlocking stress. Since the modified technique omitted the planar etch step, the indents were still present during the three-point bend. To check that the indent damage was not generating new dislocation loops, the following test was carried out. A Cz-2 specimen was indented, then annealed for 2 hours at 650°C to give at least 150MPa of oxygen dislocation locking [32]. Oxygen locking was used for this test because it is well-understood in Cz-Si material, and a large locking stress can be generated reliably. The specimen was then subjected to three-point bend with τ_{max} ~80MPa; not enough to expand any dislocation loops present during the anneal. The result was that no expanded dislocation loops were seen, showing that indents were not acting as dislocation sources, creating new dislocations during the three-point bend, at this τ_{max}.

6.1.5 Experimental results

The results of the experiments are displayed in this section. Each $\overrightarrow{\mathrm{N}}$Cz specimen was accompanied by a Cz-2 control, since oxygen was present in all the silicon used and could be expected to produce its own dislocation locking effect. If nitrogen dislocation locking was also occurring, τ_u would be higher for the $\overrightarrow{\mathrm{N}}$Cz specimens.

Low temperature anneals

Initial experiments used a short, low temperature anneal of 30 minutes at 550°C. The results, shown in Table 6.1, reveal that there was no additional nitrogen locking under these conditions, within experimental error.

	10g indent	3g indent
$\overrightarrow{\mathrm{N}}$Cz-1	39±5 MPa	46±15 MPa
Cz-2	41±10 MPa	50±10 MPa

Table 6.1: Unlocking stresses measured at 550°C for specimens annealed at 550°C for 30 minutes. τ_{max} was approximately 80MPa.

Anneals at 900°C and above

Since the $\overrightarrow{\mathrm{N}}$Cz-Si contained both nitrogen and oxygen, measurements had to distinguish between the two impurities, being sensitive to the extra locking potentially provided by nitrogen. The optimum conditions for this were thought to be high temperature anneals, since, it was believed, nitrogen might continue to lock dislocations at temperatures above 800°C, where oxygen 'boiled off' [32]. Experiments were therefore performed at high temperature using $\overrightarrow{\mathrm{N}}$Cz-2, the material with the greatest implanted nitrogen content. 900°C anneals were carried out in the RTA furnace using a nitrogen atmosphere. Nitrogen in-diffusion into the Cz-2 control was not thought to be problematic, as nitrogen's solid solubility is extremely low at the annealing temperatures used.

The results of the $\overrightarrow{\mathrm{N}}$Cz-2 900°C anneal tests are shown in Figure 6.3. It can be seen that any nitrogen-related dislocation locking effect is small; if it exists, it is masked by the large amount of random error in the experiments[2]. Figure 6.3 also shows the small extra amount of apparent dislocation locking stress associated with the 3g indents, as opposed to the 10g ones.

A further experiment was carried out using a standard furnace anneal at 1000°C for 30 minutes, and the results are shown in Table 6.2. This also failed to show any significant increase in dislocation unlocking stress in the nitrogen-implanted speci-

[2]Measurement error was found to be significantly greater with the modified dislocation unlocking technique, probably as a result of the inconsistent nature of the dislocations punched out from indents.

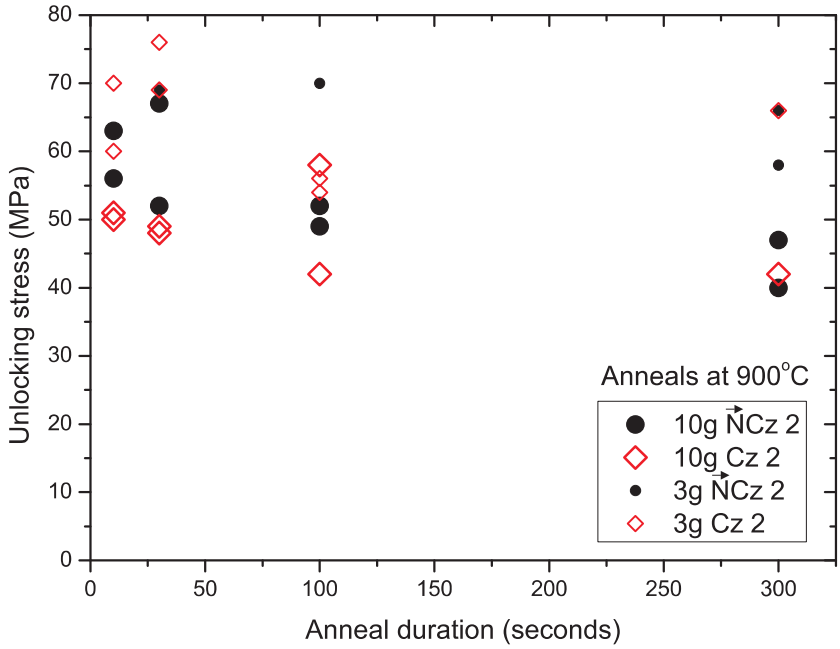


Figure 6.3: Unlocking stress measured at 550°C, for nitrogen-implanted specimens and control specimens annealed in an RTA furnace at 900°C. Error bars are not shown for clarity, but are generally of the order ±5-10MPa.

	10g indent	3g indent
$\overrightarrow{\text{N}}$Cz-2	42±5 MPa	66±15 MPa
Cz-2	36±6 MPa	58±10 MPa

Table 6.2: Unlocking stresses measured at 550°C for specimens annealed at 1000°C for 30 minutes.

mens.

Long anneals at 800°C

Experiments were also carried out using longer duration 800°C anneals. $\overrightarrow{\text{N}}$Cz-2 specimens were annealed for 4 hours at 800°C in a standard furnace using silica ampoule quenching, and unlocked with τ_{max} ~100MPa. The results from these experiments are shown in Table 6.3. Although the errors are large, there is a consistent difference between the nitrogen implanted specimens and the control, with the $\overrightarrow{\text{N}}$Cz giving about 30MPa of additional locking for both indent loads.

The experiments were discontinued at this point, as other work took precedence. Although a nitrogen dislocation locking effect had been seen, it was not of the magnitude that had originally been hoped for, and the 4 hour 800°C anneal is not in-

	10g indent	3g indent
$\overrightarrow{\mathrm{N}}$Cz-2	73±30 MPa 78±20 MPa	>104 MPa >106 MPa
Cz-2	49±9 MPa 43±6 MPa	80±30 MPa 90±20 MPa

Table 6.3: Unlocking stresses measured at 550°C for specimens annealed at 800°C for 4 hours. For the 3g $\overrightarrow{\mathrm{N}}$Cz-2 specimens '$> \tau_{max}$' is shown, as no dislocations were seen.

dustrially practical. However, it is believed that these measurements could provide a useful starting point for further study using the $\overrightarrow{\mathrm{N}}$Cz-Si material.

6.1.6 Analysis

The behaviour of nitrogen

A comparison can be made between the results presented above, and the NFZ-Si standard dislocation unlocking measurements in Chapter 5. It can be seen from Figure 5.4 that the Regime 2 saturation stress in the standard NFZ-Si experiments is about 15MPa at anneals of 900°C, and 20-30MPa at 800°C. These amounts are similar to those seen in the $\overrightarrow{\mathrm{N}}$Cz experiments. This is surprising, as it had been expected that the massively enhanced local nitrogen concentration in the $\overrightarrow{\mathrm{N}}$Cz would give a large boost to the nitrogen dislocation locking effect. It is possible that the Regime 2 saturation stress found in the standard experiments, shown in Figure 5.4, may represent a fundamental limit of nitrogen dislocation locking strength that is not [N]-dependent.

It should be noted, however, that the standard and implant-modified experiments are not directly comparable. In the standard technique, the dislocation loops are large, regular, unaffected by indent damage, and surrounded by an homogenous nitrogen atmosphere. The modified technique uses a smaller tangle of loops which are strongly affected by the strain field of the indent, and a shallow, extremely high concentration nitrogen profile. These factors make the nitrogen implant experiments harder to interpret. The greatest difficulty is that the size, and more importantly depth, of the indent-generated dislocations is not sufficiently well understood. It is not known whether the modified technique succeeded in its aim of creating dislocations shallow

enough to be contained by the nitrogen implant region. If the dislocations were deeper than this, a lack of dislocation locking could simply be due to a failure of the nitrogen to diffuse down to the dislocations.

For these reasons, the interpretation of the $\overrightarrow{\mathrm{N}}$Cz experiments is unclear. However, the length scale of the nitrogen diffusion that occurred during the experiments can be estimated using the expression for nitrogen's effective diffusivity found in the previous chapter. Using the approximation $x = 2\sqrt{Dt}$ [276], it is found that the scale of diffusion is 24μm in the 4 hour 800°C anneal, 16μm in the 300s 900°C anneal, and 130μm in the 1000°C anneal. These distances seem sufficiently large that a considerable quantity of nitrogen could have reached dislocations associated with even the 10g indents.

It should be noted, however, that if transport is by a dissociative mechanism then effective diffusivity is [N]-dependent, decreasing as [N] increases (Equation 5.10), so nitrogen transport would be slower than this in the extremely high-[N] implanted regions. The effect of this behaviour can be approximated by dividing the effective nitrogen diffusivity found in the previous chapter by the square root of the ratio of the nitrogen concentrations in the two materials ($\sqrt{(}2 \times 10^{20}\mathrm{cm}^{-3}/2 \times 10^{15}\mathrm{cm}^{-3}) = 316$). This then gives a diffusion depth of around 1μm for the 800 and 900°C anneals - a depth that may not have allowed nitrogen to reach the dislocations - and 7μm for the 1000°C anneal. Since nitrogen's dislocation locking strength is known to fall towards zero at 1000°C, the lack of a large dislocation locking effect in the $\overrightarrow{\mathrm{N}}$Cz experiments may be evidence for dissociative nitrogen transport.

Industrial application

Nitrogen implants have been suggested as a means of improving the mechanical properties of devices [242], and as such, the system is a technologically relevant one. The nitrogen-induced high-temperature dislocation locking that had been hoped for, however, has not been found, although experimental conditions were not ideal, since it is possible that the dislocations were deeper than the implanted nitrogen. Indeed, the indent data generated by the nano-indenter, displayed below, shows that the indent

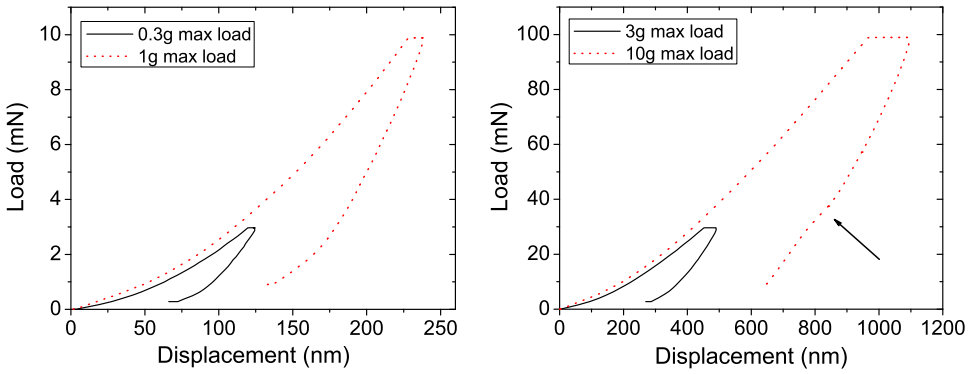


Figure 6.4: Load-displacement data from 0.3g, 1g, 3g and 10g indents. The arrow indicates a pressure-induced phase transformation ('pop-out') [289] when the 10g load is being removed.

depth was about the same as the maximum implant depth for the 3g load, and twice the implant depth for the 10g load. It is therefore likely that the dislocation tangles, which form in the damaged region directly underneath each indent, may have existed beneath the nitrogen-implanted material. Further study, using an improved experimental technique, may therefore still show that implanted nitrogen can give significant improvements in terms of near-surface dislocation pinning.

Indentation data

The nano-indenter can be used to generate detailed data from each indent test, and this provides information about the indents as well as the mechanical properties of the silicon. For this work the nano-indenter was used with non-optimised operating conditions to increase the rate at which indents could be made, as the aim was simply to damage the specimen surface, rather than conduct a detailed investigation into structural properties. Load-displacement data were taken for each indent, however, and some examples, from the different indent loads, are shown in Figure 6.4. Typical values for indent depths were 115nm, 225nm, 415nm and 850nm for the 0.3g, 1g, 3g and 10g loads respectively.

The nano-indenter's software was not set up to generate micro-hardness informa-

tion directly, but an indication of the relative hardness of the $\overrightarrow{\mathrm{N}}$Cz and Cz silicon can be found by comparing load-displacement curves for the two materials. One measure of hardness is the depth of the indent when maximum load is first reached. This value has been recorded for approximately 630 indents at each indent load in both materials, using data from approximately 10 specimens of each silicon type, and histograms of the results are presented in Figure 6.5.

A few inferences can be drawn from these results:

- The general form of the histograms is a logarithmic normal distribution. There is considerable variation in the indent depths, particularly at the higher loads, which reflects the unsophisticated way in which the nano-indenter was set up: a high 'pre-impact' indenter tip speed was used to reduce the time taken for each indent.

- The peaks of the distributions for the two materials are located at approximately the same indent depth, for each load. This indicates that the overall hardness of the silicon has not been significantly affected by the nitrogen implantation.

- The distributions of the $\overrightarrow{\mathrm{N}}$Cz specimens are all broadened slightly compared to those of the Cz-Si controls, which have sharper peaks. This would suggest that the implanted material does not have the same degree of homogeneity as the control.

However, it should be emphasised that these conclusions are only provisional, since the nano-indenter was not optimised for hardness measurements.

6.2 Arsenic-implanted Cz silicon

This section describes a small set of experiments that were carried out using arsenic-implanted Cz-silicon ($\overrightarrow{\mathrm{As}}$Cz-Si) provided by Varian Semiconductor Equipment Associates, Inc.

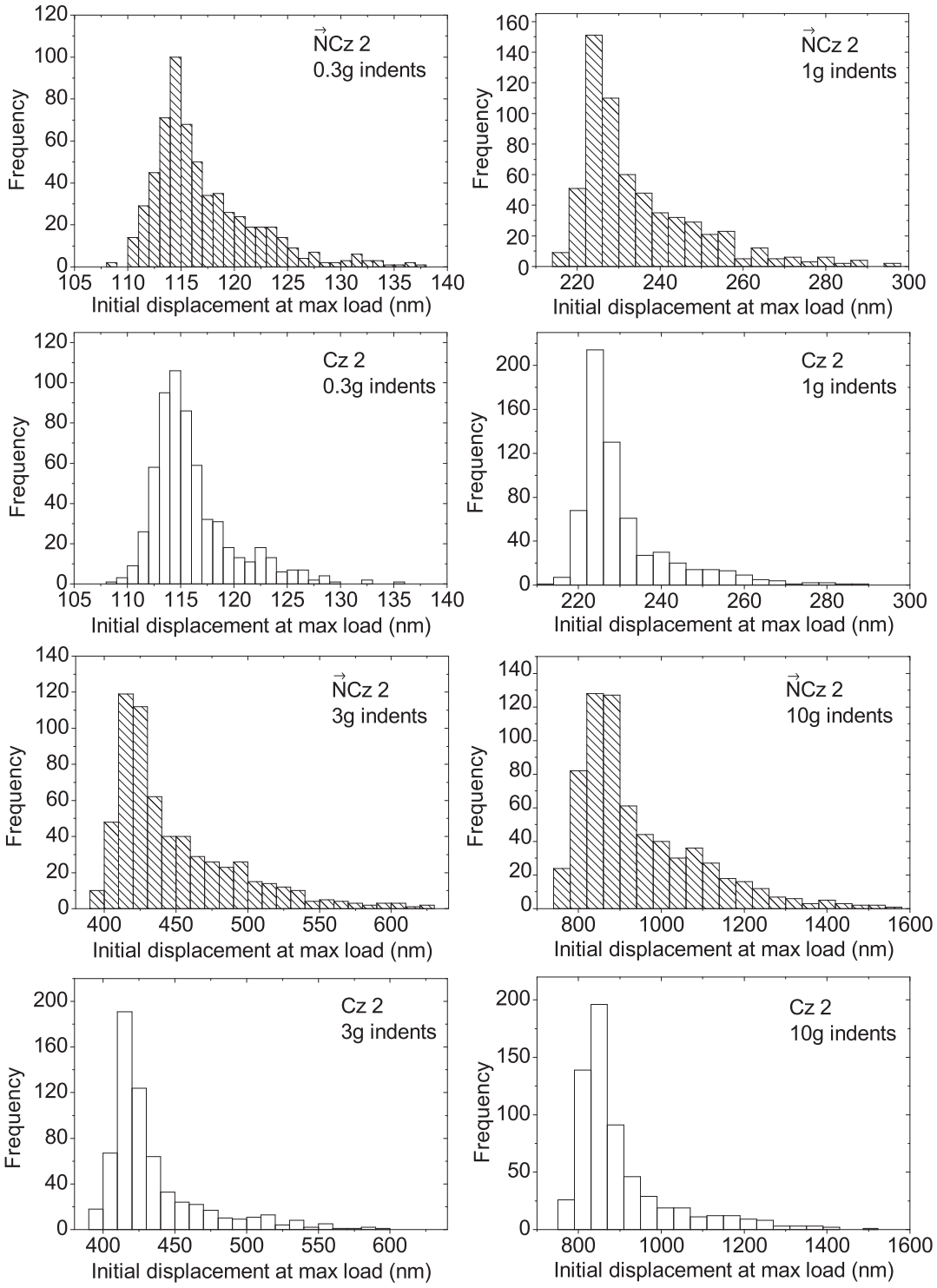


Figure 6.5: Histograms of the indent depth when maximum load is first reached, for all indent loads used, in both N-implanted and control specimens.

6.2.1 Motivation

It is well known that the annealing of ion-implanted silicon can create dislocation loops, which evolve from end-of-range damage [290]. These loops are a mixture of extrinsic faulted Frank loops [291], which can only grow by climb, and perfect loops which can glide [292]. One set of experiments, carried out in collaboration with Varian Semiconductor Equipment Associates, Inc., provided an opportunity to use these implant-generated loops to investigate implanted nitrogen's interaction with dislocations, in a system that did not suffer from the dislocation depth problem that affected the work described in §6.1.

The experiments were to use arsenic-implanted silicon, $\overrightarrow{\text{As}}$Cz-Si, which had been thermally treated to evolve dislocation loops at the implant end-of-range. Specimens from these wafers could be stressed in the three-point bend configuration at elevated temperature. It was hoped that the perfect dislocation loops would expand under this stress, and eventually encounter the specimen surface, where they could be revealed by a subsequent preferential etch. This would allow the stress required to grow the loops, which is dependent largely on their initial diameter, to be determined.

Further experiments would then use wafers that had been co-implanted with both arsenic and nitrogen, at implant energies that produced overlapping distribution profiles. These specimens would be subjected to the same tests as the arsenic-only implanted specimens, the hope being that the implanted nitrogen would create a measurable dislocation locking effect, so that the stress required to expand the loops to the surface of specimens would be greater. This new experimental technique removed one of the complications of the $\overrightarrow{\text{N}}$Cz described in §6.1, as the implanted nitrogen would surround the dislocation loops, rather than potentially having to diffuse down into the wafer to reach them.

6.2.2 Experiments

Preliminary experiments used two wafers, $\overrightarrow{\text{As}}$Cz 1 and $\overrightarrow{\text{As}}$Cz 2, which had been implanted with arsenic ions at 30keV at a dose of $5 \times 10^{15}\text{cm}^{-2}$, using 7° tilt and 22° twist. After implantation a 1050°C spike anneal had been performed on the wafers,

with the time spent above 1000°C being 1.3s [293], which served to coarsen the dislocation loops.

A simplified experimental procedure was used for $\overrightarrow{\text{As}}$Cz-Si specimens. The experiments would have to identify loops that had grown to the specimen surface, and these could potentially be very few in number. It was therefore important that the specimen surface be kept completely free from any kind of damage, to provide a clean background against which the expanded loops could be identified. For this reason, the grinding and polishing steps were removed from the experimental procedure. Specimens were cleaved from wafers, lacomit-mask etched to smooth the edges, and then subjected to three-point bend at 550°C. Planar etching of as-cleaved specimens was found to be sufficient to prevent fracture during three-point bend; however, since the specimens were not ground and polished to a regular cuboid shape, τ_{max} could only be calculated approximately.

Tests on both wafers used three-point bends with τ_{max} up to ∼340MPa, but no dislocations were seen after preferential etching. Experiments were not continued beyond this point due to time limitations, but it is believed that the method could yield information about the locking of implant-generated loops by nitrogen if pursued further. It is assumed that no dislocations were seen because the loops were too small to be expanded by the stresses used, so in further experiments specimens could be annealed before the three-point bend, so that loops grow to a detectable size.

6.3 Out-diffusion of nitrogen from NFZ-Si

6.3.1 Introduction

This section describes experiments which measured diffusion of nitrogen in silicon using an alternative approach to the standard dislocation unlocking method. While the standard technique only measures nitrogen diffusion to dislocations, the method described in this section also measures diffusion to the surface, and so is more comparable with SIMS experiments. Transport in this method also occurs over tens of microns, the length scale associated with SIMS experiments, rather than the usual

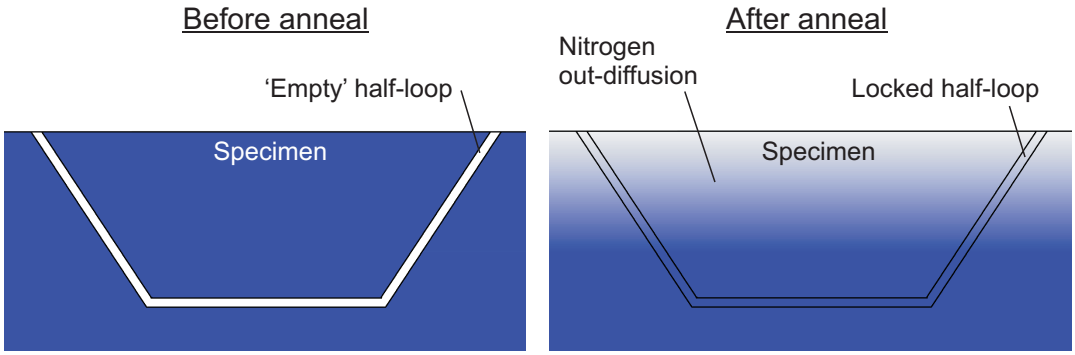


Figure 6.6: Schematic showing the effect of an out-diffused nitrogen concentration profile on dislocation locking at different depths in the specimen.

sub-micron scale associated with standard dislocation unlocking experiments.

6.3.2 Experimental technique

Experiments were performed using 'High-[N] 4', a 100Ωcm NFZ-Si wafer with [N] = 2.5×10^{15}cm^{-3}. Specimen preparation and the initial stages of the technique were identical to the standard dislocation unlocking technique, with specimens being cleaved and polished, indented, and subjected to four-point bend to introduce a dislocation array, as discussed in Chapter 3. Specimens were then all given an anneal of 15 hours at 750°C, which was calculated to give an out-diffusion profile to a depth of ~20μm, according to an extrapolation of higher-temperature SIMS data [177].

Specimens that have been annealed to produce an out-diffusion profile have a variable local nitrogen concentration, going from very low near the specimen surface to the full original concentration deep into the bulk. The dislocations introduced by indent and four-point bend run down from the surface to a depth of about 100μm, so they experience the full range of local nitrogen concentrations at different positions along their length, as shown in Figure 6.6. It is assumed that the nitrogen dislocation locking effect also varies along the dislocation length, in proportion to the local nitrogen concentration, meaning that near-surface sections of the dislocations are locked less strongly than sections deep into the specimen.

A dislocation which is locked with a varying strength is assumed to unlock at the point which is pinned the least strongly, which in this case is at the specimen surface. This is one of the reasons that a large depth planar etch is used in the standard

technique after annealing: to remove any sections of dislocations affected this way, so that the full-strength locking effect associated with the bulk nitrogen concentration will be measured. In the out-diffusion dislocation unlocking experiments, however, the variable near-surface locking strength was exploited, to give information about the nature of the out-diffusion profile.

After annealing, specimens were given planar etches of varying durations, to remove differing amounts of material from the surface[3], from 5 to 95μm. This meant that weakly-locked near-surface sections of the dislocations were still present after the etch in some cases. Specimens were then subjected to a three-point bend to unlock the dislocations. Unfortunately, bending conditions were not standardised for these tests as this was not known to be a significant factor at the time; the implications of this are discussed in the next section. The results of these measurements are displayed in Figure 6.7.

6.3.3 Results and discussion

Also presented in Figure 6.7 is a standard Fickian out-diffusion profile:

$$\frac{C - C_s}{C_0 - C_s} = \mathrm{erf}\left(\frac{x}{2\sqrt{Dt}}\right) \tag{6.1}$$

for which the surface nitrogen concentration C_s has been set to zero. C, the nitrogen concentration, is assumed to be proportional to unlocking stress, with C_0, the bulk nitrogen concentration, corresponding to the greatest value of unlocking stress measured. x is the distance from the surface at the time of the anneal, corresponding to the depth of the planar etch, and D is the effective nitrogen diffusivity, used as the fitting parameter, with a value of $4 \times 10^{-11}\mathrm{cm}^2\mathrm{s}^{-1}$.

The data show dislocation unlocking stress falling off for lightly-etched specimens, in accordance with what would be expected from the interpretation given above. The reason for the low unlocking stress of the two most highly-etched specimens was unclear when the measurements were made; further investigation to determine

[3]Planar etch depths were evaluated by measuring the separation of the two lines of dislocation etch pits associated with each indent after preferential etching, and dividing by $\sqrt{2}$, the appropriate geometric factor.

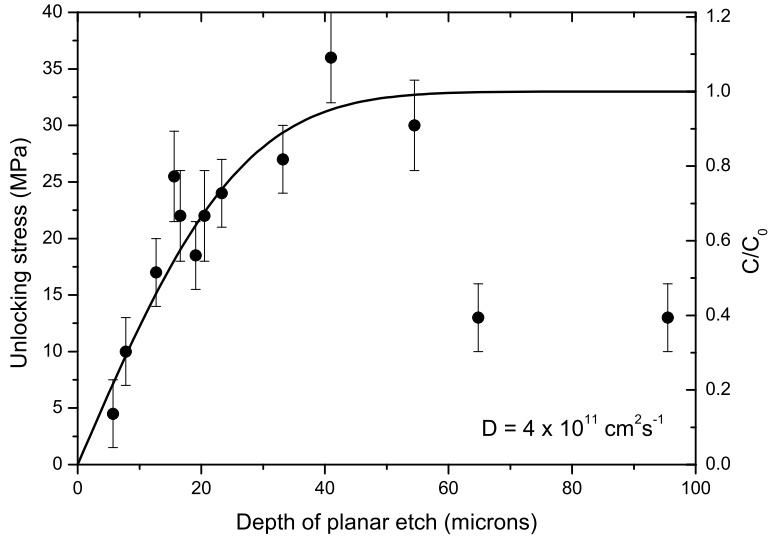


Figure 6.7: Dislocation unlocking stress measured at 550°C in 'High-[N] 4' NFZ-Si as a function of depth of material removed by planar etch. Specimens had been annealed at 750°C for 15 hours. The circles represent measured unlocking stresses (left axis). The line is an error function fit of the form $C/C_0 = \mathrm{erf}(x/2\sqrt{Dt})$, where C/C_0 is the nitrogen concentration as a proportion of the bulk concentration, D is the effective diffusivity of nitrogen at the annealing temperature, t is the anneal duration, and x is the depth into the specimen.

whether this was a real effect was not possible, as the silicon used for these experiments had run out. The value of effective diffusivity used for the fit, $4 \times 10^{-11}\mathrm{cm}^2\mathrm{s}^{-1}$, is consistent with an extrapolation of the SIMS out-diffusion nitrogen effective diffusivity found by Itoh and Abe [177], and approximately two orders of magnitude greater than the values found by Giannattasio and Murphy using standard dislocation unlocking experiments [253, 254].

Unfortunately, these experiments were performed before the relationship between three-point bend duration and unlocking stress, discussed in §4.3, was known. Following standard procedure, the lightly etched specimens were unlocked for long durations, to suit the expected low locking stresses. The three-point bend durations used for each measurement are displayed in Figure 6.8. There is a correlation between unlocking stress and three-point bend duration; this could also partially explain the low unlocking stresses of two most heavily etched specimens, which were given relatively long three-point bends.

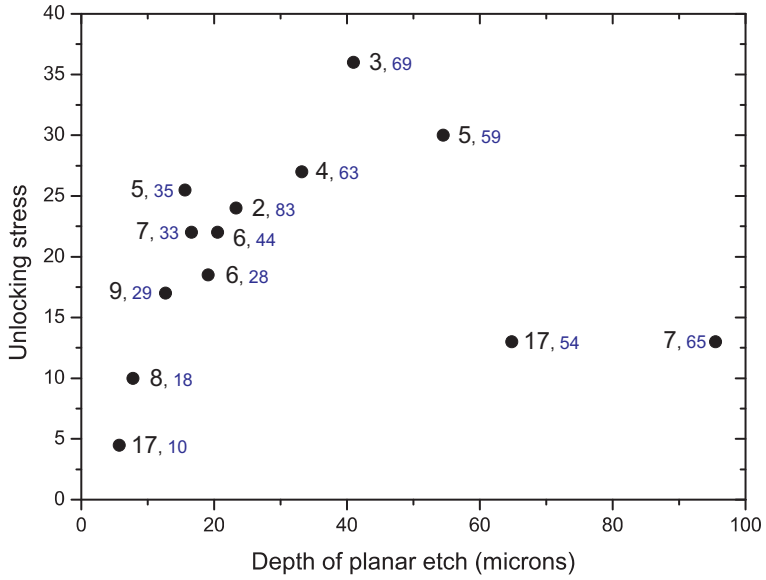


Figure 6.8: Dislocation unlocking stress measured at 550°C in 'High-[N] 4' NFZ-Si as a function of depth of material removed by planar etch. Specimens had been annealed at 750°C for 15 hours. These are the same data as presented in Figure 6.7. The two numbers next to each point give the three-point bend duration (in hours) on the left, and τ_{max} (in MPa) on the right, in blue.

It is not possible to separate the three-point bend duration effect from the real effect due to out-diffusion from the specimens. However, the data do give an indication of the general scale of the out-diffusion process at the temperature measured, which is still a useful result. The effective diffusivity of $4 \times 10^{-11} \mathrm{cm}^2\mathrm{s}^{-1}$ is consistent with that found by the new nitrogen dislocation unlocking measurements presented in Chapter 5.

6.4 Summary

Experiments using $\overrightarrow{\mathrm{N}}$Cz-Si indicate that implanted nitrogen does not produce a large dislocation locking effect at high anneal temperatures, as had been hoped. The level of nitrogen dislocation locking that was measured in these experiments was comparable to that seen in the standard NFZ-Si dislocation unlocking experiments - a surprising result, given the massively enhanced local nitrogen concentration in the $\overrightarrow{\mathrm{N}}$Cz-Si material. However, this interpretation is tentative because of uncertainty about the experimental system: the indents will have produced dislocations that ran

deeper than the implanted nitrogen. For this reason, the lack of a large locking effect may provide evidence for dissociative nitrogen diffusion, as nitrogen's diffusion length scale in the $\overrightarrow{\mathrm{N}}$Cz-Si material would be reduced due to the extremely high nitrogen concentration.

It is hoped that further study of nitrogen-implanted silicon might yield less ambiguous results. Experiments could also utilise the principle explored with the $\overrightarrow{\mathrm{As}}$Cz-Si experiments, where dislocation loops grown from implant damage are used to measure nitrogen's locking ability. The small set of $\overrightarrow{\mathrm{As}}$Cz measurements performed in this work were not able to demonstrate the proposed method successfully, but this is not thought to be due to a fundamental limitation.

The NFZ-Si nitrogen out-diffusion experiments outlined in this chapter were affected by the non-standardisation of three-point bend duration, but nevertheless give an indication of the general scale of diffusion at the temperature measured, which is consistent with higher temperature SIMS work and also the new results found using the standard dislocation unlocking technique presented in the previous chapter.

Chapter 7

Summary and further work

7.1 Nitrogen in silicon

7.1.1 Low-temperature transport

The dislocation unlocking experiments presented in Chapter 5 have been used to infer an effective diffusivity of nitrogen in silicon in the 500 - 750°C temperature range:

$$D = 173,000 \exp\left(-\frac{3.24\text{eV}}{kT}\right) \text{cm}^2\text{s}^{-1} \tag{7.1}$$

This result, believed to be the first correct measurement of nitrogen's low temperature effective diffusivity in the literature, shows that nitrogen transport in silicon behaves in a consistent way from 500°C to near the melting point. The activation energy of 3.24eV is only slightly higher than the value found from higher temperature SIMS experiments. The pre-factor of 173,000cm^2s^{-1} is unusually large for a simple diffusivity, indicating that nitrogen's transport mechanism may be more complex than simple diffusion of the interstitial dimer. If analysed in terms of a monomer-dimer dissociative mechanism, the results give a diffusivity for the nitrogen monomer of:

$$D_1 = 28 \exp\left(\frac{-(1.1 \rightarrow 1.4\text{eV})}{kT}\right) \text{cm}^2\text{s}^{-1} \tag{7.2}$$

This expression is consistent with that found by another analysis in the literature [191].

7.1.2 Interaction with dislocations

Regime 2 results

Experiments have shown that nitrogen's dislocation locking strength measured at 550°C is dependent on anneal temperature, peaking at 600 - 700°C and falling towards zero above 1000°C. This behaviour is not understood: it is not compatible with simple locking of dislocations by an atomic species. These measurements also have implications for industry since nitrogen is used in silicon wafers to improve mechanical strength.

Dependence of unlocking stress on three-point bend duration

An investigation into the dislocation unlocking technique itself showed that measured unlocking stress is dependent on the duration of the three-point bend. It has been found that the unlocking stress drops with increasing unlocking time in every type of silicon tested, an effect which has important implications for previous nitrogen dislocation unlocking results. If analysed in terms of a theory of release of dislocations from pinning points, the results show that the line density of pinning points in locked NFZ-Si specimens is approximately $10^8 \mathrm{m}^{-1}$ for all types of material tested.

Dislocation velocity

FZ- and NFZ-Si dislocation unlocking specimens have been measured to determine the dislocation velocity during the three-point bend stage. The mean velocity is broadly consistent with dislocation velocity expressions reported in the literature. While there is no dependence of dislocation velocity on anneal regime, there is a weak dependence on the nitrogen content of the material: the greater [N] is, the slower the dislocations move. This is a tentative result, however, as the number of data from the low [N] silicon types is not large.

7.1.3 Nitrogen-implanted silicon

Experiments reported in Chapter 6 used heavily N-implanted silicon in an attempt to measure nitrogen dislocation locking in a shallow implanted layer. Nitrogen im-

plantation has the potential to be useful in industry, as a massively elevated nitrogen concentration can be delivered directly to the active regions of wafers where mobile dislocations are the most damaging. The experiments used a modified version of the dislocation unlocking technique which was designed to be sensitive to the near-surface nitrogen. Measurements found modest improvements in dislocation locking strength in the N-implanted wafers over the control wafers, showing that nitrogen implantation does improve near-surface mechanical strength to some degree; however, the dislocations may have been deeper than the implanted nitrogen layer, so the results may underestimate the potential locking strength of implanted nitrogen. It is believed that further work in this area, using an improved technique, might detect a larger locking effect.

It is not known whether high concentrations of nitrogen can give a stronger dislocation locking effect than the $\sim 10^{15}\text{cm}^{-3}$ atoms found in as-grown material, which has been tested extensively in this thesis using the standard dislocation unlocking technique. However, if it is assumed that a stronger locking effect does exist, then the comparatively weak effect seen in $\overrightarrow{\text{N}}\text{Cz}$ can be used to infer the scale of nitrogen transport that was occurring in these experiments. The high temperature anneals were of sufficient duration for large quantities of nitrogen to have diffused to any dislocations associated with the indents, if nitrogen's effective diffusivity is the same as that found with the NFZ-Si work. However, if effective diffusivity is [N]-dependent, as predicted by the dissociative mechanism, then the length scale of the nitrogen transport would be far shorter and significant quantities of nitrogen may not have reached the dislocations. The lack of a strong dislocation locking effect in these experiments may therefore be evidence in favour of the dissociative model of nitrogen transport.

7.1.4 Interaction with transition metals

NFZ-Si dislocation unlocking specimens that were deliberately contaminated with transition metals have been found to give lower unlocking stress measurements (§4.1.2). The reason for this is unknown, but it seems that nitrogen transport is impeded by the presence of transition metals in some way.

7.2 The dislocation unlocking experimental method

7.2.1 Improvement in technique

The dislocation unlocking technique, as used in this work, is described in Chapter 3. It has been altered so that the three-point bend load and duration are the same for every test. Also, graphs representing the diameters of the whole array of dislocation sets are now used when determining the unlocking stress.

The alterations have resulted in the elimination of a potential systematic error due to the intentional variation of three-point bend duration. This is believed to largely explain the difference between the new nitrogen results, and the previous ones collected by Giannattasio and Murphy, which are now thought to have been affected by error. Confidence in the new results comes from the use of a standardised technique, repeat measurements using Murphy's low-[N] material, the greater number of data in the new experiments, and the correspondence between the new results and those found at higher temperatures using SIMS.

7.2.2 Usefulness of the dislocation unlocking technique

The dislocation unlocking technique is hard to learn, time-consuming to apply, and still not completely understood. It produces results which can be indirect and hard to interpret. Experiments using NFZ-Si are particularly problematic because of the low locking stresses produced by nitrogen and the high level of random error in the measurements. Despite these difficulties, however, the technique has been used in this work to successfully measure nitrogen's low temperature effective diffusivity in silicon, something that has not been achieved by any other method. This is possible largely because dislocation unlocking has the advantage of being sensitive to sub-micron impurity transport, and so can make measurements at low temperatures where diffusion is extremely slow.

Since the experiments are sensitive to impurity interactions with dislocations, they also give information about the mechanical properties of the material, in a particularly precise manner. The technique can therefore have applications in the modern

semiconductor device industry, where (for example) transistors fail because of the generation and movement of small numbers of dislocations.

For these reasons, the dislocation unlocking technique continues to be relevant and useful.

7.3 Suggestions for further work

7.3.1 Nitrogen dislocation unlocking experiments

Dependence of unlocking stress on unlocking temperature

Murphy's experiments which showed that unlocking stress fell with increasing unlocking temperature (§2.3.3, Figure 2.10) may have been affected by errors that arose with the old experimental technique, so they should be repeated. The experiment is important as it gives information about how nitrogen binds to dislocations, possibly allowing the nature of the locking species to be identified; and also the measurements are industrially useful as they concern the mechanical properties of the material.

Dependence of unlocking stress on nitrogen concentration

The lack of standardised three-point bend conditions in previous nitrogen experiments also affects the conclusions drawn about the [N]-dependence of the dislocation locking effect, and so, as above, these experiments should be repeated. The results shown in Figure 5.11, where Murphy's low-[N] material was tested using the standardised technique, do allow some initial remarks to be made, however. There are not enough results to comment on the Regime 1 behaviour, but the Regime 2 stress is clearly lower in the low-[N] material, and shows the same dependence on anneal temperature. Further experiments using material with different nitrogen concentrations would help to clarify these results. These results could also provide evidence in favour of one or other of the competing mechanisms for nitrogen transport - dimer diffusion and dissociative transport - since effective diffusivity in the latter is concentration-dependent.

Modelling dislocation unlocking experiments in terms of dissociative transport

The numerical simulation used to model the dislocation unlocking results in Chapter 5 assumes simple Fickian behaviour to calculate diffusion of nitrogen atoms to dislocations. The effective diffusivities found using this method have been analysed in terms of dissociative transport, allowing a nitrogen monomer diffusivity to be deduced (§5.2.3). However, this analysis is slightly flawed, since if transport *is* by a dissociative mechanism, then simple Fickian behaviour should not be used to model the data. Effective diffusivity in the dissociative model is concentration-dependent, and so would vary as a function of position in a concentration gradient around a dislocation.

This modelling has not been attempted here as it is beyond the scope of this work, but it should be carried out if a more complete understanding of the dislocation unlocking results is to be found.

Experiments investigating the nature of the locking species

Section 5.5.3 outlined the evidence for dislocation locking by atoms and precipitates in the new results, and suggested further experiments that might allow the locking agent to be identified. These experiments should be sensitive to the interaction energy between the locking agent and the dislocation, which is much higher for precipitates than atoms. As well as measuring the dependence of unlocking stress on unlocking temperature, as mentioned above, experiments could also explore the effect of secondary anneals on already-locked dislocations, to see whether the locking agent could be 'boiled off' easily or not.

It has also been noted that the new nitrogen data show what seems to be a slight 'stepped' shape at 600 and possibly 675°C. Unfortunately, the high level of random error in the measurements means that no firm conclusions can be drawn about this phenomenon. Further work could investigate this more thoroughly by improving the experimental technique to reduce the random error, or simply taking more data.

Double etching technique and low stress measurements

The low dislocation locking stresses produced by nitrogen are hard to measure accurately. In previous work, improvements in precision were sought by using variable three-point bend conditions, which introduced systematic error, and in this work standardised conditions have been used, eliminating the error but at the cost of reduced precision in low-stress measurements. One alternative approach would be to use 'saucer and pit' double etching. Specimens would be given an extra etch before the three-point bend, which would be slightly preferential, creating wide, shallow depressions (*i.e.* 'saucers') at each dislocation. A preferential etch would then be used after the three-point bend, to create deep narrow pits, in a similar manner to the standard technique. Each dislocation would therefore have both a saucer and a pit associated with it. This could give information about the motion of individual dislocations at very short scales, since the saucer and the pit would coincide if the dislocation had not moved during the three-point bend, but there would be a gap if it had moved.

The technique could be used in non-standard experiments which measured very low locking stresses, since the necessarily low three-point bend loads would mean that dislocations moved slowly. It could also help to improve the understanding of the dislocation unlocking technique itself, as it would give information about the number of dislocations that unlock during the three-point bends, which is currently unknown. Low stress measurements at 900°C and above are also technologically relevant, as locking stresses of just 1-2MPa are significant in this regime, for example in terms of the gravitational stresses experienced by wafers during device fabrication.

7.3.2 Oxygen dislocation unlocking experiments

It was noted in §2.2.3 that dislocation unlocking has also been used recently with highly antimony- and boron-doped Cz-Si, measuring enhanced oxygen transport at low temperatures with boron doping, but no change with antimony. This investigation could be extended to measure the effects of different shallow dopants such as arsenic, phosphorous and gallium.

7.3.3 Nitrogen-implanted silicon

The preliminary $\overrightarrow{\mathrm{N}}$Cz-Si experiments that have been carried out in this work, discussed in Chapter 6, are thought an ideal starting point for a more detailed study. The experimental technique could be improved, and characterized more fully, to allow more certainty in the results. Experiments could then investigate the dependence of unlocking stress on anneal conditions, nitrogen concentration, and other parameters such as dislocation size and depth. In addition to this, the second experimental technique which used arsenic implants to create internal dislocation loops, outlined in §6.2, could be developed further to use nitrogen co-implantation. This would remove the complication that affected the $\overrightarrow{\mathrm{N}}$Cz-Si experiments, where the mechanically created dislocation loops might have been deeper than the shallow implanted nitrogen. With co-implantation, it would be easy to ensure that the nitrogen profile coincided with the implant-generated loops.

Appendix A

Program used to model nitrogen's interaction with dislocations

The process used to model the nitrogen dislocation unlocking experiments is described in this appendix. The Fortran code of the modelling program, which was initially developed by Dr S. Senkader [32], is presented after this.

The modelling program produces a numerical solution to this equation, at each annealing temperature:

$$\frac{\partial C}{\partial t} = D_{\text{eff}} \nabla \left[\nabla C + \frac{C}{kT} \nabla \left(\Delta G_{\text{binding}} \right) \right] \tag{A.1}$$

Two boundary conditions are used. The first sets the impurity concentration far away from the dislocation as being the bulk concentration:

$$C(R) = C_0 \tag{A.2}$$

where C_0 is the background impurity concentration as above, and R is the smallest distance from the dislocation core at which there is no change in the impurity concentration, C, for all annealing temperatures and durations.

The second boundary condition relates to the capture and re-emission of impurities

from the dislocation core, located at $r = r_0$. The capture rate is given, in accordance with Fermi-Dirac statistics, by:

$$\text{capture} \propto C_1 \frac{C_a - C_c}{C_a} \tag{A.3}$$

where C_1 is the impurity concentration next to the dislocation core, C_a is the concentration of available sites at the core, and C_c is the concentration of occupied sites at the core. The emission rate is assumed to be a function of the escape probability from the core, and the impurity concentration at the core, according to:

$$\text{emission} \propto C_c \exp\left(-\frac{\Delta G_{binding}}{kT}\right) \tag{A.4}$$

The total flux of atoms passing through the dislocation core boundary at $r = r_0$ is then:

$$J = 2\pi r_0 D_0 \left[C_1 \frac{C_a - C_c}{C_a} - C_c \exp\left(\frac{\Delta S_{binding}}{k}\right) \exp\left(-\frac{\Delta H_{binding}}{kT}\right)\right] \tag{A.5}$$

as $\Delta G_{binding} = \Delta H_{binding} - T\Delta S_{binding}$. For the modelling done in this work, however, $\Delta H_{binding}$ was set at the high value of 5eV, to minimise the emission of impurities calculated to occur. The program therefore has not been used to model Regime 2.

The program uses a finite difference method to calculate the concentration of impurities at the dislocation core, from Equation A.5. A uniform impurity concentration C_0 is assumed throughout the material at the start of the operation, $t = 0$, and then the impurity distribution is calculated after small successive time steps. This allows the concentration of impurity atoms to be calculated for the appropriate anneal durations, for each temperature investigated.

The dislocation core is modelled as a cylinder of radius r_0, so that the number of impurity atoms per unit length of the core is given by:

$$N_c = C_c \pi r_0^2 \tag{A.6}$$

The number of available sites at the dislocation core is estimated as being one per Burgers vector (3.8Å for a perfect dislocation in silicon), so $n_a = 2.6 \times 10^{-7}\text{cm}^{-1}$. However, if the dislocation is far from being fully occupied and there is little competition for sites at the dislocation core, the value calculated for diffusivity is insensitive to the value used for n_a. The program calculates N_c - the number of atoms at the dislocation core. This can then be converted to an unlocking stress, since N_c is related to τ_u by:

$$\tau_u = N_c \tau_0 \tag{A.7}$$

where τ_0 is the dislocation locking stress generated by a single atom at the dislocation core. A comparison of the dependence of τ_u on three-point bend duration in Cz-Si and NFZ-Si (§4.3.2) indicates that τ_0 for nitrogen is similar to the value calculated for oxygen, 7Pacm [32], so this value has also been used here.

The geometric factors r_0 and C_a can be estimated accurately, so the modelling program effectively has three fitting parameters:

- D_{eff}, the effective diffusivity of the impurity.
- τ_0, the locking strength per impurity atom.
- ΔS, the change in entropy associated with binding to the dislocation core.

The model is insensitive to changes in the value used for ΔS, and τ_0 has been set as 7Pacm, as described above. This means that D_{eff} is the only varied fitting parameter. All the other parameters took the same values for modelling runs at the different anneal temperatures, as described below, and D_{eff} was varied until the calculated unlocking stress coincided with the Regime 1 data, at each temperature.

The values used for the inputs are shown in Table A.1. The bulk nitrogen concentration, C_0, has been set at $2 \times 10^{15}\text{cm}^{-3}$, the nitrogen concentration quoted by the manufacturer. The values used for the other parameters are those used for previous work: C_a is the number of available sites in the silicon lattice, r_{max} is the maximum diffusion length, r_0 is the dislocation core radius, and ΔS the change in entropy when an atom binds to the dislocation core.

Parameter	Value used
C_0	$2 \times 10^{15}\text{cm}^{-3}$
r_{max}	$1 \times 10^{-4}\text{cm}$
r_0	$5 \times 10^{-8}\text{cm}$
C_a	$5 \times 10^{22}\text{cm}^{-3}$
ΔS	$7.6 \times 10^{-5}\text{eVK}^{-1}$
τ_0	7Pacm
$\Delta H_{binding}$	5eV

Table A.1: Parameters used in the modelling program.

A.1 Fortran code

The following program was developed by Dr S. Senkader. In the case presented here, the diffusivity is set to $1.75 \times 10^{-16}\text{cm}^2\text{s}^{-1}$, the value found to fit the 500°C nitrogen dislocation unlocking data presented in Chapter 5.

```
      program NPairs

      implicit double precision (a-h,o-z)
      dimension flux(100),concentration(100),radi(100),deltaradi(100)
      dimension area(100)

c *** Length UNITS ARE IN Cm *****

      pi = 3.141592654
      boltz = 8.61573E-5
      cini = 2E15
      rmax = 1E-4
      rmin = 5E-8
      cav = 5E22
      pirmin = pi * rmin * rmin
      av = pirmin*cav
      entropy = 7.6E-5
      atlock = 7
      actenergy=5
      enterprob = exp(entropy/boltz)
      totf=cini*pirmin

c *** Open output file *****
      open(3,file='data.dat')

      write(*,*)'Number of annuli? (MAX 100)'
      read(*,*) n
      write(*,*)
      write(*,*)'What is the Temperature [C]?'
      read(*,*) temperature
      temperature=temperature+273.
      write(*,*)
      write(*,*)'How long does it take (in hours)?'
      read(*,*) time
```

```
      time=time*3600
      write(*,*)
      write(*,*)'Time STEP (milliseconds)?'
      read(*,*) step
      step=step*1.e-3

c *** SET THE NUMBER OF POINTS PER GRAPH (200)***
      ndata=200
      writestep=time/ndata

c *** DIFFUSIVITY AND ESCAPE PROBABILITY ***
      escapeprob = exp(-actenergy/(boltz*temperature))
      diffusivity = 1.75E-16
      pidiff = 2 * pi * diffusivity

c *** SET THE RADIUS OF ANNULI AND INITIAL CONCENTRATION ***
      i=1
      do while (i.le.n)
      radi(i)=dexp(dlog(rmin)+(i-1)*(dlog(rmax)-dlog(rmin))/n)
      concentration(i)=cini
      i = i + 1
      end do
      radi(n)=rmax


c *** SET THE DELTA-RADIUS AND DELTA-AREA ***
      i=1
      do while(i.le.n-1)
      deltaradi(i)=(radi(i+1)-radi(i))/2
      area(i)=pi*(radi(i+1)*radi(i+1)-radi(i)*radi(i))
      i=i+1
      end do


c *** START THE CALCULATION **********************************

      t=0.

      do while (t.lt.time)

c *** FLUX AT THE BOUNDARY (n=1) ***
      flux(1)=pidiff*radi(1)*(concentration(2)*(1-totf/av)
     --concentration(1)*escapeprob*enterprob)*step/deltaradi(1)

      totf=totf+flux(1)

      concentration(1)=totf/pirmin

c *** FLUX AT THE OTHER ANNULI (n=i) ***
      i=2
      do while (i.le.n-1)
      flux(i)=pidiff*radi(i)*((concentration(i+1)
     --concentration(i))/deltaradi(i))*step
c *** RECALCULATION OF THE CONCENTRATION AT THE ANNULUS i ***
      concentration(i)=concentration(i)+(flux(i)-flux(i-1))/area(i)
```

```
      i=i+1
      end do

c**** CONTROL IF ***
      if (totf.gt.av) then
      write(*,*)
      write(*,*) 'Please reduce the time step!'
      endif
      if (totf.gt.av) goto 1000
c*****************

      t=t+step

c *** WRITE THE DATA EVERY T=TIMESTEP ***
      wstep=wstep+step
      if (wstep.gt.writestep) then
      write(3,*) t/3600, totf*atlock*1.e-6
      write(*,*) 'Percentage done ',100*t/time
      wstep=0.
      endif

      end do
      write(*,*)
      write(*,*)'Data written on file every ',writestep,' sec'


1000  end
```

Bibliography

[1] J. Czochralski, Z. Phys. Chem. **92**, 219 (1917).

[2] W. C. Dash, J. Appl. Phys. **30**, 459 (1959).

[3] A. Borghesi, B. Pivac, A. Sassella, and A. Stella, J. Appl. Phys. **77**, 4169 (1995).

[4] C. W. Pearce, Crystal growth and wafer preparation, in *VLSI Technology*, edited by S. M. Sze, chap. 1, p. 21, McGraw-Hill, 1983.

[5] Y. Yatsurugi, N. Akijama, Y. Endo, and T. Nozaki, J. Electrochem. Soc. **120**, 975 (1973).

[6] I. Yonenaga, K. Sumino, and K. Hoshi, J. Appl. Phys. **56**, 2346 (1984).

[7] W. Zulehner, in *Semiconductor Silicon 1989*, edited by G. Harbeke and M. J. Schulzin, p. 2, Springer, Heidelberg, 1989.

[8] G. Lutz, *Semiconductor Radiation Detectors* (Springer, Berlin, 1999).

[9] K. J. Vinoy, H. Yoon, T. Ji, and V. K. Varadan, Proc. SPIE Int. Soc. Opt. Eng. **4981**, 164 (2003).

[10] M. B. Shabani, T. Yoshimi, and H. Abe, J. Electrochem. Soc. **143**, 2025 (1996).

[11] B. Pajot, E. Artacho, C. A. J. Ammerlaan, and J.-M. Spaeth, J. Phys.: Condens. Matter **7**, 7077 (1995).

[12] W. L. Bond and W. Kaiser, J. Phys. Chem. Solids **16**, 44 (1960).

[13] R. C. Newman, J. Phys.: Condens. Matter **12**, R335 (2000).

[14] P. D. Southgate, Proc. Phys. Soc. B **70**, 804 (1957).

[15] S.-T. Lee and D. Nichols, Appl. Phys. Lett. **47**, 1001 (1985).

[16] S.-T. Lee and D. Nichols, in *Mater. Res. Soc. Symp. Proc.* Vol. 59, p. 31, Materials Research Society, Pittsburgh, 1986.

[17] J. C. Mikkelsen Jr., Appl. Phys. Lett. **40**, 336 (1982).

[18] J. C. Mikkelsen Jr., Appl. Phys. Lett. **41**, 871 (1982).

[19] J. C. Mikkelsen Jr, Mat. Res. Soc. Symp. Proc. **59**, 19 (1986).

[20] R. Newman and R. Jones, Diffusion of oxygen in silicon, in *Semiconductors and Semimetals*, edited by F. Shimura, chap. 42, p. 289, San Diego, CA: Academic, 1994.

[21] J. W. Corbett and G. D. Watkins, Phys. Rev. Lett. **7**, 314 (1961).

[22] J. W. Corbett, R. C. McDonald, and G. D. Watkins, J. Phys. Chem. Solids **25**, 873 (1964).

[23] M. Stavola, J. R. Patel, L. C. Kimmerling, and P. E. Freeland, Appl. Phys. Lett. **42**, 73 (1983).

[24] R. C. Newman, J. H. Tucker, and F. M. Livingston, J. Phys. C: Solid State Phys. **16**, L151 (1983).

[25] C. S. Fuller, J. A. Ditzenberger, N. D. Hannay, and E. Buehler, Phys. Rev. **96**, 833 (1954).

[26] W. Kaiser, H. L. Frisch, and H. Reiss, Phys. Rev. **112**, 1546 (1958).

[27] H. Takeno, Y. Hayamizu, and K. Miki, J. Appl. Phys. **84**, 3113 (1998).

[28] S. T. Lee, P. Fellinger, and S. Chen, J. Appl. Phys. **63**, 1924 (1988).

[29] W. Bergholz, J. L. Hutchison, and P. Pirouz, J. Appl. Phys. **58**, 3419 (1985).

[30] P. Gaworzewski and G. Ritter, Phys. Stat. Sol. (a) **67**, 511 (1981).

[31] U. Gösele and T. Y. Tan, in *Defects in Semiconductors II*, edited by S. Mahajan and J. W. Corbett, , MRS Symposia Proceedings Vol. 14, p. 153, North-Holland, New York, 1983.

[32] S. Senkader, K. Jurkschat, D. Gambaro, R. J. Falster, and P. R. Wilshaw, Philos. Mag. A **81**, 759 (2001).

[33] T. Abe and M. Kimura, in *Semiconductor Silicon 1990*, edited by H. R. Huff, K. D. Baraclough, and J. Chikawa, p. 105, The Electrochemical Society, Pennington, 1990.

[34] H. Ishii, S. Shiratake, K. Oka, K. Motonami, T. Koyama, and J. Izumitani, Jpn. J. Appl. Phys., Part 2 **35**, L1385 (1996).

[35] W. Ohashi, A. Ikari, Y. Ohta, A. Tachikawa, H. Deai, H. Yokata, and T. Hoshino, in *Extended Abstracts No. 1, The 46th Spring Meeting* (Japan Society of Applied Physics, Tokyo, 1999) , p468 (1999).

[36] M. Kato, M. Tamatsuka, M. Iida, H. Takeno, T. Otogawa, and T. Matsui, in *Extended Abstracts No. 1, The 46th Spring Meeting* (Japan Society of Applied Physics, Tokyo, 1999) , p470 (1999).

[37] H. Kageshima, A. Taguchi, and K. Wada, MRS Symp. Proc. **719**, 33 (2002).

[38] L. S. Adam, M. E. Law, S. Szpala, P. J. Simpson, D. Lawther, O. Dokumaci, and S. Hegde, Appl. Phys. Lett. **79**, 623 (2001).

[39] W. von Ammon, R. Höltz, J. Virbulis, E. Dornberger, R. Schmolke, and D. Gräf, J. Cryst. Growth **226**, 19 (2001).

[40] W. von Ammon, P. Drier, W. Hensel, U. Lambert, and L. Kostler, Mater. Sci. Eng. B **36**, 33 (1996).

[41] H. D. Chiou, J. Moody, R. Sandford, and F. Shimura, in *Proceedings of the Second International Symposium on Very Large Scale Integration* Vol. PV 2004-05, High Purity Silicon VIII, 1984.

[42] J. S. Kang and D. K. Schroder, J. Appl. Phys. **64**, 6673 (1988).

[43] D. Yang, Y. W. Wang, H. N. Yao, and D. L. Que, Progress Natural Sci. **3**, 176 (1993).

[44] W. von Ammon, R. Höltz, T. Wetzel, D. Zemke, G. Raming, and M. Blietz, Microelectronic Engineering **66**, 234 (2003).

[45] R. Schmolke, The Electrochemical Society Proceedings **2000-2017**, p.3 (2000).

[46] K. Nakamura, T. Saishoji, S. Togawa, and J. Tomioka, in *Proc. Kazusa Academia Park Forum on the Science and Technology of Silicon Materials*, p. 116, Japan Tech. Inform. Service, 1999.

[47] A. L. Parakhonsky, E. B. Yakimov, and D. Yang, J. Appl. Phys. **90**, 3642 (2001).

[48] B. M. Park, G. H. Seo, and G. Kim, J. Crystal Growth **222**, 74 (2001).

[49] K. Nakai, Y. Inoue, H. Yokota, A. Ikari, J. Takahashi, A. Tachikawa, K. Kitahara, Y. Ohta, and W. Ohasi, J. Appl. Phys. **89**, 4301 (2001).

[50] V. V. Voronkov and R. Falster, J. Electrochem. Soc. **149**, G167 (2002).

[51] W. P. Lee, H. K. Yow, and T. Y. Tou, Electrochemical and Solid-State Letters **7**, G282 (2004).

[52] M. Tamatsuka, N. Kobayashi, S. Tobe, and T. Masui, Electrochem. Soc. Proc. **99**, 456 (1999).

[53] M. Iida, M. Kato, H. Takeno, M. Tamatsuka, Y. Hayamizu, M. Kimura, and T. Masui, in *Extended Abstracts No. 1, The 60th Autumn Meeting* (The Japan Society of Applied Physics, Konan University, 1999) , p356 (1999).

[54] T. Saishoji, H. Nakajima, F. Ishikawa, M. Usukubo, K. Nakamura, and J. Tomioka, in *Extended Abstracts No. 1, The 60th Autumn Meeting* (The Japan Society of Applied Physics, Konan University, 1999) , p356 (1999).

[55] H. Sawada and K. Kawakami, Phys. Rev. B **62**, 1851 (2000).

[56] F. Shimura and R. S. Hockett, Appl. Phys. Lett. **48**, 224 (1986).

[57] X. Ma, X. Yu, R. Fan, and D. Yang, Appl. Phys. Lett. **81**, 496 (2002).

[58] H. Lu, D. Yang, J. Yang, D. Tian, Y. Shen, X. Ma, L. Li, and D. Que, Physica B **308-310**, 1173 (2001).

[59] M. Pagani, R. J. Falster, G. R. Fisher, G. C. Ferrero, and M. Olmo, Appl. Phys. Lett. **70**, 1572 (1997).

[60] Q. Sun, K. H. Yao, and H. C. Gatos, J. Appl. Phys. **71**, 3760 (1992).

[61] J. Xu, X. Ma, J. Lu, C. Li, and D. Yang, Physica B **348**, 226 (2004).

[62] D. Yang and D. Que, Phys. Stat. Sol. (a) **171**, 203 (1999).

[63] I. Yonenaga, J. Appl. Phys. **98**, 023517 (2005).

[64] A. Ikari, K. Nakai, Y. Tachikawa, H. Deai, Y. Hideki, Y. Ohta, N. Masahashi, S. Hayashi, T. Hoshino, and W. Ohashi, Solid State Phenomena **69-70**, 161 (1999).

[65] T. Kumar and S. Singh, Bulletin Electrochemistry **10**, 518 (1984).

[66] H. Yamanaka, Jpn. J. Appl. Phys. **32**, 3905 (1983).

[67] T. Sinno, R. A. Brown, W. von Ammon, and E. Dornberger, J. Electrochem. Soc. **145**, 302 (1998).

[68] K. Nakai, Y. Inoue, H. Yokota, A. Ikari, J. Takahashi, and W. Ohashi, Proceedings of the 3rd International Symposium on Advanced Science and Technology of Silicon Materials, JSPS , 88 (2000).

[69] D. Gräf, U. Lambert, R. Schmolke, R. Wahlich, W. Siebert, E. Daub, and W. von Ammon, Electrochem. Soc. Proc. **2000 (17)**, 319 (2000).

[70] T. Abe and H. Takeno, Mater. Res. Soc. Symp. Proc. **262**, 3 (1992).

[71] K. Sumino, I. Yonenaga, M. Imai, and T. Abe, J. Appl. Phys. **54**, 5016 (1983).

[72] M. Akatsuka and K. Sueda, Jpn. J. Appl. Phys. Part 1 **40**, 1240 (2001).

[73] M. Heggie, R. Jones, and A. Umerski, Phys. Stat. Sol. A **138**, 383 (1993).

[74] D. Li, D. Yang, and D. Que, Physica B **273-274**, 553 (1999).

[75] H. Lu, D. Yang, L. Li, Z. Ye, and D. Que, Phys. Stat. Sol. (a) **169**, 193 (1998).

[76] V. Orlov, H. Richter, A. Fischer, J. Reif, T. Müller, and R. Wahlich, Materials Science in Semiconductor Processing **5**, 403 (2003).

[77] J. Vedde and P. Gravesen, Materials Science and Engineering B **36**, 246 (1996).

[78] G. Wang, D. Yang, D. Li, Q. Shui, J. Yang, and D. Que, Physica B **308-310**, 450 (2001).

[79] A. Giannattasio, S. Senkader, R. J. Falster, and P. R. Wilshaw, Physica B **340-342**, 996 (2003).

[80] S. Senkader, A. Giannattasio, R. J. Falster, and P. R. Wilshaw, in *Proceedings of the 202nd Meeting of the Electrochemical Society (October 2002)* Vol. PV 2002-20, High Purity Silicon VII, Salt Lake City, Utah, 2002.

[81] W. Kaiser and C. D. Thurmond, J. Appl. Phys. **30**, 427 (1959).

[82] J. B. Mitchell, J. Shewchun, D. A. Thompson, and J. A. Davies, J. Appl. Phys. **46**, 335 (1975).

[83] P. V. Pavlov, E. I. Zorin, D. I. Tetelbaum, and A. F. Khokhlov, Phys. Stat. Sol. (a) **35**, 11 (1976).

[84] M. Suezawa, K. Sumino, H. Harada, and T. Abe, Jpn. J. Appl. Phys, Part 1 **25**, L859 (1986).

[85] H. Navarro, J. Griffin, J. Weber, and L. Genzel, Solid State Commun. **58**, 151 (1986).

[86] J. A. Griffin, J. Hartung, J. Weber, H. Navarro, and L. Genzel, Appl. Phys. A: Solids Surf. **48**, 41 (1989).

[87] A. Hara, T. Fukuda, T. Miyabo, and I. Hirai, Appl. Phys. Lett. **54**, 626 (1989).

[88] A. Hara, M. Aoki, M. Koizuka, and T. Fukuda, J. Appl. Phys. **75**, 2929 (1994).

[89] D. Yang, D. Que, and K. Sumino, J. Appl. Phys. **77**, 943 (1994).

[90] D. Yang, R. Fan, L. Li, D. Que, and K. Sumino, Appl. Phys. Lett. **68**, 487 (1996).

[91] R. C. Newman, J. H. Tucker, N. G. Semaltianos, E. C. Lightowlers, T. Gregorkiewicz, I. S. Zevenbergen, and C. A. J. Ammerlaan, Phys. Rev. B **54**, 6803 (1996).

[92] R. C. Newman, M. J. Ashwin, R. E. Pritchard, and J. H. Tucker, Phys. Stat. Sol. (b) **210**, 519 (1998).

[93] D. Yang, M. Klevermann, and L. I. Murin, Physica B **2001**, 193 (2001).

[94] B. J. Heijmink Liesert, T. Gregorkiewicz, and C. A. J. Ammerlaan, Phys. Rev. B **47**, 7005 (1993).

[95] Y. V. Martynov, T. Gregorkiewicz, and C. A. J. Ammerlaan, Phys. Rev. Lett. **74**, 2030 (1995).

[96] C. P. Ewels, R. Jones, S. Öberg, J. Miro, and P. Deák, Phys. Rev. Lett. **77**, 865 (1996).

[97] V. V. Voronkov, M. Porrini, P. Collareta, M. G. Pretto, R. Scala, R. Falster, G. I. Voronkova, A. V. Batunina, V. N. Golovina, L. V. Arapkina, A. S. Guliaeva, and M. G. Milvidski, J. Appl. Phys. **89**, 4289 (2001).

[98] K. L. Brower, Phys. Rev. B **26**, 6040 (1982).

[99] T. Abe, H. Harada, N. Ozawa, and K. Adomi, Mater. Res. Soc. Symp. Proc. **59**, 537 (1986).

[100] K. Kakumoto and Y. Takano, Deep level induced by diffused n2 and vacancy complex in si, in *Proc. 2nd International Symp. on Advanced Science and Technology of Silicon Materials*, p. 437, Kona, Hawaii, 1996.

[101] Y. Tokumaru, H. Okushi, T. Masui, and T. Abe, Jpn. J. Appl. Phys. **21**, L443 (1982).

[102] N. Fuma, K. Tashiro, K. Kakumoto, and Y. Takano, Jpn. J. Appl. Phys. **35**, 1993 (1996).

[103] J. D. Murphy, C. R. Alpass, A. Giannattasio, S. Senkader, D. Emiroglu, J. H. Evans-Freeman, R. J. Falster, and P. R. Wilshaw, ECS Transactions **3**, 239 (2006).

[104] K. Nauka, M. S. Goorsky, H. C. Gatos, and J. Lagowski, Appl. Phys. Lett. **47**, 1341 (1985).

[105] R. Jones, I. Hahn, J. P. Goss, P. R. Briddon, and S. Öberg, Solid State Phenomena **95-96**, 93 (2004).

[106] J. P. Goss, I. Hahn, R. Jones, P. R. Briddon, and S. Öberg, Phys. Rev. B **67**, 045206 (2003).

[107] J. Weber, W. Schmid, and R. Sauer, Phys. Rev. B **21**, 2401 (1980).

[108] M. Tajima, T. Masui, T. Abe, and T. Nozaki, Jpn. J. Appl. Phys. **20**, L423 (1981).

[109] R. Sauer and J. Weber, Appl. Phys. Lett. **44**, 440 (1984).

[110] G. Davies, M. Zafar Iqbal, and E. C. Lightowlers, Phys. Rev. B **50**, 11520 (1994).

[111] T. Abe, Semiconductor Silicon 1981, The Electrochemical Society Proceedings **81-85**, 54 (1981).

[112] T. S. Chao, M. C. Liaw, C. H. Chu, C. Y. Chang, C. H. Chien, C. P. Hao, and T. F. Lei, Appl. Phys. Lett. **69**, 1781 (1996).

[113] L. S. Adam, M. E. Law, O. Dokumaci, and S. Hegde, J. Appl. Phys. **91**, 1894 (2002).

[114] N. Kelaidis, D. Skarlatos, V. Ioannou-Sougleridis, C. Tsamis, P. Komninou, B. Kellerman, and M. Seacrist, Mat. Sci. Eng. B **135**, 199 (2006).

[115] F. Berg Rasmussen, S. berg, R. Jones, C. Ewels, J. Goss, J. Mirod, and P. Dek, Mat. Science and Eng. B **36**, 91 (1996).

[116] M. W. Qi, S. S. Tan, B. Zhu, P. X. Cai, W. F. Gu, X. M. Xu, T. S. Shi, D. L. Que, and L. B. Li, J. Appl. Phys. **69**, 3775 (1991).

[117] H. Ono and M. Horikawa, Jpn. J. Appl. Phys. **42**, L261 (2003).

[118] M. Nakatsu, A. Hashimoto, A. Natsume, N. Inoue, and H. Ono, ECS Proceedings , 102 (2004).

[119] X. H. Shi, Solid State Commun. **106 (10)**, 669 (1988).

[120] P. Wagner, R. Oeder, and W. Zulehner, Appl. Phys. A **46**, 73 (1988).

[121] S. Binetti, S. Pizzini, R. Somaschini, A. Le Donne, D. Li, and D. Yang, Microelectronic Engineering **66**, 297 (2003).

[122] H. J. Stein, Appl. Phys. Lett. **47**, 1339 (1985).

[123] M. Porrini, M. G. Pretto, and R. Scala, Mat. Sci. Eng. B **102**, 228 (2003).

[124] A. H. Clark, J. D. MacDougall, K. E. Manchester, P. E. Roughan, and F. W. Anderson, Bull. Amer. Phys. Soc. **13**, 376 (1968).

[125] M. V. Mezhennyi, M. G. Milvidski, V. Y. Reznik, and R. J. Falster, J. Phys.: Condens. Matter **14**, 12903 (2002).

[126] G. Mannino, V. Privitera, S. Scalese, S. Libertino, E. Napolitani, P. Pichler, and N. E. B. Cowern, Electrochemical and Solid-State Letters **7**, G161 (2004).

[127] V. V. Voronkov and R. Falster, Solid State Pheonomena **95-96**, 83 (2004).

[128] R. Falster and V. V. Voronkov, Mater. Sci. Eng. **73**, 87 (2000).

[129] F. Quast, P. Pichler, H. Ryssel, and R. Falster, in *High Purity Silicon VI*, edited by C. L. Claeys, P. Rai-Choudhury, M. Watnabe, P. Stallhofer, and H. J. Dawson Vol. 2000-17, p. 156, The Electrochemical Society Proceedings Series, Pennington, NJ, 2000.

[130] J. B. Mitchell, P. P. Pronko, J. Shewchun, D. A. Thompson, and J. A. Davies, J. Appl. Phys. **46**, 332 (1975).

[131] R. Jones, S. Öberg, F. Berg Rasmussen, and B. Bech Nielsen, Phys. Rev. Lett. **72**, 1882 (1994).

[132] F. Berg Rasmussen and B. Bech Nielson, Phys. Rev. B **49**, 16353 (1994).

[133] A. Karoui, F. Sahtout Karoui, A. Kvit, and G. A. Rozgonyi, Appl. Phys. Lett. **80**, 2114 (2002).

[134] C. D. Meekison, G. R. Booker, K. J. Reeson, P. L. F. Hemment, R. F. Peart, R. J. Chater, J. A. Kilner, and J. R. Davis, J. Appl. Phys. **69**, 3503 (1991).

[135] L. S. Adam, M. E. Law, K. S. Jones, O. Dokumaci, C. S. Murthy, and S. Hegde, J. Appl. Phys. **87**, 2282 (2000).

[136] V. S. Kaushik, A. K. Datye, D. L. Kendall, B. Martinez-Tovar, D. S. Simons, and D. R. Myers, J. Mater. Res. **4**, 394 (1989).

[137] N. Stoddard, G. Duscher, A. Karoui, F. Stevie, and G. Rozgonyi, J. Appl. Phys. **97**, 083534 (2005).

[138] G. A. Rozgonyi, A. Karoui, A. Kvit, and G. Duscher, Microelectronic Engineering **66**, 305 (2003).

[139] H. Wang, X. Ma, J. Xu, X. Yu, and D. Yang, Semicond. Sci. Technol. **19**, 2004 (2004).

[140] D. Yang, X. Ma, F. Fan, J. Zhang, L. Li, and D. Que, Physica B **273-274**, 308 (1999).

[141] A. Karoui and G. A. Rozgonyi, J. Appl. Phys. **96**, 3264 (2004).

[142] S. Binetti, R. Somaschini, A. Le Donne, E. Leoni, S. Pizzini, D. Li, and D. Yang, J. Phys.: Condens. Matter **14**, 13247 (2002).

[143] A. Dörnen, G. Pensl, and R. Sauer, Phys. Rev. B **35**, 9318 (1987).

[144] A. G. Steele, L. C. Lenchyshyn, and M. L. W. Thewalt, Appl. Phys. Lett. **56**, 148 (1989).

[145] K. Aihara, H. Takeno, Y. Hayamizu, M. Tamatsuka, and T. Masui, J. Appl. Phys. **88**, 3705 (2000).

[146] K. L. Brower, Phys. Rev. Lett. **44**, 1627 (1980).

[147] K. Murakami, H. Itoh, K. Takita, and K. Masuda, Appl. Phys. Lett. **45**, 176 (1984).

[148] K. Murakami, H. Kuribayashi, and K. Masuda, Phys. Rev. B **38**, 1589 (1988).

[149] A. Karoui, F. Sahtout Karoui, and G. A. Rozgonyi, J. Appl. Phys. **96**, 3255 (2004).

[150] Y. Itoh, T. Nozaki, T. Masui, and T. Abe, Appl. Phys. Lett. **47**, 488 (1985).

[151] N. Inoue, A. Hashimoto, K. Shingu, and K. Masumoto, Solid State Phenomena **95-96**, 489 (2004).

[152] T. Gregorkiewicz, H. H. P. T. Bekman, and C. A. J. Ammerlaan, Phys. Rev. B **41**, 12628 (1990).

[153] J. A. Verges, J. Phys. C: Solid State Phys. **14**, 365 (1981).

[154] G. D. Watkins, G. G. DeLeo, and W. B. Fowler, Physica B & C **116**, 28 (1983).

[155] G. G. DeLeo, W. Beall Fowler, and G. D. Watkins, Phys. Rev. B **29**, 3193 (1984).

[156] R. P. Messmer and P. A. Schultz, Solid State Commun. **52**, 563 (1984).

[157] P. A. Schultz and R. P. Messmer, Phys. Rev. B **34**, 2532 (1986).

[158] H. P. Hjalmarson and D. R. Jennison, Phys. Rev. B **31**, 1208 (1985).

[159] F. G. Anderson, Phys. Rev. B **39**, 5392 (1989).

[160] C. Cunha, S. Canuto, and A. Fazzio, Phys. Rev. B **48**, 17806 (1993).

[161] M. Saito and Y. Miyamoto, Phys. Rev. B **56**, 9193 (1997).

[162] H. J. Stein, Nitrogen in crystalline si, in *Oxygen, Carbon, Hydrogen and Nitrogen in Crystalline Silicon*, edited by J. C. Mikkelsen Jr, S. J. Pearton, J. W. Corbett, and S. J. Pennycook Vol. 59, p. 523, Materials Research Society (MRS, Pittsbury, PA), 1985.

[163] H. J. Stein, P. S. Peercy, and C. R. Hills, in *Energy Beam-Solid Interactions and Transient Thermal Processing*, edited by D. K. Biegelsen, G. A. Rozgonyi, and C. V. Shank Vol. 35, p. 315, Materials Research Society (MRS, Pittsbury, PA), 1985.

[164] J. L. McAfee, H. Ren, and S. K. Estreicher, Phys. Rev. B **69**, 165206 (2004).

[165] H. Harada, I. Ohkubo, T. Mikayama, Y. Yamanaka, and N. Inoue, Physica B **308-310**, 244 (2001).

[166] A. Gali, J. Miro, P. Deak, C. P. Ewels, and R. Jones, J. Phys.: Condens Matter **8**, 7711 (1996).

[167] H. Kageshima, A. Taguchi, and K. Wada, Appl. Phys. Lett. **76**, 3718 (2000).

[168] P. A. Schultz and J. S. Nelson, Appl. Phys. Lett. **78**, 736 (2001).

[169] W. von Ammon, R. Höltz, J. Virbulis, E. Dornberger, R. Schmolke, and D. Gräf, Solid State Phenom. **82-84**, 17 (2002).

[170] H. J. Stein, Mat. Res. Soc. Symp. Proc. **59**, 523 (1986).

[171] M. Kaukonen, R. Jones, S. Öberg, and P. R. Briddon, Phys. Rev. B **64**, 245213 (2001).

[172] J. L. Hastings, S. K. Estreicher, and P. A. Fedders, Phys. Rev. B **56**, 10215 (1997).

[173] A. Karoui, F. Sahtout Karoui, G. A. Rozgonyi, M. Hourai, and K. Sueoka, J. Electrochem. Soc. **150**, G771 (2003).

[174] F. Sahtout Karoui, A. Karoui, G. A. Rozgonyi, M. Hourai, and K. Sueoka, Solid State Phenom. **95-96**, 99 (2004).

[175] F. Berg Rasmussen, Ph.D. Thesis, Institute of Physics and Astronomy, University of Århus, Denmark (1994).

[176] N. V. Denisova, E. I. Zorin, P. V. Pavlov, D. I. Tetelbaum, and A. F. Khokhlov, Izv. Akad. Nauk. SSSR Ser. Neorg. Mater. **11**, 2236 (1975).

[177] T. Itoh and T. Abe, Appl. Phys. Lett. **53**, 39 (1988).

[178] G. J. Willems and H. E. Maes, J. Appl. Phys. **73**, 3256 (1993).

[179] N. Fuma, K. Tashiro, K. Kakumoto, and Y. Takano, Mater. Sci. Forum **196-201**, 797 (1995).

[180] A. Giannattasio, S. Senkader, S. Azam, R. J. Falster, and P. R. Wilshaw, Microelectronic Engineering **70**, 125 (2003).

[181] A. Giannattasio, J. D. Murphy, S. Senkader, R. J. Falster, and P. R. Wilshaw, Impurity locking of dislocations in silicon, in *Proceedings of the 206th Meeting of the Electrochemical Society (October 2004)* Vol. PV 2004-05, High Purity Silicon VIII, Honolulu, Hawaii, 2004.

[182] A. Giannattasio, S. Senkader, R. J. Falster, and P. R. Wilshaw, Computational Materials Science **30**, 131 (2004).

[183] J. D. Murphy, A. Giannattasio, S. Senkader, R. J. Falster, and P. R. Wilshaw, Phys. Stat. Sol. (a) **202**, 926 (2005).

[184] J. D. Murphy, A. Giannattasio, C. R. Alpass, S. Senkader, R. J. Falster, and P. R. Wilshaw, Sol. St. Phen. **108-109**, 139 (2005).

[185] R. S. Hockett, Appl. Phys. Lett. **54**, 1793 (1989).

[186] G. Mannino, V. Privitera, S. Scalese, E. Napolitani, P. Pichler, and N. E. B. Cowern, submitted to Applied Physics Letters (2003).

[187] V. V. Voronkov and R. Falster, J. Appl. Phys. **100**, 083511 (2006).

[188] H. Sawada, K. Kawakami, A. Ikari, and W. Ohashi, Phys. Rev. B **65**, 075201 (2002).

[189] N. Fujita, R. Jones, T. Frauenheim, S. Öberg, J. P. Goss, and P. R. Briddon, Appl. Phys. Lett. **87**, 021902 (2005).

[190] N. Stoddard, P. Pichler, G. Duscher, and W. Windl, Phys. Rev. Lett. **95**, 025901 (2005).

[191] V. V. Voronkov and R. Falster, ECS Transactions **3**, 113 (2006).

[192] C. Herring and N. M. Johnson, Hydrogen in semconductors, in *Semiconductors and Semimetals*, edited by J. I. Pankove and N. M. Johnson Vol. 34, Chapter 10, Academic, San Diego, 1991.

[193] W. Windl, Solid State Phenomena **108-109**, 125 (2005).

[194] N. Fujita, R. Jones, T. A. G. Eberlein, S. Öberg, and P. R. Briddon, Solid State Phenomena **131-133**, 265 (2008).

[195] H. J. Stein, Mat. Res. Soc. Symp. Proc. **46**, 287 (1985).

[196] R. Jones, C. Ewels, J. Goss, J. Miro, P. Deák, S. Öberg, and F. Berg Rasmussen, Phys. Rev. Lett. **72**, 1882 (1994).

[197] X. Yu, D. Yang, X. Ma, J. Yang, L. Li, and D. Que, J. Appl. Phys. **92**, 188 (2002).

[198] C. Murthy, K. Lee, R. Rengarajan, O. Dokumaci, P. Ronsheim, H. Tews, and S. Inaba, Appl. Phys. Lett. **80**, 2696 (2002).

[199] D. J. Chadi, Phys. Rev. Lett. **77**, 861 (1996).

[200] P. Deák, L. C. Snyder, and J. W. Corbett, Phys. Rev. B **45**, 11612 (1992).

[201] A. Taguchi, H. Kageshima, and K. Wada, J. Appl. Phys. **97**, 053514 (2005).

[202] H. J. Stein, Appl. Phys. Lett. **43**, 296 (1983).

[203] M. Sprenger, E. G. Sieverts, S. H. Muller, and C. A. J. Ammerlaan, Solid State Commun. **51**, 951 (1984).

[204] H. Itoh, K. Murakami, K. Takita, and K. Musada, Proc. of the Fifteenth Symposium in Ion Implantation and Submicron Fabrication, Rikagaku Kenkyusho, Wako-shi Saitama, Japan **351**, 85 (1984).

[205] H. C. Alt and L. Tapfer, Proceedings of the Thirteenth International Conference on Defects in Semiconductors, edited by L. C. Kimerling and J. M. Parsey Jr., Metallurgical Society of AIME, Warrendale, PA , p. 833 (1985).

[206] E. I. Zorin, P. V. Pavlov, and D. I. Tetelbaum, Soviet Phys-Semiconductors **2**, 111 (1968).

[207] E. I. Zorin, P. V. Pavlov, D. I. Tetelbaum, and A. F. Khohlov, Soviet Phys-Semiconductors **4**, 2026 (1971).

[208] P. L. F. Hemment, R. F. Peart, M. F. Yao, K. G. Stephens, R. J. Chater, J. A. Kilner, D. Meekison, G. R. Booker, and R. P. Arrowsmith, Appl. Phys. Lett. **46**, 952 (1985).

[209] E. H. TeKaat and J. Belz, Materials Research Society Symposium **45**, 329 (1985).

[210] C. I. Drowley and T. I. Kamins, Materials Research Society Proceedings **13**, 511 (1983).

[211] J. P. Chang, M. L. Green, V. M. Donnelly, R. L. Opila, J. Eng, J. Sapjeta, P. J. Silverman, B. Weir, H. C. Lu, T. Gustafsson, and E. Garfunkel, J. Appl. Phys. **87**, 4449 (2000).

[212] M. Iida, W. Kusaki, M. Tamatsuka, E. Iino, M. Kimura, and S. Muraoka, ECS Proceedings **99-1**, 499 (1999).

[213] R. S. Hockett and D. B. Sams, ECS Proceedings **2000-2017**, 584 (2000).

[214] A. Ishitani, K. Okuno, A. Karen, and F. Soeda, Proc. Int. Conf. Materials & Process Character. VLSI. , p. 124 (1988).

[215] M. Watanabe, T. Usami, H. Muraoka, S. Matsuo, Y. Imanishi, and H. Nagashima, Semiconductor Silicon , p. 126 (1981).

[216] H. Yamanaka, H. Harada, K. Tanahashi, T. Mikayama, and H. Nagashima, Solid State Phenomena **82-84**, 63 (2002).

[217] S. M. Hu, J. Appl. Phys. **40**, 4413 (1969).

[218] H. Shimizu, S. Isomae, K. Minowa, T. Satoh, and T. Suzuki, J. Electrochem. Soc. **145**, 2523 (1998).

[219] A. Rivière-Jérôme, C. Levade, G. Vanderschaeve, I. Percheron-Garçon, and B. Forgerit, J. Phys.: Condens. Matter **12**, 10279 (2000).

[220] J. E. Lawrence, in *Semiconductor Silicon 1973*, edited by H. R. Huff and R. R. Burgess, p. 17, Pennington, NJ, 1973, The Electrochemical Society.

[221] J. P. Hirth and J. Lothe, *Theory of Dislocations*, p. 375, 2nd ed. (Wiley, 1982), .

[222] S. Schäfer, Phys. Stat. Solidi **19**, 297 (1967).

[223] I. L. F. Ray and D. J. H. Cockayne, Proc. R. Soc. Lond. A **325**, 543 (1971).

[224] J. P. Hirth and J. Lothe, *Theory of Dislocations*, 2nd ed. (Wiley, 1982).

[225] E. Schmid and W. Boas, *Plasticity of Crystals* (F.A. Hughes and Co., London, 1950).

[226] K. Sumino and M. Imai, Philos. Mag. A **47**, 753 (1983).

[227] K. Sumino, Mechanical behaviour of semiconductors, in *Handbook on Semiconductors*, edited by T. S. Moss Vol. 3, p. 96, Elsevier, 1994.

[228] A. H. Cottrell, Interaction of dislocations and solute atoms, in *Relation of Properties to Microstructure*, p. 131, Amer. Soc. Metals, Cleveland, Ohio, 1954.

[229] J. D. Eshelby, Solid State Phys. **3**, 79 (1956).

[230] A. Umerski and R. Jones, Philos. Mag. A **67**, 905 (1993).

[231] M. Heggie, R. Jones, and A. Umerski, Philos. Mag. A **63**, 571 (1991).

[232] R. Jones, A. Umerski, P. Sitch, M. Heggie, and S. Öberg, Phys. Stat. Sol. (a) **138**, 369 (1993).

[233] D. Hull and D. J. Bacon, *Introduction to Dislocations*, 4th ed. (Butterworth-Heinemann, 2001).

[234] K. Sumino, Mechanical behaviour of semiconductors, in *Handbook on Semiconductors*, edited by T. S. Moss Vol. 3, p. 125, Elsevier, 1994.

[235] H. Suzuki, in *Dislocation and Mechanical Properties of Silicon*, edited by J. C. Fisher, W. G. Johnson, R. Thompson, and T. Vreeland, p. 361, NY, John Wiley & Sons, 1957.

[236] S. M. Hu, Appl. Phys. Lett. **31**, 53 (1977).

[237] S. M. Hu, Appl. Phys. Lett. **31**, 139 (1977).

[238] S. M. Hu and W. J. Patrick, J. Appl. Phys. **46**, 1869 (1975).

[239] K. Sumino and H. Harada, Philos. Mag. A **44**, 1319 (1981).

[240] M. Imai and K. Sumino, Philos. Mag. A **47**, 599 (1983).

[241] I. Yonenaga and K. Sumino, J. Appl. Phys. **80**, 734 (1996).

[242] S. A. Galloway, *To study the mechanical properties of nitrogen ion-implanted wafers*, Part II Thesis, Department of Materials, University of Oxford, 1990.

[243] S. Senkader, R. J. Falster, and P. R. Wilshaw, J. Appl. Phys. **89**, 4803 (2001).

[244] S. Senkader, A. Giannattasio, R. J. Falster, and P. R. Wilshaw, J. Phys.: Condens. Matter **14**, 13141 (2002).

[245] S. Senkader, A. Giannattasio, R. J. Falster, and P. R. Wilshaw, Sol. St. Phen. **95–96**, 43 (2004).

[246] S. P. Murarka and G. Quintana, J. Appl. Phys. **48**, 46 (1977).

[247] N. Yarykin and V. I. Vdovin, Phys. Stat. Sol. (a) **202**, 921 (2004).

[248] J. D. Murphy, D.Phil Thesis Chapter 3, Department of Materials, University of Oxford, 2006.

[249] D. Aberg, B. G. Svensson, T. Hallberg, and J. L. Lindstrom, Phys. Rev. B **58**, 12944 (1998).

[250] L. I. Murin, T. Hallberg, V. P. Markevich, and J. L. Lindstrom, Phys. Rev. Lett. **80**, 93 (1998).

[251] J. D. Murphy, P. R. Wilshaw, B. C. Pygall, S. Senkader, and R. J. Falster, J. Appl. Phys. **100**, 103531 (2006).

[252] J. D. Murphy, S. Senkader, R. J. Falster, and P. R. Wilshaw, Mat. Sci. Eng. B **134**, 176 (2006).

[253] A. Giannattasio, Interaction of oxygen and nitrogen impurities with dislocations in silicon single-crystals, DPhil Thesis, Department of Materials, University of Oxford, 2004.

[254] J. D. Murphy, The properties of nitrogen and oxygen in silicon, D.Phil Thesis, Department of Materials, University of Oxford, 2006.

[255] J. D. Murphy, D.Phil Thesis p101ff, Department of Materials, University of Oxford, 2006.

[256] J. D. Murphy, D.Phil Thesis §4.3.1 and 2.3.8, Department of Materials, University of Oxford, 2006.

[257] J. D. Murphy, D.Phil Thesis §4.3, Department of Materials, University of Oxford, 2006.

[258] J. D. Murphy, D.Phil Thesis §2.3.8, Department of Materials, University of Oxford, 2006.

[259] P. Wilshaw, *Private communication* (2008).

[260] B. C. Pygall, Part II Thesis §8.0.7, Department of Materials, University of Oxford, 2005.

[261] K. Higashida, N. Narita, M. Tanaka, T. Morikawa, Y. Miura, and R. Onodera, Phil. Mag. A **82**, 3263 (2002).

[262] F. Shimura, J. Appl. Phys. **72**, 1642 (1992).

[263] S. P. Timoshenko and J. N. Goodier, in *Theory of Elasticity*, McGraw Hill, New York, 1970.

[264] A. Guha, Bending strength tests, in *Metals Handbook*, edited by J. R. Newman Vol. 8, p. 132, American Society for Metals, Ohio, 1985.

[265] M. Tachi, Suprijadi, S. Arai, and H. Saka, Phil. Mag. Lett. **82**, 133 (2002).

[266] M. B. Brown, Introductory solid mechanics, p. 112, Wiley, 1973.

[267] Gere and Timoshenko, in *Mechanics of Materials 2nd Ed.*, p. 359, Wordsworth International, 1985.

[268] http://www.materials.ox.ac.uk/cleanroom/equipment.htm.

[269] W. Kern, J. Electrochem. Soc. **137**, 1887 (1990).

[270] J. D. Murphy, D.Phil Thesis p70, Department of Materials, University of Oxford, 2006.

[271] W. von Ammon, Siltronic AG, *Private communication*, 2007.

[272] K. F. Kelton, R. Falster, D. Gambarro, M. Olmo, M. Cornara, and P. F. Wei, J. Appl. Phys. **85**, 8097 (1999).

[273] E. Dornberger, D. Temmler, and W. von Ammon, J. Electrochem. Soc. **149**, 226 (2002).

[274] J. L. Benton, D. C. Jacobson, B. Jackson, J. A. Johnson, T. Boone, D. J. Eaglesham, F. A. Stevie, and J. Becerro, J. Electrochem. Soc. **146**, 1929 (1999).

[275] S. M. Myers, M. Seibt, and W. Schroter, J. Appl. Phys. **88**, 3795 (2000).

[276] P. G. Shewmon, in *Diffusion in Solids*, McGraw-Hill, 1963.

[277] Properties of Silicon, *INSPEC, The Institution of Electrical Engineers, London and New York*, 1988.

[278] Instron, *Handbook for Model 1121, §5.1* .

[279] R. Jones, *Private communication*, 2008.

[280] M. Hart, Lattice parameter of si, in *Properties of Silicon*, edited by T. H. Ning, chap. 1.2, p. 7, INSPEC, 1988.

[281] C. Zener, J. Appl. Phys. **20**, 950 (1949).

[282] I. Yonenaga, T. Taishi, X. Huang, and K. Hoshikawa, J. Appl. Phys. **89**, 5788 (2001).

[283] I. Yonenaga, Solid State Phenom. **95-96**, 423 (2004).

[284] I. Yonenaga, T. Taishi, X. Huang, and K. Hoshikawa, J. Appl. Phys. **93**, 265 (2003).

[285] V. Orlov, Y. L. Iunin, M. V. Badylevich, O. Lysytskiy, and H. Richter, Solid State Phenom. **95-96**, 465 (2004).

[286] K. Sumino, Mechanical behaviour of semiconductors, in *Handbook on Semiconductors*, edited by T. S. Moss Vol. 3, p. 95, Elsevier, 1994.

[287] J. D. Murphy, *Private Communication*, 2007.

[288] P. R. Chidambaram, C. Bowen, S. Chakravarthi, C. Machala, and R. Wise, IEEE Transactions on Electron Devices **53**, 944 (2006).

[289] S. Ruffell, J. E. Bradby, J. S. Williams, and P. Munroe, J. Appl. Phys. **102**, 063521 (2007).

[290] R. J. Schreutelkamp, J. S. Custer, J. R. Liefting, W. X. Lu, and F. W. Saris, Materials Science Reports **6**, 275 (1991).

[291] A. Claverie, B. Colombeau, B. De Mauduit, C. Bonafos, X. Hebras, G. Ben Assayag, and F. Cristiano, Appl. Phys. A **76**, 1025 (2003).

[292] C. Bonafos, D. Mathiot, and A. Claverie, J. Appl. Phys. **83**, 3008 (1998).

[293] J. England, Varian Semiconductor Equipment Associates, Inc., *Private communication*, 2007.